Universidade de Lisboa

Faculdade de Medicina

Shedding Light on Enveloped Viruses Entry and its Inhibition Using Optical Techniques

Pedro Miguel Baptista de Matos

Doctorate in Biomedical Sciences

Specialty in Medical Biochemistry

2013

Universidade de Lisboa

Faculdade de Medicina

SHEDDING LIGHT ON ENVELOPED VIRUSES ENTRY AND ITS INHIBITION USING OPTICAL TECHNIQUES

Pedro Miguel Baptista de Matos

Thesis supervised by

Prof. Nuno Fernando Duarte Cordeiro Correia dos Santos

Doctorate in Biomedical Sciences

Specialty in Medical Biochemistry

A impressão desta dissertação foi aprovada pelo Conselho Científico da Faculdade de Medicina de Lisboa em reunião de 21 de Maio de 2013.

The printing of this dissertation was approved by the Scientific Council of the Faculty of Medicine of Lisbon in the meeting of May 21, 2013.

Table of contents

Preface

This Thesis compiles the work done during my doctoral studies that started in 2008 at the *Instituto de Medicina Molecular* (IMM), *Faculdade de Medicina*, *Universidade de Lisboa*. I gladly joined the *Biomembranes Unit*, headed by Prof. Nuno C. Santos, the supervisor of this Thesis, after I completed one year of research training with him, for my 4-years License degree in Biochemistry. I received a PhD fellowship from *Fundação para Ciência e Tecnologia, Ministério da Educação e Ciência* (SFRH/BD/42205/2007) which provided me the necessary funding to enroll in the *Lisbon Academic Medical Centre Doctoral Program in Biomedical Sciences* at the institution mentioned above.

The studies done at IMM relate to the membrane action of HIV-1 fusion inhibitor peptides using fluorescence spectroscopy methodologies. This theme was a common interest with another research unit at IMM, the Physical Biochemistry, led by Prof. Miguel Castanho, which we have always interacted closely. This body of work is contained in *Chapter II*. However, my research evolved to explore other aspects of viral entry besides the peptide inhibitors and I was fortunate to foster collaborations that allowed to do part of my studies abroad. Prof. Ricardo Gutiérrez Gallego accepted me in his lab in Barcelona, at the Institut Hospital del Mar d'Investigacions Mèdiques (IMIM), to explore interaction of HIV-1 glycoprotein with glycosaminoglycans. For this I used a surface plasmon resonance equipment, a technique that was not available in my lab at the time. The results related to his collaboration are presented as a submitted manuscript, in *Chapter III*. In order to seek expertise with a Virology group, I went to Prof. Gregory Melikyan's lab, at the Emory Children's Center, Emory University (Atlanta, USA). Here I studied the actual viral fusion in supported lipid bilayers and also with cells, using live confocal microscopy imaging. This work was incorporated in *Chapters IV* and *V*.

Overall, my doctoral studies have resulted in the following peer-reviewed publications:

- Matos PM, Andreu A, Santos NC*, Gutiérrez-Gallego R*. Structural requirements of glycosaminoglycans for the interaction with HIV-1 envelope glycoprotein gp120. (2013) *Submitted for publication* (*Co-corresponding authors).

- Matos PM, Marin M, Ahn B, Lam W, Santos NC, Melikyan GB. Anionic lipids are required for Vesicular Stomatitis Virus G protein-mediated single particle fusion with supported lipid bilayers. *J. Biol. Chem.* **288**:12416-12425 (2013). Journal IF: 4.773; Citations: 0 (ISI), 2 (Google Scholar).

- Hollmann A*, Matos PM*, Augusto MT, Castanho MARB, Santos NC. Conjugation of cholesterol to HIV-1 fusion inhibitor C34 increases peptide-membrane interactions potentiating its action. *PLoS ONE* **8**:e60302 (2013). (*Contributed equally to this work). Journal IF: 4.092; Citations: 0 (ISI), 0 (Google Scholar).

- Padilla-Parra S, Matos PM, Kondo N, Marin M, Santos NC, Melikyan GB. Quantitative imaging of endosome acidification and single retrovirus fusion with distinct pools of early endosomes. *Proc. Natl. Acad. Sci. U.S.A.* **109**:17627-17632 (2012). Journal IF: 9.681; Citations: 2 (ISI), 5 (Google Scholar).

- Matos PM, Freitas T, Castanho MARB, Santos NC. The role of blood cell membrane lipids on the mode of action of HIV-1 fusion inhibitor sifuvirtide. *Biochem. Biophys. Res. Commun.* **403**:270-274 (2010). Journal IF: 2.484; Citations: 5 (ISI), 7 (Google Scholar).

- Matos PM, Castanho MARB, Santos NC. HIV-1 Fusion inhibitor peptides enfuvirtide and T-1249 interact with erythrocytes and lymphocytes membranes. *PLoS ONE* **5**:e9830 (2010). Evaluated "Recommended" by Faculty of 1000 (http://f1000.com/2953959). Journal IF: 4.092; Citations: 12 (ISI), 16 (Google Scholar).

Reviews:

- Domingues MM, Matos PM, Carvalho FA, Santos NC. Protein-Biomembrane interactions as therapeutic targets. *Canal BQ (Journal of the Portuguese Biochemical Society)*, **8**:4-11 (2011).

- Matos PM, Franquelim HG, Castanho MARB, Santos NC. Quantitative assessment of peptide-lipid interactions: Ubiquitous fluorescence methodologies. *Biochim. Biophys. Acta.* 1798:1999-2012 (2010). Journal IF: 3.990; Citations: 15 (ISI), 19 (Google Scholar).

- Matos PM, Gonçalves S, Santos NC. Interaction of peptides with biomembranes assessed by potential sensitive fluorescent probes. *J. Pept. Sci.* 14:407-415 (2008). Journal IF: 1.799; Citations: 11 (ISI), 16 (Google Scholar).

Book chapter:

- Franquelim HG, Matos PM, Veiga S. "HIV vs. HIV: Turning HIV-Derived Peptides into Drugs" in *Peptide drug discovery and development – Translational research in Academia and Industry* (2011), Castanho MARB and Santos NC (eds.), Wiley-VCH, Weinheim, Germany. Citations: 1 (Google Scholar).

The four central chapters in this Thesis (II-V) are based on the inclusion of the respective article(s), preceded by a small overview explaining their context and declarations of authorship. I considered here the articles to be autonomous units, in the sense that they have their own sections, figure numbering and references. All the content of this book outside the articles or manuscripts are continuous, one sequence for figures, tables and reference numbering. All the references are at the end of the Thesis.

Acknowledgements

This Thesis is the result not only from my work and effort but also from valuable guidance, contributions and support from others that I deeply appreciate. Hence, I would like to kindly acknowledge the people and entities mentioned below:

Prof. Nuno C. Santos, my supervisor for this Thesis, for the guiding, advising and supporting my ideas and decisions throughout my doctoral program. For incentivizing us to take responsibility on developing and writing our studies, and be a part of the lab effort to evolve and seek new projects.

Prof. Miguel Castanho, for support and closely accompanying my studies related to the HIV fusion inhibitor peptides.

Instituto de Medicina Molecular, Faculdade de Medicina, Universidade de Lisboa and the **CAML PhD Program in Biomedical Sciences** staff that provided me a nice place to work and the opportunity to be a part of the PhD students activities, the annual meetings and retreats, conferences and seminars.

Prof. Ricardo Gutiérrez Gallego, for kindly accepting me in his lab in Barcelona, Spain. He taught me, helped me and supported me in my studies with the surface plasmon resonance technique. Also to **Prof. David Andreu**, in the same institution, for helping in the initial planning of the work.

Prof. Gregory Melikyan, for kindly accepting me in his lab in Atlanta, USA. His help and guidance was most valuable, suggesting new ideas whenever I hit a road block and making sure I had everything I needed for my research work.

My **Thesis Committee** members, Prof. Ana Espada de Sousa (IMM), Prof. Ana Coutinho (Instituto Superior Técnico, Universidade Técnica de Lisboa) and Prof. João Gonçalves (IMM and Faculdade de Farmácia, Universidade de Lisboa) for taking some time in evaluating my progress.

The **Nuno Santos' lab mates** (IMM Biomembranes Unit) for collaborating in the lab, being my friends, accompanying and cheering me up during these years,

either inside or outside the lab. I will keep you fondly in my "doctoral memories". Also to Teresa Freitas, Maria da Alegria Almeida and Almerinda Rodrigues for valuable technical assistance in the lab.

The **Miguel Castanho's lab mates** (IMM Physical Biochemistry Unit), for being such fun lab neighbors, collaborators and friends.

Lab mates at the Melikyan's lab in Atlanta for receiving me, supporting me and helping me in a friendly way. Also for the lab neighbors in the top floor of Emory Children's Center which always cheered me up and made me feel welcome. For all, I wish you much success in your lives.

Villa International Atlanta at the Clifton Road, headed by Camille Gaffron, for hosting me during my stay in Atlanta and to make me feel at home. Thanks to all the wonderful people from all over of the world that I met there and made sure that I was never alone.

Fundação para a Ciência e Tecnologia – Ministério da Educação e Ciência for providing the fellowship that supported me during my PhD program (SFRH/BD/42205/2007) and for the project PTDC/QUI-BIQ/104787/2008. Regarding other funding sources, I would also like to thank the **Federation for European Biochemical Societies** (FEBS) for funding my participation in their annual meeting in 2010 and in the FEBS-EMBO Advanced Lecture Course on Biomembranes in 2013; to the **European Biophysical Societies Association** (EBSA) for partially funding my visit to Ricardo Gutiérrez Gallego lab in Barcelona in 2011 and to the **Fondation pour l'Université de Lyon** for funding my participation in the BIOVISION 2013 – The World Life Sciences Forum, in France.

And last but not the least, to my **friends** and especially to my **family**, my father, mother and brother for their love and unconditional support, to whom I dedicate this Thesis.

Summary

Enveloped virus attachment and fusion into the host cells constitutes the first and crucial step for the life cycle of a virus and is mediated by the envelope glycoproteins. This Thesis aimed to clarify some important factors that influence this process and the mechanism of action at the molecular level of drugs that inhibit it.

First, the mode of action of HIV-1 fusion inhibitor peptides at the membrane level was studied using fluorescence spectroscopy. Interaction of these peptides with human cell membranes was assessed by dipole potential sensitive probes. C34-cholesterol, one of the latest generation fusion inhibitors had the highest cell membrane affinity, followed by T-1249, enfuvirtide and sifuvirtide. Sifuvirtide however showed strong preference for rigid membrane domains, mimicked by dipalmitoylphosphatidylcholine (DPPC), while C34-cholesterol strongly partitioned to cholesterol and sphingomyelin-rich model membranes. The overall results establish a relationship between these drugs antiviral activity and their membranotropism towards raft-like membrane compositions, following the trend C34-cholesterol > T-1249 > enfuvirtide. The capacity of the peptides to concentrate on lipid rafts microdomains, near the cell receptors for the virus, would make them more available to bind the viral gp41 in its exposed conformation.

We then focused on another aspect of the HIV-1 entry related to envelope-receptor interactions, namely with glycosaminoglycans. Their general structural requirements of that enable the binding to gp120 were determined by surface plasmon resonance. Binding was found to be dependent on sequence type and size, preferring heparin and heparan sulfate, with an extension of at least 12 monomers. Sulfate groups were essential for the interaction. These results help to understand some basic mechanisms of viral attachment.

Although envelope-receptor interactions play a pivotal role in the viral entry, lipids are also relevant. The role of acidic lipids in the viral fusion kinetics of vesicular stomatitis pseudoviruses (VSV) was assessed by single-particle imaging

on supported lipid bilayers. Phosphatidylserine (PS) and bis(monoacylglycero)phosphate (BMP) greatly enhanced the efficiency of hemifusion and enabled full fusion. The lag between lipid and content mixing defining the lifetime of a hemifusion intermediate were significantly shorter for BMP-containing compared to PS-containing bilayers. BMP is a late endosome-resident lipid and its effect on promoting VSV fusion makes it an important modulator on the outcome of viral entry through endocytosis.

Evolving from model membranes to cells, the internalization and fusion of a retrovirus through endocytosis was imaged. A pH-sensor consisting of two fused fluorescent proteins mTFP1-eYFP was incorporated in the envelope of an avian sarcoma and leucosis virus (ASLV). The pH values were quantified along the virus track and varied from 5.6 to 6.5 in early endosomes. Single-virus tracking showed that ASLV, upon internalization, are sorted into distinct pools of early endosomes with different dynamics, depending on using the two receptor isoforms, TVA800 or TVA950.

Overall, this Thesis sheds light on important host factors that influence enveloped virus entry and fusion, establishing lipid binding as a key player in the action of peptide fusion inhibitors.

Keywords

Avian sarcoma and leucosis virus
Confocal microscopy
Enveloped viruses
Fluorescence spectroscopy
Fusion inhibitors
Glycosaminoglycans
Human immunodeficiency virus
Membrane fusion
Single virus imaging
Surface plasmon resonance
Vesicular stomatitis virus
Viral entry

Sumário

O ciclo de vida dos vírus depende da sua capacidade de reconhecer as células do hospedeiro, ligar-se à sua superfície através de receptores específicos e transferir o seu conteúdo genético para o interior dessas células. Deste modo, os componentes virais apropriam-se da maquinaria intracelular de modo a replicarem-se. Para isso, os vírus envelopados têm de fundir a membrana lipídica que os envolve com a membrana da célula hospedeira. As glicoproteínas do envelope viral são responsáveis pelo reconhecimento do(s) receptor(es) celular(es) e pela mediação desta fusão. No entanto, os mecanismos pelos quais a entrada e fusão viral se processam ainda não estão totalmente compreendidos, por exemplo, ao nível das interacções envelope-receptor, dos intermediários de fusão e das vias de entrada para o interior das células.

Esta Tese explora detalhes moleculares da aderência, fusão e entrada de vírus envelopados usando sistemas modelo de membranas e receptores, além de mecanismos de acção de péptidos inibidores do vírus da imunodeficiência humana tipo 1 (HIV-1).

No primeiro capítulo, a influência das membranas no modo de acção de péptidos inibidores de fusão do HIV-1 foi estudada usando espectroscopia de fluorescência. Estes péptidos inibem as alterações conformacionais da gp41, proteína do envelope que permite a fusão da membrana do vírus com a da célula hospedeira. Deste modo, o vírus fica impedido de entrar na célula e prosseguir com o seu ciclo de vida. O enfuvirtide é o único fármaco deste tipo aprovado até agora para uso clínico. No entanto, estudámos também outros péptidos inibidores de fusão, mais potentes mas ainda experimentais: o T-1249, o sifuvirtide e o C34-colesterol, listados por ordem crescente de potência antiviral. Em estudos anteriores dos grupos de investigação onde estive inserido, foi estudada a interacção dos péptidos enfuvirtide, T-1249 e sifuvirtide com modelos de membrana (vesículas lipídicas) de composições definidas. Nós estendemos esse conhecimento para estudos com células sanguíneas humanas, eritrócitos e linfócitos, usando sondas fluorescentes de membrana sensíveis ao potencial

dipolar. Nos primeiros estudos, o T-1249 revelou-se como aquele que interage mais com as membranas das células, seguido do enfuvirtide, sendo o sifuvirtide o que apresentava menor afinidade. No entanto, estudos adicionais de potencial dipolar em vesículas confirmaram a preferência do sifuvirtide para domínios de membrana rígidos, mimetizados por modelos de membranas do lípido dipalmitoilfosfatidilcolina (DPPC). O membranotropismo de largo espectro, em vesículas e células, do T-1249 pode ser um dos factores que explicam a sua mais actividade em relação ao enfuvirtide. No caso do sifuvirtide, a alta especificidade para domínios rígidos de membrana, as chamadas jangadas lipídicas (*lipid rafts*), pode contribuir também para a sua potência, dado que são os locais onde a fusão viral é mais provável de ocorrer a nível das membranas das células.

O C34-colesterol é um dos inibidores de fusão de última geração, mais potente que os referenciados anteriormente. Trata-se de um conjugado formado pelo péptido C34 ligado a uma molécula de colesterol. Para este fármaco, foi efectuado um estudo completo em sistemas modelo de membranas e células humanas. O C34-colesterol teve uma partição substancialmente mais alta para vesículas lipídicas e células, comparado com a forma não conjugada, C34. O conjugado apresentava uma preferência para composições lipídicas ricas em colesterol e esfingomielina, típicas das jangadas lipídicas. De entre todos os péptidos estudados, o C34-colesterol apresentava a maior afinidade para as membranas das células: em linfócitos, 14 e 115 vezes maior afinidade que o T-1249 e o sifuvirtide, respectivamente. Ao longo destes estudos da acção dos péptidos a nível da membrana, podemos estabelecer uma relação entre actividade antiviral e a apetência para ligação às membranas e às jangadas lipídicas, seguindo a ordem C34-colesterol > T-1249 > enfuvirtide. Esta correlação pode ser explicada pela capacidade destes fármacos se concentrarem ao nível das jangadas lipídicas, onde a interacção vírus-receptor, e consequente fusão, é mais provável de ocorrer. A grande disponibilidade do péptido nesse local facilita a subsequente interacção do péptido com a conformação exposta da glicoproteína gp41.

Outro aspecto da entrada do HIV-1 relacionado com interacções envelope-receptor é apresentado no capítulo 2. Este processo, mediado pela glicoproteína do

envelope gp120 depende não só do receptor principal CD4 e co-receptores CCR5/CXCR4 mas também de receptores adjuvantes que melhoram a aderência do vírus às células. Neste caso, foi estudado a interacção da gp120 com glicosaminoglicanos, os componentes glicídicos dos proteoglicanos. Estes proteoglicanos, principalmente os de sulfato de heparano à superfície das células, são muito relevantes na dispersão e patogénese do vírus num contexto de infecção do organismo. Determinaram-se genericamente os requisitos estruturais dos glicosaminoglicanos que permitem a ligação à gp120, através da técnica de ressonância de plasmão de superfície ou espectroscopia de onda evanescente (SPR, Biacore). Esta ligação foi identificada como dependente do tipo de sequência do glicosaminoglicano, com preferência pela heparina e sulfato de heparano e menor ligação aos sulfatos de condroitano e dermatan. A extensão mínima de heparina necessária para a ligação foi definida como 12 monómeros, nas nossas condições. Também de relevância foi o facto dos grupos sulfatos serem essenciais para promover esta ligação, sendo que glicosaminoglicanos parcialmente ou totalmente desulfatados não apresentavam ligação. Estes estudos são relevantes para melhor compreender os mecanismos básicos de aderência do HIV às células, antes da interacção com o receptor principal, CD4.

A interacção envelope receptor tem um papel fundamental na fusão e entrada dos vírus envelopados. No entanto outros factores do hospedeiro podem modular este processo, nomeadamente os próprios lípidos das membranas celulares. No terceiro capítulo, o papel dos fosfolípidos aniónicos na cinética de fusão do vírus da estomatite vesicular (VSV, *vesicular stomatitis virus*) foi avaliado através de visualização de partículas individuais sobre bicamadas lipídicas suportadas. Foi utilizado uma câmara contendo dois canais microfluídicos sobre uma lamela de vidro, previamente tratada com dextrano. Nestes microcanais, as bicamadas lipídicas foram formadas sobre o dextrano. Após isto, os vírus aderiam e puderam ser observados ao microscópio. Estes vírus incorporavam duas sondas fluorescentes: um marcador lipofílico de membrana e uma proteína fluorescente no interior do vírus, acoplada à nucleocápside. Esta dupla marcação permitia a detecção da mistura dos lípidos do vírus e da bicamada aquando da hemifusão, e

também da libertação do conteúdo viral, confirmando a fusão. Estas observações revelaram que a presença de fosfatidilserina (PS) e de bis(monoacilglicero)fosfato (BMP) aumentam a eficiência da hemifusão e permitiam a progressão para fusão completa, ao contrário de membranas contendo apenas o lípido zwitteriónico fostatidilcolina (PC). Adicionalmente, o tempo entre o início da hemifusão e a libertação do conteúdo viral (isto é, o tempo de vida do passo intermediário de hemifusão) era significativamente mais curto para o caso do BMP, em comparação com a PS. O BMP é de facto um lípido que se encontra em abundância especificamente nos endossomas tardios e nos corpos multivesiculares das células, onde a fusão do VSV é mais provável de ocorrer. O BMP pode constituir um factor importante que permite a fusão completa do vírus quando este é internalizado.

No último capítulo, evoluímos da fusão de vírus em sistemas modelo de membranas para células e visualizámos a viagem intracelular de um retrovírus, contendo uma sonda de pH, pela via endossomal. Este sensor consistia em duas proteínas fluorescentes fundidas (mTFP1-eYFP) que foram incorporadas no envelope de um vírus da leucose e sarcoma aviário (ASLV, *avian sarcoma and leukosis virus*). Através de transferência de energia (FRET) entre estas duas proteínas foi possível quantificar o pH à medida que o endossoma onde se encontrava o vírus ia acidificando. Este retrovírus requer dois estímulos sequenciais para fundir com a membrana do endossoma: ligação ao receptor de membrana e pH acídico. O receptor utilizado por este vírus existe em duas isoformas: o TVA950 que é transmembranar e o TVA800 que é ancorado por um grupo glicosilfosfatidilinositol (GPI). Os valores de pH quantificados variavam ao longo do percurso de 6.5 a 5.6. A fusão foi observada pela libertação de uma proteína fluorescente associada à nucleocápside. As células que expressavam TVA950 distribuíam os vírus para endossomas que se moviam mais lentamente, ao contrário das células TVA 800 que eram indiferentes. Adicionalmente, as TVA950 suportavam uma fusão mais rápida que as TVA800, apesar dos valores de pH parecidos nos endossomas. Os resultados mostraram que após internalização, o ASLV é distribuído em diferentes grupos de endossomas, que se distinguem por

terem diferentes dinâmicas de mobilidade e que modulam a fusão de modo distinto.

Em suma, esta tese tratou de esclarecer alguns factores importantes que influenciam a fusão e entrada de vírus envelopados, nomeadamente ao nível lipídico e das interacções envelope-receptor. Estabelecemos ainda que a apetência de ligação às membranas dos péptidos inibidores de fusão do HIV-1 é um factor importante no seu modo de acção e deve ser tido em consideração no *design* de novos fármacos deste tipo.

Palavras-chave

Entrada viral

Espectroscopia de fluorescência

Espectroscopia de onda evanescente

Fusão membranar

Glicosaminoglicanos

Inibidores de fusão

Microscopia confocal

Microscopia de vírus individuais

Vírus da estomatite vesicular

Vírus da imunodeficiência humana

Vírus da leucose e sarcoma aviário

Vírus envelopados

Abbreviations

6-HB	6-helix bundle
ASLV	avian sarcoma and leukosis virus
BBB	blood brain barrier
BMP	bis(monoacylglycero)phosphate
BODIPY	4,4-Difluoro-4-bora-3a,4a-diaza-s-indacene
Chol.	Cholesterol
CHR	C-terminal heptad repeat
CS	chondroitin sulfate
DC-SIGN	dendritic cell-specific intercellular adhesion molecule-3-grabbing non-integrin
DHE	dehydroergosterol
Di-8-ANEPPS	4-[2-[6-(dioctylamino)-2-naphthalenyl]ethenyl]-1-(3-sulfopropyl)-pyridinium
DiD	1,1'-dioctadecyl-3,3,3',3'-tetramethylindodicarbocyanine
DNS	5-dimethylaminonaphthalene-1-sulfonyl
DPPC	dipalmitoylphosphatidylcholine
DS	dermatan sulfate
eYFP	enhanced yellow fluorescent protein
Fc	fragment crystallizable
FRET	Förster resonance energy transfer
GAG	glycosaminoglycan(s)
GalCer	galactosylceramide
GFP	green fluorescent protein

GPI	glycosylphosphatidylinositol
HAART	highly active antiretroviral therapy
HeV	Hendra virus
HIV	human immunodeficiency virus
HPIV3	human parainfluenza virus type 3
HS	heparan sulfate
HSPG	heparan sulfate proteoglycans
HSV	herpes simplex virus
ICAM-1	intercellular adhesion molecule 1
KS	keratan sulfate
LBD	lipid binding domain
LBPA	lysobisphosphatidic acid
LDL	low-density lipoprotein
LDLR	low-density lipoprotein receptor
LFA-1	lymphocyte function-associated antigen 1
mTFP1	monomeric teal fluorescente protein 1
NA	numerical aperture
NBD	7-nitro-2-1,3-benzoxadiazol-4-yl
NHR	N-terminal heptad repeat
NiV	Nipah virus
PALM	photoactivated localization microscopy
PBD	pocket binding domain
PC	phosphatidylcholine
PE	phosphatidylethanolamine

POPC	1-palmitoyl-2-oleoyl-sn-glycero-3-phosphocholine
POPS	1-palmitoyl-2-oleoyl-sn-glycero-3-phospho-L-serine
PS	phosphatidylserine
SIM	structure illumination microscopy
SIV	simian immunodeficiency virus
SLB	supported lipid bilayer
SM	sphingomyelin
STED	stimulated emission depletion
STORM	stochastic optical reconstruction microscopy
sTVA	soluble TVA
SU	surface subunit
TIRF	total internal reflection fluorescence
TM	transmembrane
VSV	vesicular stomatitis virus
YFP	yellow fluorescent protein

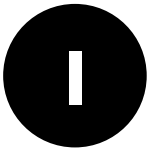

Introduction

1. General considerations on enveloped viral fusion and entry into host cells

Viruses are nano-sized infectious agents composed of structurally organized and functional biomolecules (nucleic acids, proteins and, in some cases, lipids) that require a living cell in order to replicate themselves. They are in fact obligate intracellular parasites. There is a vast diversity of viruses, with distinct sizes, shapes, structural orders and host requirements. However, the studies presented in this Thesis will comprise only enveloped viruses that infect animal cells, being focused on a particular step of their lifecycles: the attachment and entry in the host cells.

Enveloped viruses have a lipid bilayer membrane that covers and protects their capsid structures and nucleic acids. Infection of the host cells by the viruses requires their content, that is, their genome and associated viral proteins, to be delivered into the cytosol. To achieve this goal, enveloped viruses have membrane protein(s) at their surface. Envelope fusion glycoproteins have two crucial roles in the viral infection [1-4]: **i)** attach the virus to the specific host cell type it can infect, by a receptor or other cell surface molecular entities, and **ii)** promote the fusion between the host cell and virus membranes, in order to deliver the viral content to cytosol. Hence, we can say that viral envelope glycoproteins are also fusogenic proteins.

The merging of two membranes implies a very high kinetic and thermodynamic barrier, and the fusion proteins work to lower it [5]. This is done by conformation changes that occur upon certain triggers that drive the membranes together [3] (**Fig. 1**). The fusion between the two membranes most likely proceeds through an hemifusion intermediate, also designated fusion stalk [6]. This implies that the outer leaflets of the opposing membranes would merge first, allowing lipid exchange between these leaflets [6]. Only after this step, the distal leaflets merge by expansion of the fusion stalk and the pore is created, allowing content mixing between the virus and cell cytoplasm [6]. The viral membranes fusion proteins catalyze this process (**Fig. 1**).

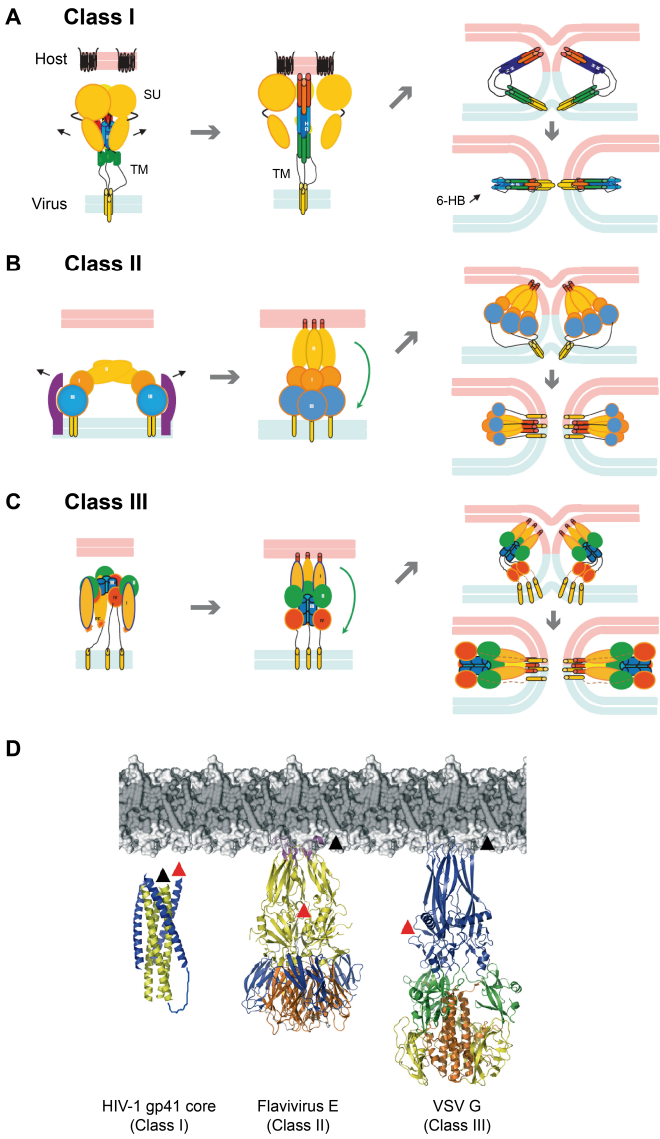

Figure 1 – Structure and mechanism of action of enveloped viruses fusion glycoproteins. (A-C) Possible models for the conformational changes of viral glycoproteins that mediate the fusion between the host cell and viral membranes. Similar steps govern the fusion process despite the structural diversity presented by class I (A), class II (B) and class III (C) fusion proteins. Interaction of the envelope glycoprotein with host cell receptor and/or contact to endosomal low pH exposes the fusion domain that is projected towards the host cell membrane, bridging the two membranes after insertion. Subsequently, the glycoprotein folds back in order to approximate the N and C-terminus and such rearrangement induces the two membranes to fuse. At the end, the two membrane anchors stay in the same continuous membrane. Adapted from [1]. (D) Post-fusion ribbon structures of representatives of the three classes of fusion glyproteins, positioned in relation to the host membrane. From left to right: HIV-1 gp41 core structure (class I); *Flavivirus* protein E (class II) and VSV protein G (class III). Black and red arrows represent the positions of the fusion peptide and the transmembrane (TM) domain, respectively. Reprinted from [4].

The diverse viral fusion proteins can be classified in three classes that are distinguished mostly by their structural motif and spatial rearrangements [7-9]. However their functional logic is similar. A transmembrane region in the C-terminus docks the protein to the viral membrane. A hydrophobic domain, the fusion peptide or loop, is present at the N-terminal region, which interacts with the host membrane in order to form a bridge between the two membranes. This fusion active conformation may be triggered by binding to the host cell receptor and/or activated by low pH, the latter when the viruses are internalized by endocytosis and fuse with the endosome membrane instead of the plasma membrane. After the binding to the host membrane, the fusion protein suffers a dramatic rearrangement in which the structure folds back or collapses, bringing the two opposing membranes together (**Fig. 1A-C**). The fusion proteins convert to a trimer of hairpins, in which the C and N-terminal parts are brought together. This fusion active trimeric structure is also a hallmark of the different viral fusion proteins [3].

Class I fusion proteins are those from, for example, Human immunodeficiency virus (HIV) and Influenza. They have two heptad repeat (HR) domains with α-helical secondary structure, between the transmembrane domain and the fusion peptide (**Fig. 1D**). They are trimers in their pre-fusion state, and their HR domains form a six-helix coiled coil bundle as a post-fusion conformation [7]. Class II fusion proteins are dimeric in their pre-fusion state and have high β-sheet content and lay low parallel to the viral surface. The fusion domains are loops at the tips of β-sheets domains and buried in the dimeric structure. They realign in trimers and project towards the host cell when primed for fusion [7] (**Fig. 1D**). Examples of viruses bearing class II fusion proteins are Dengue, Tick-borne encephalitis and Semliki forest viruses. More recently discovered, class III fusion proteins share characteristics between the two other classes. They are trimers in their pre-fusion state and have a central α-helical coiled coil; however, their fusion domains are loops in tips of β-sheet domains [10]. Vesicular stomatitis virus (VSV) and Herpes simplex virus type 1 (HSV-1) are

prime examples of this class (**Fig. 1D**). In order to summarize the characteristics that distinguish the spectrum of viral fusion proteins, refer to **Table 1**.

After fusion successfully occurs, either at the plasma membrane, or at the endosome level, the viral content is delivered and infection of the cell starts, with the virus taking over the cellular machinery to replicate itself.

Table 1 – Comparison of properties between the different classes of enveloped viruses fusion proteins. Adapted from [7].

Property	Class I	Class II	Class III
Examples	Influenza HA, Paramyxovirus F, HIV-1 gp41	Tick-borne encephalitis virus E, Semliki Forest virus E1/E2	VSV G, Herpes simplex virus type 1 gB
Requires proteolytic processing to generate fusion competent form	Yes (of fusion protein)[a]	Yes (of accessory protein)	No
Metastable on virion	Yes	Yes	No[b]
Orientation with respect to viral membrane	Perpendicular (projected as a spike)	Parallel (close to viral membrane)	Perpendicular (VSV G), HSV-1 gB not known.
Major secondary structure (of native fusion subunit)	α-helix	β-sheet	α-helix and β-sheet
Oligomeric structure of native fusion protein	Trimer	Dimer	Trimer (VSV G). HSV-1 gB not known.[c]
Location of fusion peptide in native fusion protein	Buried in subunit interface	Masked in trimer interface, at tip of extended β-strands	Exposed, at tips of extended β-strands (VSV G). HSV-1 gB not known.
Location of fusion peptide in primary sequence	At or near N-terminus	Internal	Internal (bipartite)
Activated to fusogenic form by	Low pH, receptor(s), or receptor followed by low pH	Low pH	VSV G, Low pH; HSV-1 gB, Receptors[d]
Oligomeric structure of fusion-active form (membrane-embedded prehairpin and bundles)	Trimer	Trimer	Trimer
Structure of the post-fusion form	Trimer-of-hairpins (central α-helical coiled-coil, 6HB)	Trimer-of-hairpins (mainly β-structure)	Trimer-of-hairpins (central α-helical coiled-coil and significant β-structure)

a) May not be necessary for infection.
b) VSV G is not metastable. Studies on low pH effect on HSV-1 gB also observed reversibility [11].
c) HSV-1 gB native and presumed pre-fusion structure is not yet determined.
d) In some conditions and with some strains low pH may also be required for HSV-1 gB [11-14].

2. Human Immunodeficiency Virus entry

2.1. HIV-1 envelope mediated entry and fusion

The HIV-1 envelope glycoprotein (gene designation *Env*) is constituted by two not covalently associated proteins: gp120 (surface subunit, SU) and gp41 (transmembrane subunit, TM). They form a trimer of dimers complex at the virus surface, with gp41 anchoring the complex to the viral membrane and gp120 covering it, making the outer shell [15]. gp120 is responsible for the attachment of the virus to the host cell and for the engagement with the entry receptors for HIV-1 (**Fig. 2A-B**). gp41 is the actual fusion protein that contains the fusion peptide, which anchors to the host cell membrane and drives the approximation of the membranes [16] (**Fig. 2C**). In the native state, gp120 holds gp41 in a metastable conformation, and only when gp120 binds to the receptors it allows the fusion competent conformation of gp41 to be presented [17,18].

The preferential host cells for HIV-1 are the $CD4^+$ T lymphocytes. Viruses can reach these cells either directly, or via transfer of the intact virus from one cell to another, a process called trans-infection. Some molecules or receptors can contribute to this process, such as adhesion molecules or heparan sulfate proteoglycans [19], which will be covered later in this section. These attachment helpers can maintain the virus at the cell surface before it reaches their prime receptors: CD4 [20-22] and the co-receptors CCR5 [23,24] or CXCR4 [25]. The first engagement occurs through the binding of gp120 to CD4, which triggers a conformation change that exposes a binding site to the co-receptor [26] (**Fig. 2B**). The preference for CCR5 or CXCR4 depends on the virus tropism. Double engagement leads to structural changes necessary to expose gp41 [27,28], which extends its fusion domain towards the host cell membrane. As a class I fusion protein, gp41 is composed of two helical heptad repeat domains, the C- and N-terminal heptad repeats (CHR and NHR, respectively). To catalyze membrane fusion, the two domains fold into each other, ending in a packed 6-helix bundle (6-HB) structure (**Fig. 2B**). This gp41 folding was discovered to be inhibited by

peptides derived from either CHR or NHR, competing with the binding sites for the formation of the 6-HB [29] (**Fig 2B-D**).

The viral site of fusion as long been believed to occur at the plasma membrane due to the need for receptor interaction and no requirements of low pH [33-35]. However, a recent study concluded that HIV-1 preferential route of entry is by endocytosis and fusion with endosomes [36]. Using real-time single virus imaging, the authors observed that at the plasma membrane, fusion did not progress beyond

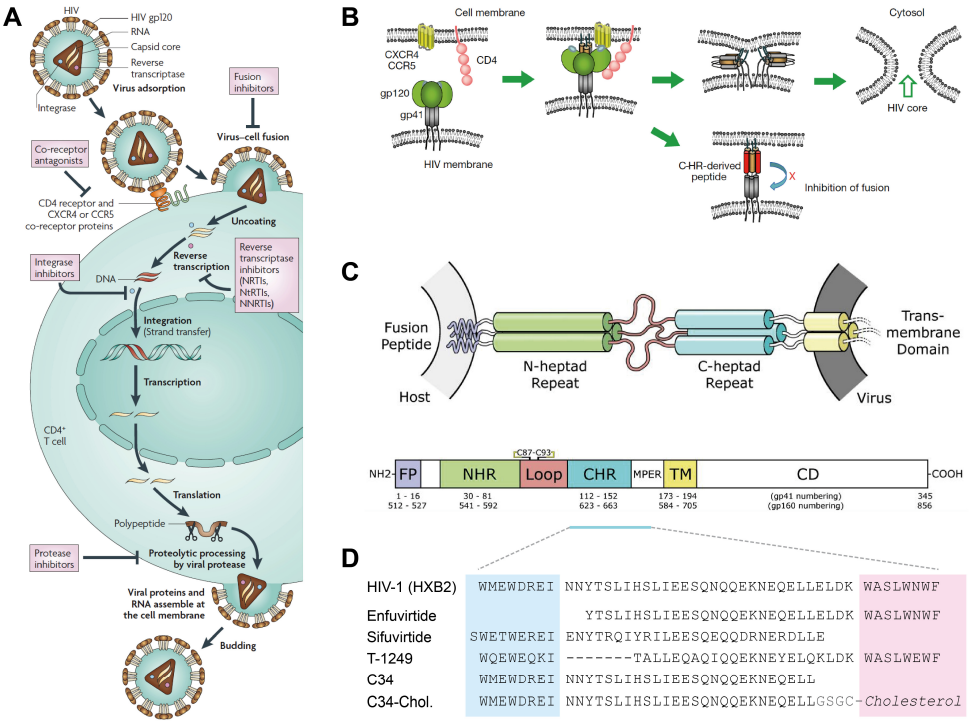

Figure 2 – HIV-1 entry and its inhibition by gp41 derived peptides. (A) HIV-1 life cycle showing the entry, intracellular replication and budding of new virions out of the host cell. The majority of the steps are now targeted by antiviral drugs (pink boxes) that impede the life cycle to progress beyond the indicated points. Reprinted from [30]. (B) Interaction of gp120 with the entry receptors CD4 and CCR5 or CXCR4. These binding steps induce conformational changes that expose gp41, which in turn will mediate membrane fusion through a hairpin or 6-helix bundle structure. Peptides derived from gp41 heptad repeat regions prevent this process and hence inhibit fusion. Adapted from [31]. (C) Schematic structure and domains of the extended conformation of gp41 when interacting with the host cell membrane, together with the numbering of amino acid residues (HXB2 strain). MPER stands for membrane-proximal region. Adapted from [32]. (D) Sequences of fusion inhibitor peptides derived from gp41 CHR domain. Colored-shading denotes the more hydrophobic and Trp-rich regions of the peptides referred in the text as pocket-binding domain (PBD, in blue) and lipid binding domain (light magenta).

lipid mixing and that complete fusion occurred at the endosomes. Moreover, this fusion process was dependent on dynamin, a GTPase that is involved in the scission of clathrin-coated pits from the plasma membrane. Further studies supported this notion by failing to force the virus to fuse at the plasma membrane [37].

2.2. HIV-1 fusion inhibitor peptides

In the early 1990s, when more knowledge became available regarding the structure and function of envelope glycoproteins of HIV-1 [15], researchers realized that small oligopeptides (up to 6-mer) derived from gp41 sequences were able to inhibit HIV-induced cell fusion [38] (**Fig. 2C-D**). Soon after, in 1992, an inhibitory 38-mer peptide derived from the NHR region was developed, named DP-107 [29]. In the following year two new potent inhibitory peptides were discovered, peptide (637-666) [39] and DP-178 [40,41], this time derived from CHR heptad repeat region (LAI strain).

While still in their infancy regarding possible clinical applications, these gp41 derived peptides came as valuable research tools to better understand the HIV-1 entry mechanisms. Two synthetic peptides, N36 and C34, from NHR and CHR, respectively, were selected by limited proteolysis of gp41, showing optimal thermodynamic properties for interactions [42]. The complex of these two peptides in solution was crystalized, which revealed a trimer of heterodimers with a complete helical structure [42]. This gave the most important insight in the understanding of the coiled coil structure of the gp41 core. Inhibitory peptides such as DP-178 could interfere with a fusion active conformation of gp41 [43]. As such, the mechanism of action of these fusion inhibitor peptides was regarded as interfering with the formation of the 6-helix bundle that brings the membrane of the virus and host cells together.

DP-178, meanwhile renamed T-20, progressed successfully into a clinical proof of concept of *in vivo* efficacy in humans [44]. With the large scale clinical trials [45,46], T-20 became the first and, until now, only HIV-1 fusion inhibitor

peptide to be approved for clinical use, as enfuvirtide (brand name Fuzeon®) [47] (**Fig. 2D**).

The success of enfuvirtide prompted for the development of new peptide drugs of this kind. Until enfuvirtide, the sequence used in the peptides was native of the reference strain HIV-1_{LAI} gp41. Rational design of sequences became crucial to this development. A second generation inhibitor developed by the same companies that led enfuvirtide to clinical trials (Roche and Trimeris) was named T-1249. Its sequenced is based not only on HIV-1 but also HIV-2 and Simian immunodeficiency virus (SIV) [48] (**Fig. 2D**). It is more potent *in vitro* than enfuvirtide and active against enfuvirtide-resistant viruses [48]. Although it did not progress in the clinical trials due to formulation problems [49], it is still tested in animal models as a component of microbicides (topical gels) to prevent HIV-1 infection [50-52].

Sifuvirtide, developed by the Chinese company Fusogen, is another second generation fusion inhibitor peptide, one of the latest drugs of this kind to complete phase IIb clinical trials, with promising results until now [53-55]. In April 2012, the Chinese State Food and Drug Administration (SFDA) approved phase III clinical trials [56]. It is a prime example of ration design, in which its sequence, based on the same C34 derived region, was modified to increase stability of the α-helix and binding to the deep pocket region of gp41 [53] (**Fig. 2D**). It is more potent than enfuvirtide in a range of primary HIV-1 isolates [53,57] and the half-life is also longer, which would require less frequent applications than enfuvirtide [53,54]. Recently, its topical gel formulation was also been proved to be safe and effective to be used as a microbicide [58].

For more information on HIV-1 fusion inhibitor peptides and how they evolved, please read the designated Book Chapter A included at the end of this Introduction section.

2.2.1. C34-cholesterol and other antiviral lipopeptides

The latest HIV-1 fusion inhibitor peptide to be studied in the context of this thesis was actually a conjugate between the C34 peptide and cholesterol, designated as C34-cholesterol [59] or L'644 [60] (**Fig. 2D**). This new compound was designed in line with previous attempts to conjugate a peptide with a lipophilic moiety, which generally improved their potency [61-63]. These lipid moieties should function as an anchor for the peptides to be displayed at the cell membrane. This way, they should be more readily available when the gp41 is exposed upon rearrangement of the HIV-1 envelope. This strategy is also sensitive to the orientation of the peptide anchoring [61]. A C-terminal derivatization of a CHR based peptides anchors the peptide in the optimal orientation for antiparallel binding to the gp41 NHR that is extended towards the host cell membrane [61].

In order to optimize such lipid anchor for inhibitory peptides, Ingallinella *et al.* [59] chose the cholesterol moiety to attach to the C34 peptide. The main reason was the importance of lipid rafts in the HIV-1 entry [64,65]. These cholesterol and sphingomyelin enriched membrane microdomains also cluster receptors at the cell surface and influence several membrane-related processes [66]. The reported evidences that lipid rafts are a preferential site of HIV-1 docking and entry [65,67,68] suggest that targeting fusion inhibitors to these sites could enhance their potency. As previously studied, T-1249 naturally adsorbs to cholesterol rich membranes, which can be one of the factors contributing for its higher activity when compared to enfuvirtide or C34 [69].

C-terminal derivatization of C34 indeed produces a very potent fusion inhibitor, with two or more orders of magnitude more potent than C34, enfuvirtide and T-1249, across multiple HIV-1 isolates [59]. An N-terminal derivatization had lower potency and lower degree of binding to the gp41 derived coiled coil 5-helix. Moreover, the use of palmitic acid instead of cholesterol rendered the conjugate with even lower activity compared to the native C34. Importantly, C34-cholesterol had an extended circulatory half-life when tested in mice, being detectable up to 24 h in the plasma when compared to 6 h of C34. This

is also a consequence of the fact that C34-cholesterol is much more resistant to the digestion by proteinase K, when compared with C34 and enfuvirtide [70].

The efficacy of C34-cholesterol as a microbicide was also evaluated against a panel of other fusion inhibitors, including C34, enfuvirtide and T-1249 [60]. This constituted a major study for preclinical evaluation of these inhibitors, using human mucosal tissue explants that included colorectal, penile and cervical tissues. C34-cholesterol was generally the most active fusion inhibitor across all tissues. Most importantly, protection provided by C34-cholesterol to the tissues was resistant to washing after pre-incubation with the inhibitors. T-1249 also presented some resistant to washing and, together with C34-cholesterol, were the only ones to have meaningful activity in penile explants [60]. This characteristic of the conjugate to offer a sustainable protection at the mucosal tissue level makes C34-cholesterol a good candidate to be used as a topical gel formulation to prevent HIV-1 infections during intercourse. This new development comes at a right time when several microbicide formulations, mainly based in polyanonic polymers, failed to have success in clinical trials [71]. Only recently the CAPRISA 004 trial showed efficacy of a 1% vaginal gel formulation of tenofovir, a reverse transcriptase inhibitor, with 39% reduction of HIV-1 infections overall. However, a year later a large scale trial for women at risk (VOICE) was cancelled prematurely due to lack of demonstrated efficacy [72].

The cholesterol tagging strategy of fusion inhibitor peptides was more recently applied to other viruses. A sequence of the C-terminal heptad repeat of the F protein of Human parainfluenza virus type 3 (HPIV3) gained 100-fold potency when C-terminally tagged with cholesterol to inhibit *in vitro* viral infection [73]. Moreover it could also inhibit two other paramyxovirus, Nipah virus (NiV) and Hendra virus (HeV), which cause lethal central nervous diseases [73]. An improved paramyxovirus peptide inhibitor was sequence optimized and cholesterol tagged, yielding potent anti-HPIV3 and NiV activity [74]. This tagged peptide was also efficacious against NiV encephalitis in an animal model, demonstrating the capability of the conjugate to cross the blood brain barrier [74].

Influenza virus was also susceptible to cholesterol conjugates of hemagglutinin derived inhibitory peptides [43]. This virus is well known to undergo low pH dependent fusion at the endosomes, demonstrating that lipophilic fusion inhibitors can be internalized with the virus in order to achieve intracellular inhibition.

New inventive ways to improve peptide fusion inhibitors continue to thrive. One of the latest efforts in the cholesterol conjugated family of inhibitors consisting of attaching two fusion inhibitor peptides to a single cholesterol moiety [75]. This strategy improved paramyxovirus inhibitors although for HIV the potency was equivalent to the monomer.

In line with the diversification of lipophilic moieties attached to peptide fusion inhibitors, the latest strategy applied by Ashkenazi *et al.* [76] consisted in using a sphinganine moiety (dihydrosphingosine) to tag these peptides. An HIV-1 gp41 NHR derived peptide N17 was endowed with antiviral activity only in its sphingopeptide form. Conjugation with palmitic acid, cholesterol and tocopherol had no effect in providing N17 antiviral activity. These results point to the fact that different peptides may require distinct lipophilic moieties for optimal potency.

2.2.2. Interaction of HIV-1 fusion inhibitor peptides with membranes

The function of gp41 is intimately tied with its membrane environment. As such, investigation of membrane interactions from gp41 derived peptides helped shed light on its function [77]. The first studies regarded the fusion peptide and how it interacts, destabilized and inserts in planar membranes and lipid vesicles [78,79]. However, the HR domain derived peptides that can inhibit the 6-HB formation and hamper fusion were also probed for direct membrane interactions in order to understand the role of the membrane in their mode of action. We will focus on CHR derived fusion inhibitor peptides, since these are the ones studied in this Thesis.

Enfuvirtide (DP-178) and C34 were first compared in their ability to bind with phosphatidylcholine (PC):cholesterol and PC:phosphatidylserine (PS):cholesterol using a Förster resonance energy transfer (FRET) based assay

between the Trp residues of the peptides and 5-dimethylaminonaphthalene-1-sulfonyl (DNS)-labeled lipid in the vesicles [80]. Energy transfer was detected in the case of enfuvirtide, contrary to C34 that showed no binding. However in small unilamellar vesicles (SUV) of PC:PS (1:1), 7-nitro-2-1,3-benzoxadiazol-4-yl (NBD)-labeled peptides interact with the membranes, with enfuvirtide having 10-fold higher surface partition coefficient when compared to C34. Moreover, enfuvirtide also formed oligomers at the membrane level. This was the first indication that membranes affect these peptides behavior and that they could influence their action. Enfuvirtide binding to PC:sphingomyelin (SM):phosphatidylethanolamine (PE):cholesterol (4.5:4.5:1:1) was also detected via surface plasmon resonance [61].

However a more complete study on enfuvirtide [81] and T-1249 [69] interactions with lipid vesicles was conducted by Veiga *et al.*, whom used the Trp fluorescence of the peptide as reporter. Enfuvirtide and T-1249 partitioned to fluid phase zwitterionic lipid vesicles containing POPC, with partition constant of $(1.6 \pm 0.1) \times 10^3$ and $(5.1 \pm 0.7) \times 10^3$, respectively. Enrichment in cholesterol significantly decreased partition for both peptides. However, a more detailed study for T-1249 using FRET (dehydroergosterol (DHE) acceptor of Trp fluorescence in the membrane) revealed that T-1249 significantly adsorbed in to cholesterol-rich POPC lipid vesicles [69], contrary to enfuvirtide. The peptides location was also determined to be in a shallow position, at the level of the phospholipids head-groups [69,81].

A study using isothermal titration calorimetry also showed interaction of enfuvirtide with POPC vesicles, while the C36 peptide showed no binding (similar to C34) [82]. However, mutation of the tryptophan rich region of enfuvirtide at its C-terminus (WNWF to ANAA) completely abrogated the ability to bind membranes. This domain is then essential for lipid binding, and can be designated as lipid binding domain (LBD). The sequence of C34 does not have this domain, having instead a WMEW motif in the N-terminus, which is important to bind to an hydrophobic pocket in the NHR domain, competing for the 6-HB formation [42]. A subsequent calorimetric study analyzed the function of these domains

using a designed heptad repeat sequence (EEYTKKI) unrelated to gp41 [83]. A peptide containing only the pocket binding domain (PBD), as the case of C34 and sifuvirtide, was designated PBD-4HR. The peptide with only the lipid binding domain was designated 4HR-LBD, equivalent to enfuvirtide, and a peptide containing the two domains PBD-4HR-LBD would be equivalent to T-1249. Membrane binding for POPC vesicles was residual for PBD-4HR, while binding constants of 6.80×10^4 and 1.27×10^4 were obtained for 4HR-LBD and PBD-4HR-LBD, respectively [83]. This was in agreement with the also previously determined higher partition of T-1249 for POPC, relative to enfuvirtide and C34. As for T-1249, PBD-4HR-LBD also had the highest antiviral activity among the three studied peptides [83].

Sifuvirtide was also studied in detail regarding its behavior in model membranes. Contrary to enfuvirtide and T-1249, sifuvirtide did not partition to POPC vesicles, instead preferring rigid, gel-like, DPPC membranes [84]. It localizes in a very shallow position, indicating more adsorption to these lipids rather than insertion. Its selectivity for rigid domains is limited to phosphatidylcholines, instead of sphingomyelins, and is also highly dependent on NaCl concentration [85]. Sifuvirtide is significantly more potent than enfuvirtide [53], and these studies shed light on the importance of targeting fusion inhibitors to rigid membrane domains, or lipid rafts, where receptors are clustered and viral entry and fusion are more likely to occur.

2.3. Role of HSPG in HIV entry and pathogenesis

In order for HIV to reach its prime receptors, is has been well established that other alternative receptor entities at the cell surface help the virus to approach and attach to the host cells, before it engages with CD4 [19]. These receptors consist of adhesion molecules, lectins, heparan sulfate proteoglycans (HSPG) and the glycolipid galactosylceramide (GalCer) [19]. For example, HIV can naturally incorporate the intercellular adhesion molecule 1 (ICAM-1) that increases infectivity for lymphocyte function-associated antigen 1 (LFA-1) bearing T $CD4^+$ lymphocytes [86,87]. Also, dendritic cell-specific intercellular adhesion molecule-3-grabbing non-integrin (DC-SIGN), is able to bind and retain HIV virus and

facilitates trans-infection to $CD4^+$ cells [88]. Importantly, HSPG also have a role similar to DC-SIGN; however, due to its ubiquitous presence in the body they end up having a major effect on spreading of the viral infection, contributing to the pathogenesis [89].

HSPG are membrane or secreted proteins that have glycosaminoglycans (GAG) chains attached, mainly heparan sulfate and chondroitin sulfate. These GAG are linear polysaccharides consisting of repeating dissacharide units of hexosamine and uronic acid, which are often sulfated [90]. Hence, GAG differ on their repeating dissacharide unit, and glycosidic linkage, to produce distinct sequences (**Fig. 3A**).

Cell surface proteoglycans, the ones that are membrane bound, exist in two forms: syndecans and glypicans (**Fig. 3B**). Syndecans are transmembrane molecules and have an extended ectodomain, with the heparan sulfate (HS) chains mainly attached in a distal position from the membrane [91]. Glypicans are glycosylphosphatidylinositol (GPI)-anchored to the plasma membrane and they form a globular ectodomain structure by disulfide links. Contrary to syndecans, glypicans have the HS chains attached in to the region proximal to the membrane [91] (**Fig. 3B**). However, only syndecans have been shown to be implicated in HIV pathogenesis [89].

In vitro studies of glycosaminoglycans-protein interactions usually rely on the soluble heparin as a GAG model. Heparin and HS have been shown to bind *in vitro* to HIV-1 gp120 [92,93]. The binding sites of gp120 to heparin were mapped and essential residues for this interaction were identified, included in the V2 and V3 loops, in the C-terminal domain and in the CD4-induced co-receptor binding site [94,95]. Also, the V3 loop was found to be essential to bind to the different types of syndecans [96]. Residues implicated in these interactions are often arginines and lysines, basic aminoacids that can interact electrostatically with negatively charged heparin.

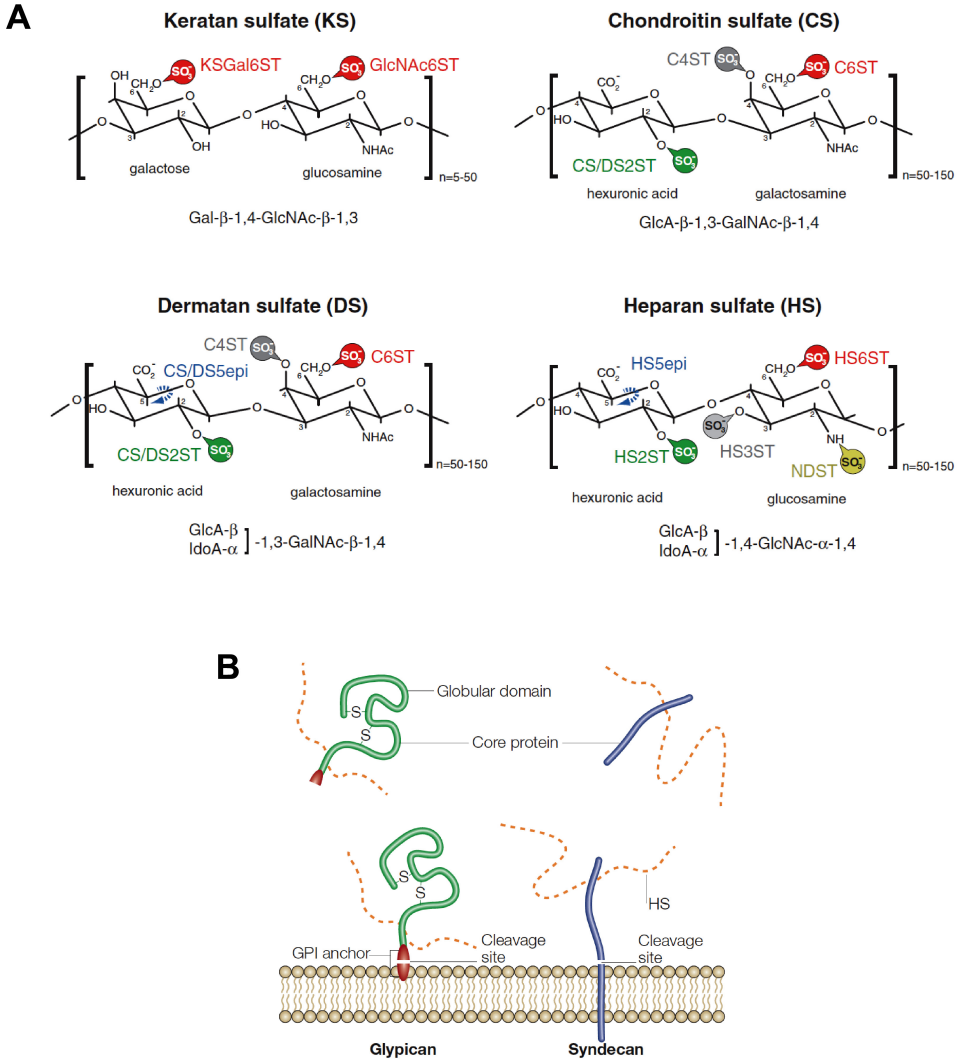

Figure 3 – Structures of glycosaminoglycans and proteoglycans. (A) Chemical structures of the typical disaccharide units that compose the different glycosaminoglycans. Colored text refers to enzymes that catalyze modifications to these chains, mainly sulfations (in balloons) but also epimerizations in the case of dermatan sulfate and heparan sulfate. Abbreviations: C4ST, chondroitin sulfate-4O-sulfotransferase; C6ST, chondroitin sulfate-6O-sulfotransferase; CS/DS2ST, chondroitin sulfate/dermatan sulfate-2O-sulfotransferase; CS/DS5epi, chondroitin sulfate/dermatan sulfate-C5-epimerase; Gal, galactose; GalNAc, N-acetyl-galactosamine; GlcA, glucuronic acid; GlcNAc, N-acetyl-glucosamine; GlcNAc6ST, N-acetyl-glucosamine-6O-sulfotransferase; HS2ST, heparan sulfate-2O-sulfotransferase; HS3ST, heparan sulfate-3O-sulfotransferase; HS6ST, heparan sulfate-6O-sulfotransferase; IdoA, iduronic acid; KSGal6ST, keratan sulfate-galactose-6O-sulfotransferase; NDST: N-deacetylase-N-sulfotransferase. Reprinted from [97]. (B) Schematic representation of the cell surface heparan sulfates syndecan (right) and glypican (left). Glypicans associate to the membrane via GPI anchor and its ectodomain is globular due to disulfide bonds. Syndecans have a transmembrane domain and an extended ectodomain. Heparan sulfate chains attach to syndecans in a distal position from the membrane, contrary to glypicans that have the chains proximal to the membrane. Reprinted from [98].

Regarding the influence of proteoglycans in in the viral infection, it was first observed that cells treated with heparitinase [99] or knocked out for GAG production [100] have much lower levels of viral attachment and infection than their *wt* counterparts. In fact, in the case of macrophages, syndecans are crucial as attachment receptors for HIV-1, as they compensate for the lower levels of CD4 of these cells, relative to T $CD4^+$ cells [101]. Syndecan-3 was also identified as a specific attachment receptor in the case of dendritic cells [102]. Importantly, the blood-brain-barrier (BBB) crossing by HIV-1 was shown to be mediated, at least in part, by proteoglycans present in the brain microvascular endothelial cells [103,104].

Proteoglycans are ubiquitously present, especially in the epithelial, endothelial and dendritic cells, as well as in macrophages. All these cell types and formed tissues (mucosas, endothelium) can capture HIV virions, protecting them and facilitating trans-infections via syndecans to the T lymphocytes in a very efficient way [8]. The endothelium can function as a major *in trans* reservoir, as it can keep virions bound to syndecans in an infectious state [89].

Strategies have already been devised to block HIV entry by taking advantage of this gp120-proteglycans interaction. A syndecan-Fc (fragment crystallizable) hybrid molecule showed potent and broad-range antiviral activity and prevented trans-infection [105]. It was effective when applied 2 h before infection, when diluted in genital fluids and at low pH, making it a promising candidate to use as a microbicide [105]. A synthetic CD4-mimetic peptide linked to an HS chain was designed taking into account that HS binds also to the CD4 induced co-receptor binding site [106]. Another version of this compound was also made with the HS chain substituted with a peptidomimetic [107]. These hybrid molecules had nanomolar antiviral activity against both CCR5- and CXCR4-tropic HIV-1 strains, making it another promising entry inhibitor [106,107].

3. Avian Sarcoma and Leukosis Virus entry

The Avian Sarcoma and Leukosis Virus (ASLV) is an alpharetrovirus that, contrary to lentiviruses (such as HIV), has a simpler genome with the *Gag-Pol* and *Env* genes, but without the accessory ones (*Vif*, *Vpr*, *Tat*, *Rev*, *Vpu* and *Nef*) [108]. These ones allow lentiviruses to replicate on non-dividing cells [108]. Its envelope fusion protein is also class I, as usual in retroviruses, and forms a 6-HB as a post-fusion conformation. There are 10 viral subgroups classified, named A-J [108], however we will focus on ASLV-A. The receptor for this virus was discovered to be TVA, a membrane protein related to the low-density lipoprotein (LDL) receptor [109,110]. Indeed, soluble forms of TVA (sTVA) pre-incubated with the virus could inhibit its infection [111,112]. Moreover, the soluble receptor was also able to induce infection in cells that do not express the cognate receptor [113], suggesting that sTVA can induce the conformational changes necessary for priming the envelope for fusion. However, in a rare case among viruses, ASLV requires not only the interaction with the receptor but also a second low pH trigger to fully activate the fusion protein [114]. ASLV two-step entry proceeds first with the interaction with the cognate receptor, which induces conformational changes that exposes the fusion peptide, still at neutral pH, and mediates its internalization [115]. Acidification of the endosomal compartment leads to the completion of the fusion reaction with the delivery of the viral contents to the cytoplasm [115,116]. As a class I fusion protein, this entry process is also inhibited by ASLV CHR-derived peptides that inhibit the formation of the 6-HB post fusion structure [117,118]. Another unusual characteristic of the viral envelope is the stability of the receptor-primed intermediate that can remain in this state for long periods of time compared to other pH-dependent viruses [114,119].

The TVA receptor exists in two different isoforms that originate from alternative splicing: TVA950 is a transmembrane receptor with a single membrane spanning domain, while TVA800 is a GPI-anchored protein. This has implication on the entry pathways of ASLV [119]. TVA800 was shown to be associated with lipid rafts (defined as detergent-resistant membranes), contrary to TVA950 [119]. Receptor usage influenced the rate at which viruses were uptaken and

internalization via TVA800 rendered the viruses more resistant to ammonium chloride arrest, a feature dependent on lipid raft association [119]. More robust imaging techniques with fluorescent labeled viruses and pH sensitive fluorophores allowed a more detailed dissection on the entry routes of ASLV-A [120,121]. Internalization of viruses was faster with TVA950; however, fusion of internalized viruses was delayed compared with TVA800 expressing cells. TVA950 supported more robust pores and higher efficiencies of infection [120]. These two receptors also likely redirect the viruses to distinct sub-cellular compartments. Viruses internalized via TVA950 are more likely to fuse at intermediate endosomes, while TVA800 internalized ones are likely to fuse in intraluminal vesicles trapped in multivesicular bodies, with the liberation of the core to the cytoplasm dependent on a second back-fusion process [121]. Recently, a cryo-EM study allowed the direct visualization of ASLV attached to liposomes in its sTVA-bound and fusion competent state [122].

4. Vesicular Stomatitis Virus entry

Vesicular stomatitis virus belongs to the *Rhabdoviridae* family of enveloped viruses with single stranded negative-sense RNA genome [123]. These viruses have also a distinct bullet shape, with a flat base and a round tip. The envelope glycoprotein is designated as G protein, a class III fusion protein forming trimers at the viral surface [124]. It enters and infects cells via endocytosis and is dependent on the low pH to trigger fusion (**Fig. 4**). The virus should attach or enter via a receptor that until very recently was not identified. Phosphatidylserine (PS) has been shown to promote VSV fusion and entry into cells and with model membranes [125-128], but it is unlikely to be the primary receptor for this virus [129]. The chaperon protein gp96 was identified as essential for VSV infection, as cells without this protein were unable to bind VSV [130]. Due to its location at the endoplasmic reticulum, gp96 is likely to act as a chaperone for a putative membrane receptor for VSV, allowing its correct folding [130]. Very recently, Finkelshtein *et al.* seem to have identified the low-density lipoprotein receptor (LDLR) and its family members as the cellular receptors for VSV [131]. To support

this claim, they presented experiments such as inhibition of VSV binding and infectivity with a soluble form of LDLR, affinity measurements of the G protein with LDLR and competition of LDL and VSV for the same binding site, among other evidences.

Rhabdovirus G protein also has a unique property among low pH dependent fusion proteins: its conformational changes due to low pH are reversible when returning to neutral pH [132]. Other pH sensitive viruses when exposed to low pH in the absence of a target membrane undergo irreversible inactivation [133]. This

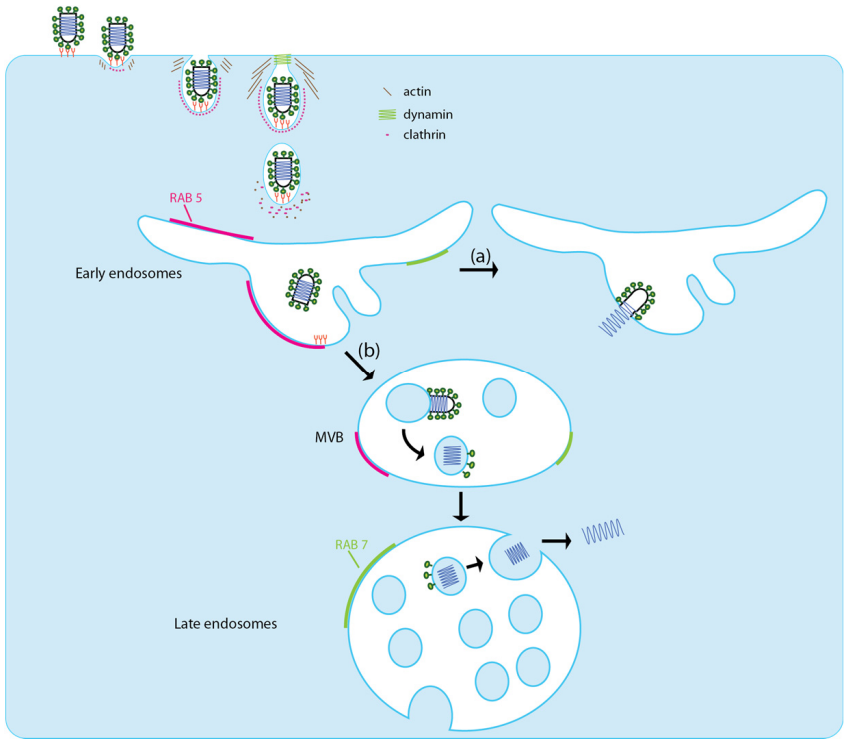

Figure 4 – Entry pathways of vesicular stomatitis virus (VSV) in the host cell. VSV should bind to the cell membrane via one or more putative receptors or attachment molecules, being internalized via partially coated clathrin vesicles. Upon arrival to early endosomes the virus can fuse in these compartments upon sufficient acidification of the lumen (a). However, should the virus progress to multivesicular bodies and late endosomes, the probability of fusion with internal vesicle is higher, releasing the capsid inside them (b). This would require a second fusion event (back-fusion) to occur in late endosomes in order to release the capsid to the cytosol. Rab5 (magenta) and Rab7 (green) are small GTPases that are present in early and late endosomes, respectively. Reprinted from [123].

reversibility allows the protein to pass through the acidic compartments of the Golgi apparatus and recover its native conformation when incorporated in the virions [134]. Other viruses require chaperones to protect these fusion proteins from undergoing irreversible changes in the Golgi.

Internalization of the virus is dependent on clathrin and dynamin-2, a GTPase involved in the release of nascent vesicles during endocytosis [135] and viruses were indeed observed inside coated vesicles [136]. Fusion was previously observed to occur within minutes in early endosomes [135], and VSV infection was dependent on Rab5 (maturation factor for early endosomes) but not Rab7 (maturation factor for late endosomes) [137]. However a recent study proposed that VSV can also fuse with intralumenal vesicles, inside multivesicular bodies [138] (**Fig. 4**). Such pathway requires a second back-fusion event with the limiting membrane of late endosomes in order to release the capsid to the cytosol. This step is dependent on the late endosome-specific lipid bis(monoacylglycero)phosphate (BMP) [138], also referred to as lysobisphosphatidic acid (LBPA) [139]. Tsg101, which is part of the endosomal sorting complexes required for transport (ESCRT), and its partner Alix were also demonstrated to regulate this late fusion step of viral capsid release [140]. Moreover, *in vitro* experiments with liposomes enriched with BMP also favored lipid mixing with VSV [141]. BMP was also shown to function as a co-factor in the fusion of dengue virus with late endosomes [142]. These examples of VSV and Dengue virus show that specific lipids can influence the entry and fusion process of enveloped viruses.

5. Methodological and technical approaches

5.1. Fluorescence-based evaluations of peptide-membrane interactions

In this Thesis we made use of fluorescence spectroscopy in order to measure interactions between peptide and membranes, either of cells or lipid vesicles. These methods were extensively reviewed in the Review Articles A and B at the end of this Introduction section.

5.2. Surface plasmon resonance

Surface plasmon resonance (SPR) is a technique that provides label-free, real-time detection of biomolecular interactions [143]. It is used to characterize the binding equilibrium and kinetics of a ligand immobilized on a thin gold surface with a binding partner in solution (analyte) [143]. This is an optical technique based on the evanescent wave phenomenon that arises from a surface of a metallic film when incident light is totally reflected, which happens above a critical angle [144] (**Fig. 5A**). The resonance is a result of energy and momentum being transformed from incident photons to surface plasmons. It is sensitive to the refractive index of the medium on the opposite side of the film. The changes in mass occurring at the surface, due to molecular interactions and increased local concentration of the analyte, lead to changes in the refractive index within the evanescent wave penetration range. The angle of incidence required associated with the SPR phenomenon is altered due to this refractive index change, and is this angle alteration that is measured as the response signal [144] (**Fig. 5A**).

SPR instruments for biomolecular interactions (in the case of this Thesis, Biacore, from GE Healthcare) usually rely on microfluidic channels to deliver small amounts of sample to the flow cells, which are in contact with the gold film surface of the chip [145] (**Fig. 5A**). This way, solution exchange and washing is easier, allowing the delivery of the ligand for immobilization, and the binding partners of interest. Usually, two or more flow cells are available for simultaneous measurements, with one serving as control.

The immobilization of a biomolecule on the chip surface can be done either covalently or non-covalently. Covalent attachment is usually done with a carboxyl presenting surfaces, than can react with proteins by different chemical strategies (**Fig. 5C**). Non-covalent attachment explore strategies such as the high-affinity of streptatividin-biotin pair, the 6-His sequence chelation of Ni^{2+} or the hydrophobic interactions for the case of lipids [146] (**Fig. 5D**).

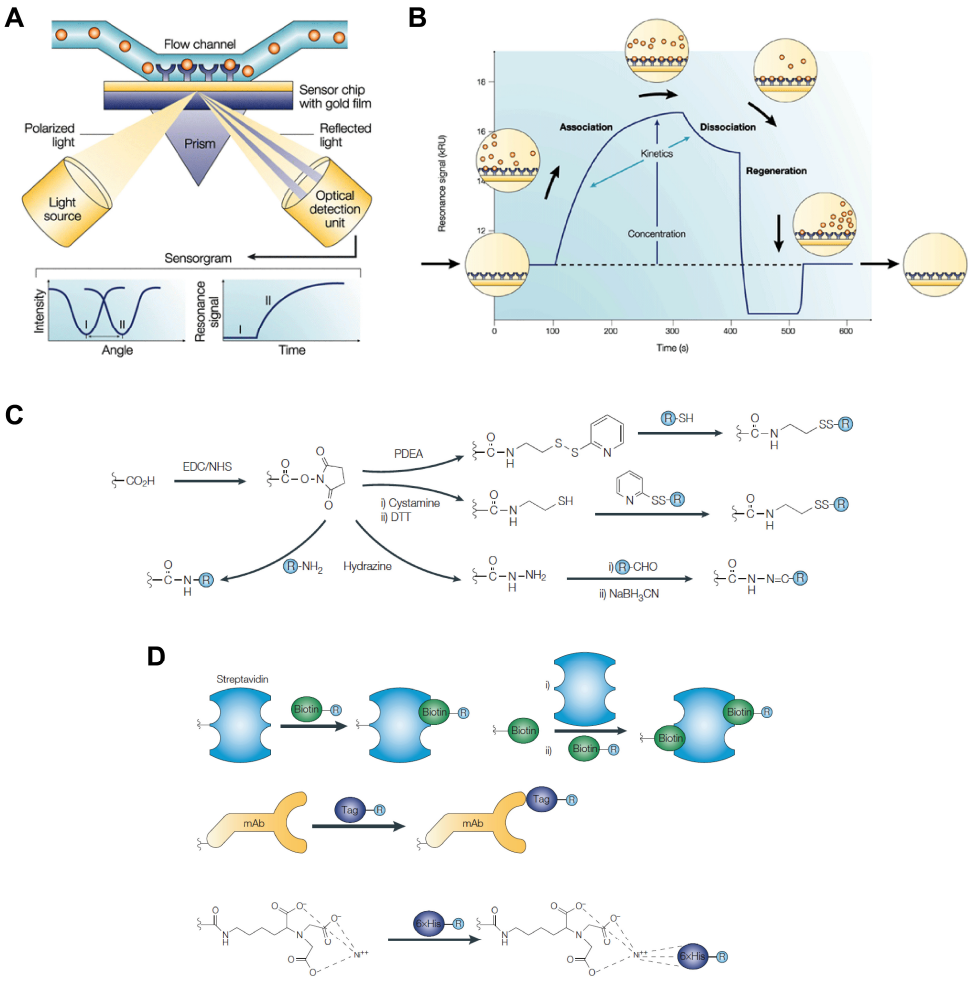

Figure 5 – Principles of surface plasmon resonance binding experiments. (A) Detection of intermolecular binding events in the flow channel of an SPR equipment (*e.g.*, Biacore), in which the changes of mass due to binding have an effect on the reflected angle of the light associated to the surface plasmon effect. (B) Typical sensorgram obtained for an SPR binding experiment. The resonance signal increases as the surface mass also increases (association). After ending the infection of the analyte, the buffer flow induces the dissociation of the molecules, decreasing the signal. Finally, regeneration procedures can return the signal to the baseline, with the surface ready for another use. (C) Chemical conjugation possibilities to covalently immobilize proteins to a carboxymethyl matrix chip via a reactive N-hydroxysuccinimide (NHS) ester. This can readily react with an amino group to form an amide linkage. Hydrazine allows coupling with aldehyde groups. Coupling via disulfide bonds can also be achieved using pyridinyldithioethanamine (PDEA) and cystamine routes. (D) Non-covalent methods to immobilize biomolecules in SPR chips: streptavidin-presenting surfaces can bind to biotin derivatized molecules (top); monoclonal antibodies immobilized through amine coupling can specifically bind proteins or other biomolecules with the respective epitopes (middle); nitrilotriacetic acid (NTA) bearing chips immobilize proteins engineered to display a 6-His sequence tag (bottom). Adapted from [146].

The need for immobilizing one of the binding partners, which can potentially hide binding sites, remains the main disadvantage of this technique. However, that can be circumvented in many cases by putting a tag (6-His or biotin) in a specific site, or using antibodies against a specific epitope as an immobilization intermediate, in order to control the immobilization orientation.

After a successful immobilization, the surface is ready to be tested with the desired analyte(s). When the analyte binds to the ligands at the surface, it induces a response signal that is recorded along the time, constituting the sensorgram [144] (**Fig. 5B**). During the binding phase, or association phase, the response increases until the binding sites are saturated and equilibrium is reached. When the analyte injection is stopped and the flow substituted by the running buffer, the analyte dissociation causes the response to decrease. In this way, association and dissociation kinetics, as well as affinity constants can be extracted from these time-course measurements data [144]. After each run, the surface is usually regenerated, typically using a solution with modifications in pH, salts or other compounds that accelerated the dissociation of the analyte and brings the response signal back to the original baseline. This allows the chip to be reused for several individual runs until it wears off.

For binding reactions that occur at 1:1 stoichiometry, we can represent as the following chemical equation:

$$A + B \underset{k_d}{\overset{k_a}{\rightleftharpoons}} AB \tag{1}$$

The rate equations that characterize the association and dissociation kinetics, respectively, are [147]:

$$\frac{d[AB]}{dt} = k_a \cdot [A] \cdot [B] \tag{2}$$

$$-\frac{d[AB]}{dt} = k_d \cdot [AB] \tag{3}$$

The net equation is:

$$\frac{d[\mathrm{AB}]}{dt} = k_{\mathrm{a}} \cdot [\mathrm{A}] \cdot [\mathrm{B}] - k_{\mathrm{d}} \cdot [\mathrm{AB}] \tag{4}$$

When the reaction reaches equilibrium, the rate of association is the same as the rate of dissociation:

$$k_{\mathrm{a}} \cdot [\mathrm{A}] \cdot [\mathrm{B}] = k_{\mathrm{d}} \cdot [\mathrm{AB}] \tag{5}$$

The equilibrium constants are defined by:

Equilibrium association constant: $$K_{\mathrm{A}} = \frac{k_{\mathrm{a}}}{k_{\mathrm{d}}} = \frac{[\mathrm{AB}]}{[\mathrm{A}] \cdot [\mathrm{B}]} \tag{6}$$

Equilibrium dissociation constant: $$K_{\mathrm{D}} = \frac{k_{\mathrm{d}}}{k_{\mathrm{a}}} = \frac{[\mathrm{A}] \cdot [\mathrm{B}]}{[\mathrm{AB}]} \tag{7}$$

All these kinetic and affinity constants can be quantified by this technique.

Surface plasmon resonance based sensors can be very versatile, characterizing the binding over a range of biomolecules. It has been possible for a while to also run relatively high throughput screenings in which this technique is valuable to identify high affinity drugs or antibodies to a specific target [148,149]. Technological advances should drive a more applied use of these sensors in medicine, where they could serve as rapid and efficient diagnostic tools in laboratories [150].

5.3. Imaging viral entry and fusion in model membranes and cells

Virus life cycles are a complex sequence of steps that are challenging to study and follow. Viruses intimately interact with the cellular structures of their host cells to carry out replication. In the past two decades, microscopy techniques have advanced in order to allow the discrimination of single virus interactions with cells and dissect the pathways of the infection process [151]. In practical terms, viral

and cellular structures must be fluorescently labeled and the microscope powerful enough for the detection of single viruses or viral components in real time. As such, two main technical aspects are crucial: the fluorescent labeling, and the imaging instrument and configuration.

Virus labeling can be done either with chemical probes or genetically engineered fluorescent proteins. Covalent labeling with fluorescent chemical probes is a very versatile method, as an array of amine reactive dyes (fluoresceins, rhodamines, Alexas and BODIPY, among others) can be attached to viral surface proteins. Viral membranes can be labeled with lipophilic dyes that incorporate in the bilayer leaflets. Nucleic acids intercalating dyes such as acridine orange or neutral red [152] can label viral genomes, although only recently the use of Syto82 allowed for live replication imaging [153]. Indirect labeling when virus components are already inside the cell is also possible with the use of biarsenical dyes [154] that bind tetracystein motifs engineered in the proteins of interest [155,156].

The advent of the genetically encoded fluorescent proteins, starting with the development of the green fluorescent protein (GFP) variants [157,158], greatly expanded the capabilities of imaging specific proteins in biological systems. Since then, an array of fluorescent proteins of all colors is available [159,160]. These fluorescent proteins can be fused to structural proteins of the virus (usually matrix or capsid proteins), with more than one copy per virus, in order to improve detection by the microscope.

Microscopy equipment and configuration is the other important factor in these viral imaging experiments. The objective is to reduce the background as much as possible and detect the labeled viral particles, which are nanometric in scale. Conventional widefield epifluorescence microscopy collects light emitted by the entire depth of the sample [161]. This is usually not suited for viruses due to higher background and poor distinction of detailed structures. However, applying deconvolution techniques greatly improves image quality by computational removal of out of focus light, while still retaining the advantage of fast acquisition of widefield [162]. Confocal systems remove this out of focus light through a

pinhole before the light reaches the detector, producing sharper images [161]. In these systems, with the use of laser excitation lines that allow higher flexibility on multicolor imaging, defined specific regions for illumination (useful for photobleaching experiments) and increased technological advances in detectors over time, confocal is now a widespread method in fluorescence imaging for biological sciences. If one wants to visualize events at the membrane level, or structures close to the coverglass, TIRF (total internal reflection fluorescence) microscopy allows for sensitive and reduced background detection [163]. This is done by illuminating the glass at a critical angle for total internal reflection, producing an envanescent wave of limited depth that will excite the nearby fluorophores (similar to what was explained earlier in this introduction for SPR instrumentation).

The resolution limit of these optical microscopies is around 200 nm, which is derived from the inherent diffraction effect of light, described by the Abbe equation [164,165]:

$$d = \frac{\lambda}{2(n \cdot \sin\theta)} \tag{8}$$

in which d is the resolution, λ the light wavelength, n the refractive index and θ the converging angle of the light (n sin θ is also defined as the numerical aperture, NA).

Most viruses sizes are below that value, which limits the way these viral structures can be distinguished when imaged. In the recent years, sub-diffraction imaging technologies have been developed that brought the resolution down to 10 nm, in what is called super-resolution microscopies [165,166]. This encompasses techniques such as SIM (structure illumination microscopy), STED (stimulated emission depletion), PALM (photoactivated localization microscopy) and STORM (stochastic optical reconstruction microscopy) [166]. These methods still have to mature in order to provide fast, real time imaging, although significant progress has already been made [167].

Early studies with labeled viruses provided the first glimpses on how they enter and traffic inside the cell, mainly in the endosomes. Semliki forest virus and reovirus serotype 1, chemically labeled with rhodamine or fluorescein, were among the first viruses to be used in this kind of approach [168,169]. Application of GFP in virus labeling was first done with herpes simplex type 1 by fusing it either with capsid or matrix protein components [170,171], enabling to follow the structural components of the virus after fusion. Viral trafficking studies also helped to uncover novel cell biology concepts related, for example, with microtubules dynamics via Texas red labeled adenovirus [172] or a new, caveolae and actin dependent, entry pathway for SV40 [173,174]. Also, GFP-labeled HIV-1 imaging in cells clarified the implications of the microtubules and dynein in the intracellular trafficking of the virus [175]. As the technology advanced, single molecule detection and computational tracking capabilities allowed for higher sensitivity of detection and quantitative characterization of the entry pathways and motion of single viruses [176]. Enveloped viruses trafficking together with fusion events observation was achieved using influenza virus labeled with the lipophilic dye 1,1'-dioctadecyl-3,3,3',3'-tetramethylindodicarbocyanine (DiD) [177]. The fusion after acidification was detected when dye dequenching and redistribution occurred upon lipid mixing. Using different labeling for outer and inner leaflets of the viral membrane (DiD and palmitoylated yellow fluorescent protein (YFP)), the fusion process of ALSV was characterized in terms of kinetics and pH dependence [178]. Observing HIV-1 fusion in live cells was possible using DiD labeled virions together with fluorescent protein marked nucleocapsid [179]. This kind of robust double-labeled, single virus tracking in live cells was also the base to unveil the previously unknown entry pathway of HIV-1 through fusion at the endosome level, instead of the plasma membrane [36]. HIV-1 spreading via virological sinapses, cell-cell adhesions that facilitate viral transfer, was also directly observed via Gag labeling using high speed 3D video microscopy [180]. ASLV entry pathways and the two step entry process dependent on low pH and receptor binding were dissected via single virus live imaging using pH sensitive markers, allowing to distinguish the sorting of the virions in distinct intracellular compartments [120,121]. As super-resolution paves the way for the future of

imaging, more detailed viral structures can be distinguished in infected cells, such as the conical shaped HIV-1 capsid, and if the virus is mature or immature [181].

However, when we want to look at details on how specific molecules modulate the fusion process, it is useful to simplify the system and use minimal components to mimic and isolate the phenomenon under study. For long, virus fusion requirements were also studied with membrane model systems, such as lipid vesicles, that offered a simple mean of manipulating lipid composition and buffer conditions (salt and pH), in order to identify specific requirements or dependences. For imaging, however, only recently virus-membrane fusion was directly imaged using supported lipid bilayers (SLB) in glass supports [182,183] (**Fig. 6**). SLB consist of a single phospholipid bilayer on top of a clean planar surface, in an aqueous environment [184]. An ideal SLB should be uniform and fluid, allowing lateral mobility of the phospholipids. It can be formed by lipid vesicle rupture at the surface (**Fig. 6C**) or using a Langmuir–Blodgett trough to compress monolayers on a water surface that can be transferred to the glass surface [184]. Wessels *et al.* reported direct influenza and Sindbis viruses fusion with glass supported lipid bilayers [183]. The viruses were membrane labeled with octadecyl rhodamine (R18) at self-quenching concentrations and the fusion was observed by the dequenching and radial spreading of the dye upon lipid mixing. Floyd *et al.* improved this technique by using double labeled influenza virus (membrane dye and content dye) to measure the kinetics of lipid mixing and content release, providing a full picture of fusion kinetics [182]. The same methodology was later modified to use proton uncaging by UV for lowering the pH, instead of buffer exchange [185]. Such methods allow to measure single particle fusion kinetics and detail the mechanism in levels difficult to obtain when using live cells.

Virus imaging studies are now essential to understand the full picture of the viral life cycles. New technological advances will certainly benefit the field as they also become increasingly accessible to researchers.

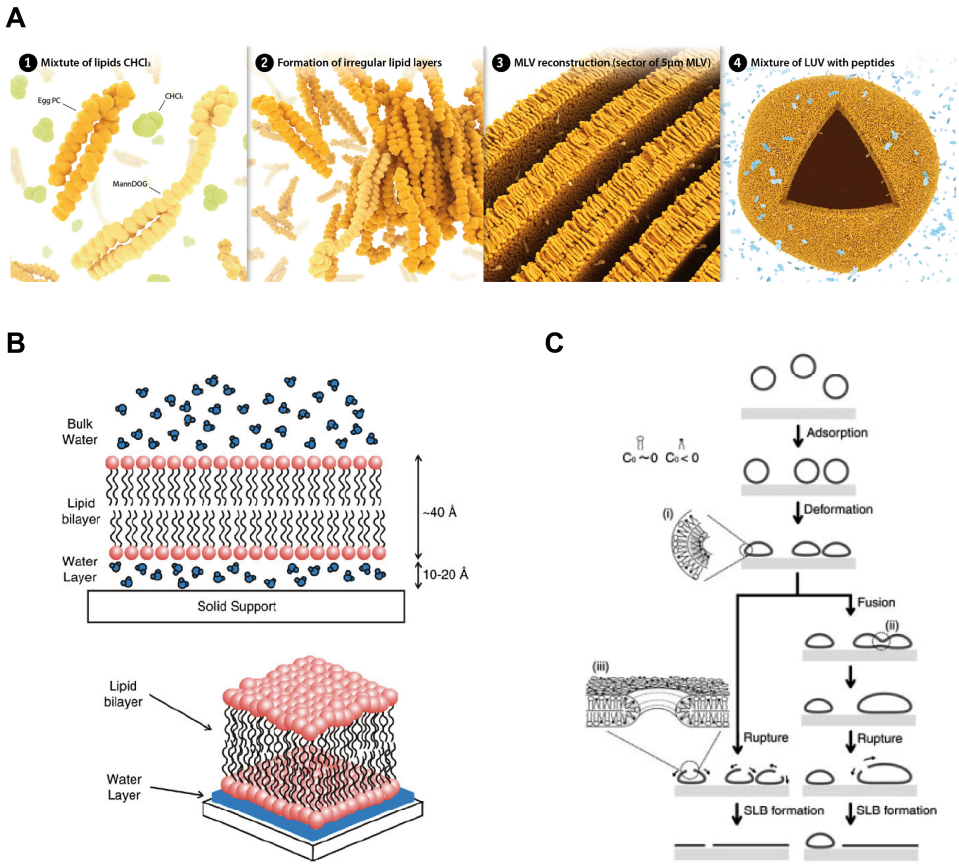

Figure 6 – Model membranes for biophysical studies. (A) Schematic representation of the general steps for the formation of the lipid vesicles used in this Thesis for peptide-membrane interactions and formation of supported lipid bilayers. Adapted from [186,187] (B) Lipid bilayer supported on a solid planar surface, in an aqueous environment. A water sheet remains between the bilayer and the support, allowing for some degree of lipid mobility. Reprinted from [184]. (C) Possible mechanisms of SLB formation by successive events of vesicle adsorption, deformation, fusion and rupture. Reprinted from [188].

6. Review articles and book chapter

In order to complement this introduction, we present a book chapter related to HIV-1 fusion inhibitor peptides and two review articles that explain the methodological approaches based on fluorescence to study peptide-membrane interactions.

Book Chapter A

Franquelim HG, Matos PM, Veiga S. "HIV vs. HIV: Turning HIV-Derived Peptides into Drugs" in *Peptide drug discovery and development – Translational research in Academia and Industry* (2011), Castanho MARB and Santos NC (eds.), Wiley-VCH, Weinheim, Germany.

Review Article A

Matos PM, Gonçalves S, Santos NC. Interaction of peptides with biomembranes assessed by potential sensitive fluorescent probes. *J. Pept. Sci.* **14**:407-415 (2008).

Review Article B

Matos PM, Franquelim HG, Castanho MARB, Santos NC. Quantitative assessment of peptide-lipid interactions: Ubiquitous fluorescence methodologies. *Biochim. Biophys. Acta.* **1798**:1999-2012 (2010).

Book Chapter A

Declaration of authorship

I, Pedro Miguel Baptista de Matos, declare that the manuscript preparation and writing was carried out by me, Henri Franquelim and Dr. Ana Salomé Veiga.

I, Ana Salomé Veiga, as senior author of the article mentioned above, hereby acknowledge and confirm that the information above is correct.

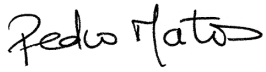

Pedro M. Matos

Ana Salomé Veiga

10
HIV vs. HIV: Turning HIV-Derived Peptides into Drugs

Henri G. Franquelim, Pedro M. Matos, and A. Salomé Veiga

10.1
Introduction

Human immunodeficiency virus (HIV) is the causative agent of the acquired immunodeficiency syndrome (AIDS). There are two types of HIV: HIV-1 and HIV-2, HIV-1 being the most virulent [1]. HIV can be transmitted by blood and blood products, vertically (from mother to child), or through sexual activity. By the end of 2009, the United Nations Programme on AIDS (UNAIDS)/World Health Organization (WHO) epidemic update estimated 33.4 million (31.1–35.8 million) people worldwide living with HIV [2]. Despite much effort, no curative treatment or effective vaccine has yet been achieved.

The rational design of anti-HIV-1 therapeutics is based on detailed knowledge of the biology of the virus. Combination therapy with reverse transcriptase and protease inhibitors is the most common current treatment of HIV-1 infection [3]. Despite the success of this therapy, namely by reducing morbidity and mortality of HIV-1 infected patients [4], it has adverse effects and drug resistant HIV-1 strains have emerged [5]. This demands the development of new classes of drugs targeting different stages of the viral life cycle. A new class of antiviral agents in development, the entry inhibitors, exhibits promising inhibition profiles. Unlike reverse transcriptase and protease inhibitors, which target post-entry steps inside the host cells, entry inhibitors act extracellularly preventing viral entry into target cells [6].

10.2
HIV-1 Envelope Protein

HIV-1 is an enveloped virus that infects $CD4^+$ T cells, dendritic cells, and macrophages [1]. The HIV-1 envelope glycoprotein is the protein responsible for the viral entry into the target cells. It is expressed on the surface of the viral membrane as a trimer [7]. It is composed of two subunits noncovalently associated: the gp120 subunit, a globular-shaped subunit at the surface of the membrane that interacts

Peptide Drug Discovery and Development: Translational Research in Academia and Industry, First Edition.
Edited by Miguel Castanho and Nuno C. Santos.

Published 2011 by WILEY-VCH Verlag GmbH & Co. KGaA

with cellular receptors, and the gp41 transmembrane subunit, responsible for the fusion between the viral and cellular membranes (reviewed in [6, 8, 9]).

gp41 is composed of an ectodomain (extracellular domain), a transmembrane domain (TM) and an endodomain (intracellular domain or cytoplasm tail (CT)). Several functional domains have been identified in the ectodomain. The fusion peptide (FP) is located at the ectodomain N-terminal. This region, hydrophobic and rich in glycine residues, interacts with the target cell membrane and plays an important role in membrane fusion (reviewed in [10]). Two heptad repeat regions ((HR(), with the tendency to form α-helical coiled-coils [11], are also present: the first (NHR or HR1) near the N-terminal is adjacent to the FP; the second (CHR or HR2) is located at the ectodomain C-terminal. Peptides derived from them are referred to as N- and C-peptides, respectively. The two HR are separated by a loop region (LR) that contains an intramolecular cysteine bridge. At the C-terminal between the CHR and the TM is located a Trp-rich domain (TRD), the membrane proximal external region (MPER), which also seems to play an important role during the viral membrane fusion [12]. As several monoclonal antibodies bind to this region, the MPER is seen as the major target for vaccine development (reviewed in [13]).

Protein dissection combined with biophysical analysis has demonstrated that the two HR regions within gp41 form a helical trimer of antiparallel dimers [14]. The crystal structures of portions of the ectodomain [15, 16] confirmed that the gp41 core tends to form a trimer of hairpins (also called trimeric coiled coil or six-helix bundle (6HB)). A central trimeric coiled coil formed by the N-peptide region is surrounded by three helical C-peptides that bind to conserved hydrophobic grooves on the coiled-coil surface in an antiparallel orientation. This structure represents the fusion-active conformation of gp41.

10.3 HIV Entry and Its Inhibition

HIV-1 entry into target cells is believed to be a multi-step and complex process (reviewed in [6, 8]). The first step is the binding of gp120 to the target cell surface molecule CD4, which serves as the main receptor for HIV-1 [17]. However, CD4 alone is not sufficient for HIV-1 to fuse with the cells [18, 19]. Two chemokine receptors, known as CCR5 and CXCR4, are the major HIV-1 coreceptors and all viral strains can use one (R5 and X4 viruses) or both (R5X4 viruses). The gp120-CD4 binding induces conformational changes in gp120 leading to the exposure or the formation of the coreceptor binding site. gp120 binding to the CD4 and coreceptor results in further conformational changes that lead to gp41 activation into its fusion-active state. The gp41 conformational changes lead to the insertion of its FP into the target cell membrane and the formation of an extended prehairpin intermediate that bridges the viral and cellular membranes. Subsequent changes within the gp41 ectodomain involve the interaction of CHR and NHR, and a 6HB structure is formed. The hairpin formation brings the viral and cell

membrane into close proximity, allowing fusion of the membranes and then entry of the virus.

Each of the HIV-1 entry steps can be a target for entry inhibitors. The ones currently under development fall into one of three categories: gp120-CD4 binding inhibitors (or attachment inhibitors), gp120-coreceptors binding inhibitors (or chemokine coreceptors inhibitors), and fusion inhibitors (reviewed in [20, 21]). Several molecules that block gp120 binding to CD4 receptor and coreceptors have been identified and are reviewed elsewhere. This chapter reviews the molecular bases of fusion inhibition and the involvement of gp41. As such, the discussion will focus on peptide-based fusion inhibitors (Figure 10.1).

Fusion inhibitors, such as enfuvirtide (also known as DP-178, T-20, or Fuzeon) and T-1249 (Tifuvirtide), both from Trimeris, Inc. and Hoffmann-La Roche, Inc., are peptides whose mode of action involves binding to gp41. They interfere with the conformational changes that lead to the 6HB formation and membrane fusion. These kinds of inhibitors are the leading compounds, enfuvirtide being approved by the FDA since 2003 [23, 24]. Enfuvirtide remains the standard in HIV fusion inhibitor peptides as the only drug to complete the whole development track up to clinical use.

10.4
HIV-1 Fusion Inhibitors: from Bench to Clinical Administration

The initial development of HIV-1 fusion inhibitors was based on peptides that were derived from the HR regions of gp41, mainly obtained by protein dissection strategies. Some synthetic C-peptides, such as C34 and enfuvirtide, are highly potent inhibitors of HIV-1 infection at low nanomolar range [25, 26]. It has been proposed that these C-peptides act by interfering with the formation of the 6HB in a dominant negative fashion, by binding to the NHR region of gp41 exposed in the prehairpin intermediate [8, 14, 27].

Synthetic N-peptides also exhibit inhibitory activity against HIV. They are less potent inhibitors (micromole range) than the C-peptides [14, 28, 29]. It was proposed that one of the main reasons for this behavior is their tendency to aggregate in solution [14]. N36 and DP107 are examples of N-peptide inhibitors. In their mode of action, N-peptides may either target the CHR region [14] or intercalate with the NHR region [30].

A critical aspect of the inhibition by HR-derived peptides is the propensity of the central NHR core to form a highly stable helical 6HB complex with CHR peptides. Structural analysis of gp41 indicated that the NHR core formed deep hydrophobic pockets. A complementary specific region of CHR, named the pocket binding domain (PBD), packs into those domains on the NHR core faces enabling effective interactions within the helical complex [31].

C34, a 34 amino acid residues peptide, was the C-peptide used to discover the trimeric coiled coil structure of gp41 [15]. It can be used as a fusion inhibitor and is one of the most potent early-discovered fusion inhibitors. This peptide overlaps the

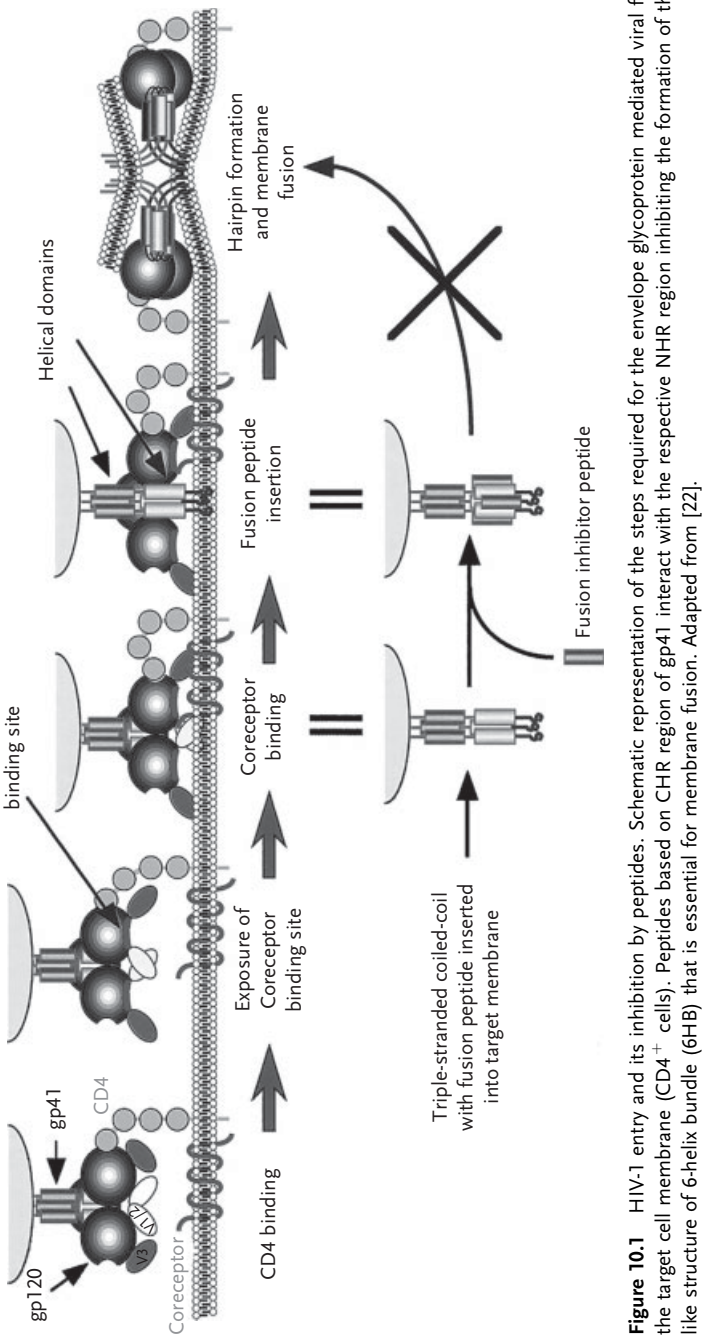

Figure 10.1 HIV-1 entry and its inhibition by peptides. Schematic representation of the steps required for the envelope glycoprotein mediated viral fusion with the target cell membrane ($CD4^+$ cells). Peptides based on CHR region of gp41 interact with the respective NHR region inhibiting the formation of the hairpin-like structure of 6-helix bundle (6HB) that is essential for membrane fusion. Adapted from [22].

CHR region, including the PBD region, which is essential for its antiviral effectiveness [31]. In terms of activity, it showed an increased *in vitro* activity. At a molecular level, C34 forms highly stable helical complexes with N-peptides, such as N36 [29]. Considering the mode of action, evidence (using the C34-like 36 residues inhibitor T649) suggests that the hydrophobic pocket domain and the LLSGIV sequence of the NHR are both preferential docking sites for this peptide, explaining its increased inhibition efficacy [32]. Nevertheless, despite being more potent, C34 is not a good drug candidate due to its low solubility [33].

Enfuvirtide is a 36 amino acid residues peptide that was developed as a novel anti-HIV drug [26, 34]. It is currently the more advanced fusion inhibitor drug approved for clinical application. Since 2003, enfuvirtide has been licensed by the FDA for the treatment of HIV patients who failed to respond to current antiretroviral therapeutics [23].

Enfuvirtide shares 24 identical residues with C34, but lacks the PBD at the N-terminal. In terms of molecular interaction, unlike C34, enfuvirtide does not form stable helical complexes with N36 [35]. Despite the reduced helicity, it possesses high antiretroviral activity. Crucial for this inhibitory effect are the C-terminal residues not included in C34 [36]. Mutations and deletions of the C-terminal domain have been shown to impair the antiretroviral activity of enfuvirtide [35]. This region overlaps the TRD and is responsible for efficient lipid membrane binding [37, 38]. Lipid membranes play an important role during HIV inhibition, since the fusion process must occur in extreme confinement between the viral envelope and the cellular plasma membrane [39]. Membranes participate in enfuvirtide's action, by increasing its concentration at its site of action. It was demonstrated that enfuvirtide incorporates extensively into neutral liquid-crystal lipid membranes and occupies a shallow position in the lipid membrane [40] (Figure 10.2).

The mode of action by which enfuvirtide inhibits viral fusion is still not completely clear and is rather complex. Several proposals have been presented involving different target sites in gp41, gp120, and at the membrane level. The most currently accepted mechanism is the one proposed for C-peptides in general, involving interaction with the gp41 NHR region, thus preventing the conformational changes that lead to the fusion-active arrangement [26, 41, 42].

However, accumulated evidence suggests that this assumption may be too simplistic. Due to the lack of the PBD region, it was suggested that enfuvirtide binding affinity to the NHR region cannot justify its strong inhibitory activity and the peptide should have at least two different interactions modes with gp41 [43].

In addition, Kliger *et al.* [44] showed that enfuvirtide can bind to membranes and oligomerize on their surface. The involvement of lipids in the mechanism of interaction of enfuvirtide, by contrast with C34, has also been reported by Jiang and coworkers [37]. Therefore, two possible enfuvirtide target sites in gp41 can be proposed, both contributing to fusion inhibition: interaction with the NHR region in aqueous solution prevents the formation of the 6HB structure, while interaction with gp41 in the membrane environment inhibits fusion pore formation [43–45].

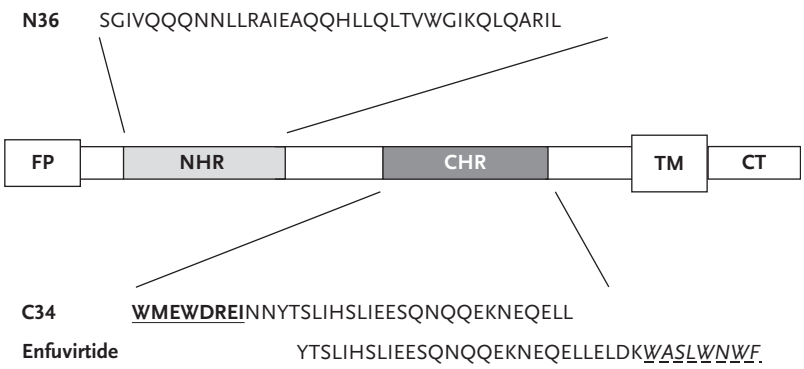

Figure 10.2 Peptide fusion inhibitors and respective gp41 domains. Schematic representation of the location of the N- and C-terminal heptad repeats domains (NHR and CHR, respectively) on gp41 and the sequences from which three first-generation fusion inhibitors are derived: N-peptide N36 (residues 546–581) and C-peptides C34 (residues 628–661) and enfuvirtide (residues 638–673). The underlined and bold sequence in C34 represents the pocket-binding domain (PBD), whereas the underlined and italic sequence in enfuvirtide represents the Trp-rich domains (TRD). FP – fusion peptide, TM – transmembrane domain, CT – cytoplasmic tail.

Less accepted, but also proposed modes of action for enfuvirtide involve its binding to the gp41 FP, preventing the insertion of the latter into the target cell membrane and thus membrane fusion [46], and binding to the gp120 subunit, as an additional target site contributing to its inhibitory activity [47].

During pre-clinical and clinical trial phases, enfuvirtide was demonstrated to be effective against a broad spectrum of HIV-1 strains. Maximum efficacy and safety were achieved with a dose of 90 mg injected subcutaneously twice daily [48]. Though it possess potent anti-HIV activity, enfuvirtide has several pitfalls, such as a short half-life *in vivo*, local side effects and induction of drug-resistant strains.

Based on the knowledge gathered on the structure, activity, and function of fusion inhibitors such as enfuvirtide or C34, several modified peptides have been created, in an attempt to achieve better antiretroviral activity *in vivo* (reviewed in [35]).

One of these new molecules is the rationally designed second generation fusion inhibitor T-1249. This 39 amino acid residues peptide is composed of sequences derived from HIV-1, HIV-2, and simian immunodeficiency virus (SIV) [49], and incorporates both PBD and TRD regions, which explains the efficacy enhancement. Despite the need for clarification, it is believed that, in its mechanism of action, T-1249 acts like most C-peptides, interacting with the NHR region and preventing 6HB formation [23]. It is also able to concentrate on lipid membranes. At variance with enfuvirtide, T-1249 adsorbs on the surface of raft-like platforms in lipid membranes, this difference being one possible explanation for its improved activity. Pre-clinical and clinical studies have demonstrated that this peptide is more potent (2 to 100-fold increase in activity *in vitro* [35]) and has a higher half-life than enfuvirtide, thus enabling a once-daily subcutaneous dose. Furthermore,

T-1249 has been demonstrated to be active against enfuvirtide resistant HIV-1 isolates [50]. Nevertheless, in spite of these optimistic results, the clinical development of T-1249 was discontinued due to formulation difficulties [35, 48].

Another peptide that has recently completed phase IIb clinical trials (http://www.fusogen.com/en/news.asp?id=146) is Sifuvirtide. This 36 aa peptide designed by FusoGen Pharmaceuticals Inc. has been engineered using 3D structure information of HIV-1 gp41 and computer modeling analysis [51]. Sifuvirtide has 16 different residues compared to C34 and 22 compared to enfuvirtide. Like C34, it maintains the PBD region and lacks the TRD region important for membrane binding [52]. Its mode of action is believed to be similar to C34. Nevertheless, it was demonstrated that this peptide adsorbs selectively on the surface of rigid phosphatidylcholine membranes [53, 54]. Sifuvirtide can form a stable 6HB structure with the N-peptide N36 and has potent inhibitory activity against enfuvirtide-resistant strains. Phase Ia clinical studies demonstrated that this peptide has a better safety profile, tolerability, and pharmacokinetic properties than enfuvirtide [52, 55]. This peptide presents low injection side reactions, a longer half-life *in vivo* and a 20-fold higher potency *in vitro*, which enables the administration of a lower once-daily dose compared to enfuvirtide [52, 55]. This peptide was modified by introducing several salt bridges, which favored its solubility, α-helicity, durability and antiviral potency [52]. In the next section new modifications of the C- and N-peptides, as those applied in Sifuvirtide, will be discussed in more detail.

10.5
New Strategies for Creating New HIV Fusion Inhibitor Peptides

Understanding the trimeric gp41 structure and the putative interaction of the CHR and NHR explained why peptides derived from sequences of gp41 inhibited HIV infection of cells. This unlocked a new wave of research that aimed to discover new peptide drugs that target gp41-mediated fusion. In fact, the peptide nature of these drugs gives the researcher a particularly flexible framework with defined rules, which can be played in a myriad of ways. Also, exploring these diverse combinations gives important information on the factors that are most important for the effectiveness of these drugs. In this setting, and not surprisingly, the majority of the fusion inhibitor peptides that were or will be described did not proceed to clinical trials nor were intended to. Hence, many of the peptides were created for research purposes only, as intermediates or precursors for possible future drugs.

In this section we will describe new fusion inhibitor peptides and the strategies behind their design to improve their activity. The starting point is always the wild type (wt) sequence of gp41 (HXB2) or an already modified gp41-based peptide. The rational design of new sequences for these types of drugs usually takes into account factors such as binding to native gp41, secondary structure (helicity), solubility, oligomerization, isomerism, or even lipophilicity.

10.5.1 Increasing Helicity and Binding to gp41

One of the first practical rationalizations in order to improve enfuvirtide activity was to increase the helicity of the peptide in solution [56]. Enfuvirtide does not have a defined secondary structure in solution [26], but assumes an α-helical structure when bundled with a corresponding gp41 N-terminal peptide [14]. Hence, forcing a helical conformation in solution could reduce the energy necessary for the interaction to occur. For this, HIV35, a shorter derivative of enfuvirtide in which the hydrophobic C-terminal TRD (KWASLWNWF) is absent, was used. Ablation of this domain actually results in a peptide with substantially decreased antiviral activity. Covalent crosslinks between aminoacids at positions i and $i+7$ were used to lock the α-helical conformation. Peptides derived from HIV35 with one (HIV24) or two (HIV31) cross-links were prepared, and circular dichroism studies confirmed the increased helicity of these forms. The cross-linking in HIV24 partially restored the activity of the truncated peptide, while in HIV31 it increased it to levels similar to enfuvirtide. This proved the importance of the secondary structure in determining the binding with gp41, even when an important domain for activity is ablated.

A similar approach was used with other short C-peptides that were targeted to the hydrophobic pocket region [57]. The α-helix was stabilized via chemical crosslinking with a diaminoalkane group linking two Glu residues at i and $i+7$ and with the use of an unnatural aminoacid that favors helicity (α-aminoisobutyric acid). The sequence C14wt (gp160 HXB2 626–639) showed very weak antiviral activity, measured by cell–cell fusion assay. The highest antiviral activity was obtained for the version of the peptide cross-linked in the middle at positions 629 and 636 (C14linkmid) followed by an unlinked version but with those positions substituted by α-aminoisobutyric acid (C14Aib). For this case, an important binding site, targeting the hydrophobic pocket, was maintained, and the short sequences used proved to be sufficient for inhibition but modifications to achieve helical constrain were mandatory.

A possible disadvantage of this kind of approach is that cross-linking strategies are not favorable to large scale manufacturing, if a peptide of this kind is able to reach broad clinical use.

Besides these two examples of peculiar use of chemical crosslinking, the majority of the approaches for modifying this kind of peptide involves aminoacid residue changes, rearrangements, and shortening/elongation.

A good example of rational design by modifying the aminoacid sequence was done for C34. It is less soluble than enfuvirtide which is one of the reasons why C34 never progressed in a clinical setting. Otaka *et al.* [33] modified C34 with the following rationale: (i) maintenance of the aminoacids responsible for the interaction with gp41, when represented in a helical-wheel diagram against a trimer of N36; (ii) substitution of non-conserved aminoacids of the solvent accessible site by Glu and Lys that should form ions pairs at positions i and $i+4$. This would enhance solubility and helicity due to formation of intrahelical salt bridges [58].

Two main peptides were derived, SC34 and SC34EK, with the latter neglecting the maintenance of some conserved aminoacids in favor of more salt bridges to stabilize the helix. These two peptides had significantly higher antiviral activity *in vitro* than enfuvirtide, SC34EK being a little more potent than SC34. An extreme version of these peptides (SC35EK) was also synthesized in the form Z-EE-ZZ-KK (with Z representing an arbitrary aminoacid), maintaining the interactive site while the solvent accessible was exclusively Glu and Lys, with activity still comparable with the other peptides. The stable structure of SC34EK with N36 was later confirmed by X-ray crystallography [59]. This shows that increasing helicity by aminoacid substitution while maintaining the residues that interact with gp41 NHR is a successful strategy to increase the activity of fusion inhibitor peptides (Figure 10.3).

The same approach was taken for enfuvirtide, by introducing the same motif Z-EE-ZZ-KK resulting in an increase in the antiviral activity [60]. Shorter versions of SC35EK were also produced with 29 (SC29EK) and 22 (SC22EK) aminoacids by truncation at the C-terminal region [61]. Only SC29EK maintained activity similar to SC34EK and also inhibited enfuvirtide-resistant strains of HIV.

In an effort to screen for the next generation fusion inhibitor that would follow enfuvirtide and T-1249, scientists from Trimeris designed a new set of peptides to improve helical propensity and affinity to gp41 NHR that self-associate to stable

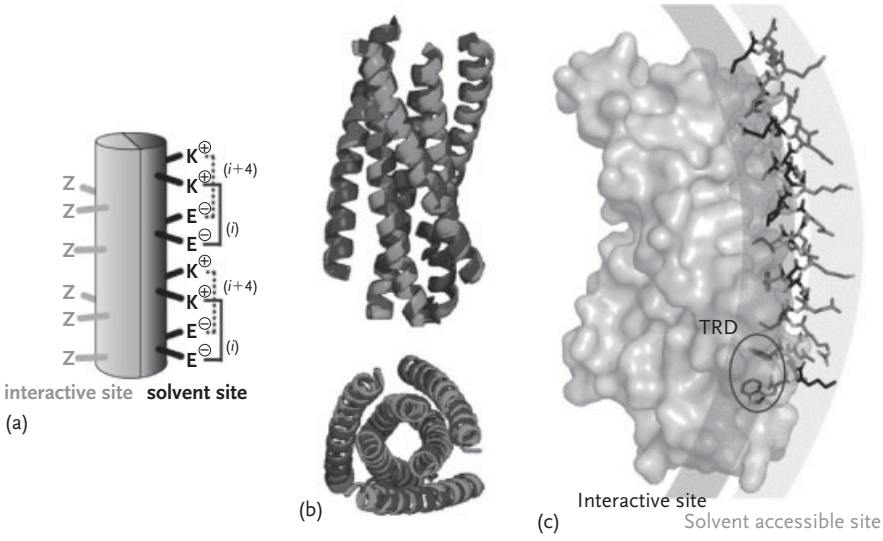

Figure 10.3 Design and structure of SC34EK. (a) The C34 sequence was modified by introducing EK (i, $i+4$) motif in the solvent accessible site, while maintaining the aminoacid residues (Z) of the interactive site. (b) Side and top views of the structure of the 6HB formed by N36/SC34EK (gray), superimposed by the gp41 native core structure (black). (c) Stick model representation of SC34EK modeled in interaction with part of a N36/SC34EK bundle (gray structure). The location of the N-terminal Trp rich domain is indicated by a circle (TRD). Adapted from [59].

oligomers in solution and are active against enfuvirtide-resistant strains [62]. The starting peptide was named T-2410, a wt sequence from gp41 CHR that included the hydrophobic pocket binding sequence. Residues that could be changed without compromising antiviral activity and 6HB stability were selected by Ala scanning. Charged aminoacids Glu and Arg were introduced in spaced positions i and $i + 4$ in order to favor formation of salt bridges. To further increase helicity, some noncritical aminoacids not participating in salt bridges were substituted by Ala, an aminoacid with high helical propensity. Up to 15 peptides were obtained with this rational design, from which we will highlight T-2635. This peptide was found, by circular dichroism, to be 75% helical, compared with the starting point of only 7% for T-2410 (enfuvirtide is 12%). It oligomerizes in solution, being a trimer in the concentration range from 50 to 1000 μM and a mixture of trimer and monomer below 50 μM. Its *in vitro* activity can be up to >3600-fold greater than enfuvirtide in certain strains. Importantly, it takes much longer for the virus to aquires mutations to resist these peptides than with enfuvirtide and they have improved pharmacokinetics in cynomolgus monkeys, including extended half-life. Besides the usual structural refinements, this work also emphasizes the role of the oligomerization state in the antiviral activity.

Although the majority of the peptides described here contain the pocket binding sequence and/or the TRD lipid binding domain, He *et al.* identified a new motif upstream of the pocket binding domain important for the stabilization of gp41 6HB (621QIWNNMT627) [63]. A series of peptides containing this sequence was obtained, from which we will highlight CP621–652. This peptide was able to interact with a counterpart NHR peptide in a more stable way than C34. Moreover, improved activity was observed compared to enfuvirtide and the peptide also inhibited strains resistant to enfuvirtide and C34. Based on CP621–652, a new peptide was designed by introducing Lys and Glu in order to create ion pairs, and the first residue at the C-terminal was changed to Val to enhance hydrophobic interaction with the NHR counterpart [64]. This new peptide, CP32M, had improved characteristics over its predecessor and we can emphasize the high potency in low picomolar amounts against enfuvirtide- and C42-resistant strains. These peptides do not rely on the 547GIV549 motif to interact with NHR, a sequence previously shown to be a major determinant of resistance to enfuvirtide and C34 [65].

However, creating peptides that are effective against resistant strains should not be more difficult. Single aminoacid residue modification of enfuvirtide or C34 can overcome such resistance. Izumi *et al.* [66] took into account that the CHR mutations S138A and N126K enhance resistance to enfuvirtide and C34, respectively, and created a peptide with modified aminoacids on those positions. For enfuvirtide, substitution with all natural aminoacids was tried, resulting in the fact that only T-20S138A inhibited replication of enfuvirtide-resistant virus as efficiently as the wt clone. Other efficient substitutions were for smaller hydrophobic residues (Ala, Leu, Ile) or more flexible ones (Met, Thr). The same happened for a C34 modified through the mutation N126K, which became active against the respective resistant strain. This case highlights the importance of having

resistance information in order to specifically tailor the peptides to overcome such barrier.

Another example of an innovative approach comes from the creation of C34coil, a derivative of C34 grafted into a GCN4 Leu zipper [67]. In this case, residues of C34 critical for binding to NHR are transferred to a GCN4 sequence, functioning as a scaffold. After that, the C34-GCN4 peptide was disulfide linked to a GCN4 peptide only in order to form a coiled coil dimer. This resulted in a more stable and structurally defined peptide, with enhanced solubility and helicity. Importantly, C34coil was 1000 times more resistant to proteolytic degradation than C34 itself. This new peptide is not more potent than C34; however, IC50 values for cell–cell fusion and infectivity assays are within an order of magnitude.

We should also not forget that computational biology is nowadays a major tool to design new drugs tailored to a specific molecular target. The computation power available makes the simulation of structures and interactions increasingly accessible and informative. A series of 10 variants of C34 (KYK01 to 10) was designed based on molecular dynamics simulations of 6HB stability to increase the binding to the gp41 NHR region [68]. KYK01, KYK02, and KYK03 were more efficient in inhibiting virus replications than the original C34; however, they were inactive against enfuvirtide-resistant viruses. To overcome this, KYK02 was modified to carry the previously mentioned S138A substitution. For this case more than one strategy was applied in order to design a truly efficient drug.

10.5.2
Isomeric Peptides and Resistance to Proteolysis

To specifically tackle the problem of the oral bioavailability of these drug peptides, due to rapid preoteolytic degradation in the gastrointestinal tract, the main strategy that emerged was to design peptides with different chirality from the natural ones: D-peptides. Using once again the pocket binding site as a target, a D-peptide IQN17 was designed to properly present this target to serve as a template for the new peptides [69]. Using mirror-image phage display, several D-peptides were identified (D10-p1 through D10-p12). They presented a 10 residues consensus sequence to the binding of the pocket region. Cys flanking the consensus sequence generated an intramolecular disulfide bond to yield a cyclic peptide. Lys were added at the N-terminus to increase solubility. These peptides were capable of inhibiting HIV-1 entry into cells in the micromolar concentration range. This kind of approach was refined in a later study [70] in which the authors locked the consensus residues and randomized the other ones in the phage-display rounds. The new peptides were more potent than those obtained in the first studies and were active against laboratory-adapted strains (HXB2) and primary isolates.

In another attempt to create proteolysis resistant fusion inhibitors, the C34 sequence was modified by introducing D-aminoacid point substitutions at sites not directly involved in 6HB integrity [71]. These modifications were able to create stable and helical peptides with similar activity to C34.

10.5.3
Bacterially Expressed Peptides

From the pharmaceutical point of view, even if a peptide is very potent, it may not be feasible for commercialization if its manufacturing is difficult and costly. To address the problem of large scale manufacturing, Deng *et al.* tried, for the first time, to express a fusion inhibitor peptide, C52L in *E. coli* [72]. This peptide spans the sequence of enfuvirtide and C34, containing at the C-terminus a heptad register of three residues from the N-terminus of GCN4-pII isoleucine trimer to enhance helicity. The peptide was produced by extraction from insoluble bacterial inclusion bodies. It possessed broad activity, inhibiting infection of all clades of HIV-1 group M and also enfuvirtide resistant variants. This was the first and only time that this kind of production was tried, aiming at a solution for getting more affordable drugs of this type.

10.5.4
Modification of Peptides by Derivatization with Lipids or Proteins

In the constant search for ways to optimize and increase the effectiveness of HIV fusion inhibitor peptides, sometimes it takes more than just residue substitutions to achieve a better result. In this section we will describe how HIV fusion inhibitor peptides can be modified by covalently attaching another molecular entity to increase potency.

An unconventional approach was taken by Hildinger *et al.* by expressing a membrane-anchored version of enfuvirtide [73]. In this case enfuvirtide was expressed fused with a membrane protein, so that the peptide was displayed at the surface of a T-helper cell line. In this way, the peptide potently inhibited viral replication in these transduced cell lines. In contrast, a construct that attached enfuvirtide to a secreted protein instead of a membrane spanning one, did not inhibit the replication. This indicates that attachment of the drug to the cell membrane, where viral fusion occurs, increases the efficacy of the drug.

Following different observations of the enhanced efficacy of membrane associated peptides, Peisajovich *et al.* [74] synthesized SIV-derived enfuvirtide peptides acylated at their C-terminus. Octylation of enfuvirtide rendered the peptide significantly more potent than the peptide itself. The same did not happen for propyl and hexyl variations and for N-terminal acylation. Moreover, an inactive enfuvirtide mutant in which part of the TRD, GNWF, was substituted by ANAA, was rescued when octylated. The acylation seemed to mimic the role of the hydrophobic C-terminal region of the peptide. This C-terminal modification to the peptide could direct the peptide to the cell membranes in order to be readily available if the virus infects the cell, and with the favorable orientation to interact with gp41 NHR. This membrane association effect is similar to the previously presented case of enfuvirtide covalently attached to a membrane spanning protein.

A series of enfuvirtide peptides was truncated at this region to arrive at a minimal inhibitory sequence, named DP [75]. In this version, the entire region containing the three C-terminal Trp residues was removed. This peptide was then attached to fatty acids of 8, 12, or 16 carbons to assess the effect of chain length. Indeed, the higher the length the more potent was the conjugate in inhibiting viral fusion. N-terminal conjugation did not lead to similar improved efficacy, hence the importance of the orientation of the peptide. The hydrophobic anchor of these modified peptides permitted higher potency, presumably due to membrane targeting and concentration effects.

Trimeris, the company behind enfuvirtide and T-1249, also developed a peptide conjugated with fatty-acid. TRI-999 is a peptide that includes the pocket binding domain regions but not the C-terminal hydrophobic tail. Instead, a C18 fatty acid is attached to the only Lys residue near the C-terminus through a PEG3 linker [76]. This peptide was more potent than enfuvirtide, having an IC50 up to 250-fold lower. Importantly, the pharmacokinetics clearance values were up to sixfold slower than enfuvirtide, showing a slow and steady release of the drug [77].

In an effort by scientists of Merck Research Laboratories to increase the efficacy of C34, a new type of conjugate was synthesized with a cholesteryl moiety attached [78]. The rationale for the use of cholesterol instead of a fatty acid was the higher affinity towards membranes and targeting of the drug to the receptor-rich membrane microdomains (lipid rafts) where HIV-cell fusion is likely to occur. This modification increases the antiviral activity from 15-fold to 300-fold compared to enfuvirtide and T-1249, and increases significantly the half-life of the peptide *in vivo*. Moreover, the activity is retained *in vitro* if pre-treated host cells are washed. Contrary to C34, the addition of cholesterol to enfuvirtide does not have the same effects of enhancing potency, probably due to the existence of the lipid binding domain already. Interestingly, this cholesterol tagging strategy was also later used for fusion inhibitor peptides of paramoxyvirus [79].

Beside these lipopeptide conjugates that turned out to be quite successful, protein conjugates were recently considered. The C34 fusion inhibitor peptide was conjugated with human serum albumin and tested for *in vitro* and *in vivo* action [80]. A maleimido-C34 derivative was reacted with cysteine 34 of HSA, the only cysteine of this protein, resulting in a 1 : 1 complex, named PC-1505. The potency of this conjugate was still similar to C34 and enfuvirtide, indicating that the accessory protein did not prevent the peptide from reaching gp41 in the pre-fusion state. More importantly, the PC-1505 activity *in vivo* was 3 times higher than the unconjugated form and was more sustained, resulting in an improved pharmacokinetic profile. A similar approach was taken by Xie *et al.* [81], where they modified a C34 peptide in order to carry a maleimido group in Lys 13 (FB006M). When injecting this modified peptide in SCID/hu mouse model the peptide reacted with Cys 34 of albumin in the blood, generating a 1 : 1 complex which prolonged the half-life of the drug while maintaining its efficacy.

Another interesting approach was taken by Ji *et al.* [82]. They created a construct CD4-BFFI which consists of two HIV-1 fusion inhibitor peptides T-651 [62] fused to the Fc (fragment, crystallizable) end of a humanized anti-CD4 monoclonal

antibody. This antibody part would direct the conjugate to the CD4 receptor making the peptides available at the exact site of viral attachment. CD4-BFFI presented improved antiviral activities over nonconjugated T-651, as well as improved serum stability and pharmacokinetics, with a half-life of several days. This demonstrates once again the utility of using peptide conjugates to improve the pharmacological profiles of these kinds of peptide drugs.

10.6
Drug-Resistance and Combination Therapy

The emergence of drug-resistant HIV-1 variants in patients under fusion inhibitor therapy is one of the aspects that should be taken into consideration in the development of novel compounds. Resistance to enfuvirtide has been observed both *in vitro* and during clinical studies and is governed by changes in the NHR region, especially in and around the GIV motif (amino acids 35–45 of gp41) (reviewed in [83]). Those mutations have been shown to reduce the level of enfuvirtide binding and sensitivity, but at a fitness cost. These mutations interfere in the interaction between the viral NHR and CHR domains, thus decreasing viral bundle stability, which may alter fusion kinetics, pathogenicity, replicative fitness, and other aspects of the viral fusion process. Nevertheless, the virus may further evolve to repair its fitness loss by introducing a compensatory mutation, normally in the CHR domain. For instance, Baldwin and Berkhout reported that, for the V38A mutated virus, the compensatory mutation N126K promoted a drug-dependent phenotype [83]. Alternatively, Bai *et al.* [84] and Tolstrup *et al.* [85] reported the E137K mutation that partially compensated the loss of stability at the helical bundle level for N43D-mutated viruses and further increased its resistance to enfuvirtide.

A way to delay the emergence of drug resistance and/or take advantage of the loss of replicative fitness of drug-resistant strains could be the use of combination therapy. The simultaneous use of antiretroviral drugs with different targets is able to increase the antiviral potency because of the synergistic effect resulting from the combination. For instance, strong synergistic activity was reported when entry inhibitors targeting gp120 (e.g., PRO 542), gp41 (e.g., enfuvirtide), and the co-receptor, CXCR4 (e.g., AMD3100) or CCR5 (e.g., SCH-C), were used in combination [86–88]. Additionally, some studies demonstrated that combination of fusion inhibitors targeting different sites would also result in a similar phenomenon. Hrin *et al.* demonstrated that a combination of enfuvirtide and $(CCIZN17)_3$, a trimer of N-peptides targeting the CHR domain, worked synergistically in inhibiting the entry of primary HIV-1 isolates in an *in vitro* infectivity assay [89]. The combinations of enfuvirtide with other C-peptides have also demonstrated potent synergistic effects. For instance, the combination of enfuvirtide (which possesses the TRD) and Sifuvirtide (which presents the PBD) exhibited strong synergic activity against laboratory-adapted and primary HIV-1 strains [90]. More recently,

Pan *et al.* tested the combination of enfuvirtide with both second-generation T-1249 and next-generation fusion inhibitor T-1144 (drug similar to T-2635) against HIV-1 induced cell–cell fusion [91]. The double combination exhibited strong synergism, leading to two orders of dose reduction. Exceptional synergistic activity was retrieved using the triple combination, where a three-order dose reduction was demonstrated. Furthermore, combination therapy with enfuvirtide, T-1249 and T-1144 led also to strong synergism against enfuvirtide- and T-1249-resistant HIV-1 variants. Enfuvirtide, T-1249 and T-1144, and also Sifuvirtide, contain different functional domains and present distinct primary binding sites. The binding of one of those C-peptides to the viral gp41 NHR domain may extend the temporal window period of the already transient fusion intermediate, which would then become more accessible to the other C-peptides, resulting in a potent synergism [51].

To conclude, synergistic strategies may provide higher efficacy with lower antiretroviral doses, overcoming limitations of a one-drug therapy to patients, such as ineffectiveness against resistant-strains, requirement of high doses per injection and serious injection side effects. In the end, the use of a combination of fusion inhibitors may result in lower costs and lower rejection of the antiretroviral therapy.

10.7
Concluding Remarks

The notions underlying the HIV-1 membrane fusion process and the contribution of gp41 fusion intermediate are nowadays well accepted among the scientific community. The discovery of the structure of the gp41 hairpin, prior and after gp41 NHR and CHR reorganization, contributed significantly to the development of new strategies to inhibit HIV-1. To ensure a competent viral and plasma membrane fusion, the CHR and NHR domains of the viral protein gp41 must interact to form a trimeric hairpin structure. The inhibition of this viral process is the basis of the mode of action, potency, efficacy and selectivity of fusion inhibitors. Since the early 1990s, when the first peptide inhibitors were discovered, major advances have occurred in the way we understand and design these peptidic compounds. The development of more potent and novel fusion inhibitors is being addressed, understanding the contribution of structural features and specific domains that are needed for a stronger and efficient interaction with gp41. Enfuvirtide is still the only licensed and FDA-approved drug of the fusion inhibitor class, but other drugs are now in pre-clinical or clinical development. Moreover, new insights on the mechanism of resistance and tolerance of these compounds have been discovered and several strategies involving synergistic approaches are being tested. Therefore, we can expect better outcomes and more compounds to appear in the near future, thus providing new hope for the treatment not only of AIDS but also of other viral diseases.

References

1 Janeway, C.A., Travers, P., Walport, M., and Shlomchik, M. (2005) *Immunobiology: The Immune System in Health and Disease*, Garland Science, New York, NY.

2 UNAIDS/WHO. (2009) AIDS epidemic update 2009. http://data.unaids.org/pub/Report/2009/JC1700_Epi_Update_2009_en.pdf (7 October 2010).

3 De Clercq, E. (2002) New developments in anti-HIV chemotherapy. *Biochim. Biophys. Acta*, **1587** (2–3), 258–275.

4 Palella, F. J. Jr, Delaney, K.M., Moorman, A.C., Loveless, M.O., Fuhrer, J., Satten, G.A., Aschman, D.J., and Holmberg, S.D. (1998) Declining morbidity and mortality among patients with advanced human immunodeficiency virus infection. HIV outpatient study investigators. *N. Engl. J. Med.*, **338** (13), 853–860.

5 Carr, A. (2003) Toxicity of antiretroviral therapy and implications for drug development. *Nat. Rev. Drug Discov.*, **2** (8), 624–634.

6 Eckert, D.M. and Kim, P.S. (2001) Mechanisms of viral membrane fusion and its inhibition. *Annu. Rev. Biochem.*, **70**, 777–810.

7 Center, R.J., Leapman, R.D., Lebowitz, J., Arthur, L.O., Earl, P.L., and Moss, B. (2002) Oligomeric structure of the human immunodeficiency virus type 1 envelope protein on the virion surface. *J. Virol.*, **76** (15), 7863–7867.

8 Chan, D.C. and Kim, P.S. (1998) HIV entry and its inhibition. *Cell*, **93** (5), 681–684.

9 Wyatt, R. and Sodroski, J. (1998) The HIV-1 envelope glycoproteins: fusogens, antigens, and immunogens. *Science*, **280** (5371), 1884–1888.

10 Tamm, L.K. and Han, X. (2000) Viral fusion peptides: a tool set to disrupt and connect biological membranes. *Biosci. Rep.*, **20** (6), 501–518.

11 Chambers, P., Pringle, C.R., and Easton, A.J. (1990) Heptad repeat sequences are located adjacent to hydrophobic regions in several types of virus fusion glycoproteins. *J. Gen. Virol.*, **71** (Pt 12), 3075–3080.

12 Lorizate, M., Huarte, N., Saez-Cirion, A., and Nieva, J.L. (2008) Interfacial pre-transmembrane domains in viral proteins promoting membrane fusion and fission. *Biochim. Biophys. Acta*, **1778** (7–8), 1624–1639.

13 Montero, M., van Houten, N.E., Wang, X., and Scott, J.K. (2008) The membrane-proximal external region of the human immunodeficiency virus type 1 envelope: dominant site of antibody neutralization and target for vaccine design. *Microbiol. Mol. Biol. Rev.*, **72** (1), 54–84, table of contents

14 Lu, M., Blacklow, S.C., and Kim, P.S. (1995) A trimeric structural domain of the HIV-1 transmembrane glycoprotein. *Nat. Struct. Biol.*, **2** (12), 1075–1082.

15 Chan, D.C., Fass, D., Berger, J.M., and Kim, P.S. (1997) Core structure of gp41 from the HIV envelope glycoprotein. *Cell*, **89** (2), 263–273.

16 Weissenhorn, W., Dessen, A., Harrison, S.C., Skehel, J.J., and Wiley, D.C. (1997) Atomic structure of the ectodomain from HIV-1 gp41. *Nature*, **387** (6631), 426–430.

17 Maddon, P.J., Dalgleish, A.G., McDougal, J.S., Clapham, P.R., Weiss, R.A., and Axel, R. (1986) The T4 gene encodes the AIDS virus receptor and is expressed in the immune system and the brain. *Cell*, **47** (3), 333–348.

18 Chesebro, B., Buller, R., Portis, J., and Wehrly, K. (1990) Failure of human immunodeficiency virus entry and infection in CD4-positive human brain and skin cells. *J. Virol.*, **64** (1), 215–221.

19 Clapham, P.R., Blanc, D., and Weiss, R.A. (1991) Specific cell surface requirements for the infection of CD4-positive cells by human immunodeficiency virus types 1 and 2 and by Simian immunodeficiency virus. *Virology*, **181** (2), 703–715

20 Briz, V., Poveda, E., and Soriano, V. (2006) HIV entry inhibitors: mechanisms of action and resistance

pathways. *J. Antimicrob. Chemother.*, **57** (4), 619–627.
21 De Clercq, E. (2009) Anti-HIV drugs: 25 compounds approved within 25 years after the discovery of HIV. *Int. J. Antimicrob. Agents*, **33** (4), 307–320.
22 Doms, R.W. and Trono, D. (2000) The plasma membrane as a combat zone in the HIV battlefield. *Genes Dev.*, **14** (21), 2677–2688.
23 Kilby, J.M. and Eron, J.J. (2003) Novel therapies based on mechanisms of HIV-1 cell entry. *N. Engl. J. Med.*, **348** (22), 2228–2238.
24 Robertson, D. (2003) US FDA approves new class of HIV therapeutics. *Nat. Biotechnol.*, **21** (5), 470–471.
25 Kilby, J.M., Hopkins, S., Venetta, T.M., DiMassimo, B., Cloud, G.A., Lee, J.Y., Alldredge, L., Hunter, E., Lambert, D., Bolognesi, D., Matthews, T., Johnson, M.R., Nowak, M.A., Shaw, G.M., and Saag, M.S. (1998) Potent suppression of HIV-1 replication in humans by T-20, a peptide inhibitor of gp41-mediated virus entry. *Nat. Med.*, **4** (11), 1302–1307.
26 Wild, C.T., Shugars, D.C., Greenwell, T. K., McDanal, C.B., and Matthews, T.J. (1994) Peptides corresponding to a predictive alpha-helical domain of human immunodeficiency virus type 1 gp41 are potent inhibitors of virus infection. *Proc. Natl. Acad. Sci. U. S. A.*, **91** (21), 9770–9774.
27 Kilgore, N.R., Salzwedel, K., Reddick, M., Allaway, G.P., and Wild, C.T. (2003) Direct evidence that C-peptide inhibitors of human immunodeficiency virus type 1 entry bind to the gp41 N-helical domain in receptor-activated viral envelope. *J. Virol.*, **77** (13), 7669–7672.
28 Eckert, D.M. and Kim, P.S. (2001) Design of potent inhibitors of HIV-1 entry from the gp41 N-peptide region. *Proc. Natl. Acad. Sci. U. S. A.*, **98** (20), 11187–11192.
29 Naider, F. and Anglister, J. (2009) Peptides in the treatment of AIDS. *Curr. Opin. Struct. Biol.*, **19** (4), 473–482.
30 Wild, C., Dubay, J.W., Greenwell, T., Baird, T. Jr, Oas, T.G., McDanal, C., Hunter, E., and Matthews, T. (1994) Propensity for a leucine zipper-like domain of human immunodeficiency virus type 1 gp41 to form oligomers correlates with a role in virus-induced fusion rather than assembly of the glycoprotein complex. *Proc. Natl. Acad. Sci. U. S. A.*, **91** (26), 12676–12680.
31 Chan, D.C., Chutkowski, C.T., and Kim, P.S. (1998) Evidence that a prominent cavity in the coiled coil of HIV type 1 gp41 is an attractive drug target. *Proc. Natl. Acad. Sci. U. S. A.*, **95** (26), 15613–15617.
32 Chang, D.K. and Hsu, C.S. (2007) Biophysical evidence of two docking sites of the carboxyl heptad repeat region within the amino heptad repeat region of gp41 of human immunodeficiency virus type 1. *Antiviral Res.*, **74** (1), 51–58
33 Otaka, A., Nakamura, M., Nameki, D., Kodama, E., Uchiyama, S., Nakamura, S., Nakano, H., Tamamura, H., Kobayashi, Y., Matsuoka, M., and Fujii, N. (2002) Remodeling of gp41-C34 peptide leads to highly effective inhibitors of the fusion of HIV-1 with target cells. *Angew. Chem. Int. Ed. Engl.*, **41** (16), 2937–2940.
34 Wild, C., Greenwell, T., and Matthews, T. (1993) A synthetic peptide from HIV-1 gp41 is a potent inhibitor of virus-mediated cell-cell fusion. *AIDS Res. Hum. Retroviruses*, **9** (11), 1051–1053.
35 Liu, S., Wu, S., and Jiang, S. (2007) HIV entry inhibitors targeting gp41: from polypeptides to small-molecule compounds. *Curr. Pharm. Des.*, **13** (2), 143–162.
36 Jiang, S., Zhao, Q., and Debnath, A.K. (2002) Peptide and non-peptide HIV fusion inhibitors. *Curr. Pharm. Des.*, **8** (8), 563–580.
37 Liu, S., Jing, W., Cheung, B., Lu, H., Sun, J., Yan, X., Niu, J., Farmar, J., Wu, S., and Jiang, S. (2007) HIV gp41 C-terminal heptad repeat contains multifunctional domains. Relation to mechanisms of action of anti-HIV peptides. *J. Biol. Chem.*, **282** (13), 9612–9620.
38 Liu, S., Lu, H., Niu, J., Xu, Y., Wu, S., and Jiang, S. (2005) Different from the HIV fusion inhibitor C34, the anti-HIV

drug Fuzeon (T-20) inhibits HIV-1 entry by targeting multiple sites in gp41 and gp120. *J. Biol. Chem.*, **280** (12), 11259–11273.

39 Bar, S. and Alizon, M. (2004) Role of the ectodomain of the gp41 transmembrane envelope protein of human immunodeficiency virus type 1 in late steps of the membrane fusion process. *J. Virol.*, **78** (2), 811–820.

40 Veiga, S., Henriques, S., Santos, N.C. and Castanho, M. (2004) Putative role of membranes in the HIV fusion inhibitor enfuvirtide mode of action at the molecular level. *Biochem. J.*, **377** (Pt 1), 107–110

41 Kliger, Y. and Shai, Y. (2000) Inhibition of HIV-1 entry before gp41 folds into its fusion-active conformation. *J. Mol. Biol.*, **295** (2), 163–168.

42 Rimsky, L.T., Shugars, D.C., and Matthews, T.J. (1998) Determinants of human immunodeficiency virus type 1 resistance to gp41-derived inhibitory peptides. *J. Virol.*, **72** (2), 986–993.

43 Ryu, J.R., Jin, B.S., Suh, M.J., Yoo, Y.S., Yoon, S.H., Woo, E.R., and Yu, Y.G. (1999) Two interaction modes of the gp41-derived peptides with gp41 and their correlation with antimembrane fusion activity. *Biochem. Biophys. Res. Commun.*, **265** (3), 625–629.

44 Kliger, Y., Gallo, S.A., Peisajovich, S.G., Munoz-Barroso, I., Avkin, S., Blumenthal, R., and Shai, Y. (2001) Mode of action of an antiviral peptide from HIV-1 Inhibition at a post-lipid mixing stage. *J. Biol. Chem.*, **276** (2), 1391–1397.

45 Munoz-Barroso, I., Salzwedel, K., Hunter, E., and Blumenthal, R. (1999) Role of the membrane-proximal domain in the initial stages of human immunodeficiency virus type 1 envelope glycoprotein-mediated membrane fusion. *J. Virol.*, **73** (7), 6089–6092.

46 Mobley, P.W., Pilpa, R., Brown, C., Waring, A.J., and Gordon, L.M. (2001) Membrane-perturbing domains of HIV type 1 glycoprotein 41. *AIDS Res. Hum. Retroviruses.*, **17** (4), 311–327.

47 Alam, S.M., Paleos, C.A., Liao, H.X., Scearce, R., Robinson, J., and Haynes, B.F. (2004) An inducible HIV type 1 gp41 HR-2 peptide-binding site on HIV type 1 envelope gp120. *AIDS Res. Hum. Retroviruses.*, **20** (8), 836–845.

48 Veiga, A.S., Santos, N.C., and Castanho, M.A. (2006) An insight on the leading HIV entry inhibitors. *Recent. Pat. Antiinfect. Drug Discov.*, **1** (1), 67–73.

49 Eron, J.J., Gulick, R.M., Bartlett, J.A., Merigan, T., Arduino, R., Kilby, J.M., Yangco, B., Diers, A., Drobnes, C., DeMasi, R., Greenberg, M., Melby, T., Raskino, C., Rusnak, P., Zhang, Y., Spence, R., and Miralles, G.D. (2004) Short-term safety and antiretroviral activity of T-1249, a second-generation fusion inhibitor of HIV. *J. Infect. Dis.*, **189** (6), 1075–1083.

50 Lalezari, J.P., Bellos, N.C., Sathasivam, K., Richmond, G.J., Cohen, C.J., Myers, R.A. Jr, Henry, D.H., Raskino, C., Melby, T., Murchison, H., Zhang, Y., Spence, R., Greenberg, M.L., Demasi, R. A., and Miralles, G.D. (2005) T-1249 retains potent antiretroviral activity in patients who had experienced virological failure while on an enfuvirtide-containing treatment regimen. *J. Infect. Dis.*, **191** (7), 1155–1163.

51 Pan, C., Liu, S., and Jiang, S. (2010) HIV-1 gp41 fusion intermediate: a target for HIV therapeutics. *J. Formos. Med. Assoc.*, **109** (2), 94–105.

52 He, Y., Xiao, Y., Song, H., Liang, Q., Ju, D., Chen, X., Lu, H., Jing, W., Jiang, S., and Zhang, L. (2008) Design and evaluation of Sifuvirtide, a novel HIV-1 fusion inhibitor. *J. Biol. Chem.*, **283** (17), 11126–11134.

53 Franquelim, H.G., Loura, L.M., Santos, N.C., and Castanho, M.A. (2008) Sifuvirtide screens rigid membrane surfaces. Establishment of a correlation between efficacy and membrane domain selectivity among HIV fusion inhibitor peptides. *J. Am. Chem. Soc.*, **130** (19), 6215–6223.

54 Franquelim, H.G., Veiga, A.S., Weissmuller, G., Santos, N.C., and Castanho, M.A. (2010) Unravelling the molecular basis of the selectivity of the HIV-1 fusion inhibitor Sifuvirtide towards phosphatidylcholine-rich rigid

membranes. *Biochim. Biophys. Acta*, **1798** (6), 1234–1243.
55 Wang, R.R., Yang, L.M., Wang, Y.H., Pang, W., Tam, S.C., Tien, P., and Zheng, Y.T. (2009) Sifuvirtide, a potent HIV fusion inhibitor peptide. *Biochem. Biophys. Res. Commun.*, **382** (3), 540–544.
56 Judice, J.K., Tom, J.Y., Huang, W., Wrin, T., Vennari, J., Petropoulos, C.J., and McDowell, R.S. (1997) Inhibition of HIV type 1 infectivity by constrained alpha-helical peptides: implications for the viral fusion mechanism. *Proc. Natl. Acad. Sci. U. S. A.*, **94** (25), 13426–13430.
57 Sia, S.K., Carr, P.A., Cochran, A.G., Malashkevich, V.N., and Kim, P.S. (2002) Short constrained peptides that inhibit HIV-1 entry. *Proc. Natl. Acad. Sci. U. S. A.*, **99** (23), 14664–14669.
58 Marqusee, S. and Baldwin, R.L. (1987) Helix stabilization by Glu-... Lys + salt bridges in short peptides of de novo design. *Proc. Natl. Acad. Sci. U. S. A.*, **84** (24), 8898–8902.
59 Nishikawa, H., Nakamura, S., Kodama, E., Ito, S., Kajiwara, K., Izumi, K., Sakagami, Y., Oishi, S., Ohkubo, T., Kobayashi, Y., Otaka, A., Fujii, N., and Matsuoka, M. (2009) Electrostatically constrained alpha-helical peptide inhibits replication of HIV-1 resistant to enfuvirtide. *Int. J. Biochem. Cell Biol.*, **41** (4), 891–899.
60 Oishi, S., Ito, S., Nishikawa, H., Watanabe, K., Tanaka, M., Ohno, H., Izumi, K., Sakagami, Y., Kodama, E., Matsuoka, M., and Fujii, N. (2008) Design of a novel HIV-1 fusion inhibitor that displays a minimal interface for binding affinity. *J. Med. Chem.*, **51** (3), 388–391.
61 Naito, T., Izumi, K., Kodama, E., Sakagami, Y., Kajiwara, K., Nishikawa, H., Watanabe, K., Sarafianos, S.G., Oishi, S., Fujii, N., and Matsuoka, M. (2009) SC29EK, a peptide fusion inhibitor with enhanced alpha-helicity, inhibits replication of human immunodeficiency virus type 1 mutants resistant to enfuvirtide. *Antimicrob. Agents Chemother.*, **53** (3), 1013–1018.
62 Dwyer, J.J., Wilson, K.L., Davison, D.K., Freel, S.A., Seedorff, J.E., Wring, S.A., Tvermoes, N.A., Matthews, T.J., Greenberg, M.L., and Delmedico, M.K. (2007) Design of helical, oligomeric HIV-1 fusion inhibitor peptides with potent activity against enfuvirtide-resistant virus. *Proc. Natl. Acad. Sci. U. S. A.*, **104** (31), 12772–12777.
63 He, Y., Cheng, J., Li, J., Qi, Z., Lu, H., Dong, M., Jiang, S., and Dai, Q. (2008) Identification of a critical motif for the human immunodeficiency virus type 1 (HIV-1) gp41 core structure: implications for designing novel anti-HIV fusion inhibitors. *J. Virol.*, **82** (13), 6349–6358.
64 He, Y., Cheng, J., Lu, H., Li, J., Hu, J., Qi, Z., Liu, Z., Jiang, S., and Dai, Q. (2008) Potent HIV fusion inhibitors against enfuvirtide-resistant HIV-1 strains. *Proc. Natl. Acad. Sci. U. S. A.*, **105** (42), 16332–16337.
65 Trivedi, V.D., Cheng, S.F., Wu, C.W., Karthikeyan, R., Chen, C.J., and Chang, D.K. (2003) The LLSGIV stretch of the N-terminal region of HIV-1 gp41 is critical for binding to a model peptide, T20. *Protein Eng.*, **16** (4), 311–317.
66 Izumi, K., Kodama, E., Shimura, K., Sakagami, Y., Watanabe, K., Ito, S., Watabe, T., Terakawa, Y., Nishikawa, H., Sarafianos, S.G., Kitaura, K., Oishi, S., Fujii, N., and Matsuoka, M. (2009) Design of peptide-based inhibitors for human immunodeficiency virus type 1 strains resistant to T-20. *J. Biol. Chem.*, **284** (8), 4914–4920.
67 Sia, S.K. and Kim, P.S. (2003) Protein grafting of an HIV-1-inhibiting epitope. *Proc. Natl. Acad. Sci. U. S. A.*, **100** (17), 9756–9761.
68 Soonthornsata, B., Tian, Y.S., Utachee, P., Sapsutthipas, S., Isarangkura-na-Ayuthaya, P., Auwanit, W., Takagi, T., Ikuta, K., Sawanpanyalert, P., Kawashita, N., and Kameoka, M. (2010) Design and evaluation of antiretroviral peptides corresponding to the C-terminal heptad repeat region (C-HR) of human immunodeficiency virus type 1 envelope glycoprotein gp41. *Virology*, **405** (1), 157–164.

69 Eckert, D.M., Malashkevich, V.N., Hong, L.H., Carr, P.A., and Kim, P.S. (1999) Inhibiting HIV-1 entry: discovery of D-peptide inhibitors that target the gp41 coiled-coil pocket. *Cell*, **99** (1), 103–115.

70 Welch, B.D., VanDemark, A.P., Heroux, A., Hill, C.P., and Kay, M.S. (2007) Potent D-peptide inhibitors of HIV-1 entry. *Proc. Natl. Acad. Sci. U. S. A.*, **104** (43), 16828–16833.

71 Gaston, F., Granados, G.C., Madurga, S., Rabanal, F., Lakhdar-Ghazal, F., Giralt, E., and Bahraoui, E. (2009) Development and characterization of peptidic fusion inhibitors derived from HIV-1 gp41 with partial D-amino acid substitutions. *ChemMedChem.*, **4** (4), 570–581.

72 Deng, Y., Zheng, Q., Ketas, T.J., Moore, J.P., and Lu, M. (2007) Protein design of a bacterially expressed HIV-1 gp41 fusion inhibitor. *Biochemistry (Mosc.)*., **46** (14), 4360–4369.

73 Hildinger, M., Dittmar, M.T., Schult-Dietrich, P., Fehse, B., Schnierle, B.S., Thaler, S., Stiegler, G., Welker, R., and von Laer, D. (2001) Membrane-anchored peptide inhibits human immunodeficiency virus entry. *J. Virol.*, **75** (6), 3038–3042.

74 Peisajovich, S.G., Gallo, S.A., Blumenthal, R., and Shai, Y. (2003) C-terminal octylation rescues an inactive T20 mutant: implications for the mechanism of HIV/SIMIAN immunodeficiency virus-induced membrane fusion. *J. Biol. Chem.*, **278** (23), 21012–21017.

75 Wexler-Cohen, Y. and Shai, Y. (2007) Demonstrating the C-terminal boundary of the HIV 1 fusion conformation in a dynamic ongoing fusion process and implication for fusion inhibition. *FASEB J.*, **21** (13), 3677–3684.

76 Zhang, H.Y., Schneider, S.E., Bray, B.L., Friedrich, P.E., Tvermoes, N.A., Mader, C.J., Whight, S.R., Niemi, T.E., Silinski, P., Picking, T., Warren, M., and Wrings, S.A. (2008) Process development of TRI-999, a fatty-acid-modified HIV fusion inhibitory peptide. *Org. Process Res. Dev.*, **12** (1), 101–110

77 Stanfield-Oakley, S.A., Mosier, S.M., Davison, D.K., Medinas, R.J., Jin, L., Delmedico, M.K., Dwyer, J.J., Heilek-Snyder, G., and Greenberg, M.L. (2006) Next generation HIV peptide fusion inhibitors TRI-999 and TRI-1144 display enhanced activity against enfuvirtide sensitive and resistant viruses. *Antivir. Ther.*, **11** (5), S25–S25.

78 Ingallinella, P., Bianchi, E., Ladwa, N.A., Wang, Y.J., Hrin, R., Veneziano, M., Bonelli, F., Ketas, T.J., Moore, J.P., Miller, M.D., and Pessi, A. (2009) Addition of a cholesterol group to an HIV-1 peptide fusion inhibitor dramatically increases its antiviral potency. *Proc. Natl. Acad. Sci. U. S. A.*, **106** (14), 5801–5806.

79 Porotto, M., Yokoyama, C.C., Palermo, L.M., Mungall, B., Aljofan, M., Cortese, R., Pessi, A., and Moscona, A. (2010) Viral entry inhibitors targeted to the membrane site of action. *J. Virol.*, **84** (13), 6760–6768.

80 Stoddart, C.A., Nault, G., Galkina, S.A., Thibaudeau, K., Bakis, P., Bousquet-Gagnon, N., Robitaille, M., Bellomo, M., Paradis, V., Liscourt, P., Lobach, A., Rivard, M.E., Ptak, R.G., Mankowski, M.K., Bridon, D., and Quraishi, O. (2008) Albumin-conjugated C34 peptide HIV-1 fusion inhibitor: equipotent to C34 and T-20 *in vitro* with sustained activity in SCID-hu Thy/Liv mice. *J. Biol. Chem.*, **283** (49), 34045–34052.

81 Xie, D., Yao, C., Wang, L., Min, W., Xu, J., Xiao, J., Huang, M., Chen, B., Liu, B., Li, X., and Jiang, H. (2010) An albumin-conjugated peptide exhibits potent anti-HIV activity and long *in vivo* half-life. *Antimicrob. Agents Chemother.*, **54** (1), 191–196.

82 Ji, C., Kopetzki, E., Jekle, A., Stubenrauch, K.G., Liu, X., Zhang, J., Rao, E., Schlothauer, T., Fischer, S., Cammack, N., Heilek, G., Ries, S., and Sankuratri, S. (2009) CD4-anchoring HIV-1 fusion inhibitor with enhanced potency and *in vivo* stability. *J. Biol. Chem.*, **284** (8), 5175–5185.

83 Baldwin, C. and Berkhout, B. (2007) HIV-1 drug-resistance and drug-dependence. *Retrovirology*, **4**, 78.

84 Bai, X., Wilson, K.L., Seedorff, J.E., Ahrens, D., Green, J., Davison, D.K., Jin, L., Stanfield-Oakley, S.A., Mosier, S.M., Melby, T.E., Cammack, N., Wang, Z., Greenberg, M.L., and Dwyer, J.J. (2008) Impact of the enfuvirtide resistance mutation N43D and the associated baseline polymorphism E137K on peptide sensitivity and six-helix bundle structure. *Biochemistry (Mosc.)*, **47** (25), 6662–6670.

85 Tolstrup, M., Selzer-Plon, J., Laursen, A. L., Bertelsen, L., Gerstoft, J., Duch, M., Pedersen, F.S., and Ostergaard, L. (2007) Full fusion competence rescue of the enfuvirtide resistant HIV-1 gp41 genotype (43D) by a prevalent polymorphism (137K). *AIDS*, **21** (4), 519–521.

86 Nagashima, K.A., Thompson, D.A., Rosenfield, S.I., Maddon, P.J., Dragic, T., and Olson, W.C. (2001) Human immunodeficiency virus type 1 entry inhibitors PRO 542 and T-20 are potently synergistic in blocking virus-cell and cell-cell fusion. *J. Infect. Dis.*, **183** (7), 1121–1125.

87 Tremblay, C.L., Giguel, F., Kollmann, C., Guan, Y., Chou, T.C., Baroudy, B.M., and Hirsch, M.S. (2002) Anti-human immunodeficiency virus interactions of SCH-C (SCH 351125), a CCR5 antagonist, with other antiretroviral agents *in vitro*. *Antimicrob. Agents Chemother.*, **46** (5), 1336–1339.

88 Tremblay, C.L., Kollmann, C., Giguel, F., Chou, T.C., and Hirsch, M.S. (2000) Strong *in vitro* synergy between the fusion inhibitor T-20 and the CXCR4 blocker AMD-3100. *J. Acquir. Immune Defic. Syndr.*, **25** (2), 99–102.

89 Hrin, R., Montgomery, D.L., Wang, F., Condra, J.H., An, Z., Strohl, W.R., Bianchi, E., Pessi, A., Joyce, J.G., and Wang, Y.J. (2008) Short communication: *in vitro* synergy between peptides or neutralizing antibodies targeting the N- and C-terminal heptad repeats of HIV type 1 gp41. *AIDS Res. Hum. Retroviruses*, **24** (12), 1537–1544.

90 Pan, C., Lu, H., Qi, Z., and Jiang, S. (2009) Synergistic efficacy of combination of enfuvirtide and sifuvirtide, the first- and next-generation HIV-fusion inhibitors. *AIDS*, **23** (5), 639–641.

91 Pan, C., Cai, L., Lu, H., Qi, Z., and Jiang, S. (2009) Combinations of the first and next generations of human immunodeficiency virus (HIV) fusion inhibitors exhibit a highly potent synergistic effect against enfuvirtide-sensitive and -resistant HIV type 1 strains. *J. Virol.*, **83** (16), 7862–7872.

Review Article A

Declaration of authorship

I, Pedro Miguel Baptista de Matos, declare that the manuscript preparation and writing was carried out by me, Dr. Sónia Gonçalves and Prof. Nuno S. Santos.

I, Nuno C. Santos, as supervisor of Pedro Matos and as corresponding author of the article mentioned above, hereby acknowledge and confirm that the information above is correct.

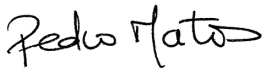

Pedro M. Matos

Nuno C. Santos

Journal of Peptide Science
J. Pept. Sci. 2008; **14**: 407–415
Published online 14 January 2008 in Wiley InterScience (www.interscience.wiley.com). DOI: 10.1002/psc.1005

JOURNAL OF PEPTIDE SCIENCE

Review

Interaction of peptides with biomembranes assessed by potential-sensitive fluorescent probes‡

PEDRO M. MATOS, SÓNIA GONÇALVES and NUNO C. SANTOS*

Instituto de Medicina Molecular, Faculdade de Medicina da Universidade de Lisboa, Av. Prof. Egas Moniz, 1649-028 Lisboa, Portugal

Received 30 June 2007; Revised 31 October 2007; Accepted 16 November 2007

Abstract: Peptide–membrane interaction is an important step to be evaluated in a study of the activity and mode of action of several bioactive peptides. A variety of methods are available; however, few of them satisfy the criteria of being sensitive, biocompatible, versatile, easy to perform, and allowing real-time monitoring as the use of potential-sensitive fluorescent probes. Here we review methods for detecting the effects of membrane-active peptides, even those that are not intrinsically fluorescent, on the different types of membrane potentials, with a special emphasis on studies conducted with living cells. FPE is a probe sensitive to surface potential and detects electrostatic interactions at the water-lipid interface. Di-8-ANEPPS is sensitive to dipole potential and detects membrane incorporations. Transmembrane potential changes reveal major membrane destabilizations, such as in pore formation. The combination of the information obtained from the three potential variations can lead to a more elucidative picture of the mechanisms of the interaction of relevant peptides with biomembranes. Copyright © 2008 European Peptide Society and John Wiley & Sons, Ltd.

Keywords: biomembranes; bioactive peptides; fluorescent probes; surface potential; dipole potential; transmembrane potential

INTRODUCTION

The cell membrane is the interface between the cytoplasm and the outer environment, where all the exchanges and interactions take place, allowing cells to obtain nutrients and energy, export, attach, communicate and sense, with the aid of a myriad membrane-associated proteins. The numerous roles of membranes are indicative of its extraordinary functional flexibility.

Interaction of peptides with lipid bilayers, either cell membranes or artificial vesicles, is an expanding research field, as peptides are a very versatile and heterogeneous group of molecules. Depending on the peptide sequence, charge, hydrophobicity and secondary structure, it can be prone to interact with lipid bilayers by simple electrostatic surface interaction, incorporation due to the hydrophobic effect, translocation or pore formation. All of this brings consequences for membrane structure, namely on lipid organization and packaging, induction of events such as fusion, aggregation or content leakage.

Measuring these types of interactions can help to unveil the mode of action of these membrane-active peptides. These studies are particularly important in drug research, where interaction with membrane lipids can determine the drug effects, delivery, and bioavailability [1,2]. Even for peptides whose targets are membrane proteins, the membrane can act as a catalyst in the reaction, the so-called 'membrane catalysis model', as it is much more probable that the peptide establishes contact first with the membrane and not directly with the receptor [3]. Studies on peptides can also serve as a simple model to understand interactions at higher levels of complexity, such as the interaction of proteins with the membrane [4].

Fluorescence methods are very sensitive, relatively simple to perform and can provide reliable results. In the specific case of the use of simple mimetic systems of biological membranes (lipid vesicles) and if the peptide have intrinsic fluorescent amino acid residues, especially tryptophan, the peptide–membrane binding can be followed by fluorescence spectroscopy due to microenvironment induced changes on quantum yields, spectral changes, fluorescence anisotropy or fluorescence lifetimes of these residues [5]. However, this technique is not suitable for peptides lacking fluorescent aminoacid residues and/or if we want to study the interaction with biomembranes, where other proteic components are already present. In order to face these limitations, alternative strategies were developed to indirectly measure peptide interactions with membranes. This can be achieved by monitoring the effects of these interactions on the different types of membrane potentials, using membrane incorporated fluorescent

* Correspondence to: Nuno C. Santos, Unidade de Biomembranas, Instituto de Medicina Molecular, Faculdade de Medicina da Universidade de Lisboa, Av. Prof. Egas Moniz, 1649-028 Lisboa, Portugal; e-mail: nsantos@fm.ul.pt

‡ This article is part of the Special Issue of the Journal of Peptide Science entitled "2nd workshop on biophysics of membrane-active peptides".

BIOGRAPHIES

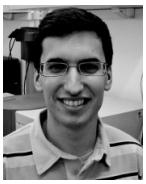

Pedro Miguel Matos was born in Batalha, Portugal, in 1985. He graduated in Biochemistry, in 2007, at the Faculty of Sciences, University of Lisbon. His present research comprises the application of biophysical approaches such as fluorescence spectroscopy to understand the action of HIV fusion inhibitor peptides at the cell membrane level. He is heading towards his doctoral studies, focused on viral entry mechanisms, in the Institute of Molecular Medicine (Lisbon, Portugal).

Sónia Gonçalves was born in Caracas, Venezuela, in 1972. She graduated in Chemistry at the Central University of Venezuela, in 1998, and obtained her Ph.D in Physical Chemistry from the same University, in 2002. She worked as researcher at the Laser Spectroscopy Laboratory (Caracas, Venezuela). Currently, she is working as Assistant Researcher in the Biophysics area, with medical applications, at the Faculty of Medicine, University of Lisbon (Portugal). Her research interests mainly comprise the resolution of problems related with the interaction of proteins with membranes by the application of spectroscopic techniques, such as fluorescence, light scattering, and reflectometric interference (biochip technology).

Nuno C. Santos was born in Lisbon, Portugal, in 1972. Lipid membranes have been the common element of his research specialization since 1994. After a majoring in Biochemistry, Nuno C. Santos conducted his Ph.D. research work in the Technical University of Lisbon (Portugal) and in the University of California at Santa Barbara (USA). He completed his Ph.D. in 1999, and joined the Faculty of Medicine of the University of Lisbon as Assistant Professor. He is now also Principle Investigator at the Institute of Molecular Medicine (Lisbon, Portugal). His research is focused on the following: (i) structural characterization of biomolecules and interaction with lipid membranes, using fluorescence spectroscopy, light scattering and AFM; (ii) viral fusion and assembly; (iii) LPS-binding protein-derived drugs; and (iv) nanomedicine.

probes. This is a minimally invasive method and avoids the necessity of peptide derivatization, which modifies its native structure and can potentially lead to biased results.

In this article, we will focus on methods for measuring the interaction of peptides with membrane-model systems and cell membranes based on the use of fluorescent dyes that are sensitive to different types of membrane potential, namely, surface, dipole and transmembrane potentials.

SURFACE POTENTIAL

The surface potential arises from the net excess charges that accumulate in the outer surface of the membrane, in contact with the external medium (Figure 1). It is therefore the potential difference between the membrane surface and the bulk medium. The sources of these charges are mainly charged lipid head-groups and ions electrostatically interacting with them [6–8]. Any interaction of a charged entity with the membrane surface is likely to alter the surface potential and hence it is susceptible to be detected by a fluorescent probe.

Fluorescein phosphatidylethanolamine (FPE) is a probe sensitive to surface potential (Figure 2) [9]. It was first used to measure pH changes in the internal compartment of lipid vesicles due to the variation of its quantum yield with the protonation state of the fluorescein (increased fluorescence with increased deprotonation) [10]. Later it was described more generically for the measure of pH at the water/lipid interface [11], a property that permits, for instance, the assessment of a proton pump activity [12,13]. During these experiments it was realized that changes in the medium ionic strength could compromise the pH measurements, which led to studies concerning the

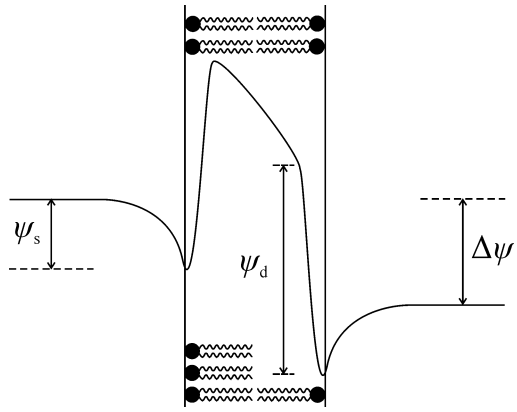

Figure 1 Electrical potential profile across a phospholipid bilayer. The surface potential (ψ_s) arises from charge accumulation at the membrane surface, the dipole potential (ψ_d) is a consequence of the alignment and distribution of lipid and water dipoles, and the difference in charge concentration in the two bulk mediums separated by the membrane constitutes the transmembrane potential ($\Delta\psi$).

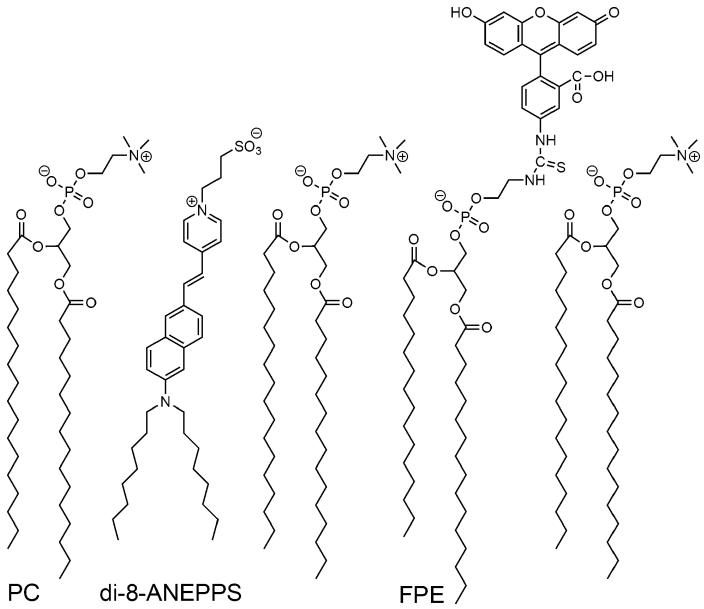

Figure 2 Structures of the membrane potential probes FPE and di-8-ANEPPS, incorporated in a phosphatidylcholine membrane leaflet.

effect of peptides in lipid membrane surface potentials [9].

When incorporated into lipid membranes, the fluorescein moiety of this probe stands precisely in the water–lipid interface, and hence it has the ability to detect pH or charge distribution changes at the membrane surface [9]. FPE behavior can be explained by the Handersen–Hasselbach equation, taking into account the surface potential [14]:

$$\log\left(\frac{c_F}{c_{HF}}\right) = \mathrm{pH} - \left(\mathrm{p}K - \frac{F\psi_s}{RT\ln 10}\right) \qquad (1)$$

where c_F and c_{HF} are the concentrations of the dissociated and protonated forms, respectively, of the fluorophore located at the membrane surface, and the expression $\mathrm{p}K - F\psi_s/(RT\ln 10)$ is the apparent pK, where ψ_s is the surface potential. It can be easily understood that for the fluorescein moiety of FPE, standing at the membrane surface, changes in the surface potential at constant bulk phase pH, will affect its apparent pK and consequently, its protonation state, resulting in changes in the quantum yield [9,15]. The simplest test to verify the correct incorporation and responsiveness of FPE in vesicles or cells is the addition of calcium ions to the medium, which will lead to an increased surface potential and consequently decreased fluorescein apparent pK, increased deprotonation, and increased fluorescence intensity [9]. A possible interference factor is the adsorption of proteins, which may change the dielectric constant in the vicinity of the fluorescent probe, so that fluorescence changes may not only reflect surface potential alterations.

The first experiments that used FPE to assess peptide–membrane interactions were done with phospholipid vesicles and involved the study of the peptides pyrularia thionin (PT), CTX (*Naja naja kaouthia* cardiotoxin), p25 (leader peptide of subunit IV of cytochrome *c* oxidase) and melittin, known to be membrane-active [9]. FPE was characterized in terms of its fluorescence spectra in phospholipid vesicles and pH titrations were done to determine the pK_{app} in different ionic conditions. The correct incorporation of FPE in the outer leaflet of the vesicles was tested. PT and CTX were shown to interact with phosphatidylcholine/phosphatidylserine (PC/PS) phospholipid vesicles, as addition of each peptide caused an increase in the fluorescence of membrane-bound FPE. Melittin and p25 had a slightly different behavior: they also caused an increase in the fluorescence intensity upon addition (increase in electropositivity of the membrane surface) but followed by a slow decrease until saturation (Figure 3). This biphasic interaction was more clearly observed using a stopped-flow rapid mixing technique, as it allowed resolving of the initial fluorescence increase in the millisecond time-scale. The final decrease can be explained by the insertion of regions of the peptides, or even its translocation, placing the positive charges away from the membrane surface, no longer affecting its potential. Melittin has a short hydrophobic *N*-terminal helix bearing two positive charges (in a total of six) that can insert into the

DOI: 10.1002/psc

lipid bilayer [16]. This is in agreement with the results mentioned above [9], because the extent of the signal decrease following the insertion event is approximately 1/3 of the initial change, as stated by the original authors. For the case of p25, it has been reported that the *N*-terminal region of the peptide, containing positive charged aminoacid residues, inserts into the lipid bilayer with its axis perpendicular to the membrane surface [17]. Pore-formation and peptide translocation, which can also explain the decreased number of positive charges in contact with the surface upon peptide-membrane interaction, have actually been reported for melittin [18], and can be advanced as a hypothesis for the case of p25. Titrating FPE-labeled PC/PS vesicles with p25 held a hyperbolic binding curve with an approximate half saturation point of 4 μM.

A more systematic study of the interaction of p25 with membrane vesicles was done later [19]. Relying on the stopped-flow technique, fluorescence changes were recorded over time and the dependence of fluorescence change with the p25 concentration was found to be described by a cooperative model (sigmoidal curve). It was the first time that a cooperative behavior was identified in a signal-sequence peptide and denotes the complexity of peptide–membrane interactions.

FPE labeling of living cells is also possible and was done, for the first time, with erythrocytes and lymphocytes [15]. Systematic studies for B-lymphocytes were carried out with BSA. Serial additions of this protein caused a decrease in fluorescence intensity, as expected, considering BSA negative net charge at the pH of the experiment (pH 7.5). Changes on fluorescence upon BSA addition were plotted and analyzed according to a single binding site model, resulting in a K_d of 2.85 ± 0.48 μM (Figure 4). The choice of this specific fitting model can be controversial. However this does not imply that there is only one possible molecular explanation for the process. The majority of the peptide–membrane interactions actually follow a simple water–membrane partition [5] but this cannot be quantified directly by these methods. For assessing the response of FPE to protein–ligand interactions at the membrane level, assays were done using MHC class II monoclonal antibodies and a fluorescence decrease was observed. By the opposite, testing with an antibody that lacks binding site in B-lymphocyte membranes, GaM-IgG, showed no alterations in fluorescence. For studying peptide interactions with FPE-labeled erythrocyte membrane, melittin, poly-L-lysine, and BSA were chosen. The first two macromolecules, being positive at the pH of the experiments, should increase membrane-bound FPE fluorescence. However, the opposite was observed instead. Only when FPE-labeled erythrocytes were previously treated with neuraminidase, the expected fluorescence increases were observed. It seems that for the specific case of erythrocytes, the abundant negatively charged sialic acid residues of membrane glycoproteins affects the response of FPE. It can be speculated that binding of melittin or poly-L-lysine to these moieties may alter its organization and disposition in such a way that their influence on the microenvironment on the close vicinity of the membrane surface would change the FPE response, explaining the decrease in fluorescence.

HIV-1 infection of T-lymphocytes involves the interaction of its membrane glycoprotein gp120 with CD4 receptors and co-receptors. When that happens, gp41 is exposed and its fusion peptide domain is inserted in the target cell membrane [20]. The interaction of this 16 residues gp41 fusion peptide ($gp41_{FP}$) with

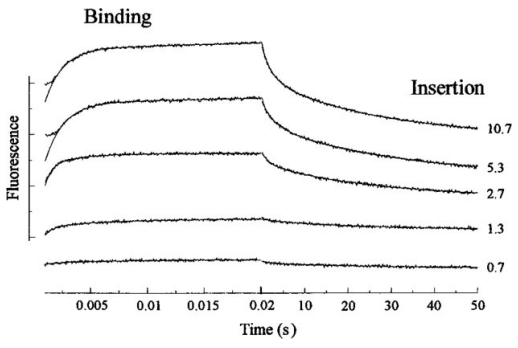

Figure 3 Time-course variation of FPE-labeled PC vesicles fluorescence during mixing with p25 at the concentrations (μM) indicated in each trace. Traces were offset for clarity and for each one, two experimental traces were combined covering time periods with different scales. Reprinted with permission from [19]. Copyright 1996 American Chemical Society.

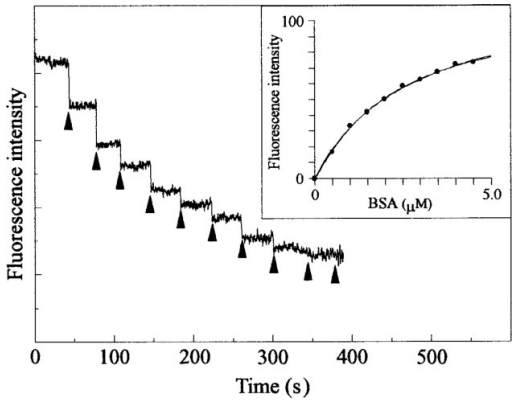

Figure 4 Effect of serial additions of BSA on the fluorescence of FPE-labeled B-lymphocytes. Fluorescence decreases over time as BSA has a net negative charge at pH of the assay (7.5). The inset represents the absolute fluorescence changes as a function of BSA concentration, in which solid lines represent the fittings to a single binding site and a cooperative model [15]. Reproduced with permission of the Company of Biologists.

T-lymphocyte membranes was assessed using FPE [21]. Assays with FPE-labeled PC vesicles show increased fluorescence in the presence of this peptide and a cooperative behavior on the variation of fluorescence with peptide concentration. These results were confirmed using Jurkat T-lymphocytes. Moreover, the effects of interleukin 8 (IL-8), heparitinase, heparin, and heparan sulfate were also investigated. The presence of IL-8 or heparan sulfate in soluble forms, or treatment of the cells with heparitinase, significantly decreased the interaction between the peptide and the cell membrane. Heparin apparently affects the interactions in a much lower extent. These results indicate that $gp41_{FP}$ interacts specifically with heparan sulfate in the cell surface, revealing that the latter may have an important role in the virus attachment to the cell and subsequent membrane fusion.

FPE was also used to study the interaction between fibronectin, an extracellular matrix protein, and the osteoblast membranes [22]. The variation profile of the fluorescence against fibronectin concentration followed a single binding site hyperbolic model, yielding an affinity constant of 120 nM. Treating osteoblasts with heparitinase reduced the binding capacity of fibronectin to almost 50%. In the presence of the RGD peptide, which sequence is involved in the binding of fibronectin to integrin α5b1, the binding capacity is also reduced, but at a lesser extent. Cell-surface proteoglycans are then an essential way by which fibronectin binds to the osteoblast membrane and not only to the integrins.

The versatility of FPE extends also to prokaryotic cells. A successful labeling of *Escherichia coli* and *Helicobacter pylori* was reported, after inactivation with heat or UV light [23]. Although requiring some optimizations, the authors managed to obtain an adequate response with calcium ions and poly-L-lysine. The interaction of the VacA (*H. pylori* vacuolating toxin) p37 subunit with *H. pylori* membrane was studied and a K_d value of 1.7 nM was obtained by a cooperative binding model. The interaction of this peptide with FPE-labeled PC/PS vesicles (model system of eukaryotic cell membranes) was also studied [23], showing a much lower affinity. This indicates that the preferential interaction of p37 with the bacterial membrane can be due to its particular lipid composition or to the existence of a specific receptor.

DIPOLE POTENTIAL

The dipole potential of lipid membranes, or alterations to it, can also reveal interactions at the membrane level. This type of potential originates from the alignment of dipolar residues of lipids (polar headgroups and glycerol–ester regions) and oriented water molecules hydrating the outer surface of the membrane (Figure 1) [24,25]. Various methods are described to measure dipole potentials in planar lipid bilayers and lipid vesicles [26]. In terms of lipid vesicles and cells, the easier to use, the most biocompatible and allowing real-time monitoring and imaging is the method using voltage-sensitive fluorescent dyes. Such dyes are di-8-ANEPPS (4-[2-[6-(dioctylamino)-2-naphthalenyl]ethenyl]-1-(3-sulfopropyl)-pyridinium) (Figure 2) [27] and RH421 (N-(4-sulfobutyl)-4-[4-[4-(dipentylamino)phenyl]butadienyl]-pyridinium) [28]. Beside the aliphatic chains, these probes possess a conjugated structure (the chromophore region), therefore providing an extensive degree of electron delocalization, a reason for its fluorescence and relatively high stokes shift. They incorporate in the outer leaflet of the membranes and the chromophore group stays near the lipid head-group region, sensing the local electric field derived from the dipoles [27]. The mechanism by which di-8-ANEPPS, and RH421 and other aminostyry1pyridinium dyes operate in order to sense dipole potential is believed to be electrochromic [29]. Absorption and emission peaks shift in response to a nearby electrical field that differentially interacts with the ground-state and excited-state dipole moments of the chromophore [30,31]. Therefore these kinds of probes suggest a dual wavelength ratiometric measurements strategy, similar to what is done with some ion indicators, such as for Ca^{2+} [32]. This approach has several advantages because the signal is independent of probe or cell concentration and avoids photobleaching artifacts [27].

Emphasis will be put in di-8-ANEPPS, the most used dye for dipole potential measurement. Although the vast majority of the work with di-8-ANEPPS relies on the excitation spectrum shift to measure dipole potential, only recently a systematic study was done to compare excitation and emission ratiometric fluorescence methods for this dye, concluding that only the former can be used [33]. Membrane fluidity is another aspect for concern and has been addressed in previous papers. Gross *et al.* [27] states that membrane microviscosity does not significantly influence the fluorescence excitation ratio and Clarke and Kane [34] suggested that in order to eliminate the possible effects of membrane fluidity, fluorescence should be detected at the red-edge of the emission spectra, at 670 nm. It is also relevant to refer that the use of a fluorescent probe is not the most adequate method to measure absolute values of dipole potential, mainly because a rigorous calibration method has not been established yet. An equation for converting fluorescence excitation ratio to voltage is available [35], but is based on potential values calculated on previous and distinct papers, by different methods. However, in the presented cases, the use of absolute values of dipole potential is not relevant.

The influence of dipole potential on p25 interaction with lipid vesicles was studied with di-8-ANEPPS along

with the above-mentioned FPE measurements for surface potential [36]. In the presence of p25, the dipole potential of di-8-ANEPPS labeled PC vesicles decreased, as indicated by the decrease of the ratio of the fluorescence intensities at two excitation wavelengths, 460 and 520 nm, for the same emission wavelength of 580 nm, with the increase of peptide concentration. The dipole potential of PC vesicles was also manipulated adding phloretin and 6-ketocholestanol (6-KC), previously known to decrease and increase the dipole potential, respectively [27,37]. The results showed that the larger the initial dipole potential, the larger is its decrease caused by the interaction of the peptide with the membrane (Figure 5). Kinetic studies using stopped-flow technique and the comparison with the kinetic results obtained from FPE experiments also led to the conclusion that the decrease in dipole potential occurs when the peptide inserts into the membrane rather than during the initial binding event.

A similar study was done for assessing the interaction between the fusion peptide from simian immunodeficiency virus (SIV) gp32 with phosphatidylcholine/phosphatidylethanolamine (PC/PE) vesicles [38]. Addition of the SIV fusion peptide to the vesicles suspension caused a decrease in the dipole potential, and the larger the initial dipole potential, the larger the magnitude of the decrease, as for p25. The influence of the magnitude of the dipole potential in the peptide-dependent membrane fusion was assessed by a fluorescence resonance energy transfer (FRET) based

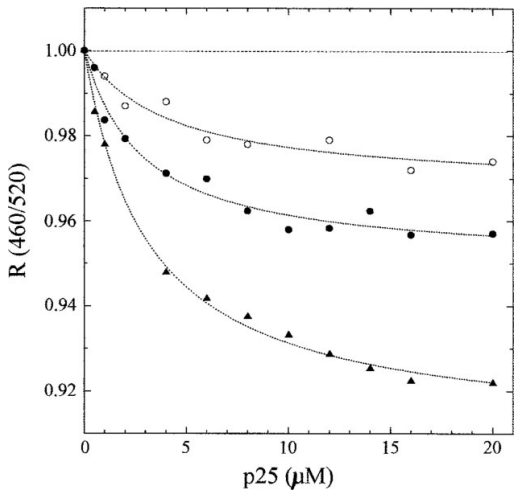

Figure 5 Variation of the ratio of the di-8-ANEPPS fluorescence intensities at two excitation wavelengths, 460 and 520 nm, R(460/520), as a function of p25 concentration. The emission wavelength was kept at 580 nm. Each trace refers to a different vesicle composition: ●, pure PC vesicles; ○, phloretin-enriched PC vesicles; ▲, 6-KC enriched PC vesicles [36]. Reproduced with permission of the Biophysical Society.

lipid-mixing fusion assay. It was clearly demonstrated that increasing dipole potential with 6-KC enhanced the fusion process and the opposite was true for phloretin. The HIV-1 gp41 fusion peptide interaction with PC/PE vesicles was also studies with FPE and di-8-ANEPPS [39]. Apart from demonstrating once again that 6-KC and, at a lesser extent, cholesterol increases membrane dipole potential, the authors related the K_d derived from FPE kinetic studies with the dipole potential of vesicles with different cholesterol/6-KC compositions. The fusion peptide had a higher affinity for membranes with higher dipole potential. As a high-dipole potential enhances fusion and cholesterol has an increased proportion on SIV and HIV membrane [40,41], the results of these two studies shed some light on the importance of membrane lipid composition for the infectivity of SIV/HIV.

The modulation of membrane dipole potential can bring new possibilities in the drug delivery research area. With this in mind two different studies are presented involving the drugs saquinavir and bacitracin.

Saquinavir is a peptidomimetic inhibitor of HIV protease and its interaction with Caco-2 cell membrane was studied [42]. The human intestinal epithelial cell line Caco-2 is often used to assess intestinal permeability of drugs [43]. The shift in the excitation spectra of di-8-ANEPPS, indicative of alterations in the dipole potential, revealed that saquinavir decreases this potential when binding to Caco-2 cell membranes and, at a lower extent, to PC/PS vesicles. Analyzing the dependence of the ratio with the saquinavir concentration, it was shown that for Caco-2 cells the data followed a cooperative binding profile, in contrast with the results obtained for vesicles, which followed a hyperbolic single binding site model. This is indicative that a receptor-mediated process may take place besides the membrane binding *per se*, as it is known to be a substrate of the P-glycoprotein, the product of *MDR1* gene [44]. Membrane dipole potentials were modulated by 6-KC or phloretin, yielding a larger decrease of the fluorescence ratio for 6-KC, both for Caco-2 and lipid vesicles. Moreover, the binding capacity of saquinavir for cholesterol depleted cell membranes was also assessed and found to be decreased relative to normal ones. It is shown that increasing membrane dipole potential enhances saquinavir binding to Caco-2 cells. Such dipole potential modulation can be a strategy to increase intestinal absorption.

The interaction of bacitracin with PC vesicles was studied in the context of enhancing the transdermal delivery of this cyclic peptide antibiotic [45]. The red shift in the excitation spectra of di-8-ANEPPS labeled vesicles showed that bacitracin binding decreases the membrane dipole potential. With 6-KC enriched vesicles, the dipole potential decreased at a higher extent in the presence of bacitracin. The opposite

DOI: 10.1002/psc

effect was observed for phloretin. The variation of the surface potential over time was also measured using FPE, upon adding bacitracin to PC vesicles suspension. Those enriched with 6-KC yielded an increased signal. All these studies were done to help to interpret the initial experiment in which FITC-labeled bacitracin penetrated more deeply in epidermis pretreated with 6-KC-enriched PC vesicles, as visualized by confocal microscopy. The more efficient binding of bacitracin to 6-KC enriched membranes suggests a new and more efficient way of delivering this peptide for the treatment of skin infections.

Although di-8-ANEPPS has been the most used probe for measuring dipole potential, recently developed probes based on the 3-hydroxyflavone fluorescent moiety promise better detection [46]. The probes F4N1 and BPPZ were synthesized and tested for their ability to sense dipole potential. These probes have the particularity of undergoing excited-state intramolecular proton-transfer (ESIPT), yielding two tautomeric forms, revealed by the presence of two emission peaks in the fluorescence spectrum. The presence of a nearby electrical field not only originates a shift in the absorption and emission bands, but also alters the intensity ratio of the two emission peaks. These two types of ratios, using two wavelengths at each side of the excitation band and using the two emission peaks, correlated well with the typical excitation ratio used for di-8-ANEPPS. The fact that emission ratios can be used facilitates fluorescence microscopy imaging of the dipole potential in membranes, as for a single excitation wavelength the emission of the probes can be collected on two separate detectors at the same time. This is a very useful approach for visualizing dipole potential distribution in membranes of living cells [47].

TRANSMEMBRANE POTENTIAL

The last member of the membrane potential club is the transmembrane potential. As it is the most well-known and well-studied type of potential, just a contextualization in this case will be given. In simple terms, it is defined as the potential difference between the intra and extracellular aqueous phases (Figure 1). This is a consequence of the selective nature of the membrane, that allows the flux of specific charged solutes (e.g. ions), creating a concentration gradient.

Measuring the transmembrane potential in a context of a peptide–membrane interaction is especially important for antimicrobial peptides, which usually form pores or channels in membranes, enabling the dissipation of an established potential, or for cell-penetrating peptides, whose mode of action may depend on this potential [48,49]. In fact, membrane potential tests are routinely used to assay the membrane potential alterations that occur when these types of peptides are added to a vesicle or cell suspension. There are several fluorescent dyes available for the detection of transmembrane potential alterations, from slow response carbocyanines (DiI, DiS, and DiO derivatives) and oxonols (DiBAC and DiSBAC) to fast response styryl dyes (ANEP and RH dyes) [50].

The majority of the studies test the ability of a certain peptide to alter the transmembrane potential in vesicles or even bacteria, using slow-response dyes. In vesicles, a transmembrane potential is achieved by adding valinomycin to vesicles prepared in a KCl buffer and suspended in NaCl buffer. Some peptides are able to dissipate the potential [51–53] while others simply do not [54], depending on the degree of membrane disruption. Moreover, monitoring transmembrane potential of bacteria when they are exposed to antimicrobial peptides often reveals membrane depolarization [55–57].

CONCLUDING REMARKS

There is no doubt that when certain peptides have the ability to interact with membranes they alter some of their properties, and membranes potentials are no exception. For the three types of membrane potential, there are different types of fluorescent dyes capable of measuring each of them. This is an advantage, as it permits the establishment of similar protocols, based on the same concept of fluorescent dye detection, in order to build a combined study, with readily comparable results. Such combined studies, involving the different membrane potentials, permit a wider vision of what is happening at the membrane level when certain peptides are present.

Alterations in surface potential sensed by FPE can reveal the very first electrostatic binding events at the membrane surface and even peptide insertion or translocation. Di-8-ANEPPS is the most used probe for measuring dipole potential and allows the monitoring of insertion events, as these tend to change the disposition of the molecular dipoles of membrane phospholipids. It has the advantage of being sensitive to uncharged molecules. A study of the effect of transmembrane potential is important to find out if a more extensive disruption is made on the membrane by the peptide, such as pore or channel formation.

These tools, although available for a while, can be more extensively explored, especially in the context of *in vivo* environments, in conjunction also with fluorescence imaging and real-time observation of the interaction events.

Acknowledgments

This work was partially supported by the Fundação para a Ciência e Tecnologia (FCT) of the Portuguese Ministry of Science, Technology and Higher Education (MCTES).

REFERENCES

1. Burton PS, Conradi RA, Ho NF, Hilgers AR, Borchardt RT. How structural features influence the biomembrane permeability of peptides. *J. Pharm. Sci.* 1996; **85**: 1336–1340.
2. Fahr A, van Hoogevest P, May S, Bergstrand N, Leigh MLS. Transfer of lipophilic drugs between liposomal membranes and biological interfaces: consequences for drug delivery. *Eur. J. Pharm. Sci.* 2005; **26**: 251–265.
3. Castanho MA, Fernandes MX. Lipid membrane-induced optimization for ligand-receptor docking: recent tools and insights for the "membrane catalysis" model. *Eur. Biophys. J.* 2006; **35**: 92–103.
4. Killian JA, Nyholm TK. Peptides in lipid bilayers: the power of simple models. *Curr. Opin. Struct. Biol.* 2006; **16**: 473–479.
5. Santos NC, Prieto M, Castanho MA. Quantifying molecular partition into model systems of biomembranes: an emphasis on optical spectroscopic methods. *Biochim. Biophys. Acta* 2003; **1612**: 123–135.
6. McLaughlin S. The electrostatic properties of membranes. *Annu. Rev. Biophys. Biophys. Chem.* 1989; **18**: 113–136.
7. Langner M, Kubica K. The electrostatics of lipid surfaces. *Chem. Phys. Lipids* 1999; **101**: 3–35.
8. Cevc G. Membrane electrostatics. *Biochim. Biophys. Acta* 1990; **1031**: 311–382.
9. Wall J, Golding CA, Van Veen M, O'Shea P. The use of fluorescein phosphatidylethanolamine (FPE) as a real-time probe for peptide-membrane interactions. *Mol. Membr. Biol.* 1995; **12**: 183–192.
10. Thelen M, Petrone G, O'Shea PS, Azzi A. The use of fluorescein-dipalmitoylphosphatidylethanolamine for measuring pH-changes in the internal compartment of phospholipid vesicles. *Biochim. Biophys. Acta* 1984; **766**: 161–168.
11. Soucaille P, Prats M, Tocanne JF, Teissie J. Use of a fluorescein derivative of phosphatidylethanolamine as a pH probe at water/lipid interfaces. *Biochim. Biophys. Acta* 1988; **939**: 289–294.
12. Yuanbo C, Fan Z, Jiachang Y. Detecting proton flux across chromatophores driven by F_0F_1-ATPase using *N*-(fluorescein-5-thiocarbamoyl)-1,2-dihexadecanoyl-*sn*-glycero-3-phosphoethano lamine, triethylammonium salt. *Anal. Biochem.* 2005; **344**: 102–107.
13. Thelen M, O'Shea PS, Petrone G, Azzi A. Proton translocation by a native and subunit III-depleted cytochrome c oxidase reconstituted into phospholipid vesicles. Use of fluorescein-phosphatidylethanolamine as an intravesicular pH indicator. *J. Biol. Chem.* 1985; **260**: 3626–3631.
14. O'Shea P. Intermolecular interactions with/within cell membranes and the trinity of membrane potentials: kinetics and imaging. *Biochem. Soc. Trans.* 2003; **31**: 990–996.
15. Wall J, Ayoub F, O'Shea P. Interactions of macromolecules with the mammalian cell surface. *J. Cell Sci.* 1995; **108**: 2673–2682.
16. Bechinger B. Structure and functions of channel-forming peptides: magainins, cecropins, melittin and alamethicin. *J. Membr. Biol.* 1997; **156**: 197–211.
17. Chupin V, Leenhouts JM, de Kroon AI, de Kruijff B. Cardiolipin modulates the secondary structure of the presequence peptide of cytochrome oxidase subunit IV: a 2D 1H-NMR study. *FEBS Lett.* 1995; **373**: 239–244.
18. Matsuzaki K, Yoneyama S, Miyajima K. Pore formation and translocation of melittin. *Biophys. J.* 1997; **73**: 831–838.
19. Golding C, Senior S, Wilson MT, O'Shea P. Time resolution of binding and membrane insertion of a mitochondrial signal peptide: correlation with structural changes and evidence for cooperativity. *Biochemistry* 1996; **35**: 10931–10937.
20. Chan DC, Kim PS. HIV entry and its inhibition. *Cell* 1998; **93**: 681–684.
21. Cladera J, Martin I, O'Shea P. The fusion domain of HIV gp41 interacts specifically with heparan sulfate on the T-lymphocyte cell surface. *EMBO J.* 2001; **20**: 19–26.
22. Sim B, Cladera J, O'Shea P. Fibronectin interactions with osteoblasts: identification of a non-integrin-mediated binding mechanism using a real-time fluorescence binding assay. *J. Biomed. Mater. Res. A* 2004; **68**: 352–359.
23. Fitchen N, O'Shea P, Williams P, Hardie KR. Electrostatic sensor for identifying interactions between peptides and bacterial membranes. *Mol. Immunol.* 2003; **40**: 407–411.
24. Gawrisch K, Ruston D, Zimmerberg J, Parsegian VA, Rand RP, Fuller N. Membrane dipole potentials, hydration forces, and the ordering of water at membrane surfaces. *Biophys. J.* 1992; **61**: 1213–1223.
25. Zheng C, Vanderkooi G. Molecular origin of the internal dipole potential in lipid bilayers: calculation of the electrostatic potential. *Biophys. J.* 1992; **63**: 935–941.
26. Clarke RJ. The dipole potential of phospholipid membranes and methods for its detection. *Adv. Colloid Interface Sci.* 2001; **89–90**: 263–281.
27. Gross E, Bedlack RS, Loew LM. Dual-wavelength ratiometric fluorescence measurement of the membrane dipole potential. *Biophys. J.* 1994; **67**: 208–216.
28. Zouni A, Clarke RJ, Holzwarth JF. Kinetics of the solubilization of styryl dye aggregates by lipid vesicles. *J. Phys. Chem.* 1994; **98**: 1732–1738.
29. Fluhler E, Burnham VG, Loew LM. Spectra, membrane binding, and potentiometric responses of new charge shift probes. *Biochemistry* 1985; **24**: 5749–5755.
30. Loew LM, Bonneville GW, Surow J. Charge shift optical probes of membrane potential. theory. *Biochemistry* 1978; **17**: 4065–4071.
31. Bublitz GU, Boxer SG. Stark spectroscopy: applications in chemistry, biology, and materials science. *Annu. Rev. Phys. Chem.* 1997; **48**: 213–242.
32. Grynkiewicz G, Poenie M, Tsien RY. A new generation of Ca2+ indicators with greatly improved fluorescence properties. *J. Biol. Chem.* 1985; **260**: 3440–3450.
33. Vitha MF, Clarke RJ. Comparison of excitation and emission ratiometric fluorescence methods for quantifying the membrane dipole potential. *Biochim. Biophys. Acta* 2007; **1768**: 107–114.
34. Clarke RJ, Kane DJ. Optical detection of membrane dipole potential: avoidance of fluidity and dye-induced effects. *Biochim. Biophys. Acta* 1997; **1323**: 223–239.
35. Clarke RJ. Effect of lipid structure on the dipole potential of phosphatidylcholine bilayers. *Biochim. Biophys. Acta* 1997; **1327**: 269–278.
36. Cladera J, O'Shea P. Intramembrane molecular dipoles affect the membrane insertion and folding of a model amphiphilic peptide. *Biophys. J.* 1998; **74**: 2434–2442.
37. Franklin JC, Cafiso DS. Internal electrostatic potentials in bilayers: measuring and controlling dipole potentials in lipid vesicles. *Biophys. J.* 1993; **65**: 289–299.
38. Cladera J, Martin I, Ruysschaert JM, O'Shea P. Characterization of the sequence of interactions of the fusion domain of the simian immunodeficiency virus with membranes. Role of the membrane dipole potential. *J. Biol. Chem.* 1999; **274**: 29951–29959.
39. Buzon V, Cladera J. Effect of cholesterol on the interaction of the HIV GP41 fusion peptide with model membranes. Importance of the membrane dipole potential. *Biochemistry* 2006; **45**: 15768–15775.
40. Aloia RC, Jensen FC, Curtain CC, Mobley PW, Gordon LM. Lipid composition and fluidity of the human immunodeficiency virus. *Proc. Natl. Acad. Sci. U.S.A.* 1988; **85**: 900–904.
41. Aloia RC, Tian H, Jensen FC. Lipid composition and fluidity of the human immunodeficiency virus envelope and host cell plasma membranes. *Proc. Natl. Acad. Sci. U.S.A.* 1993; **90**: 5181–5185.
42. Asawakarn T, Cladera J, O'Shea P. Effects of the membrane dipole potential on the interaction of saquinavir with phospholipid membranes and plasma membrane receptors of Caco-2 cells. *J. Biol. Chem.* 2001; **276**: 38457–38463.
43. Shah P, Jogani V, Bagchi T, Misra A. Role of Caco-2 cell monolayers in prediction of intestinal drug absorption. *Biotechnol. Prog.* 2006; **22**: 186–198.
44. Lee CG, Gottesman MM, Cardarelli CO, Ramachandra M, Jeang KT, Ambudkar SV, Pastan I, Dey S. HIV-1 protease

inhibitors are substrates for the MDR1 multidrug transporter. *Biochemistry* 1998; **37**: 3594–3601.
45. Cladera J, O'Shea P, Hadgraft J, Valenta C. Influence of molecular dipoles on human skin permeability: Use of 6-ketocholestanol to enhance the transdermal delivery of bacitracin. *J. Pharm. Sci.* 2003; **92**: 1018–1027.
46. Klymchenko AS, Duportail G, Mely Y, Demchenko AP. Ultrasensitive two-color fluorescence probes for dipole potential in phospholipid membranes. *Proc. Natl. Acad. Sci. U.S.A.* 2003; **100**: 11219–11224.
47. Shynkar VV, Klymchenko AS, Duportail G, Demchenko AP, Mely Y. Two-color fluorescent probes for imaging the dipole potential of cell plasma membranes. *Biochim. Biophys. Acta* 2005; **1712**: 128–136.
48. Deshayes S, Plenat T, Charnet P, Divita G, Molle G, Heitz F. Formation of transmembrane ionic channels of primary amphipathic cell-penetrating peptides. Consequences on the mechanism of cell penetration. *Biochim. Biophys. Acta* 2006; **1758**: 1846–1851.
49. Terrone D, Sang SL, Roudaia L, Silvius JR. Penetrating and related cell-penetrating cationic peptides can translocate across lipid bilayers in the presence of a transbilayer potential. *Biochemistry* 2003; **42**: 13787–13799.
50. Haugland RP. Probes for membrane potential. *The Handbook – A Guide to Fluorescent Probes and Labelling Technologies*. Invitrogen Molecular Probes: Eugene, OR, 2005; 973–986.
51. Moll GN, Brul S, Konings WN, Driessen AJ. Comparison of the membrane interaction and permeabilization by the designed peptide Ac-MB21-NH2 and truncated dermaseptin S3. *Biochemistry* 2000; **39**: 11907–11912.
52. Rintoul MR, de Arcuri BF, Morero RD. Effects of the antibiotic peptide microcin J25 on liposomes: role of acyl chain length and negatively charged phospholipid. *Biochim. Biophys. Acta* 2000; **1509**: 65–72.
53. Ibrahim HR, Sugimoto Y, Aoki T. Ovotransferrin antimicrobial peptide (OTAP-92) kills bacteria through a membrane damage mechanism. *Biochim. Biophys. Acta* 2000; **1523**: 196–205.
54. Tiriveedhi V, Butko P. A fluorescence spectroscopy study on the interactions of the TAT-PTD peptide with model lipid membranes. *Biochemistry* 2007; **46**: 3888–3895.
55. Zhu WL, Lan H, Park IS, Kim JI, Jin HZ, Hahm KS, Shin SY. Design and mechanism of action of a novel bacteria-selective antimicrobial peptide from the cell-penetrating peptide Pep-1. *Biochem. Biophys. Res. Commun.* 2006; **349**: 769–774.
56. Nuding S, Fellermann K, Wehkamp J, Mueller HA, Stange EF. A flow cytometric assay to monitor antimicrobial activity of defensins and cationic tissue extracts. *J. Microbiol. Methods* 2006; **65**: 335–345.
57. Yang ST, Shin SY, Kim JI. Interaction mode of a symmetric Trp-rich undeca peptide PST11-RK with lipid bilayers. *FEBS Lett.* 2007; **581**: 157–163.

Review Article B

Declaration of authorship

I, Pedro Miguel Baptista de Matos, declare that the manuscript preparation and writing was carried out by me, Henri Franquelim, Prof. Miguel A. R. B. Castanho and Prof. Nuno S. Santos.

I, Nuno C. Santos, as supervisor of Pedro Matos and as corresponding author of the article mentioned above, hereby acknowledge and confirm that the information above is correct.

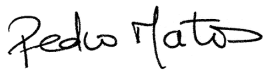

Pedro M. Matos

Nuno C. Santos

Biochimica et Biophysica Acta 1798 (2010) 1999–2012

Contents lists available at ScienceDirect

Biochimica et Biophysica Acta

journal homepage: www.elsevier.com/locate/bbamem

Review

Quantitative assessment of peptide–lipid interactions. Ubiquitous fluorescence methodologies

Pedro M. Matos, Henri G. Franquelim, Miguel A.R.B. Castanho, Nuno C. Santos *

Instituto de Medicina Molecular, Faculdade de Medicina da Universidade de Lisboa, Av. Prof. Egas Moniz, 1649-028 Lisbon, Portugal

ARTICLE INFO

Article history:
Received 27 March 2010
Received in revised form 13 July 2010
Accepted 13 July 2010
Available online 18 July 2010

Keywords:
Peptide
Protein
Lipid
Membrane
Fluorescence
Partition

ABSTRACT

Peptide–membrane interactions have been gaining increased relevance, mainly in biomedical investigation, as the potential of the natural, nature-based and synthetic peptides as new drugs or drug candidates also expands. These peptides must face the cell membrane when they interfere with or participate in intracellular processes. Additionally, several peptide drugs and drug leads actions occur at the membrane level (e.g., antimicrobial peptides, cell-penetrating peptides and enveloped viruses membrane fusion inhibitors). Here we explore fluorescence spectroscopy methods that can be used to monitor such interactions. Two main approaches are considered, centered either on the peptide or on the membrane. On the first, we consider mainly the methodologies based on the intrinsic fluorescence of the aminoacid residues tryptophan and tyrosine. Regarding membrane-centric approaches, we review methods based on lipophilic probes sensitive to membrane potentials. The use of fluorescence constitutes a simple and sensitive method to measure these events. Unraveling the molecular mechanisms that govern these interactions can unlock the key to understand specific biological processes involving natural peptides or to optimize the action of a peptide drug.

Contents

1. Introduction

The interaction of peptides with lipid bilayers is attracting the attention of a growing community of scientists. Innovative applications of atomic force microscopy, NMR and fluorescence spectroscopy [1], for instance, allow detailed information on peptide conformation, orientation and association in the confined space of the bilayer to be obtained. Along with academic interest, industry (mainly pharmaceutical) has been achieving important milestones on the development of peptide products. Enfuvirtide (T-20) is a 36-aminoacid peptide HIV-1 fusion inhibitor in clinical use. Other clinically relevant peptides may follow,

Abbreviations: 6-KC, 6-ketocholestanol; AMP, antimicrobial peptide; BPPZ, 3-(4-{4-[4′-(3-Hydroxybenzo[*f*]flavonyl)phenyl]piperazino}-1-pyridiniumyl)-1-propanesulfonate; CL, cardiolipin; CPP, cell-penetrating peptide; DHE, dehydroergosterol; di-8-ANEPPS, 4-[2-[6-(dioctylamino)-2-naphthalenyl]ethenyl]-1-(3-sulfopropyl)-pyridinium; DNS, dansil; DPH, 1,6-diphenylhexatriene; DPPC, 1,2-dipalmitoylphophatidylcholine; ESIPT, excited-state intramolecular proton-transfer; F4N1, *N*-[(4′-dimethylamino)-3-hydroxy-6-flavonyl]methyl-*N*,*N*-trimethyl ammonium bromide; FPE, fluorescein phosphatidylethanolamine; FRET, Förster resonance energy transfer; HIV, human immunodeficiency virus; MccJ25, microcin J25; NMR, nuclear magnetic resonance; PC, phosphatidylcholine; PG, phospatidylglycerol; POPC, 1-palmitoyl-2-oleoyl-phospatidylcholine; POPG, 1-palmitoyl-2-oleoyl-phospatidylglycerol; PrP, prion protein; RD, reduction of dimensionality; RH421, N-(4-sulfobutyl)-4-[4-[4-(dipentylamino)phenyl]butadienyl]-pyridinium

* Corresponding author. Tel.: +351 217999480; fax: +351 217999477.
E-mail address: nsantos@fm.ul.pt (N.C. Santos).

0005-2736/$ – see front matter © 2010 Elsevier B.V. All rights reserved.
doi:10.1016/j.bbamem.2010.07.012

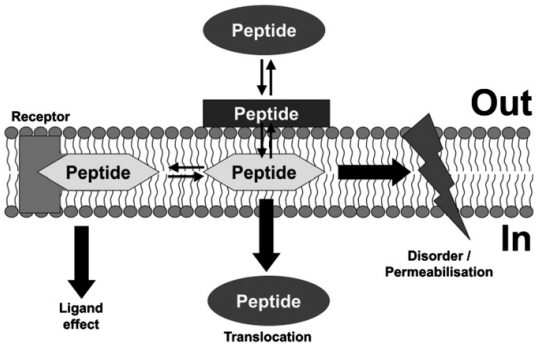

Fig. 1. Outline of peptide–membrane interactions. Peptides in contact with membranes may change conformation, which may facilitate proper binding to a receptor. Peptides may also exert local specific effects, such as disorder or permeabilization (e.g., antimicrobial peptides). Other peptides have the ability to translocate across the membrane, having no apparent effect in the lipid bilayer. Reprinted from [10].

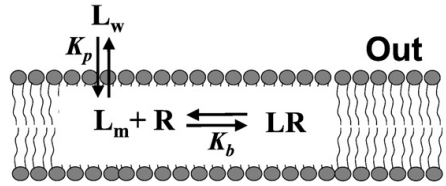

Fig. 2. Simplified scheme for membrane-mediated ligand–receptor interaction, where no membrane binding sites are considered and partition is described by a single equilibrium step. K_p and K_b are equilibrium constants for partition into the membrane and binding to receptor, respectively (L_w refers to ligand L in the bulk aqueous phase; L_m refers to ligand in the membrane; R — receptor). Reprinted from [10].

not only in the field of antimicrobials, but also on central nervous system-targeted drugs [2–5]. In the long term, cell-penetrating peptides (CPP) may also play an important role in gene therapy [6].

Many of the peptides that gather academic and industrial interest are membrane-active (i.e., lipid-interactive) peptides (Fig. 1), but while antimicrobial peptides (AMP) target bacterial membranes, others (such as enfuvirtide [7,8]) may bind lipids in a pre-stage for receptor docking. This concept was put forward in 1986 [9] and has been refined over the years (for a review see [10]). The lipid palisade influences the peptide concentration, conformation, location, and orientation in ways that improve peptide ligand–receptor interaction relative to free solution. The first conceptualization [9] considered the docking of a ligand to a membrane receptor to be a three-step process: (i) adsorption of the ligand to the membrane and formation of an accumulation layer; (ii) insertion in the membrane for which binding sites were considered to exist; and, (iii) receptor docking in the membrane matrix. Whilst electrostatic accumulation in adsorption is important, as shown by the fact that receptor-binding kinetics may be 10^5 times faster than in its absence [9], steady-state considerations can be made clearer considering the bulk aqueous medium vs. membrane concentration balance. Fig. 2 depicts the equilibria involved in membrane-mediated ligand–receptor docking in a more simplified way. Membrane insertion is accounted for in a single step and no membrane binding sites for insertion are evoked, because this membrane binding sites have an elusive physical counterpart. There are however other frameworks that account for multi-step binding processes of peptides to membranes, taking into account water–lipid interfacial regions and also the folding of the peptide or protein itself [11,12].

The concentrating effect of the membrane is expected to increase the occupied-to-unoccupied receptor-binding sites ratio by a partition coefficient (K_p) factor (see below) that combines adsorption and insertion in the lipid palisade [10]. The ratio of bound to unbound receptors is:

$$\frac{[LR]_m}{[R]_m} = K_p K_b [L]_w \quad (1)$$

where $[LR]_m$ is the concentration of the ligand–receptor complex in the membrane, $[R]_m$ is the concentration of the receptor in the membrane, K_b is the binding constant and $[L]_w$ is the ligand concentration in aqueous environment. In the absence of membranes, the ratio of bound to unbound receptors would be $K_b[L]_w$.

Typical moderate values of K_p are 10^3–10^4 in the absence of an electrostatic contribution and 10^5–10^6 when an electrostatic attraction is present [7,8,13]. Thus, the extent of ligand–receptor binding can be improved up to several orders of magnitude. However, the power of membranes to concentrate the ligand is not effective unless receptor-binding site and ligand are located at the same depth in the membrane. Three main methods exist to estimate the depth or depth distribution of fluorophores in the membrane. The Parallax Method [14] adapts the common simple methodology of the three-dimensional quenching sphere-of-action model to two dimensions. The underlying concept of static (non-diffusive) quenching [15] remains unchanged. This assumption confines the appropriate applicability of the model to few experimental cases, although it is often used without checking for this premise. The Distribution Analysis of Depth-Dependent Fluorescent Quenching (Distribution Analysis, in short) is an alternative that overcame these limitations [16]. For instance, compared to the Parallax Method, the Distribution Analysis yields additional valuable information on the fluorophore's transverse heterogeneity and lipid exposure and it can be used to evaluate wide ranges of membrane penetrations [17]. A second alternative to overcome some of the formal weaknesses of the Parallax Method [18] applies the simple diffusional quenching concepts to the restricted dimensionality of a bilayer, which is treated as a slab where fluorophores and quenchers locate, having a certain in-depth distribution. Single-molecule Brownian Dynamics simulations were carried out to ascertain the quencher statistical location distributions. Pairs of quenchers (either brominated or doxyl-derivatized acyl chains in fatty acids or phospholipids) are then used to quench the fluorophore. The relative degree of quenching between them depends on the known distributions of the quenchers and on the fluorophore distribution to be determined. This methodology was applied to study the location of the HIV fusion inhibitors enfuvirtide (T-20), T-1249 and sifuvirtide, which were proposed to use membrane-mediated steps in their mechanism of action [7,8,19]. A shallow average position of the Trp residues was determined, which helps to position the whole molecular ensemble in the lipid bilayer.

Along with concentration and conformation modulation, the most important role of membranes is the modulation of the ligand orientation. The most common spectroscopic methods used to determine the orientation of foreign molecules in membranes were reviewed in reference [20]. These include IR spectroscopy, UV–Vis linear dichroism, time-resolved fluorescence anisotropy decays, Raman spectroscopy, Surface Plasmon Resonance and NMR. UV–Vis linear dichroism methodologies have been applied in a large number of studies involving different classes of molecules, including multi-functional peptides [21,22].

An eventual advantage in membrane mediation relates to the reduction of dimensionality from 3D to 2D. Adam and Delbrück [23] theorized that reaction rates between ligands and surface bound receptors would be increased by non-specific ligand adsorption and 2D diffusion towards receptors. This effect is referred to as reduction of dimensionality (RD) reaction rate enhancement. Since then, several theoretical models attempted to describe the relevance of underlying factors to this behavior [24–28]. However, as justly referred by

Martins et al. [29], caution must be exerted when comparing a 2D reaction with a 3D counterpart, namely not disregarding the clause "other factors being equal". When going from 3D to 2D some factors will face changes inherent to the reduction of dimensionality, as it happens for the diffusion coefficient. While there is RD enhancement in most cases for reaction-limited processes, for diffusion limited processes there is a disadvantage in conditions plausible to occur in biological systems [10].

This review is focused on methods to monitor membrane interaction that avoid chemical modification of the peptides and proteins involved in the study, as this may change their membrane binding properties (e.g., [30,31]). This is achieved mainly by taking advantage of the intrinsic fluorescence of the peptides and the use of membrane fluorescent probes to indirectly monitor perturbations caused by peptide interaction. However, it is important to mention that in many cases of peptides that are not intrinsically fluorescence, the derivatization with a suitable fluorophore can be a valuable solution to measure their interaction with membranes, provided that it does not significantly alter the peptide structural and functional properties. This labeling may also enable the use of other fluorescence-based techniques, such as microscopy imaging and fluorescence correlation spectroscopy (FCS) [32,33]. Moreover, this can also be useful to obtain more insightful information regarding peptide orientation in membranes [34,35].

2. Quantification of the partition of a peptide to a membrane using intrinsic fluorescence

2.1. Basic concept

The partition constant or partition coefficient of a solute between an aqueous and a lipid phase can be defined, based on the free energy of transfer of the solute between the two phases, as:

$$K_{p,x} = \frac{\frac{n_{S,L}}{n_L + n_{S,L}}}{\frac{n_{S,W}}{n_W + n_{S,W}}} \tag{2}$$

where n_W and n_L are the moles of water and lipid, and $n_{S,i}$ are the moles of solute present in each phase (i = W, aqueous phase; i = L, lipid phase). As under most experimental conditions the quantities of water and lipid are considerably higher than the quantity of solute on the aqueous and lipid phases, respectively, the equation is usually simplified to:

$$K_{p,x} \approx \frac{\frac{n_{S,L}}{n_L}}{\frac{n_{S,W}}{n_W}} \tag{3}$$

However, in most of the literature the partition coefficient is presented as a function of the volumes of the phases, V_i, instead of using the quantity of lipid and water:

$$K_p = \frac{\frac{n_{S,L}}{V_L}}{\frac{n_{S,W}}{V_W}} \tag{4}$$

This parameter, sometimes named Nernst partition coefficient, can be related with the previous one by the expression:

$$K_p = K_{p,x}\frac{\gamma_W}{\gamma_L} \tag{5}$$

where γ_i is the molar volume of water (i = W) or lipid (i = L).

A different way to describe the interaction of a solute with a membrane is by considering a binding mechanism. In this case, a chemical equilibrium between the solute and one or more lipid molecules is considered, and a conventional binding isotherm is obtained (e.g., [36,37]), in which two parameters describe the process: a dissociation constant, K_d (or an association constant) and the number of lipid molecules that are associated with a solute molecule. The main disadvantage of this option relatively to the partition formalisms is that there is no molecular counterpart for describing those binding sites in the membrane, as if some kind of receptors for the solute would exist. In fact, the membrane is a supramolecular system and the solute interaction is controlled by the lipid ensemble.

The partition quantification has been previously extensively reviewed elsewhere [38], including the use of several optical spectroscopies and non-optical techniques. Experimental artifacts, practical limitations and the determination of membrane inter-domain partitions are also discussed in that review.

2.2. Determination of K_p by intrinsic fluorescence parameters

For most of the cases, the partition coefficient of a molecule between a lipid and an aqueous phase can be evaluated by fluorescence spectroscopy as long as: (i) there is a difference in a fluorescence parameter (e.g., quantum yield, fluorescence anisotropy or fluorescence lifetime) of the partitioning molecule when in aqueous solution and after incorporation in the membrane or, (ii) the incorporation of the molecule in the membrane leads to a change on a fluorescence property of a membrane probe. The first situation will be treated in this section.

The intrinsic fluorescence of peptides containing tryptophan (Trp) or tyrosine (Tyr) residues is a valuable tool to quantify their insertion on lipid membranes. Due to the strong dependence of the fluorescence of these aromatic amino acids (specially Trp) on the physical properties of their micro-environment, the insertion of the peptide on a lipid membrane can lead to substantial changes on the quantum yield, wavelength of the emission maximum, fluorescence anisotropy and fluorescence lifetime [39].

As long as there is a significant difference between the quantum yield of the peptide in the aqueous environment and in the lipid membrane, its partition constant can be determined by conducting fluorescence intensity, I, measurements with a fixed concentration of peptide and increasing lipid concentrations ([L]). This usually yields a hyperbolic-like I vs. [L] variation profile, which can be fitted using [40,41]:

$$I = \frac{I_W + K_p\gamma_L[L]I_L}{1 + K_p\gamma_L[L]} \tag{6}$$

where γ_i is the molar volume of water (i = W) or lipid (i = L). Ideally, I should be the integrated fluorescence emission intensity but, if no significant spectral shifts occur upon increasing [L], I may be measured at a chosen emission wavelength. Typical examples of the use of this equation on the quantification of the interaction of peptides with membranes are the studies of the lipid selectivity of the previously mentioned different HIV-1 membrane fusion inhibitors [7,8,19].

To use the steady-state fluorescence anisotropy, r, to calculate the partition coefficient of a fluorescent molecule, it is not only necessary that this parameter has a significant change between the lipid and aqueous phases, but also the fluorescence intensity from both phases must be comparable. Using an experimental design identical to that indicated for the fluorescence intensity-based methodology, the data should be fitted using [42]:

$$r = \frac{r_W\left((\gamma_L[L])^{-1} - 1\right) + r_L K_p \varepsilon_L \phi_L / (\varepsilon_W \phi_W)}{(\gamma_L[L])^{-1} - 1 + K_p \varepsilon_L \phi_L / (\varepsilon_W \phi_W)} \tag{7}$$

where ϕ is the fluorescence quantum yield and ε is the molar absorption.

In addition to the steady-state fluorescence spectroscopy methodologies, partition coefficients can also be obtained by time-resolved fluorescence spectroscopy. When carrying out a time-resolved fluorescence spectroscopic study of the interaction of a fluorescent molecule with a membrane system, ideally two exponentials would describe the experimental fluorescence intensity decay, one corresponding to the molecules in aqueous media and the other to the molecules in the lipid environment:

$$I(t) = a_W \exp(-t/\tau_W) + a_L \exp(-t/\tau_L) \quad (8)$$

(where t is time and τ_i is the fluorescence lifetime of the molecules in each phase). In this ideal case, the relative concentration of each specie could be calculated from the pre-exponential factors ratio (a_L/a_W), if the radiative rate constants and absorption coefficient ratios in both phases are known [43]. However, in most of the cases (including intrinsically fluorescent peptides), the decays both in the aqueous phase and on the membrane are complex. Thus, the total decay must be described by a sum of exponentials, mixing up all the contributions. Therefore, an average of the fluorescent lifetime should be used. The average fluorescence lifetime of a fluorophore, $<\tau>$, is given by (e.g., [44]),

$$\langle\tau\rangle = \frac{\sum a_i \tau_i^2}{\sum a_i \tau_i} \quad (9)$$

However, if $<\tau>$ is used for K_p determination, a complex equation would be attained, where steady-state and transient-state data must be combined [40]:

$$\langle\tau\rangle = \langle\tau\rangle_W + (\langle\tau\rangle_L - \langle\tau\rangle_W)\frac{K_p\gamma_L[L]}{K_p\gamma_L[L] + \frac{\varepsilon_W\phi_W}{\varepsilon_L\phi_L}} \quad (10)$$

Therefore, it is more convenient to calculate the variation of the fluorescence lifetime averaged by the pre-exponentials, $\overline{\tau}$,

$$\overline{\tau} = \frac{\sum a_i \tau_i}{\sum a_i} \quad (11)$$

leading to the formalism for the determination of K_p [40],

$$\overline{\tau} = \frac{\overline{\tau}_W + K_p\gamma_L[L]\,\overline{\tau}_L}{1 + K_p\gamma_L[L]} \quad (12)$$

This simpler equation is similar to Eq. (6) because both $\overline{\tau}$ and I are additive parameters. These cases can be assigned to the same general equation [38]:

$$p = \frac{p_W + K_p\gamma_L[L]p_L}{1 + K_p\gamma_L[L]} \quad (13)$$

where p stands for any additive parameter, such as I or $\overline{\tau}$. If $\varepsilon_W\phi_W \approx \varepsilon_L\phi_L$ and $\gamma_L[L] \ll 1$ (a condition present in most experimental conditions) are assumed in Eq. (7), then p may also stand for r.

2.3. Complex partition curves

As an exception to the general rule of the increase of I, r and τ of a fluorophore upon incorporation in a membrane system, Vermeir et al. [45] reported a decrease on the fluorescence intensity of the partitioning molecule when in the membrane. This quenching process was used as a simple methodology to obtain the value of the partition coefficient, by a linear fit:

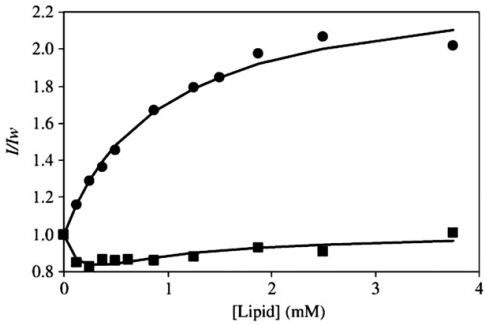

Fig. 3. Fluorescence emission intensity of pep-1 (6.88 μM), normalized by dividing by I_W, upon titration with large unilamellar vesicles of palmitoyloleoylphosphatidylcholine (POPC; circles; normal hyperbolic increase of I) or dipalmitoylphosphatidylcholine (DPPC; squares; system where self-quenching occurs). Eqs. (6) and (15), respectively, were used for data fitting and K_p quantification. Reprinted from [46].

$$\frac{I_W}{I} = 1 + K_p\gamma_L[L] \quad (14)$$

This equation is in fact a special case of Eq. (6) for a situation in which it is assumed that $I_L = 0$. More recently, in a study of the membrane and environmental parameters that influence the activity of the cell-penetrating peptide pep-1 [46], a less strict model was proposed to quantify the partition constants of systems in which fluorescence quenching (usually self-quenching) can occur upon insertion in the membrane (Fig. 3):

$$I = \frac{K_p\gamma_L[L]I_L}{1 + K_p\gamma_L[L] + k_2K_pI_L} + \frac{I_W}{1 + K_p\gamma_L[L]} \quad (15)$$

where,

$$k_2 = \frac{k_q}{\varepsilon l k_f} \quad (16)$$

l is the optical path, k_q is the kinetic constant of the quenching process, k_f is the radiative fluorescence constant and ε is the molar absorption. Pina et al. adapted this model to a more complex and specific situation, in which there is a combined effect of the partition of the Shiga toxin B-subunit to the bulk lipid membrane, with self-quenching, and the subsequent binding of the protein to its specific ligand (a glycolipid) with an increase on the quantum yield [47].

Other types of deviations from the normal hyperbolic behavior of partition curves were reported on the study of the interaction of the antimicrobial peptide omiganan with biomembrane model systems with different lipid compositions [3]. Upon titration of the peptide solution with some of the lipid vesicles, a spike was registered, deviating from the hyperbolic-like behavior just on a restrict range of lipid concentrations (Fig. 4). This critical-point was explained by a model, tested by curve simulation, where a sequence of events is taken into account, in which it is considered that the apparent K_p is dependent on peptide concentration: firstly, at high peptide/lipid ratios, a saturated regime in which the local concentration of the peptide in the membrane is constant and independent of the concentration of the peptide in solution. In this situation, the constant parameter that describes the system, instead of K_p, is the local peptide/lipid ratio in the membrane, σ. Secondly, at low peptide/lipid ratios, the excess of lipid enables the use of the previously described common partition formalisms, with a constant K_p. On the critical-

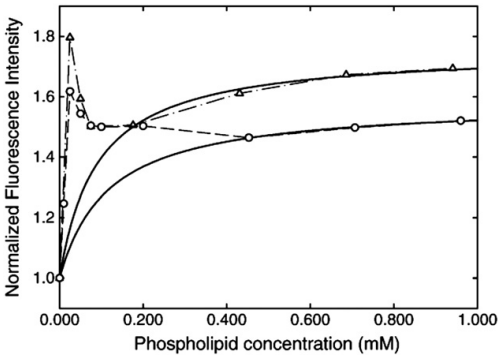

Fig. 4. Partition curves of the antimicrobial peptide omiganan to lipid vesicles of palmitoyloleoylphosphatidylglycerol (POPG; triangles) and dipalmitoylphosphatidylglycerol (DPPG; circles). Fluorescence emission intensities were normalized by dividing by I_W. The peptide concentration was 7.7 μM. Reprinted from [3].

points, both σ and K_p are valid to describe the system. These points can be identified from the partition curves experimentally obtained with different peptide concentrations and fitted by:

$$[P]_s = \frac{\sigma}{K_p \gamma_L} + \sigma[L] \tag{17}$$

where $[P]_s$ is the peptide concentration at the saturation point for a concentration of lipid, [L]. On a study of the membrane insertion of a possible dengue virus fusion peptide [48], the use of this formalism was further extended to systems in which peptide oligomerization occurs, driven by its local high concentration in the membrane, but not strictly resulting from saturation (Fig. 5).

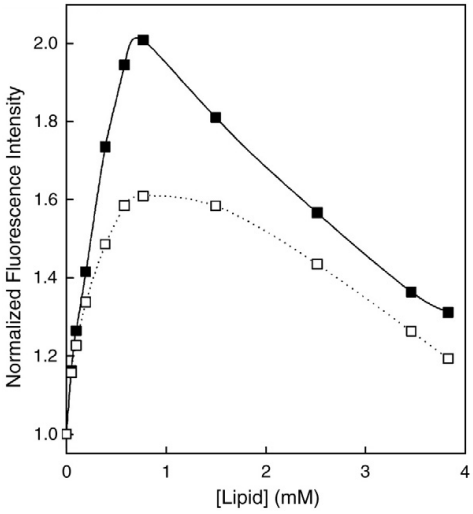

Fig. 5. Partition of a possible dengue virus fusion peptide to lipid vesicles of POPC:POPG (4:1) at pH 5.5 (filled squares) and pH 8.0 (open squares). Fluorescence emission intensities were normalized by dividing by I_W. The peptide concentration was 18 μM. Reprinted from [48].

2.4. Adsorption quantification by Förster Resonance Energy Transfer methodologies

As previously shown, the evaluation of the interaction of fluorescent peptides and proteins with lipid membranes can be easily followed by recording the changes on the fluorescence properties of the aromatic amino acid residues. Nevertheless, generally, the adsorption of peptides or proteins on the surface of lipid membranes will not induce significant changes in the fluorescence parameters or will lead to changes not large enough to allow a correct determination of a partition coefficient. Therefore, it can be advantageous to follow the interaction of fluorescent peptides with lipid membranes adding molecules that will perturb the fluorescence properties of the aromatic residues of the peptides. Simple dynamic quenching approaches, as recently described [49], or even Förster Resonance Energy Transfer (FRET) methodologies can be used with this purpose. For instance, FRET methodologies can be a quite powerful approach, yielding information about the extent and the topological range of the molecular interaction of peptides with membranes [39,44].

FRET is the process in which a molecule in the excited state (donor) returns to the ground state by transferring its energy to another molecule (acceptor) without the emission of a photon or contact between molecules. The extent of the energy transfer is determined by the distance between donor and acceptor and the overlap of the donor's fluorescence emission spectrum and the acceptor's adsorption spectrum [39]. An important parameter to describe this phenomenon is the Förster radius, R_0, which can be calculated from the spectroscopic data of the donor and acceptor, using:

$$R_0 = 0.2108\left[\kappa^2 \phi_D n^{-4} J\right]^{1/6} \tag{18}$$

where κ^2 is a factor that depends on the relative orientation of donors and acceptor (the value $\kappa^2 = 2/3$, relative to the dynamic isotropic limit, is usually assumed [50]), ϕ_D is the donor quantum yield in the absence of the acceptor and n is the refractive index ($n = 1.4$ is used as refractive index within lipid vesicles [51]). The parameter J represents the spectral overlap integral between the emission spectrum of the donor and the absorption spectrum of the acceptor:

$$J = \int_0^\infty I(\lambda)\varepsilon(\lambda)\lambda^4 d\lambda \tag{19}$$

where $I(\lambda)$ is the normalized donor emission spectrum and $\varepsilon(\lambda)$ is the acceptor molar absorption spectrum, in the interval of wavelengths centered in λ and with width dλ. The numerical constant in Eq. (18) implies the use of λ is in nm, ε in M^{-1} cm^{-1}, and R_0 in Å.

The efficiency of energy transfer, E, is defined as the fraction of the energy of the photons absorbed by the donor that is transferred to the acceptor, and is given by,

$$E = \frac{k_T}{k_T + \tau_D^{-1}} = \frac{R_0^6}{R_0^6 + R^6} \tag{20}$$

k_T represents the rate of energy transfer from a donor to an acceptor separated by a distance R. Therefore, the Förster radius, R_0, represents the distance for which the efficiency of energy transfer is 0.5. Experimentally, the efficiency of energy transfer, E, can be calculated using the equation:

$$E = 1 - \frac{\overline{\tau}_{DA}}{\overline{\tau}_D} = 1 - \frac{I_{DA}}{I_D} \tag{21}$$

where $\overline{\tau}_{DA}$ and $\overline{\tau}_D$ are the fluorescence lifetimes averaged by the pre-exponential factors (Eq. (11)) and I_{DA} and I_D are the fluorescence

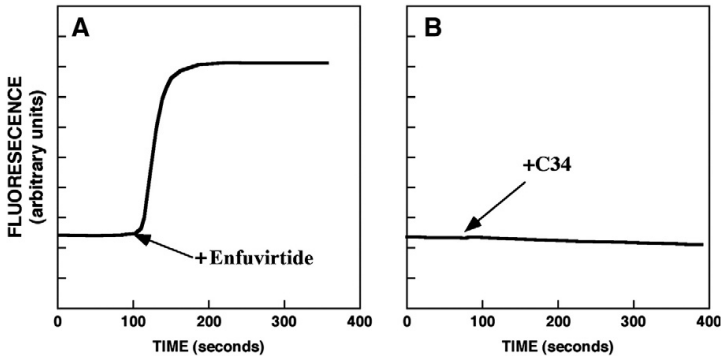

Fig. 6. Detection of peptide binding to the membrane by FRET. Fusion inhibitors enfuvirtide (A) or C34 (B) at 0.45 μM, were added to phosphatidylcholine/phosphatidylserine/cholesterol/DNS-phosphatidyletanolamine (8:8:2:1 (w/w), 68 μM) lipid vesicles. Excitation at 280 nm and emission at 518 nm. Reprinted from [54].

emission intensities of the donor in the presence and absence of the acceptor, respectively.

Here, we will use the interaction of HIV gp41 derived peptides with lipid bilayers to illustrate FRET applications on the quantification of adsorption. The HIV fusion process mediated by the gp120–gp41 complex occurs in an extreme confinement between the viral envelope and the cell membrane [52]. The ability of certain domains and regions of these proteins to interact with membranes is important for various steps of the entry and even for the inhibition of the fusion process. As previously referred, some HIV gp41 derived peptides have a peculiar interaction with lipid model systems, which can be related to their molecular mode of action [7,8,19]. In all the examples that will be given, the donor groups are the Trp residues of the peptides, whereas the acceptor molecules are localized within the lipid bilayers.

Kliger et al. studied the binding of a recombinant protein corresponding to the ectodomain of gp41 [53] and HIV-1 fusion inhibitor peptides (enfuvirtide and C34 [54]) with lipid membranes by measuring the energy transfer from the Trp residues of these proteins and peptide to dansyl (DNS) chromophores incorporated into lipid vesicles. They detected the binding by measuring the increase in the sensitized DNS fluorescence emission upon excitation of Trp (Fig. 6).

Other studies using fluorescence spectroscopy methodologies [7,8,19] found a correlation between membrane-interaction properties of HIV fusion inhibitor peptides and their efficacy. The adsorption of T-1249 to cholesterol-rich membranes and the adsorption of sifuvirtide to DPPC gel phase membranes were demonstrated by several fluorescence approaches and confirmed by FRET, using as acceptors dehydroergosterol (DHE), an intrinsically fluorescent cholesterol analogue, and 1,6-diphenylhexatriene (DPH), a rigid rod-like fluorescent probe that partitions deeply within the core of a lipid bilayer [55], respectively.

Using a specific FRET methodology to describe the adsorption events, it was possible to quantify the fraction of molecules that was adsorbed on the surface of the bilayers. The formalism [7,19,51] assumes several planes parallel to the bilayer surface (Fig. 7A): two acceptor planes and a donor plane (Trp residues) at a distance W_i from that of the acceptors, in the case of T-1249, for instance. Firstly, the decay of the donor fluorescence intensity in the absence of acceptor is given by:

$$I_D(t) = A_W I_{D,W}(t) + (1-A_W)\cdot I_{D,L}(t) \quad (22)$$

where $I_{D,W}$ and $I_{D,L}$ are the fluorescence decays of the donor in the buffer and adsorbed to the lipid vesicles, respectively, and A_W is the fraction of the molecules in aqueous solution. For T-1249 in the presence of the acceptor in the membrane, the fluorescence decay of the sub-population in solution is not affected, but the adsorbed donor's fluorescence is extinct by acceptors localized in two parallel planes (Fig. 7A). The donor fluorescence decay, in the presence of the acceptor is:

$$I_{D,A}(t) = A_W I_{D,W}(t) + (1-A_W)\cdot I_{D,L}(t)\cdot \rho_1(t)\cdot \rho_2(t) \quad (23)$$

The $\rho_i(t)$ functions denote the FRET rates to acceptors located on the planes W_1 and W_2 away from the donor, respectively, and are given by [51]:

$$\rho_i(t) = \exp\left\{-2\left(\frac{W_i}{R_0}\right)^2 n\pi R_0^2 \int_0^1 \frac{1-\exp\left[\left(-\frac{t}{\langle\tau\rangle}\right)\left(\frac{R_0}{W_i}\right)^6 \alpha^6\right]}{\alpha^3} d\alpha\right\} \quad (24)$$

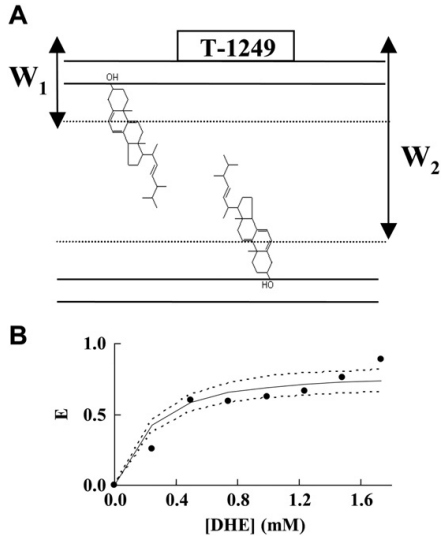

Fig. 7. Detection of the binding of T-1249 to cholesterol-enriched membranes by FRET. (A) Diagram representing the donor–acceptor geometry in the lipid bilayer: T-1249 adsorbed at the surface and DHE in both leaflets of the membrane. (B) Energy transfer efficiency from Trp residues of T-1249 (donor) to DHE (acceptor) in POPC/cholesterol vesicles. The boundaries $A_W = 0.2$ and $A_W = 0.4$ are also represented (dashed lines). Reprinted from [7].

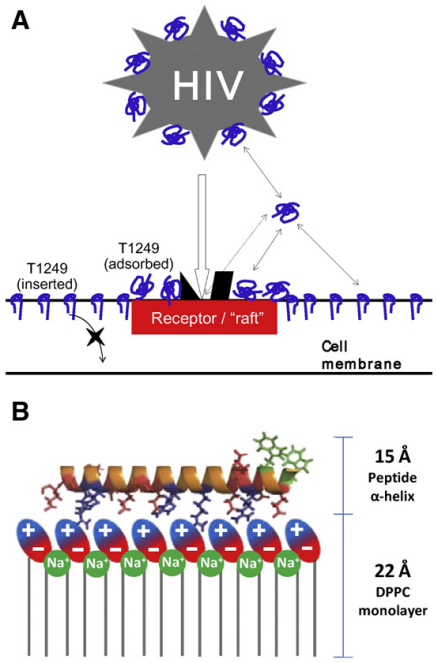

Fig. 8. Putative modes of action at the membrane level of T-1249 and sifuvirtide, revealed after combining overall partition and more detailed FRET approaches. (A) Schematic representation of the involvement of lipid membranes in T-1249 inhibition mechanism, as described in [7], displaying the adsorption on cholesterol-enriched membrane domains. The translocation of the peptide is prevented due to charge repulsion of negatively charged phospholipids of the inner leaflet. The term raft refers to cholesterol-rich liquid-ordered membrane microdomains. (B) Schematic representation of the adsorption of sifuvirtide on the surface of DPPC gel phase membranes in the presence of physiological NaCl concentration, as described in [49]. Reprinted from [7,49].

where n is the acceptor density (molecules/unit area), which was computed from:

$$n = \frac{[DHE]}{[POPC]\cdot\left(a_{POPC} + \frac{1}{2}a_{chol} - b\right)} \quad (25)$$

where a_{POPC} and a_{chol} are the areas per POPC and the cholesterol molecule on the bilayer plane, respectively, and b is the condensation effect of cholesterol on the bilayer area. In this equation, the area of cholesterol is divided by 2 due to the fact that the POPC:cholesterol mixture ratio used in that original work was 2:1. R_0 was calculated using Eq. (18) and the FRET efficiency according to Eq. (21), where I_D and I_{DA} were obtained by the numerical integration of the theoretical decay laws:

$$I_D = \int_0^\infty i_D(t)dt \quad (26)$$

$$I_{D.A} = \int_0^\infty i_{D.A}(t)dt \quad (27)$$

A_W, was obtained from the non-linear regression analysis of experimental data (Fig. 7B). It is worth of notice that the interactions of T-1249 and sifuvirtide with the lipid vesicles for which there is peptide adsorption were difficult to quantify by the fluorescence spectroscopy approaches mentioned in the previous sections, because these peptide–membrane interactions only cause minor changes in the Trp fluorescence parameters [7,19]. Overall, the use of a FRET methodology allowed retrieving detailed information (Fig. 8) and revealed a correlation between the efficacy and membrane domain selectivity among HIV fusion inhibitor peptides [7,19].

3. Peptide–lipid interactions studied using membrane potential-sensitive probes

In many cases, it is not possible to rely on the intrinsic fluorescence of peptides or proteins due to the lack of fluorescent amino acids. Moreover, on the study of cell systems, interference of other cellular proteic components makes Trp and Tyr fluorescence a useless tool. However, when a molecule is interacting with a lipid membrane, it alters some of the intrinsic properties of the membrane, such as the different types of membrane potentials, lipid fluidity, curvature, polarity or packing. Lipophilic fluorescent probes sensitive to these properties can be used to indirectly report parameters of protein–membrane or peptide–membrane interactions. We will focus on the use of potential-sensitive fluorescent probes, as fluidity and polarity probes are more commonly used to study membrane properties themselves [56]. This strategy also avoids the necessity of peptide or protein derivatization, which can modify native structures and lead to biased results. This advantage is particularly important when peptides are used. The use of these probes has also been recently reviewed elsewhere [57].

3.1. Membrane surface potential perturbation

The surface potential is a consequence of the net excess charges that accumulate in the outer surface of the cell membrane, in contact with the external medium (Fig. 9). It is therefore the potential difference between the membrane surface and the bulk medium. The sources of these charges are mainly ionized lipid head-groups and ions electrostatically interacting with them [58–60]. Hence, the approach of a charged entity, such as a peptide or protein, to the membrane outer surface is likely to alter the surface potential by itself or altering the ion distribution.

Fluorescein phosphatidylethanolamine (FPE) has been the main probe used to detect alterations in the membrane surface potential [61]. When incorporated into lipid membranes, the fluorescein moiety of this probe stands precisely in the water–lipid interface, and hence it has the ability to detect pH or charge distribution changes at the membrane surface (Fig. 10) [61]. FPE behavior can be explained by the

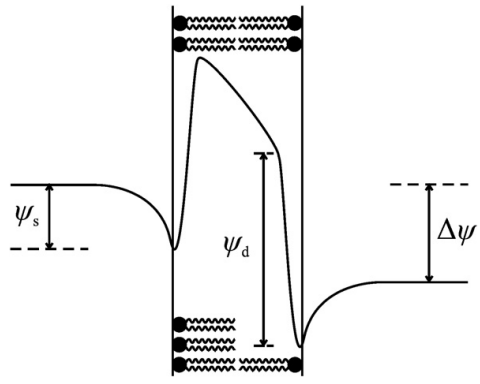

Fig. 9. Schematic representation of the three types of membrane potential by tracing the electrical potential profile across the membrane. Surface potential (ψ_s) arises from the accumulation of charges at the membrane surface. Dipole potential (ψ_d) derives from the sum of the dipolar components of the phospholipids and interface water. Ion concentration gradients account for transmembrane potential ($\Delta\psi$). Reprinted from [57].

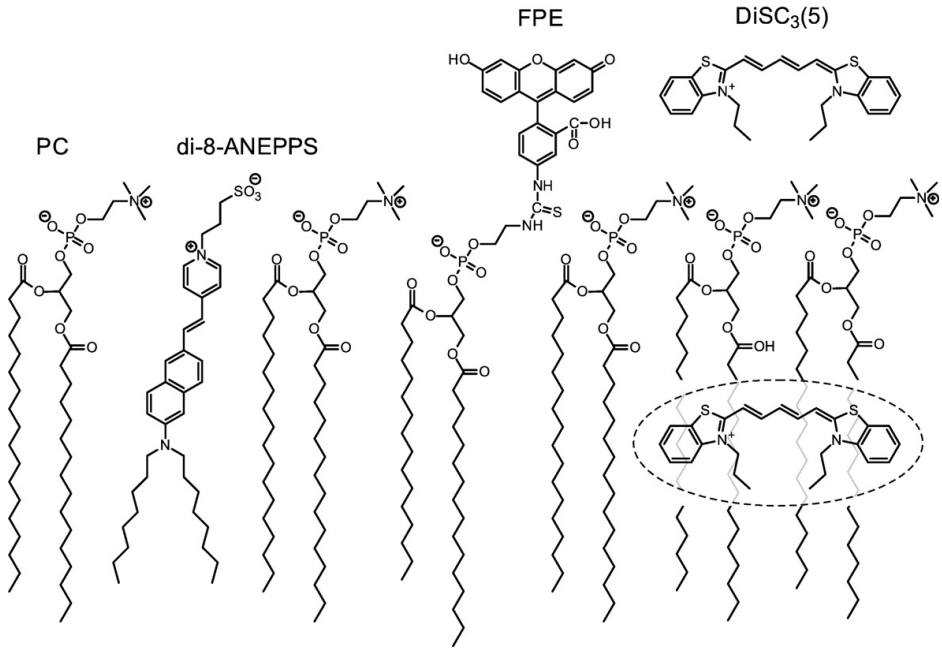

Fig. 10. Structural representation of different potential sensitive probes in the membrane leaflet environment. FPE and di-8-ANEPPS are the main probes for use in the detection of surface and dipole potential, respectively. $DiSC_3(5)$ is depicted as an example of slow response transmembrane potential probe that partitions to the membrane. The structures of the probes are represented as inserted in a portion of a phosphatidylcholine (PC) lipid layer.

Henderson–Hasselbalch equation, taking into account the surface potential [62]:

$$\log\left(\frac{c_F}{c_{HF}}\right) = \mathrm{pH} - \left(\mathrm{p}K - \frac{F\psi_s}{RT\ln 10}\right) \tag{28}$$

where c_F and c_{HF} are the concentrations of the dissociated and protonated forms of the fluorophore located at the membrane surface, respectively, and the expression $\mathrm{p}K - F\psi_s/(RT\cdot\ln 10)$ is the apparent pK, where ψ_s is the surface potential. Changes in the surface potential at constant bulk phase pH affect the apparent pK of FPE and, consequently, its protonation state, resulting in changes in the quantum yield [61,62]. The simplest test to verify the correct incorporation and responsiveness of FPE in vesicles or cells is the addition of calcium ions (cation to which the membranes are impermeable) to the medium, which will lead to an increased surface potential (accumulation of positive charges at the surface) and, consequently, decreased fluorescein apparent pK, increased deprotonation and increased fluorescence intensity [61]. This effect is observed not only for negatively charged phospholipids that attract the calcium ions, but also for the zwitterionic ones, which complex the calcium ions via the phosphate groups [63,64] or even possibly through the carbonyl oxygens [65]. The dielectric environment appears not to influence significantly the probe [66]. However, this is a possible interference factor, as protein adsorption may alter the dielectric environment of the probe and not only the surface potential.

As a lipophilic dye, FPE is suitable for labeling both lipid vesicles and cell membranes. Lipid vesicles are usually obtained by extrusion methods, and the incorporation of FPE can be done by two different experimental approaches: (i) co-solubilizing the probe in the lipid mixture prior to the extrusion, or (ii) labeling the vesicles after they are formed, by incubating them with the probe, followed by gel filtration to remove unbound fluorophore [61]. The first option is a simpler and faster method, but both inner and outer leaflets of the bilayers get labeled. In most of the cases where just the interaction with the outer leaflet is concerned, the labeled inner leaflet does not interfere (provided that translocation of the interacting molecule to the vesicle interior and changes in the inner leaflet environment are not significant). Cell membranes can be easily labeled by incubating them with FPE. There is no need for gel filtration, as the unbound probe can be removed by centrifugation and washing with fresh buffer. In some specific cases of its application to studies with cells, the response of FPE may not be the expected due to complex membrane features, such as the extensive glycocalix in erythrocytes [67,68] or the extracellular matrix of B12 microglial cells [67]. Successful FPE changes could be observed after treatment with neuraminidase and collagenase, respectively, to remove such features.

The interactions of the peptides melittin (component of the bee venom) and p25 (leader sequence of subunit IV of cytochrome *c* oxidase) with membrane model systems were among the first experiments to use FPE as surface potential reporter [61]. When p25 or melittin was added to a FPE-labeled vesicles suspension, an immediate increase of fluorescence intensity was observed as a consequence of their overall positive charge, followed by a slower decrease in fluorescence until stabilization. This biphasic response was better observed using stopped-flow rapid mixing method, as it allowed resolving the initial fluorescence increase event in the millisecond time scale [61,69]. The most plausible explanation for this kinetic profile, advanced by the original authors, is that the cationic peptide reaches the membrane surface, increasing the surface potential and consequently the probe fluorescence. After that, a partial insertion into the membrane would bury positive charges, which would no longer contribute to the potential and hence a fluorescence decrease would be observed. The dependence of FPE

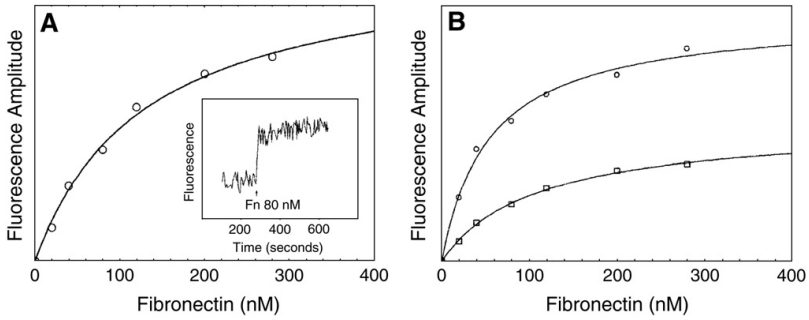

Fig. 11. Interaction of fibronectin with osteoblast membranes. (A) FPE-labeled osteoblasts fluorescence intensity variation profile with concentration, upon serial addition of fibronectin. A typical time course variation of fluorescence intensity at the addition moment is shown in the inset. The data was fitted to a single binding site model. (B) Heparitinase treatment reduced the binding significantly. Comparison of the fluorescence changes between FPE-labeled osteoblasts (○) with those previously treated with heparitinase (□) that removes cell surface heparan sulfate. The experiments were conducted at 37 °C with a cell concentration of 5×10^4/mL. Reprinted from [71].

fluorescence change with p25 concentration was also shown to follow a cooperative binding model, never demonstrated before for a free signal-sequence peptide [69].

The prion protein (PrP) is a cell membrane-associated protein that can be converted, via post-translational modifications, to a pathogenic scrapie form, which causes spongiform encephalopathies [70]. Interaction with membranes can have a role in this conversion. The binding of Syrian hamster prion protein, which closely resembles human prion protein, to biomembrane model systems was assessed with FPE [70]. The interaction with POPG vesicles follows a complex kinetic in which a rapid fluorescence intensity increase is observed due to initial interaction events, followed by a fluorescence decrease, probably due to protein partial insertion, and a third slower phase of less perceptible fluorescence increase, hypothesized as being caused by lipid rearrangements. However, for the POPC:POPG mixture 70:30 (molar ratio), only the initial binding phase was observed, but with a slower kinetics. This is an example of how FPE can dissect the different stages of a peptide–membrane interaction.

FPE was also used to study the interaction between the extracellular matrix protein fibronectin and the membranes of osteoblast, cells responsible for bone formation [71]. Upon addition of fibronectin to FPE-labeled osteoblasts, an immediate increase on fluorescence is observed (Fig. 11A, inset), revealing that an interaction occurred rapidly. These fluorescence variations were analyzed as a function of protein concentration, enabling the calculation of a dissociation constant (K_d) of 120 nM. The treatment of these cells with heparitinase previously to the interaction experiments lead to a 50% decrease in binding (Fig. 11B), indicating that cell surface heparan sulfate proteoglycans are partly responsible for the binding. Moreover, in the presence of the integrin-binding motif RGD peptide, fibronectin membrane binding was also reduced, due to competition with integrin receptors. Therefore, fibronectin appetence for osteoblasts is modulated by cell surface integrins and proteoglycans.

3.2. Membrane dipole potential perturbation

Dipole potential is another type of membrane potential, originating from the sum of the dipolar residues of lipids (polar head-groups and glycerol-ester regions) due to its rather aligned organization and oriented water molecules hydrating the surfaces of the membrane (Fig. 9) [72,73]. Macromolecules interacting with the membrane can destabilize this organization and/or contribute with their own dipoles to the membrane dipole potential; hence, the detection of alterations on this property can be used to report such interactions. The first fluorescent membrane probes described as sensitive to dipole potential were di-8-ANEPPS (4-[2-[6-(dioctylamino)-2-naphthalenyl]ethenyl]-1-(3-sulfopropyl)-pyridinium) [74] and RH421 (N-(4-sulfobutyl)-4-[4-[4-(dipentylamino)phenyl]butadienyl]-pyridinium) [75]. They possess a considerably conjugated chromophore region (high stokes shift) in which two aliphatic chains are attached to facilitate the incorporation of the probe in a phospholipid layer. The chromophore stays near the lipid head group and glycerol backbone, sensing the local electric fields derived from the dipoles [74]. The mechanism by which di-8-ANEPPS and RH421 sense the dipole potential is believed to be electrochromical [76]. Absorption and emission peaks shift in response to a nearby electrical field that differentially interacts with the ground-state and excited-state dipole moments of the chromophore [77]. Thus, changes in dipole potential are measured in terms of spectral shifts of the lipid bilayer incorporated probe. Therefore, this type of probes is specially suitable for a dual wavelength ratiometric measurements strategy, similar to what is done with some ion indicators, such as for Ca^{2+} [78]. This approach is very advantageous because the signal is independent of probe or cell concentration and avoids photobleaching-induced artifacts [74].

In this section, we present some examples regarding only the use of di-8-ANEPPS, as it is the most commonly used dye for dipole potential-related interaction studies (Fig. 10). Although the vast majority of the work conducted with di-8-ANEPPS relies on the measurement of excitation spectrum shifts, only recently a systematic study was carried out to compare excitation and emission ratiometric fluorescence methods for this dye, concluding that only the former can be used [79]. Shifts in the excitation spectra can be better observed by transforming data in differential spectra, that is, subtracting the normalized excitation spectra of the probe without the molecule of interest from the normalized excitation spectra of di-8-ANEPPS in the presence of the interacting molecules. This typically yields a sinusoidal curve crossing the abscissa axis with one maximum and one minimum. A blue shift is denoted when the minimum occurs at a lower wavelength than the maximum and the opposite for the red shift. However, one has to know what this means in terms of dipole potential variation. This is revealed by modulating the dipole potential of phospholipid vesicles with phloretin and 6-ketocholestanol (6-KC) [74], previously shown to decrease and increase the membrane dipole potential, respectively [80]. A blue shift is induced by 6-KC, meaning that blue shifts indicate the increase in dipole potential, and the opposite for phloretin. In addition, the ratio of the fluorescence intensity produced at the wavelengths of the maximum and minimum of the differential spectra (the value at lower wavelength divided by the value at higher wavelength) is a quantitative parameter that can be used for the same purpose. Addition of 6-KC to di-8-ANEPPS labeled vesicles increased the ratio, while such parameter was decreased by phloretin [74]. To summarize, increasing the dipole potential leads to a blue shift in the excitation spectrum and

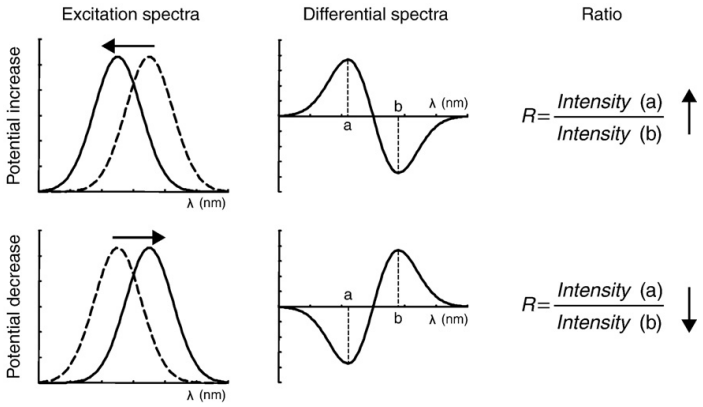

Fig. 12. Sensing the membrane dipole potential with di-8-ANEPPS. The excitation spectrum of membrane-bound di-8-ANEPPS shifts in response to changes in the dipole potential. The differential spectra help to visualize these shifts and to determine the wavelengths of maximal variation, in order to define the ratio *R*.

increase of the ratio value; at variance, decreasing of this potential leads to a red shift and decrease of the ratio (Fig. 12).

A problem that may arise is the fact that di-8-ANEPPS, as other fast response voltage sensitive probes, is also sensitive to transmembrane potential variations [81] and hence it is advised that, during measurements, transmembrane potential, if any, should be kept constant. Membrane fluidity is another aspect for concern. Gross et al. [74] stated that membrane microviscosity does not significantly influence the fluorescence excitation ratio, and Clarke and Kane [82] suggested that, in order to eliminate the possible effects of membrane fluidity, fluorescence should be detected at the red-edge of the emission spectra.

The influence of dipole potential on p25 interaction with lipid vesicles was studied with di-8-ANEPPS, along with the above mentioned FPE measurements for surface potential [83]. This peptide induced a decrease in the dipole potential of phosphatidylcoline lipid vesicles, as evaluated by the di-8-ANEPPS differential spectrum. The excitation ratio of this probe was also measured for different concentrations of p25, yielding a K_d of 2.8 μM. The initial dipole potential of lipid vesicles was also modulated via phloretin or 6-KC, changing the maximum extension of binding for the peptide. These results, together with those from stopped-flow fluorescence measurements with FPE, elucidated that p25 rapidly interacts with the membrane surface before inserting into the membrane, affecting the dipole potential only in this latter step.

The propensity of HIV-1 fusion inhibitor peptides enfuvirtide and T-1249 to interact with blood cell membranes was also evaluated using di-8-ANEPPS, as a Trp fluorescence-based approach would be impracticable with cells [84]. Human isolated erythrocytes and peripheral blood mononuclear cells with their membranes labeled with the probe were incubated with either one of the peptides. Differential excitation spectra were obtained in order to observe the probe response, showing that the presence of the peptides decreased the dipole potential of the membrane in a concentration-dependent manner (Fig. 13A). The kinetics of this interaction could be followed by measuring the excitation ratio in real-time (Fig. 13B). To quantify the affinity of these peptides to the cell membranes, the variation of the ratio with the peptide concentration was analyzed using a hyperbolic binding curve, in order to obtain the peptide–biomembrane dissociation constants (Fig. 13C). T-1249 was shown to have an approximately eight-fold higher affinity when compared with enfuvirtide. This enhanced interaction of T-1249 with cell membranes correlates with its higher efficacy *in vivo*, due to a possible effect of membrane-enhanced drug transfer to the membrane-associated gp41 in its pre-fusion conformation.

Besides di-8-ANEPPS, other probes have been shown to be sensitive to dipole potential. Variants of NBD-labeled lipids were tested for their sensitivity to membrane dipole potential [85]. The probes relative fluorescence intensity had a linear dependency on the dipole potential of the labeled vesicles. No shifts or broadening of the probe spectrum were observed when the dipole varied; hence, no ratiometric approach can be used. Probes derived from 3-hydroxyflavone, such as F4N1 (*N*-[(4′-dimethylamino)-3-hydroxy-6-flavonyl] methyl-*N*,*N*-trimethyl ammonium bromide) and BPPZ (3-(4-{4-[4′-(3-Hydroxybenzo[*f*]flavonyl)phenyl]piperazino}-1-pyridiniumyl)-1-propanesulfonate), were more recently developed [86]. These probes have the particularity of undergoing excited-state intramolecular proton-transfer (ESIPT), yielding two tautomeric forms, revealed by the presence of two peaks on their fluorescence emission spectra. Excitation spectrum shifts were observed for both probes and, more importantly, the intensity ratio of the two emission bands also changed as a response to potential variations. These two types of ratio, at two wavelengths of the excitation spectrum edges and at the two emission peaks, correlated very well with di-8-ANEPPS excitation ratio, proving the usefulness of these new probes for detecting dipole potential. The two-band emission ratio is also very useful for microscopy, as the emissions can be collected from two emission filters corresponding to the bands, enabling the production of ratio images.

3.3. Transmembrane potential perturbation

The transmembrane potential can be defined, in simple terms, as the difference of potentials between the intra and extracellular aqueous phases. This is a consequence of the selective nature of the membrane, which may allow the flux of specific charged solutes (e.g., ions), creating a concentration gradient (Fig. 9).

There are many fluorescent probes available to detect changes in the transmembrane potential. They can be divided in two major groups, depending on their slow or fast response [87]. The slow response probes include carbocyanins, such as its indo-(DiI), thio-(DiS) and oxo-(DiO) derivatives, and oxonols, including bis-barbituric acid (DiBAC) and bis-thiobarbituric acid (DiSBAC) derivatives. The mode of detection of this type of probes may vary depending on the molecule, but it is often based on the partition equilibrium between the membrane and the aqueous medium, or through a Nernst equilibrium-dependent translocation to the cell or mitochondria interior [88]. On the other hand, fast response probes (that include ANEP and RH families) sense potential alterations by electrochromic mechanisms and intramolecular charge rearrangements, as

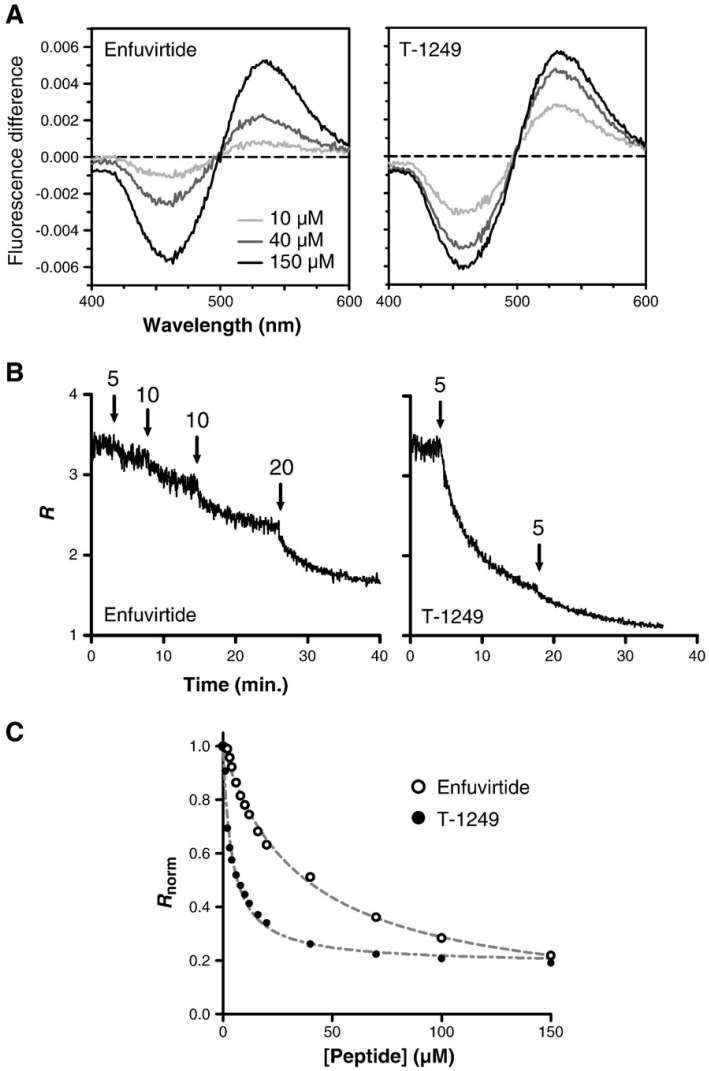

Fig. 13. Interaction of HIV fusion inhibitor peptides with erythrocyte membrane. (A) Differential spectra showing the dipole potential changes in the presence of enfuvirtide or T-1249. (B) The decrease in the dipole potential when the peptides are added can be followed through time by measuring the ratio (R) of fluorescence intensities (I) at two excitation wavelengths of maximum variation according to the differential spectra, $R = I_{455nm}/I_{525nm}$. (C) Quantification of the affinity of the two peptides towards the erythrocyte membrane by fitting the data to a hyperbolic binding model (single binding site). T-1249 dissociation constant (4.16 μM) is approximately eight times lower than for enfuvirtide (35.4 μM). For peripheral blood mononuclear cells the variation trend was similar. Ratios were normalized for the initial value. Adapted from [84].

previously explained for di-8-ANEPPS. Such electronic changes are much faster than molecular translocations, justifying the nomenclature.

The monitoring of alterations in transmembrane potential during the interaction of macromolecules with membranes is important in cases where major membrane destabilizations (such as pore formation or loosening of the lipid matrix) take place, dissipating ionic gradients. The most representative examples are from antimicrobial peptides, which often form pores or channels in bacterial membranes, in order to induce leakage and, consequently, cell death. Additionally, cell-penetrating peptides, able to translocate cargo molecules inside the cell without major membrane disruption, can depend on transmembrane potential for their mode of action [30,89].

The antimicrobial family of microcins consists of low molecular weight peptides synthesized mainly by *Escherichia coli* [90]. The interaction of the peptide Microcin J25 (MccJ25) with membrane vesicles was assessed by various methods, including transmembrane potential monitoring with the slow response probe $DiSC_3(5)$ (3,3′-dipropylthiadicarbocyanine iodide, Fig. 10) [91]. A transmembrane potential was achieved by adding valinomycin to vesicles prepared in a KCl-containing buffer and suspended in a NaCl-containing buffer. In the presence of MccJ25, the preformed potential is significantly dissipated, as indicated by an increase in the fluorescence of the probe, both for vesicles of PC and PC/PG/CL (phosphatidylcoline/phosphatidylglycerol/cardiolipin), a mixture that mimics bacteria membrane (Fig. 14). Therefore, it was shown that the peptide is

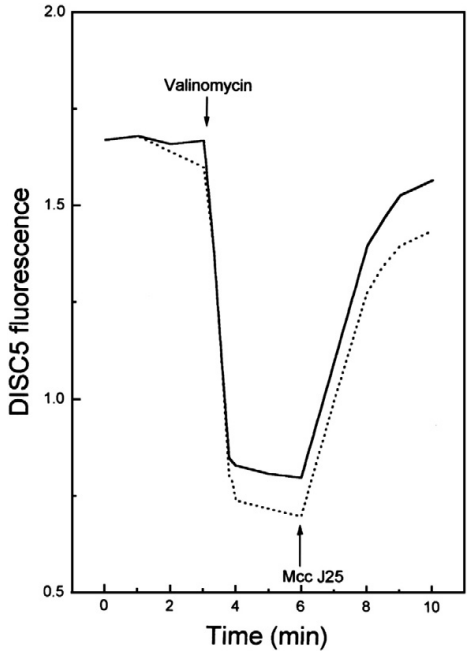

Fig. 14. Perturbation of lipid membranes by the antimicrobial peptide microcin J25. Transmembrane potential monitoring with the probe $DiSC_3(5)$ for K^+-loaded lipid vesicles of PC (solid line) or PC:PG:CL 7:2:1 (dotted line) in Na^+-containing buffer. Addition of valinomycin induced a transmembrane potential that was dissipated with the addition of the peptide. Reprinted from [91].

capable of inducing membrane permeabilization. A similar study was done with the rationally designed peptide PST11-RK, based on the structural motifs of the antimicrobial peptide tritrpticin. The effect that this peptide has on bacterial membranes was assessed via $DiSC_3$ (5) fluorescence for *Staphylococcus aureus* and *E. coli* [92]. In the presence of PST11-RK, a fluorescence increase was observed due to bacterial membrane depolarization (dissipation of potential) in a concentration-dependent manner. Membrane permeabilization should then represent a major killing factor upon PST11-RK application.

4. Conclusions

Visualizing, monitoring and understanding biological and biophysical processes in real-time are of key importance for life sciences research. Focusing on processes that occur at the cell membrane level, it has been described how intrinsic features of peptides and proteins, namely fluorescence, can help to observe their behavior towards this important cell structure.

The interaction of proteins or peptides with the cell membrane or membrane model systems can be conveniently followed using fluorescence spectroscopy. This can be regarded simply as a qualitative tool, but the main advantages of fluorescence spectroscopy application at this level are related with its use for quantitative purposes, on the direct evaluation of peptide–membrane and protein–membrane interactions, together with the elucidation of the factors that influence the extension of the process. The changes in some of the intrinsic fluorescence parameters of peptides containing fluorescent amino acid residues can be easily used to measure the insertion of a peptide on a membrane, without the need of peptide labeling (a process that can lead to significant changes on the structure and properties of the molecule and consequent biased observations). Additionally, the fluorescent amino acid residues of a protein can also be used as energy transfer donors, enabling the quantification of the extension even of the weak interactions associated with most of the membrane adsorption processes.

Many studies are centered in the interacting macromolecule, meaning that it is such the entity that produces the fluorescence signal, whether it has intrinsic fluorescent amino acid residues or it is derivatized with a fluorophore. However it can be more advantageous to perform membrane-centered studies, in which a property of the membrane is monitored by means of a lipophilic fluorescent probe while the interaction is occurring. We reviewed how probes sensitive to the different types of membrane potential can translate such interactions. FPE is the main probe sensitive to surface potential and can report interactions of charged macromolecules with the membrane surface. It is capable of distinguishing different moments of interaction, such as initial binding events and insertion, allowing multiphasic kinetics to be observed. The membrane dipole potential sensor di-8-ANEPPS detects interactions of molecules that do not need to be charged and is particularly sensitive to molecules rich in dipole chemical groups. It reports insertions in the lipid layer or surface interactions that disturb the organizations of dipolar residues of the phospholipids. Transmembrane potential probes are useful to assess interactions that lead to membrane disruption, causing potential dissipation and eventually content leakage or lysis. Real-time imaging with membrane potential sensitive probes is becoming a reality and it will be very interesting to follow the evolution of these techniques to enable the mapping of interaction events at the membrane level.

Several studies use more than one of these experimental approaches in order to obtain more information about the interaction events. All these methodologies, as well as their combination provide molecular level information useful in the fields of drug development, cell signaling, trafficking and interactomics.

Acknowledgments

This work was partially supported by projects PTDC/QUI/69937/2006 and PTDC/QUI-BIQ/104787/2008 from Fundação para a Ciência e Tecnologia of the Portuguese Ministery of Science, Technology and Higher Education (FCT-MCTES). PMM and HGF also thank FCT-MCTES for grants SFRH/BD/42205/2007 and SFRH/BD/39039/2007, respectively.

References

[1] M. Castanho (Ed.), Structure and function of membrane-active peptides, International University Line Publishers (IUL Press), La Jolla, CA, 2010.
[2] S.C.D.N. Lopes, A. Fedorov, M.A.R.B. Castanho, Chiral recognition of D-kyotorphin by lipidic membranes: relevance toward improved analgesic efficiency, ChemMedChem 1 (2006) 723–728.
[3] M.N. Melo, M.A.R.B. Castanho, Omiganan interaction with bacterial membranes and cell wall models. Assigning a biological role to saturation, Biochim. Biophys. Acta 1768 (2007) 1277–1290.
[4] M.N. Melo, D. Dugourd, M.A.R.B. Castanho, Omiganan pentahydrochloride in the front line of clinical applications of antimicrobial peptides, Recent Patents Anti-Infect, Drug Disc. 1 (2006) 201–207.
[5] V.J. Hruby, W. Kazmierski, A.M. Kawasaki, T.O. Matsunaga, Peptide pharmaceuticals, in: D.A. Ward (Ed.), Synthetic Chemistry and the Design of Peptide-based Drugs, Open University Press, Buckingham, UK, 1991, pp. 135–184.
[6] J.S. Wadia, M. Becker-Hapak, S.F. Dowdy, Protein transport, in: Ü. Langel (Ed.), Cell-penetrating Peptides — Processes and Applications, CRC Press, Boca Raton, FL, 2002, pp. 365–375.
[7] A.S. Veiga, N.C. Santos, L.M. Loura, A. Fedorov, M.A.R.B. Castanho, HIV fusion inhibitor peptide T-1249 is able to insert or adsorb to lipidic bilayers. Putative correlation with improved efficiency, J. Am. Chem. Soc. 126 (2004) 14758–14763.
[8] S. Veiga, S. Henriques, N.C. Santos, M. Castanho, Putative role of membranes in the HIV fusion inhibitor enfuvirtide mode of action at the molecular level, Biochem. J. 377 (2004) 107–110.
[9] D.F. Sargent, R. Schwyzer, Membrane lipid phase as catalyst for peptide–receptor interactions, Proc. Natl. Acad. Sci. U. S. A. 83 (1986) 5774–5778.

[10] M.A.R.B. Castanho, M.X. Fernandes, Lipid membrane-induced optimization for ligand–receptor docking: recent tools and insights for the "membrane catalysis" model, Eur. Biophys. J. 35 (2006) 92–103.
[11] S.H. White, W.C. Wimley, Hydrophobic interactions of peptides with membrane interfaces, Biochim. Biophys. Acta 1376 (1998) 339–352.
[12] S.H. White, W.C. Wimley, Membrane protein folding and stability: physical principles, Annu. Rev. Biophys. Biomol. Struct. 28 (1999) 319–365.
[13] S.T. Henriques, M.A.R.B. Castanho, Consequences of nonlytic membrane perturbation to the translocation of the cell penetrating peptide pep-1 in lipidic vesicles, Biochemistry 43 (2004) 9716–9724.
[14] A. Chattopadhyay, E. London, Parallax method for direct measurement of membrane penetration depth utilizing fluorescence quenching by spin-labeled phospholipids, Biochemistry 26 (1987) 39–45.
[15] M.A.R.B. Castanho, M.J.E. Prieto, Fluorescence quenching data interpretation in biological systems. The use of microscopic models for data analysis and interpretation of complex systems, Biochim. Biophys. Acta 1373 (1998) 1–16.
[16] A.S. Ladokhin, Distribution analysis of depth-dependent fluorescence quenching in membranes: a practical guide, Methods Enzymol. 278 (1997) 462–473.
[17] E. London, A.S. Ladokhin, Measuring the depth of amino acid residues in membrane-inserted peptides by fluorescence quenching, Curr. Top. Membr. 52 (2002) 89–115.
[18] M.X. Fernandes, J. Garcia de la Torre, M.A.R.B. Castanho, Joint determination by Brownian dynamics and fluorescence quenching of the in-depth location profile of biomolecules in membranes, Anal. Biochem. 307 (2002) 1–12.
[19] H.G. Franquelim, L.M. Loura, N.C. Santos, M.A.R.B. Castanho, Sifuvirtide screens rigid membrane surfaces. establishment of a correlation between efficacy and membrane domain selectivity among HIV fusion inhibitor peptides, J. Am. Chem. Soc. 130 (2008) 6215–6223.
[20] S.C.D.N. Lopes, M.A.R.B. Castanho, Overview of common spectroscopic methods to determine the orientation/alignment of membrane probes and drugs in lipidic bilayers, Curr. Org. Chem. 9 (2005) 889–898.
[21] S.C.D.N. Lopes, A. Fedorov, M.A.R.B. Castanho, Cholesterol modulates maculosin's orientation in model systems of biological membranes. Relevance towards putative molecular recognition, Steroids 69 (2004) 825–830.
[22] S.C.D.N. Lopes, A. Fedorov, M.A.R.B. Castanho, Lipidic membranes are potential "catalysts" in the ligand activity of the multifunctional pentapeptide neokyotorphin, Chembiochem 6 (2005) 697–702.
[23] G. Adam, M. Delbrück, Reduction of dimensionality in biological diffusion processes, in: A. Rich, N. Davidson (Eds.), Structural Chemistry and Molecular Biology, W. H. Freeman & Co., San Francisco, 1968, pp. 198–215.
[24] C. DeLisi, The biophysics of ligand–receptor interactions, Q. Rev. Biophys. 13 (1980) 201–230.
[25] N.D. Gershon, K.R. Porter, B.L. Trus, The cytoplasmic matrix: its volume and surface area and the diffusion of molecules through it, Proc. Natl. Acad. Sci. U.S.A. 82 (1985) 5030–5034.
[26] M. Baldo, A. Grassi, A. Raudino, Diffusion-controlled reactions among ligands and receptor clusters: effects of competition for ligands, J. Phys. Chem. 95 (1991) 6734–6740.
[27] J. Erickson, B. Goldstein, D. Holowka, B. Baird, The effect of receptor density on the forward rate constant for binding of ligands to cell surface receptors, Biophys. J. 52 (1987) 657–662.
[28] R.I. Cukier, The effect of surface diffusion on surface reaction rates, J. Chem. Phys. 79 (1983) 2430–2435.
[29] J. Martins, E. Melo, K.R. Naqvi, Reappraisal of four different approaches for finding the mean reaction time in the multi-trap variant of the Adam–Delbruck problem, J. Chem. Phys. 120 (2004) 9390–9393.
[30] S.T. Henriques, J. Costa, M.A.R.B. Castanho, Re-evaluating the role of strongly charged sequences in amphipathic cell-penetrating peptides: a fluorescence study using Pep-1, FEBS Lett. 579 (2005) 4498–4502.
[31] H.H. Szeto, P.W. Schiller, K. Zhao, G. Luo, Fluorescent dyes alter intracellular targeting and function of cell-penetrating tetrapeptides, FASEB J. 19 (2005) 118–120.
[32] E. Rhoades, T.F. Ramlall, W.W. Webb, D. Eliezer, Quantification of alpha-synuclein binding to lipid vesicles using fluorescence correlation spectroscopy, Biophys. J. 90 (2006) 4692–4700.
[33] L. Rusu, A. Gambhir, S. McLaughlin, J. Radler, Fluorescence correlation spectroscopy studies of peptide and protein binding to phospholipid vesicles, Biophys. J. 87 (2004) 1044–1053.
[34] S. Haldar, H. Raghuraman, A. Chattopadhyay, Monitoring orientation and dynamics of membrane-bound melittin utilizing dansyl fluorescence, J. Phys. Chem. B 112 (2008) 14075–14082.
[35] H. Raghuraman, A. Chattopadhyay, Orientation and dynamics of melittin in membranes of varying composition utilizing NBD fluorescence, Biophys. J. 92 (2007) 1271–1283.
[36] M.K. Jain, J. Rogers, L. Simpson, L.M. Gierasch, Effect of tryptophan derivatives on the phase properties of bilayers, Biochim. Biophys. Acta 816 (1985) 153–162.
[37] A.S. Ito, A.M. Castrucci, V.J. Hruby, M.E. Hadley, D.T. Krajcarski, A.G. Szabo, Structure–activity correlations of melanotropin peptides in model lipids by tryptophan fluorescence studies, Biochemistry 32 (1993) 12264–12272.
[38] N.C. Santos, M. Prieto, M.A.R.B. Castanho, Quantifying molecular partition into model systems of biomembranes: an emphasis on optical spectroscopic methods, Biochim. Biophys. Acta 1612 (2003) 123–135.
[39] N.C. Santos, M. Castanho, Fluorescence spectroscopy methodologies on the study of proteins and peptides. On the 150th anniversary of protein fluorescence, Trends. Appl. Spectr. 4 (2002) 113–125.
[40] N.C. Santos, M. Prieto, M.A.R.B. Castanho, Interaction of the major epitope region of HIV protein gp41 with membrane model systems. A fluorescence spectroscopy study, Biochemistry 37 (1998) 8674–8682.
[41] A. Coutinho, M. Prieto, Self-association of the polyene antibiotic nystatin in dipalmitoylphosphatidylcholine vesicles: a time-resolved fluorescence study, Biophys. J. 69 (1995) 2541–2557.
[42] M.A.R.B. Castanho, M.J.E. Prieto, Fluorescence study of the macrolide pentaene antibiotic filipin in aqueous solution and in a model system of membranes, Eur. J. Biochem. 207 (1992) 125–134.
[43] W.L.C. Vaz, E. Melo, Fluorescence spectroscopic studies on phase heterogeneity in lipid bilayer membranes, J. Fluoresc. 11 (2001) 255–271.
[44] J.R. Lakowicz, Principles of Fluorescence Spectroscopy, 2nd ed., Kluwer Academic/Plenum Publishers, New York, NY, 1999.
[45] M. Vermeir, N. Boens, K.P. Heirwegh, Interaction of 7-n-alkoxycoumarins with cytochrome P-450(2) and their partitioning into liposomal membranes. Assessment of methods for determination of membrane partition coefficients, Biochem. J. 284 (1992) 483–490.
[46] S.T. Henriques, M.A.R.B. Castanho, Environmental factors that enhance the action of the cell penetrating peptide pep-1 A spectroscopic study using lipidic vesicles, Biochim. Biophys. Acta 1669 (2005) 75–86.
[47] D.G. Pina, L. Johannes, M.A.R.B. Castanho, Shiga toxin B-subunit sequential binding to its natural receptor in lipid membranes, Biochim. Biophys. Acta 1768 (2007) 628–636.
[48] F. Stauffer, M.N. Melo, F.A. Carneiro, F.J. Sousa, M.A. Juliano, L. Juliano, R. Mohana-Borges, A.T. Da Poian, M.A.R.B. Castanho, Interaction between dengue virus fusion peptide and lipid bilayers depends on peptide clustering, Mol. Membr. Biol. 25 (2008) 128–138.
[49] H.G. Franquelim, A.S. Veiga, G. Weissmuller, N.C. Santos, M.A.R.B. Castanho, Unravelling the molecular basis of the selectivity of the HIV-1 fusion inhibitor sifuvirtide towards phosphatidylcholine-rich rigid membranes, Biochim. Biophys. Acta (2010).
[50] R.E. Dale, J. Eisinger, W.E. Blumberg, The orientational freedom of molecular probes. The orientation factor in intramolecular energy transfer, Biophys. J. 26 (1979) 161–193.
[51] L. Davenport, R.E. Dale, R.H. Bisby, R.B. Cundall, Transverse location of the fluorescent probe 1, 6-diphenyl-1, 3, 5-hexatriene in model lipid bilayer membrane systems by resonance excitation energy transfer, Biochemistry 24 (1985) 4097–4108.
[52] S. Bar, M. Alizon, Role of the ectodomain of the gp41 transmembrane envelope protein of human immunodeficiency virus type 1 in late steps of the membrane fusion process, J. Virol. 78 (2004) 811–820.
[53] Y. Kliger, S.G. Peisajovich, R. Blumenthal, Y. Shai, Membrane-induced conformational change during the activation of HIV-1 gp41, J. Mol. Biol. 301 (2000) 905–914.
[54] Y. Kliger, S.A. Gallo, S.G. Peisajovich, I. Munoz-Barroso, S. Avkin, R. Blumenthal, Y. Shai, Mode of action of an antiviral peptide from HIV-1. Inhibition at a post-lipid mixing stage, J. Biol. Chem. 276 (2001) 1391–1397.
[55] T. Le Doan, M. Takasugi, I. Aragon, G. Boudet, T. Montenay-Garestier, C. Helene, Excitation energy transfer from tryptophan residues of peptides and intrinsic proteins to diphenylhexatriene in phospholipid vesicles and biological membranes, Biochim. Biophys. Acta 735 (1983) 259–270.
[56] R.M. Epand, R. Kraayenhof, Fluorescent probes used to monitor membrane interfacial polarity, Chem. Phys. Lipids 101 (1999) 57–64.
[57] P.M. Matos, S. Goncalves, N.C. Santos, Interaction of peptides with biomembranes assessed by potential-sensitive fluorescent probes, J. Pept. Sci. 14 (2008) 407–415.
[58] S. McLaughlin, The electrostatic properties of membranes, Annu. Rev. Biophys. Biophys. Chem. 18 (1989) 113–136.
[59] M. Langner, K. Kubica, The electrostatics of lipid surfaces, Chem. Phys. Lipids 101 (1999) 3–35.
[60] G. Cevc, Membrane electrostatics, Biochim. Biophys. Acta 1031 (1990) 311–382.
[61] J. Wall, C.A. Golding, M. Van Veen, P. O'Shea, The use of fluoresceinphosphatidylethanolamine (FPE) as a real-time probe for peptide-membrane interactions, Mol. Membr. Biol. 12 (1995) 183–192.
[62] P. O'Shea, Intermolecular interactions with/within cell membranes and the trinity of membrane potentials: kinetics and imaging, Biochem. Soc. Trans. 31 (2003) 990–996.
[63] H. Binder, O. Zschornig, The effect of metal cations on the phase behavior and hydration characteristics of phospholipid membranes, Chem. Phys. Lipids 115 (2002) 39–61.
[64] L. Herbette, C.A. Napolitano, R.V. McDaniel, Direct determination of the calcium profile structure for dipalmitoyllecithin multilayers using neutron diffraction, Biophys. J. 46 (1984) 677–685.
[65] R.A. Bockmann, H. Grubmuller, Multistep binding of divalent cations to phospholipid bilayers: a molecular dynamics study, Angew. Chem. Int. Ed Engl. 43 (2004) 1021–1024.
[66] P. Soucaille, M. Prats, J.F. Tocanne, J. Teissie, Use of a fluorescein derivative of phosphatidylethanolamine as a pH probe at water/lipid interfaces, Biochim. Biophys. Acta 939 (1988) 289–294.
[67] J. Cladera, P. O'Shea, Generic techniques for fluorescence measurements of protein–ligand interactions; real time kinetics and spatial imaging, in: S.E. Harding, B.Z. Chowdhry (Eds.), Protein–ligand Interactions, Oxford University Press, Oxford, 2001, pp. 169–200.
[68] J. Wall, F. Ayoub, P. O'Shea, Interactions of macromolecules with the mammalian cell surface, J. Cell Sci. 108 (1995) 2673–2682.
[69] C. Golding, S. Senior, M.T. Wilson, P. O'Shea, Time resolution of binding and membrane insertion of a mitochondrial signal peptide: correlation with structural changes and evidence for cooperativity, Biochemistry 35 (1996) 10931–10937.
[70] N. Sanghera, T.J. Pinheiro, Binding of prion protein to lipid membranes and implications for prion conversion, J. Mol. Biol. 315 (2002) 1241–1256.

[71] B. Sim, J. Cladera, P. O'Shea, Fibronectin interactions with osteoblasts: identification of a non-integrin-mediated binding mechanism using a real-time fluorescence binding assay, J. Biomed. Mater. Res. A 68 (2004) 352–359.
[72] H. Brockman, Dipole potential of lipid membranes, Chem. Phys. Lipids 73 (1994) 57–79.
[73] R.J. Clarke, The dipole potential of phospholipid membranes and methods for its detection, Adv. Colloid Interface Sci. 89–90 (2001) 263–281.
[74] E. Gross, R.S. Bedlack, L.M. Loew, Dual-wavelength ratiometric fluorescence measurement of the membrane dipole potential, Biophys. J. 67 (1994) 208–216.
[75] A. Zouni, R.J. Clarke, J.F. Holzwarth, Kinetics of the solubilization of styryl dye aggregates by lipid vesicles, J. Phys. Chem. 98 (1994) 1732–1738.
[76] E. Fluhler, V.G. Burnham, L.M. Loew, Spectra, membrane binding, and potentiometric responses of new charge shift probes, Biochemistry 24 (1985) 5749–5755.
[77] L.M. Loew, G.W. Bonneville, J. Surow, Charge shift optical probes of membrane potential. Theory, Biochemistry 17 (1978) 4065–4071.
[78] G. Grynkiewicz, M. Poenie, R.Y. Tsien, A new generation of Ca2+ indicators with greatly improved fluorescence properties, J. Biol. Chem. 260 (1985) 3440–3450.
[79] M.F. Vitha, R.J. Clarke, Comparison of excitation and emission ratiometric fluorescence methods for quantifying the membrane dipole potential, Biochim. Biophys. Acta 1768 (2007) 107–114.
[80] J.C. Franklin, D.S. Cafiso, Internal electrostatic potentials in bilayers: measuring and controlling dipole potentials in lipid vesicles, Biophys. J. 65 (1993) 289–299.
[81] R.S. Bedlack Jr., M. Wei, L.M. Loew, Localized membrane depolarizations and localized calcium influx during electric field-guided neurite growth, Neuron 9 (1992) 393–403.
[82] R.J. Clarke, D.J. Kane, Optical detection of membrane dipole potential: avoidance of fluidity and dye-induced effects, Biochim. Biophys. Acta 1323 (1997) 223–239.
[83] J. Cladera, P. O'Shea, Intramembrane molecular dipoles affect the membrane insertion and folding of a model amphiphilic peptide, Biophys. J. 74 (1998) 2434–2442.
[84] P.M. Matos, M.A.R.B. Castanho, N.C. Santos, HIV-1 fusion inhibitor peptides enfuvirtide and T-1249 interact with erythrocyte and lymphocyte membranes, PLoS ONE 5 (2010) e9830.
[85] J.I. Alakoskela, P.K. Kinnunen, Control of a redox reaction on lipid bilayer surfaces by membrane dipole potential, Biophys. J. 80 (2001) 294–304.
[86] A.S. Klymchenko, G. Duportail, Y. Mely, A.P. Demchenko, Ultrasensitive two-color fluorescence probes for dipole potential in phospholipid membranes, Proc. Natl. Acad. Sci. U.S.A. 100 (2003) 11219–11224.
[87] R.P. Haugland, The Handbook — A Guide to Fluorescent Probes and Labelling Technologies, 10th ed, 2005 Molecular Probes, Eugene, OR.
[88] J. Plasek, K. Sigler, Slow fluorescent indicators of membrane potential: a survey of different approaches to probe response analysis, J. Photochem. Photobiol. B 33 (1996) 101–124.
[89] S.T. Henriques, J. Costa, M.A.R.B. Castanho, Translocation of beta-galactosidase mediated by the cell-penetrating peptide pep-1 into lipid vesicles and human HeLa cells is driven by membrane electrostatic potential, Biochemistry 44 (2005) 10189–10198.
[90] C. Asensio, J.C. Perez-Diaz, A new family of low molecular weight antibiotics from enterobacteria, Biochem. Biophys. Res. Commun. 69 (1976) 7–14.
[91] M.R. Rintoul, B.F. de Arcuri, R.D. Morero, Effects of the antibiotic peptide microcin J25 on liposomes: role of acyl chain length and negatively charged phospholipid, Biochim. Biophys. Acta 1509 (2000) 65–72.
[92] S.T. Yang, S.Y. Shin, J.I. Kim, Interaction mode of a symmetric Trp-rich undeca peptide PST11-RK with lipid bilayers, FEBS Lett. 581 (2007) 157–163.

7. General objectives

The studies presented in this Thesis aim to clarify and improve the knowledge on molecular aspects of enveloped virus entry through membrane fusion and its inhibition, with a focus on the role of host factors. For this, we used optical based biophysical techniques, mainly fluorescence spectroscopy, single-particle microscopy and surface plasmon resonance. Overall, the objectives of this Thesis are:

- Evaluate the interaction of HIV-1 fusion inhibitor peptides with model and cell membranes;
- Correlate the antiviral activity of fusion inhibitor peptides with their membranotropic properties;
- Determine the general structural requirements of glycosaminoglycans to bind the HIV-1 envelope glycoprotein gp120;
- Visualize single enveloped virus fusion on supported lipid bilayers under the microscope;
- Study the role of anionic lipids in modulating the VSV G protein mediated viral fusion in model membranes.
- Clarify the entry pathway of ASLV in cells by simultaneous imaging of single virus fusion and quantification of endosomal pH along virus trafficking.

II

Membranotropic properties of HIV-1 fusion inhibitor peptides and its relation to antiviral activity

Overview

This section presents 3 articles related to the studies of HIV-1 fusion inhibitor peptide interactions with model and cell membranes.

Article A describes the peptide-membranes interactions detected by a dipole potential sensitive fluorescent probe. This allowed the quantification of membrane binding of enfuvirtide and T-1249 to human isolated blood cells, erythrocytes and lymphocytes. These studies were extended to sifuvirtide in Article B, a fusion peptide rationally designed in order to be more potent than enfuvirtide.

A comprehensive membrane interactions study with model membranes and cells was done for the latest generation and highly potent peptide conjugate C34-cholesterol, presented in Article C. The overall results for the fusion inhibitors studied emphasize the role of membrane interaction in their mode of action and as an important factor to take into account when designing drugs of this type.

All these studies were performed at IMM in Lisbon.

Article A

Matos PM, Castanho MARB, Santos NC. HIV-1 Fusion inhibitor peptides enfuvirtide and T-1249 interact with erythrocytes and lymphocytes membranes. *PLoS ONE* **5**:e9830 (2010).

Article B

Matos PM, Freitas T, Castanho MARB, Santos NC. The role of blood cell membrane lipids on the mode of action of HIV-1 fusion inhibitor sifuvirtide. *Biochem. Biophys. Res. Commun.* **403**:270-274 (2010).

Article C

Hollmann A*, Matos PM*, Augusto MT, Castanho MARB, Santos NC. Conjugation of cholesterol to HIV-1 fusion inhibitor C34 increases peptide-membrane interactions potentiating its action. *PLoS ONE* **8**:e60302 (2013). (*Contributed equally to this work).

Article A

Declaration of authorship

I, Pedro Miguel Baptista de Matos, declare that the experimental design, all the experimental work, data analysis and writing of initial manuscripts drafts were carried out by me, under the supervisions of Prof. Nuno C. Santos and the help of Prof. Miguel Castanho.

I, Nuno C. Santos, as supervisor of Pedro Matos and as corresponding author of the article mentioned above, hereby acknowledge and confirm that the information above is correct.

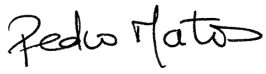

Pedro M. Matos

Nuno C. Santos

OPEN ACCESS Freely available online

PLoS one

HIV-1 Fusion Inhibitor Peptides Enfuvirtide and T-1249 Interact with Erythrocyte and Lymphocyte Membranes

Pedro M. Matos, Miguel A. R. B. Castanho, Nuno C. Santos*

Instituto de Medicina Molecular, Faculdade de Medicina da Universidade de Lisboa, Lisboa, Portugal

Abstract

Enfuvirtide and T-1249 are two HIV-1 fusion inhibitor peptides that bind to gp41 and prevent its fusogenic conformation, inhibiting viral entry into host cells. Previous studies established the relative preferences of these peptides for membrane model systems of defined lipid compositions. We aimed to understand the interaction of these peptides with the membranes of erythrocytes and peripheral blood mononuclear cells. The peptide behavior toward cell membranes was followed by di-8-ANEPPS fluorescence, a lipophilic probe sensitive to the changes in membrane dipole potential. We observed a fusion inhibitor concentration-dependent decrease on the membrane dipole potential. Quantitative analysis showed that T-1249 has an approximately eight-fold higher affinity towards cells, when compared with enfuvirtide. We also compared the binding towards di-8-ANEPPS labeled lipid vesicles that model cell membranes and obtained concordant results. We demonstrated the distinct enfuvirtide and T-1249 membranotropism for circulating blood cells, which can be translated to a feasible *in vivo* scenario. The enhanced interaction of T-1249 with cell membranes correlates with its higher efficacy, as it can increase and accelerate the drug binding to gp41 in its pre-fusion state.

Citation: Matos PM, Castanho MARB, Santos NC (2010) HIV-1 Fusion Inhibitor Peptides Enfuvirtide and T-1249 Interact with Erythrocyte and Lymphocyte Membranes. PLoS ONE 5(3): e9830. doi:10.1371/journal.pone.0009830

Editor: Linqi Zhang, Tsinghua University, China

Received October 23, 2009; **Accepted** March 2, 2010; **Published** March 23, 2010

Funding: This work was supported by Fundação para a Ciência e Tecnologia (FCT, http://www.fct.mctes.pt) of the Portuguese Ministry of Science, Technology and Higher Education (MCTES), including project PTDC/QUI-BIQ/104787/2008. P.M.M. was funded by the FCT-MCTES PhD grant SFRH/BD/42205/2007. The funders had no role in study design, data collection and analysis, decision to publish, or preparation of the manuscript.

Competing Interests: The authors have declared that no competing interests exist.

* E-mail: nsantos@fm.ul.pt

Introduction

The Human Immunodeficiency Virus type 1 (HIV-1) is a highly pathogenic, evasive and difficult to eradicate agent that causes Acquired Immunodeficiency Syndrome (AIDS). This discovery in the early 1980s triggered major international scientific efforts in antiviral drug discovery and development [1]. As a consequence, many drugs are now available to manage this condition, allowing the use of drug combination therapy known as HAART (highly active antiretroviral therapy). The majority of the drugs inhibit the different enzymes vital for the HIV-1 life cycle: reverse transcriptase, integrase and protease. However, the entry inhibitors target steps before the viral content is released into the host cell cytoplasm [2]. Infection of T $CD4^+$ cells begins with the binding of the viral envelope trimeric glycoprotein gp120 with the CD4 receptor and a chemokine receptor (CCR5 or CXCR4) of the host cell. This engagement triggers the exposure of the hydrophobic N-terminal region of another envelope glycoprotein, gp41. This fusion peptide anchors to the membrane of the host cell, enabling the two gp41 helical heptad repeat domains, the C-terminal (CHR or HR2) and the N-terminal (NHR or HR1), to fold into each other to form a hairpin-like structure (6-helix bundle). This approximates the cell and the viral membranes, facilitating their fusion and the release of the viral content into the cell [3].

Besides maraviroc, a recently approved CCR5 antagonist blocking gp120 co-receptor engagement [4], enfuvirtide is the other only entry inhibitor approved for clinical use [5]. Enfuvirtide (formerly known as T-20 and DP-178) is a peptide drug selected from chemically synthesized peptides derived from various regions of gp41 [6]. The core structure of gp41 was only revealed later and helped to understand the inhibitory activity of enfuvirtide [7]. The peptide sequence (sequence 643–678 of HIV-1_{LAI} [6]) corresponded partially to the CHR region of gp41 and it would bind to the opposite NHR region, preventing the formation of the hairpin structure and consequently, the fusion. The same consortium that led enfuvirtide to clinical approval (Trimeris, Inc. and Roche) developed a second generation fusion inhibitor, T-1249. It is a 39-mer peptide which sequenced was designed taking into account the gp41 CHR sequences from HIV-1, HIV-2 and SIV (Simian Immunodeficiency Virus) [8]. A successful short-term evaluation of antiretroviral activity and safety in humans proved the potential of this new drug [8], although further clinical development was put on hold [9].

Since the first appearance of enfuvirtide, the search for peptide drugs against HIV has been a growing field of research and several candidates proved to be efficient *in vitro* [10]. As our knowledge of HIV structure and function progresses, more sophisticated peptide designs are developed in order to overcome viral resistance to previous drugs. The initial view of the mechanism of action of these peptides, that is, binding to NHR region and block 6-helix bundle formation, has been refined over the years. Other factors besides gp41-peptide binding can contribute to explain the mode of action of these peptides. In fact enfuvirtide does not form stable 6-helix bundle structures with N36, a NHR derived peptide, contrary to C34, another CHR derived peptide [11]. Moreover, peptides derived from the membrane-spanning domain in gp41 and the co-receptor binding site in gp120 inhibited enfuvirtide

antiviral activity [11], meaning that other sites in the viral envelope could be targeted by enfuvirtide.

Membrane binding/tropism emerged as an important factor to take into account concerning the mode of actions of these peptides. Previous studies evaluated the preferences of enfuvirtide and T-1249 to membrane model systems. Partition of these peptides to fluid phase and cholesterol-rich lipid vesicles was followed by intrinsic tryptophan fluorescence present in both peptides [12,13]. Both enfuvirtide [13] and T-1249 [12] partitioned to fluid phase zwitterionic phospholipid vesicles (POPC, 1-palmitoyl-2-oleoyl-*sn*-glycero-3-phosphocholine) with partition constants (K_p [14]) of 1.6×10^3 and 5.1×10^3, respectively. However, regarding interaction with cholesterol-rich POPC vesicles (up to 33% mol) enfuvirtide showed residual association, while T-1249 binding was significant, despite also presenting a low partition (membrane insertion) [12]. T-1249 improved preference for lipid environment correlated with its higher antiviral activity.

In this study, we aim to understand the nature of HIV-1 fusion inhibitors-membrane interactions using human blood cells, namely erythrocytes and PBMC (peripheral blood mononuclear cells). We made use of an indirect reporter, the fluorescent lipophilic probe di-8-ANEPPS, as direct measure of the peptide intrinsic tryptophan fluorescence was impracticable with cells. This probe incorporates in the outer leaflet of the cell membranes and is sensitive to the local dipole potential by shifting its excitation spectrum [15]. Interaction of peptides or other molecules with membranes can change the lipid and interfacial water dipoles organization. Moreover, the peptide dipoles themselves can contribute to the potential. These overall dipolar changes occurring at the membrane can then be translated by the probe both qualitatively and quantitatively [16].

Results

Labeling of erythrocytes and PBMC with di-8-ANEPPS membrane probe

Isolated human erythrocytes and PBMC membranes were successfully labeled with di-8-ANEPPS. Confocal microscopy images clearly show the delineated labeled membrane (Fig. 1A,B). Importantly, no intracellular staining of di-8-ANEPPS was observed. The emission and excitation spectra of the probe were taken for the two cell types (Fig. 1C). Labeled erythrocytes and PBMC had different spectral maxima (specially for the emission) due to the probe sensitivity to the differences in the composition and nature of the membrane lipids.

Enfuvirtide and T-1249 induce changes in the dipole potential of cell membranes

Incubation of the labeled erythrocytes and PBMC with enfuvirtide or T-1249, lead to changes in spectral properties of the membrane-bound di-8-ANEPPS. Excitation spectra were deviated to the red meaning that a decrease in the dipole potential occurs. Differential spectra can be used in order to help the visualization of the spectral shift (Fig. 2). In this case, the minimum of the differential spectra comes at a lower wavelength than the maximum, indicative of a decrease in the dipole potential (see methods section). These changes depend on the peptide and its concentration. T-1249 is more effective in decreasing the membrane potential than enfuvirtide.

To follow the time course of the interaction, we used the ratio between the approximate maximum and minimum of the differential spectra ($R = I_{455\ nm}/I_{525\ nm}$), that correlates with the dipole potential variations. After the addition of each peptide, we observed a decrease on the dipole potential within the first minutes for erythrocytes (Fig. 3) and lymphocytes.

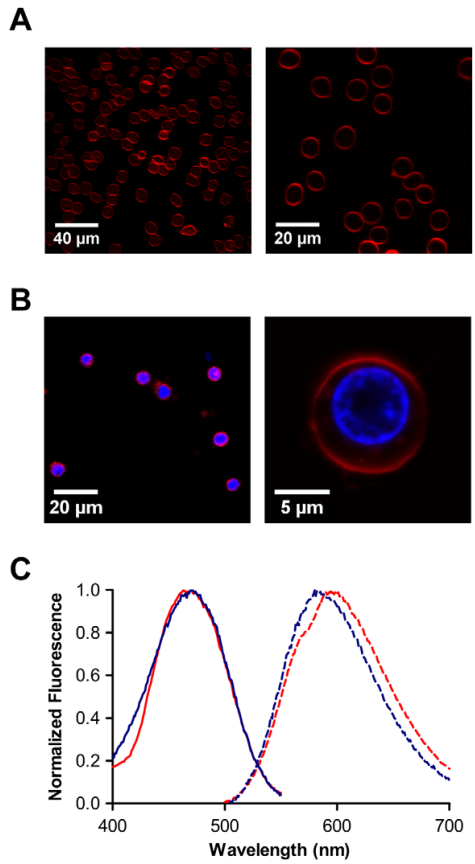

Figure 1. Visualization and spectral characterization of di-8-ANEPPS labeled cells. Labeled erythrocytes (A) and PBMC (B) were observed under a confocal fluorescence microscope to confirm that only the plasma membrane was stained (shown in red). Additional staining of the nucleus with Hoechst dye (blue) was performed for PBMC, only for microscopy observation. Excitation and emission spectra (C) were taken for each labeled cell type, differing on peaks due to different membrane environments (blue trace for PBMC and red trace for erythrocytes; filled line for excitation and dashed line for emission spectra). Excitation at 465 nm for both cell types; emission at 600 nm and 585 nm for erythrocytes and PBMC, respectively.
doi:10.1371/journal.pone.0009830.g001

Quantification of the membrane-peptide interaction for erythrocytes and PBMC

In order to quantify the affinity of the peptides to the cell membranes, we set to investigate the variation of the dipole potential as a function of peptide concentration (Fig. 4). The ratio R was measured for a range of concentrations of enfuvirtide and T-1249. The decrease of the potential as a function of concentration followed a hyperbolic curve. The data was analyzed according to a single binding site model [17] to yield dissociation constants (K_d) for each peptide (Table 1). For both cell types, the K_d for T-1249 was much smaller (one order of magnitude), accounting for a higher preference for the cell membrane. The

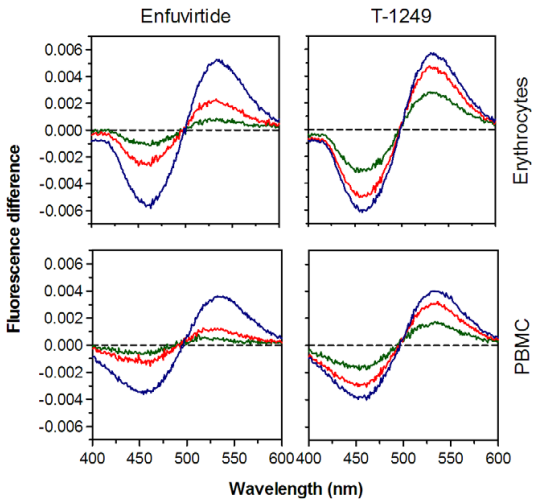

Figure 2. Differential spectra of membrane-bound di-8-ANEPPS in the presence of HIV-1 fusion inhibitor peptides. The shape of the difference spectra reveal spectral shift to the red, indicative of a decrease in membrane dipole potential. For erythrocytes (top row) and PBMC (bottom row), the higher the peptide concentration (150 μM in blue, 40 μM in red and 10 μM in green), the higher the spectral shifts.
doi:10.1371/journal.pone.0009830.g002

relative behavior of the peptide towards the erythrocyte and PBMC membrane seems to be maintained: the ratios $K_{d,ENF}/K_{d,T\text{-}1249}$ are similar for both cell type (8.5 and 8.1 for erythrocytes and PBMC, respectively).

Comparison of peptide-induced dipole changes in biomimetic lipid vesicles

As stated earlier, interaction of enfuvirtide and T-1249 with lipid vesicles has been previously studied by means of their tryptophan residues fluorescence. For the sake of comparison with the data obtained for the interaction with blood cells membranes and in order to validate the comparison with previous data, we used di-8-ANEPPS labeled lipid vesicles to assess the interaction of these peptides, reported by changes on membrane dipole potential (Fig. 5). The lipid vesicles were composed entirely of POPC, to mimic most of the outer leaflets of mammalian cell membranes, in the liquid disordered state, or a mixture of POPC with cholesterol 33% mol, as an approximation to the membrane microdomains in the liquid ordered state (lipid rafts). This is especially relevant for the erythrocyte membranes, which are particularly cholesterol-rich [18]. Concerning the POPC vesicles, the binding of T-1249 was again more pronounced than for enfuvirtide (Fig. 5). When the vesicles are enriched with cholesterol, significant changes occur in terms of peptide association to the membrane. Enfuvirtide binds less extensively to membranes rich in cholesterol, while T-1249 increases the extension of membrane association (Fig. 5). This is in agreement with previous results obtained for lipid vesicles [12], in which the adsorption of T-1249 on cholesterol enriched domains was identified, in contrast to enfuvirtide.

Discussion

Designing peptide drugs based in gp41 sequence to prevent viral entry into host cells has been in focus in the antiretroviral research field. Several factors related to their mode of action must be taken into account in order to optimize efficacy. For the first time, we addressed the interactions of HIV-1 fusion inhibitors with human cell membranes to better understand their membranotropic behavior *in vivo*. We made use of a dipole potential membrane probe, di-8-ANEPPS, to indirectly assess the membrane binding of enfuvirtide and T-1249 to erythrocytes and mononuclear leukocytes. These peptides decreased the membrane dipole potential of the two cell types, indicating that an interaction is occurring. Quantitatively, T-1249 was found to have approximately 8 times more affinity towards these cell membranes than enfuvirtide. Furthermore, studies with di-8-ANEPPS labeled POPC vesicles corroborated this by showing higher binding of T-1249 in comparison with enfuvirtide. Concerning POPC/cholesterol vesicles, the relative binding affinity between the two peptides was maintained. The presence of cholesterol reduced the binding extension of enfuvirtide and had an opposite effect in the case of T-1249, in agreement with our previous results that followed the interaction by tryptophan fluorescence [12]. Due to the fact that erythrocyte membranes contain significantly more cholesterol than PBMC [18] it could be expected that peptide binding characteristics for these two cell types would be more distinct. However, these composition differences seem not to be sufficient to change significantly the interaction behavior of the

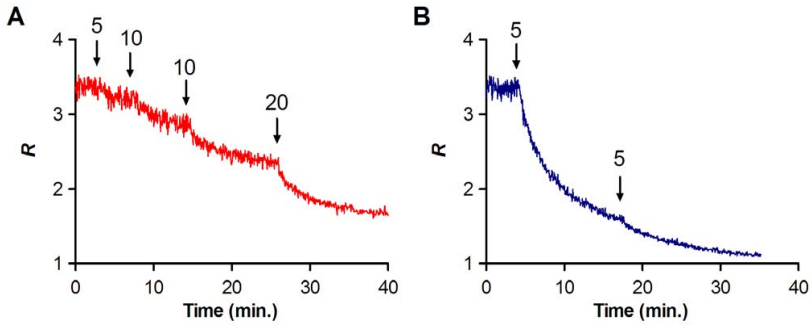

Figure 3. Time course variation of dipole potential in response to the peptides. The effect of the addition of indicated concentrations (μM) of enfuvirtide (A, red) and T-1249 (B, blue) to labeled erythrocytes was followed by measuring the ratio in real-time. Stepwise additions decreases the ratio within minutes.
doi:10.1371/journal.pone.0009830.g003

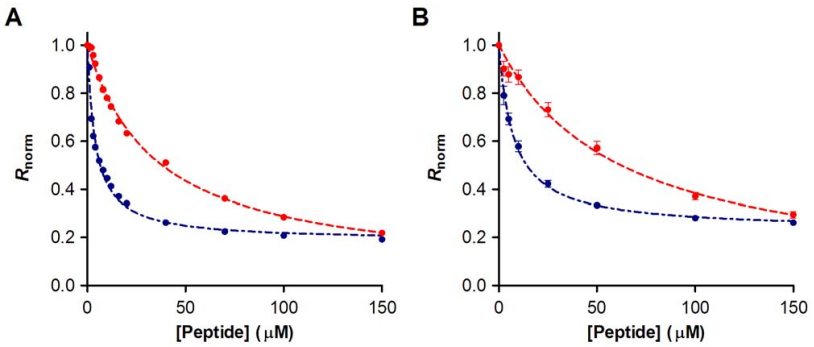

Figure 4. Peptide affinity towards erythrocytes and PBMC cell membranes. The dependence of the ratio on the enfuvirtide (red) and T-1249 (blue) concentrations for erythrocytes (A) and PBMC (B) was analyzed by a single binding site model (dashed lines) in order to quantify the dissociation constants (see Table 1). Ratio values were normalized for the initial value of zero peptide concentration. Plotted values represent the mean ± SEM (error bars not visible in erythrocytes due to small errors). N = 6 for erythrocytes and N = 7 for PBMC.
doi:10.1371/journal.pone.0009830.g004

peptides, as we can see confronting POPC with POPC/cholesterol (33% mol) vesicles. Other factors such as the diversity of lipidic, proteic and glycidic components seem to superimpose to the effect of differences in cholesterol content. In fact, we checked if cholesterol depletion of erythrocytes membranes by methyl-β-cyclodextrin would reflect on changes in peptide binding and no significant alterations were detected (data not shown).

The membranotropism of these peptides can be explained in molecular terms by their structure and aminoacid sequence. It has been identified in the CHR and adjacent regions specific motifs that account for different roles in the interaction with NHR and membrane environment. Some of these regions also translate to the CHR derived peptides. Towards the N-terminus of CHR, there is a pocket binding domain (PBD, HIV-1_{LAI} 628–635) that binds to a hydrophobic groove in the NHR region [7]. It was established that this PBD was a crucial region for the binding of CHR and NHR in order to form the 6-helix bundle hairpin-like structure [7]. Another region identified in the far C-terminus of CHR is the lipid binding domain (LBD), a hydrophobic Trp-rich region by which CHR derived peptides can apparently bind to lipid membranes [19]. The sequence of enfuvirtide contains only the LBD while T-1249 was designed to contain both LBD and PBD (Fig. 6A). Thus, binding to cell and mimetic membranes is related to this putative LBD. Interestingly, by mutating the LBD region of enfuvirtide WNWF to ANAA, the antiviral activity of the peptide was abrogated [20] as well as its ability to bind to POPC vesicles [19]. Moreover, when an ANAA enfuvirtide mutant was octylated, its inhibitory activity was restored to a level similar to standard enfuvirtide [21]. This indicates the importance of the LBD for the efficacy of enfuvirtide, as the octylation of enfuvirtide also increased its potency. A similar result was obtained when enfuvirtide and ANAA mutant were expressed attached to a membrane protein in a T-helper cell line [22]. Another example comes from the addition of a cholesteryl group to C34, another peptide fusion inhibitor that lacks a LBP but contains the PBD sequence [23]. The potency of the derivatized C34 increased significantly; however, this effect was not observed when cholesterol was attached to enfuvirtide, which already has a LBD. TRI-999, another LBD lacking C-peptide, was synthesized with an attached C18 chain [24], showing improved efficiency over enfuvirtide.

All these findings that relate membrane binding to improved efficiency of the peptides mean that this is a major factor to take into account when rationally designing drugs of this type. Enfuvirtide and T-1249 have membranotropic behavior towards POPC lipid vesicles and now this study confirms that they both

Table 1. Quantification of peptide binding.

Cells	Peptide	$R_{min,\ norm}$	K_d (μM)	$K_{d,\ ENF}/K_{d,\ T\text{-}1249}$
Erythrocytes	T-1249	−0.81±0.0063	4.16±0.13	8.5
	Enfuvirtide	−0.97±0.015	35.4±1.33	
PBMC	T-1249	−0.77±0.014	7.71±0.61	8.1
	Enfuvirtide	−1.0±0.071	62.2±10.2	

Comparison of the values of the dissociation constant, K_d and the parameter R_{min} obtained by non-linear regression with equation (1). The values represent mean ± SEM.
doi:10.1371/journal.pone.0009830.t001

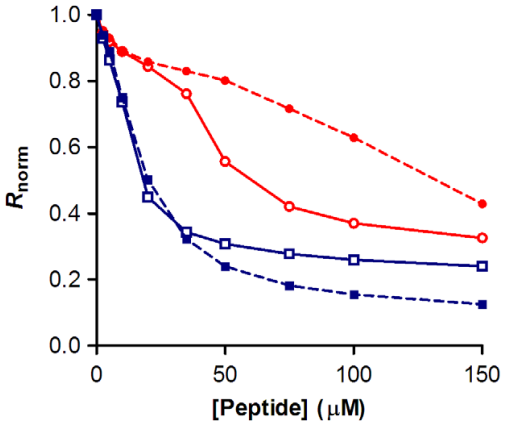

Figure 5. Interaction of the peptides with membrane model systems. The binding profiles for enfuvirtide (red) and T-1249 (blue) were obtained for large unilamellar vesicles composed of POPC (open symbols) and POPC/cholesterol 33% mol (filled symbols).
doi:10.1371/journal.pone.0009830.g005

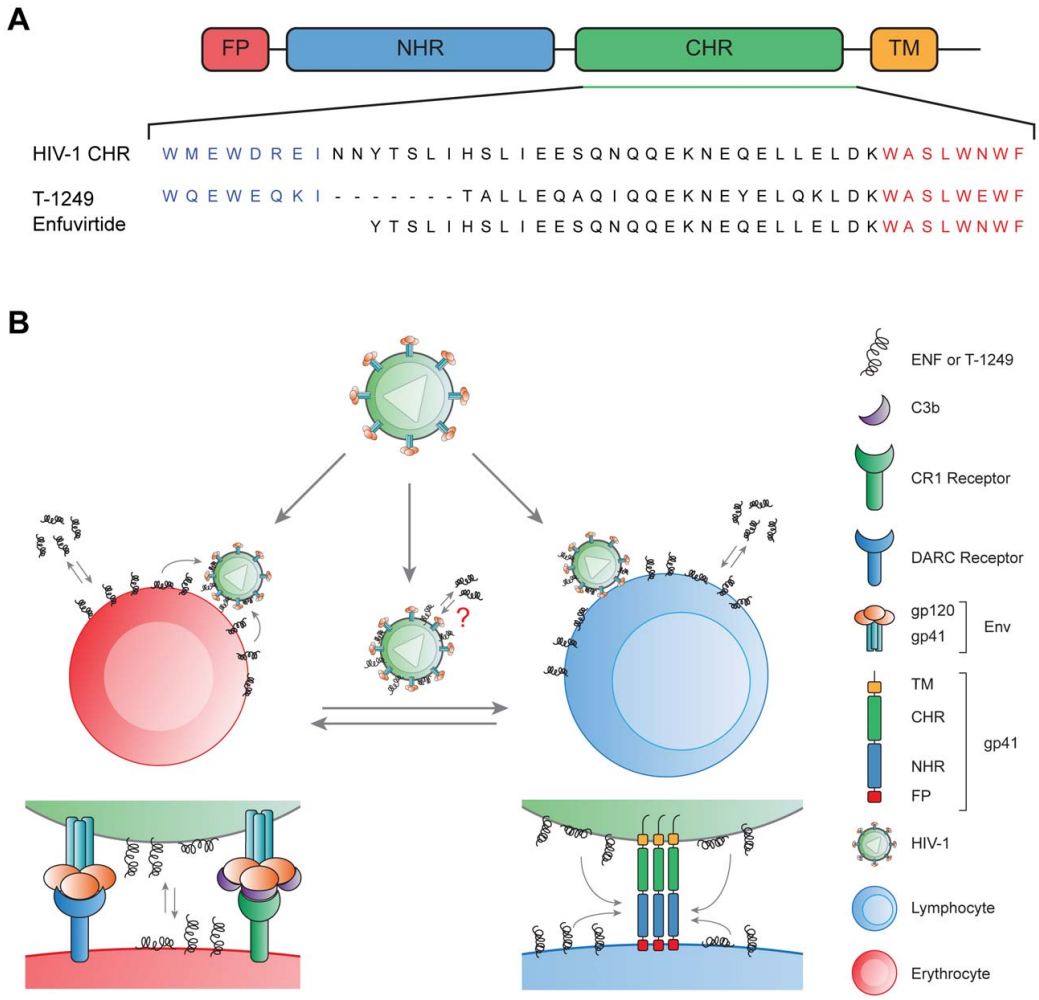

Figure 6. Proposed mode of action of enfuvirtide and T-1249 in circulation with blood cells. A) Sequence alignment of enfuvirtide and T-1249 with native gp41 (PDB code: 1ENV), showing the pocket binding domain (PBD) in blue and the putative lipid binding domain (LBD) close to the membrane proximal region in red. B) Peptides partition to the membranes of circulating blood cells creating a peptide-rich environment, when the virus interact both with erythrocytes and lymphocytes. HIV associates with erythrocytes via DARC receptor or complement opsonized virus via CR1. Exchanges of peptide between cells and virus and partition of peptide directly to the viral membrane can occur. When infecting the preferential $CD4^+$ T cells, the membrane binding of peptide inhibitors should facilitate its interaction with the exposed conformation of gp41, preventing the 6-helix bundle formation. If the virus is internalized and fuses with the cell membrane at the endosome level, as recently described [27], the partition of the peptides to the membranes ensures that a considerable amount of peptides enters upon endocytosis in order to be available during the intracellular fusion event.
doi:10.1371/journal.pone.0009830.g006

also interact with circulating blood cells. These peptides have a restricted temporal and spatial window of opportunity to bind to their molecular target: the NHR region of gp41 in its extended conformation when the virus and host cell are closely engaged. This makes aqueous diffusion of the peptide to the target less efficient. The capacity that these peptides have to bind to the cell membranes facilitates the delivery of the peptides to this confined environment, as some peptide is already locally present. Ultimately, the membrane can act as a "catalyst" to the binding reaction between the gp41 and the peptides, as it has been postulated in other receptor-ligand scenarios in the membrane environment [25]. Thus, for this case, the higher potency of T-1249 in relation to enfuvirtide seems to correlate with its higher membranes binding to the blood cells, particularly the lymphocytic fraction, where the preferential target cells are included. Then, its membrane binding capacity is possibly one of the factors that explain their relative potency (Fig. 6B). In terms of its structure and sequence, both peptides have the LBD sequence that accounts almost totally for enfuvirtide membrane binding. Nevertheless, T-1249 should have some other structural charac-

teristic that account for its higher binding affinity. The PBD region additionally present on T-1249 is also a hydrophobic region and has 2 tryptophan residues (LBD has 3 Trp). This could account for a weak membrane binding domain. However, the membrane binding capacity of a C-peptide with an altered heptad repeat sequence and containing a PBD but not a LBD (PBD-4HR, similar do C34) is very poor, similar to a C-peptide that does not have any of these domains [26]. We could speculate that a possible, but not certain, synergistic action between the PBD and LBD domains present on T-1249 to increase its membranotropism. Another contributing factor could be the increased helicity of T-1249 in solution compared to enfuvirtide [12], a structural characteristic that favors insertion and stability in the membrane. Summarizing, T-1249 would be more effective due to: a) a LBD sequence motif, shared with enfuvirtide, that allows the peptide to anchor to the membrane as a platform to reach the target sequence in gp41 and explains part of its membranotropism; b) a PBD sequence motif that accounts for an enhanced gp41 binding and c) the higher overall affinity towards cell membranes of T-1249 (especially cholesterol-rich domains) not explained by the sum of the membrane binding effects of PBD and LBD.

Recently, a novel discovery about the HIV-1 entry into host cells challenged the current knowledge of viral-cell membrane fusion at the cell surface. Miyauchi *et al.* [27] showed that HIV-1 tends to prefer an endocytic route of entry and that fusion preferentially occurs at the endosomes. This would elicit protection to HIV from fusion inhibitors, as the surface exposition of the gp41 extended conformation is reduced. Hence, the capability of peptide fusion inhibitors to partition to the membrane and remain there while the virus is internalized, together with a cell membrane patch, can prove to be a decisive factor concerning their inclusion on the endosome, leading to increased antiretroviral efficacy and potency.

The relevance of peptide binding to erythrocytes is not to be diminished. In fact, HIV can be found associated with erythrocytes *in vivo* [28] and binds to erythrocyte membrane *in vitro* [29]. The virus can bind to erythrocytes *via* the DARC (Duffy Antigen Receptor for Chemokines) [30,31] or *via* the complement receptor 1 (CR-1), that binds C3b or C3bi opsonized virus [32,33]. Moreover, erythrocytes can mediate trans-infection of these bound viruses to other immune system cells that circulate in the blood and reside in the spleen [30,32]. Interestingly, depending on which complement proteins are opsonizing the virus, they can direct the virus through various immune system cells that express different complement receptors, creating a dynamic circulation of the virus and facilitating its spreading through the body [34]. Therefore, we can speculate that by contacting with erythrocytes with pre-bound fusion inhibitor peptides, the virus itself can take peptide in its own membrane (Fig. 6B). In fact, Aloia *et al.* [35] found the lipid composition of the erythrocyte membrane to be similar to the HIV membrane itself; thus, peptide-viral membrane interaction seems to be very feasible. This peptide-membrane interaction can occur also for other circulating cells.

In a therapeutic context, several factors can influence the availability of the antiretroviral peptides in circulation. The drug is distributed to different components of the blood, namely, dissolved in the plasma, bound to plasma proteins (namely, albumin) and, as we established with this study, bound to cell membranes. The membrane-bound fraction would enhance the availability towards the molecular target in the virus, as explained earlier in this section, opposing to the fraction bound to plasma proteins, a factor that enhances peptide clearance. In conclusion, the dynamics between the peptide interaction among the different cell populations and with the virus, along with emerging new perspectives of HIV entry are complex factors that should the taken in consideration when rationally designing the next generation of fusion inhibitor peptides.

Materials and Methods

Isolation and labeling of human erythrocytes and PBMC

Human blood samples were obtained from healthy volunteer donors at the public blood bank Instituto Português do Sangue (Lisbon, Portugal), with their informed written consent. These samples were obtained under an institutional agreement between IPS Lisboa and Instituto de Bioquímica from Faculdade de Medicina da Universidade de Lisboa. This study was approved by the Ethics Committee of Faculdade de Medicina da Universidade de Lisboa. Donors were asked to give up to 10 mL of blood for research purposes additionally to their common blood donation of 450 mL to the blood bank. The blood collection was made anonymously as the data treatment resulting from the experiences made with these samples. The samples were drawn to K_3EDTA anticoagulant tubes (Vacuette, Greiner Bio-one, Kremsmünster, Austria). For erythrocytes, the blood samples were centrifuged at 1200 *g* during 10 min to remove plasma and buffy-coat. The erythrocytes were washed at least two times with working buffer (HEPES 10 mM pH 7.4, in NaCl 150 mM, both from Sigma, St. Louis, MO, USA). For labeling, they were prepared at 1% hematocrit in working buffer supplemented with 0.05% (m/V) Pluronic F-127 (Sigma) and di-8-ANEPPS 10 μM (Molecular Probes, Invitrogen, Carlsbad, CA, USA). PBMC were isolated by density gradient using Ficoll-Paque Plus (GE Healthcare, Little Chalfont, UK), accordingly to manufacturer's instructions. Cells were counted in Cell-Dyn 1600 analyzer (Abbott, Abbott Park, IL, USA) and were prepared at 3000 cells/μL in Pluronic supplemented buffer with di-8-ANEPPS 3.3 μM. The suspensions of erythrocytes or PBMC with probe were incubated at room temperature with gentle agitation for 1 h. Unbound di-8-ANEPPS was removed by two wash cycles, with centrifugations at 1500 *g* for 5 min.

Preparation and labeling of lipid vesicles

Large unilamellar vesicles (LUV) with ~100 nm diameter, composed of pure POPC (Avanti Polar Lipids, Alabaster, AL, USA) or POPC with 33% mol cholesterol (Sigma), were obtained by extrusion of multi-lamellar vesicles (MLV) as described elsewhere [36]. Briefly, a chloroform dissolved lipid was dried in round-bottom flasks to obtain a film. MLV were obtained by dissolving the film in working buffer and subjecting to 8 freeze-thaw cycles. The suspension was extruded, first through a polycarbonate filter with 400 nm pores, followed by passages trough 100 nm pores filters in a custom made extruder. For cholesterol enriched vesicles, the extruder was heated by a water bath. Lipid vesicles suspensions with 500 μM of total lipid were incubated overnight with di-8-ANEPPS 10 μM, to ensure maximum incorporation of the probe.

Fusion inhibitor peptides

The HIV-fusion inhibitors enfuvirtide (T-20) and T-1249 (kind gifts of Roche, Palo Alto, CA, USA) were prepared in working buffer at maximum stock concentration of 250 μM. These peptides were incubated at different concentrations with labeled erythrocytes (0.02% hematocrit), PBMC (100 cells/μL) or lipid vesicles (200 μM of total lipid) during 1 h for cells or 90 min for vesicles, with gentle agitation before measurements.

Microscopy imaging

Erythrocyte microscopy images were obtained in a laser scanning confocal microscope Zeiss LSM 5 Live (Jena, Germany) using a water immersion objective Zeiss C-Apochromat 20× (1.20 numerical aperture). PBMC images were obtained in a Zeiss LSM510 Meta using an oil immersion objective Zeiss Plan-Apochromat 63× (1.4 numerical aperture). Di-8-ANEPPS was excited by a 488 nm laser (LP 505 filter for erythrocytes, BP 575–615 for PBMC). For the PBMC, Hoescht dye (Molecular Probes, Invitrogen) was also used for nucleus labeling, excited by a 405 nm laser (LP 420 filter).

Membrane dipole potential assessed by di-8-ANEPPS

The membrane probe di-8-ANEPPS assesses dipole potential by shifting its excitation spectrum. Differential spectra for detecting these shifts are obtained by subtracting the excitation spectrum of labeled cells in the presence of peptide from the spectrum in its absence. Before subtraction the spectra were normalized to the integrated areas to reflect only spectral shifts. The differential spectra are waveform shaped, which amplitude directly correlates with the peak shifting magnitude, and hence, with the dipole potential variation. Blue-shifts will result in differential spectra in which a maximum comes at a lower wavelength than the maximum, and the opposite for red-shifts.

To qualitatively define a value for the spectral shift and hence, the dipole potential, a ratio was established from fluorescence intensities at two wavelengths on the sides of excitation spectrum peak [15,37]. We chose them by taking the corresponding wavelength values for the minimum and the maximum of the differential spectra, defining the ratio R for this case as $I_{455\ nm}/I_{525\ nm}$ (I, fluorescence intensity). It was already established that an increase in the membrane dipole potential leads to a blue-shift in the membrane incorporated di-8-ANEPPS and, consequently, to an increase in the ratio [15,37]. We also made a simple test for erythrocytes by adding 6-ketocholestanol (Sigma), an agent that increases dipole potential, and we observed the expected behavior of di-8-ANEPPS.

The variation of R with the peptide concentration was analyzed by a single binding site model [17], following equation 1, with the R values normalized for R_0, the value at zero peptide concentration. R_{min} defines the asymptotic minimum value of R and K_d is the dissociation constant.

$$R/R_0 = 1 + \frac{R_{min}/R_0[\text{Peptide}]}{K_d + [\text{Peptide}]} \qquad \text{(Eq.1)}$$

Fluorescence spectroscopy measurements

All the fluorescence spectroscopy measurements were made in a Varian Cary Eclipse (Mulgrave, Australia) fluorescence spectrophotometer. Membrane-bound di-8-ANEPPS excitation spectra and ratios were taken with emission at 670 nm in order to avoid membrane fluidity effects, as previously tested for lipid vesicles [38]. We also tested if this was observed in labeled erythrocytes (data not shown). The R values were measured through temperatures from 15°C to 50°C, with emissions at 580, 600 and 670 nm. The slope was lower for 670 nm, meaning a lower interference of fluidity effect at this wavelength. Excitation and emission slits for all measurements were 5 nm and 10 nm, respectively.

Acknowledgments

We thank Dr. Henrique Sobral do Rosário for the help on microscopy imaging and Mrs. Teresa Freitas for the technical support on PBMC isolation. The peptides enfuvirtide and T-1249 were a kind gift of Roche (Palo Alto, CA, USA).

Author Contributions

Conceived and designed the experiments: PMM MARBC NCS. Performed the experiments: PMM. Analyzed the data: PMM NCS. Wrote the paper: PMM MARBC NCS.

References

1. Greene WC (2007) A history of AIDS: looking back to see ahead. Eur J Immunol 37 Suppl 1: S94–102.
2. Tilton JC, Doms RW (2009) Entry inhibitors in the treatment of HIV-1 infection. Antiviral Res 85: 91–100.
3. Moore JP, Doms RW (2003) The entry of entry inhibitors: a fusion of science and medicine. Proc Natl Acad Sci U S A 100: 10598–10602.
4. Fatkenheuer G, Pozniak AL, Johnson MA, Plettenberg A, Staszewski S, et al. (2005) Efficacy of short-term monotherapy with maraviroc, a new CCR5 antagonist, in patients infected with HIV-1. Nature Medicine 11: 1170–1172.
5. Matthews T, Salgo M, Greenberg M, Chung J, DeMasi R, et al. (2004) Enfuvirtide: the first therapy to inhibit the entry of HIV-1 into host CD4 lymphocytes. Nat Rev Drug Discov 3: 215–225.
6. Wild CT, Shugars DC, Greenwell TK, McDanal CB, Matthews TJ (1994) Peptides corresponding to a predictive alpha-helical domain of human immunodeficiency virus type 1 gp41 are potent inhibitors of virus infection. Proc Natl Acad Sci U S A 91: 9770–9774.
7. Chan DC, Fass D, Berger JM, Kim PS (1997) Core structure of gp41 from the HIV envelope glycoprotein. Cell 89: 263–273.
8. Eron JJ, Gulick RM, Bartlett JA, Merigan T, Arduino R, et al. (2004) Short-term safety and antiretroviral activity of T-1249, a second-generation fusion inhibitor of HIV. Journal of Infectious Diseases 189: 1075–1083.
9. Martin-Carbonero L (2004) Discontinuation of the clinical development of fusion inhibitor T-1249. AIDS Reviews 6: 61–61.
10. Naider F, Anglister J (2009) Peptides in the treatment of AIDS. Curr Opin Struct Biol 19: 473–482.
11. Liu S, Lu H, Niu J, Xu Y, Wu S, et al. (2005) Different from the HIV fusion inhibitor C34, the anti-HIV drug Fuzeon (T-20) inhibits HIV-1 entry by targeting multiple sites in gp41 and gp120. J Biol Chem 280: 11259–11273.
12. Veiga AS, Santos NC, Loura LMS, Fedorov A, Castanho MARB (2004) HIV fusion inhibitor peptide T-1249 is able to insert or adsorb to lipidic bilayers. Putative correlation with improved efficiency. Journal of the American Chemical Society 126: 14758–14763.
13. Veiga S, Henriques S, Santos NC, Castanho M (2004) Putative role of membranes in the HIV fusion inhibitor enfuvirtide mode of action at the molecular level. Biochemical Journal 377: 107–110.
14. Santos NC, Prieto M, Castanho MARB (2003) Quantifying molecular partition into model systems of biomembranes: an emphasis on optical spectroscopic methods. Biochimica Et Biophysica Acta-Biomembranes 1612: 123–135.
15. Gross E, Bedlack RS, Jr., Loew LM (1994) Dual-wavelength ratiometric fluorescence measurement of the membrane dipole potential. Biophys J 67: 208–216.
16. Matos PM, Goncalves S, Santos NC (2008) Interaction of peptides with biomembranes assessed by potential-sensitive fluorescent probes. J Pept Sci 14: 407–415.
17. Cladera J, O'Shea P (1998) Intramembrane molecular dipoles affect the membrane insertion and folding of a model amphiphilic peptide. Biophys J 74: 2434–2442.
18. Leidl K, Liebisch G, Richter D, Schmitz G (2008) Mass spectrometric analysis of lipid species of human circulating blood cells. Biochim Biophys Acta 1781: 655–664.
19. Liu S, Jing W, Cheung B, Lu H, Sun J, et al. (2007) HIV gp41 C-terminal heptad repeat contains multifunctional domains. Relation to mechanisms of action of anti-HIV peptides. J Biol Chem 282: 9612–9620.
20. Lawless MK, Barney S, Guthrie KI, Bucy TB, Petteway SR, Jr., et al. (1996) HIV-1 membrane fusion mechanism: structural studies of the interactions between biologically-active peptides from gp41. Biochemistry 35: 13697–13708.
21. Peisajovich SG, Gallo SA, Blumenthal R, Shai Y (2003) C-terminal octylation rescues an inactive T20 mutant: implications for the mechanism of HIV/SIMIAN immunodeficiency virus-induced membrane fusion. J Biol Chem 278: 21012–21017.
22. Hildinger M, Dittmar MT, Schult-Dietrich P, Fehse B, Schnierle BS, et al. (2001) Membrane-anchored peptide inhibits human immunodeficiency virus entry. J Virol 75: 3038–3042.

23. Ingallinella P, Bianchi E, Ladwa NA, Wang YJ, Hrin R, et al. (2009) Addition of a cholesterol group to an HIV-1 peptide fusion inhibitor dramatically increases its antiviral potency. Proc Natl Acad Sci U S A 106: 5801–5806.
24. Zhang HY, Schneider SE, Bray BL, Friedrich PE, Tvermoes NA, et al. (2008) Process development of TRI-999, a fatty-acid-modified HIV fusion inhibitory peptide. Organic Process Research & Development 12: 101–110.
25. Castanho MA, Fernandes MX (2006) Lipid membrane-induced optimization for ligand-receptor docking: recent tools and insights for the "membrane catalysis" model. Eur Biophys J 35: 92–103.
26. Qi Z, Shi W, Xue N, Pan C, Jing W, et al. (2008) Rationally designed anti-HIV peptides containing multifunctional domains as molecule probes for studying the mechanisms of action of the first and second generation HIV fusion inhibitors. J Biol Chem 283: 30376–30384.
27. Miyauchi K, Kim Y, Latinovic O, Morozov V, Melikyan GB (2009) HIV enters cells via endocytosis and dynamin-dependent fusion with endosomes. Cell 137: 433–444.
28. Hess C, Klimkait T, Schlapbach L, Del Zenero V, Sadallah S, et al. (2002) Association of a pool of HIV-1 with erythrocytes in vivo: a cohort study. Lancet 359: 2230–2234.
29. Beck Z, Brown BK, Wieczorek L, Peachman KK, Matyas GR, et al. (2009) Human erythrocytes selectively bind and enrich infectious HIV-1 virions. PLoS One 4: e8297.
30. He W, Neil S, Kulkarni H, Wright E, Agan BK, et al. (2008) Duffy antigen receptor for chemokines mediates trans-infection of HIV-1 from red blood cells to target cells and affects HIV-AIDS susceptibility. Cell Host Microbe 4: 52–62.
31. Lachgar A, Jaureguiberry G, Le Buenac H, Bizzini B, Zagury JF, et al. (1998) Binding of HIV-1 to RBCs involves the Duffy antigen receptors for chemokines (DARC). Biomed Pharmacother 52: 436–439.
32. Banki Z, Wilflingseder D, Ammann CG, Pruenster M, Mullauer B, et al. (2006) Factor I-mediated processing of complement fragments on HIV immune complexes targets HIV to CR2-expressing B cells and facilitates B cell-mediated transmission of opsonized HIV to T cells. J Immunol 177: 3469–3476.
33. Horakova E, Gasser O, Sadallah S, Inal JM, Bourgeois G, et al. (2004) Complement mediates the binding of HIV to erythrocytes. J Immunol 173: 4236–4241.
34. Stoiber H, Banki Z, Wilflingseder D, Dierich MP (2008) Complement-HIV interactions during all steps of viral pathogenesis. Vaccine 26: 3046–3054.
35. Aloia RC, Jensen FC, Curtain CC, Mobley PW, Gordon LM (1988) Lipid composition and fluidity of the human immunodeficiency virus. Proc Natl Acad Sci U S A 85: 900–904.
36. Mayer LD, Hope MJ, Cullis PR (1986) Vesicles of variable sizes produced by a rapid extrusion procedure. Biochim Biophys Acta 858: 161–168.
37. Vitha MF, Clarke RJ (2007) Comparison of excitation and emission ratiometric fluorescence methods for quantifying the membrane dipole potential. Biochim Biophys Acta 1768: 107–114.
38. Clarke RJ, Kane DJ (1997) Optical detection of membrane dipole potential: avoidance of fluidity and dye-induced effects. Biochim Biophys Acta 1323: 223–239.

Appendix to Article A

This PLoS ONE article was selected for recommendation in the Faculty of 1000 (F1000) website, a post-publication evaluation service. Available in http://f1000.com/2953959.

Article B

Declaration of authorship

I, Pedro Miguel Baptista de Matos, declare that the experimental design, all the experimental work, data analysis and writing of initial manuscripts drafts were carried out by me, under the supervisions of Prof. Nuno C. Santos and the help of Prof. Miguel Castanho. Teresa Freitas helped in the isolation of human cells.

I, Nuno C. Santos, as supervisor of Pedro Matos and as corresponding author of the article mentioned above, hereby acknowledge and confirm that the information above is correct.

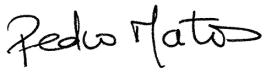

Pedro M. Matos

Nuno C. Santos

Biochemical and Biophysical Research Communications 403 (2010) 270–274

Contents lists available at ScienceDirect

Biochemical and Biophysical Research Communications

journal homepage: www.elsevier.com/locate/ybbrc

The role of blood cell membrane lipids on the mode of action of HIV-1 fusion inhibitor sifuvirtide

Pedro M. Matos, Teresa Freitas, Miguel A.R.B. Castanho, Nuno C. Santos *

Instituto de Medicina Molecular, Faculdade de Medicina da Universidade de Lisbon, Av. Prof. Egas Moniz, 1649-028 Lisboa, Portugal

ARTICLE INFO

Article history:
Received 12 October 2010
Available online 12 November 2010

Keywords:
HIV-1
Erythrocytes
Lymphocytes
Sifuvirtide
Dipole potential
Membrane

ABSTRACT

Sifuvirtide is a gp41 based peptide that inhibits HIV-1 fusion with the host cells and is currently under clinical trials. Previous studies showed that sifuvirtide partitions preferably to saturated phosphatidylcholine lipid membranes, instead of fluid-phase lipid vesicles. We extended the study to the interaction of the peptide with circulating blood cells, by using the dipole potential sensitive probe di-8-ANEPPS. Sifuvirtide decreased the dipole potential of erythrocyte and lymphocyte membranes in a concentration dependent manner, demonstrating its interaction. Also, the lipid selectivity of the peptide towards more rigid phosphatidylcholines was confirmed based on the dipole potential variations. Overall, the interaction of the peptide with the cell membranes is a contribution of different lipid preferences that presumably directs the peptide towards raft-like domains where the receptors are located, facilitating the reach of the peptide to its molecular target, the gp41 in its pre-fusion conformation.

1. Introduction

The search for new antiretroviral drugs has been an ongoing effort in order to manage HIV pathogenesis, leading to AIDS in humans. With the evolving technology, the paradigm has shifted to rationally designed drugs, tailored for a specific target of the viral life cycle [1]. HIV-1 fusion inhibitor peptides have been the object of intense research in the recent years as a consequence of the successful approval for clinical use of enfuvirtide (formerly T-20) [2]. Sifuvirtide is a second generation HIV-1 fusion inhibitor that is currently undergoing phase II clinical trials [3,4]. As previous HIV-1-fusion inhibitors, this peptide is based on the C-terminal heptad repeat (CHR) region of gp41, in order to bind to the N-terminal heptad repeat (NHR) region of gp41 and inhibit its pre-fusion conformation. Sifuvirtide was designed to increase the stability of the α-helix and to cover the deep pocket binding region of gp41 [3]. It shares some features with C34, another peptide that covers only the deep pocket region, differing from it in 16 out of 36 residues. Contrary to enfuvirtide, sifuvirtide lacks the region close to the membrane proximal region, which presumably accounts for lipid binding characteristics. T-1249, another second generation fusion inhibitor [5,6], has both the pocket (PBD) and lipid (LBD) binding domains.

Enfuvirtide and T-1249 were previously reported to partition to lipid model membranes [7,8] and blood cell membranes [9], a characteristic that correlated with antiviral efficacy, as T-1249, a more potent drug, has more affinity towards membranes than enfuvirtide. These peptides face a limited spatial and temporal window in which gp41 is susceptible in its pre-fusion conformation; therefore, a local concentration of peptide in the membrane environment makes the peptide delivery more efficient than via aqueous diffusion only. However, sifuvirtide was found not to partition towards POPC (1-palmitoyl-2-oleoyl-*sn*-glycero-3-phosphocholine) and POPC/cholesterol membranes, preferring instead more rigid choline phospholipids (DPPC, 1,2-dipalmitoyl-*sn*-glycero-3-phosphocholine) [10,11], which mimic more rigid lipid domains enriched in receptors at the cell membrane context. These are also the preferred sites of action for the HIV-1 gp41 fusion peptide [12,13]. Moreover, the viral envelope membrane is enriched in saturated phosphatidylcholines (PC), relative to the host cell, with DPPC constituting up to 20% of total PC [14].

We aimed to explore the membranotropism of sifuvirtide towards circulating blood cells (erythrocytes and peripheral blood mononuclear cells, PBMC) by monitoring its interaction using a membrane fluorescent probe. This probe, di-8-ANEPPS (4-[2-[6-(dioctylamino)-2-naphthalenyl]ethenyl]-1-(3-sulfopropyl)-pyridinium), is sensitive to alterations on the membrane dipole potential,

Abbreviations: CHR, C-terminal heptad repeat; NHR, N-terminal heptad repeat; TM, transmembrane domain; FP, fusion peptide; PBD, pocket binding domain; LBD, lipid-binding domain; Env, envelope; PC, phosphatidylcholine; POPC, 1-palmitoyl-2-oleoyl-*sn*-glycero-3-phosphocholine; DPPC, 1,2-dipalmitoyl-*sn*-glycero-3-phosphocholine; PBMC, peripheral blood mononuclear cells; di-8-ANEPPS, 4-[2-[6-(dioctylamino)-2-naphthalenyl]ethenyl]-1-(3-sulfopropyl)-pyridinium; LUV, large unilamellar vesicles; MLV, multi-lamellar vesicles.

* Corresponding author. Fax: +351 217999477.
E-mail address: nsantos@fm.ul.pt (N.C. Santos).

0006-291X/$ - see front matter © 2010 Elsevier Inc. All rights reserved.
doi:10.1016/j.bbrc.2010.11.013

which occur when molecules containing dipoles, such as this peptide, adsorb or insert into the lipid bilayer [15–18]. The membrane-incorporated di-8-ANEPPS reports dipole potential changes due to a shift in its excitation spectrum. The spectral shift is proportional to the magnitude of the potential change. This makes fluorescence differential ratiometric measurements an appropriate approach to quantify these changes [17].

2. Materials and methods

Human blood samples were collected from healthy blood donors, with their previous written informed consent, following a protocol established with the Portuguese Blood Institute (Lisbon), approved by the Ethics Committee of the Faculty of Medicine of the University of Lisbon. Erythrocytes and PBMC were isolated and labeled with di-8-ANEPPS (Invitrogen, Carlsbad, CA, USA) as previously described [9]. Briefly, erythrocytes were isolated by repeated centrifugation and washing with isotonic buffer and incubated at 1% hematocrit with 10 μM di-8-ANEPPS and buffer supplemented with 0.05% (m/V) Pluronic F-127 (Sigma, St. Louis, MO, USA). PBMC were isolated by density gradient using Ficoll-Paque Plus (GE Healthcare, Litlle Chalfont, UK) and incubated at 3000 cells/μL in Pluronic-supplemented buffer with 3.3 μM di-8-ANEPPS. Incubations lasted for 1 h and unbound probe was washed by centrifugation. Large unilamellar vesicles (LUV) with ~100 nm diameter, composed of pure POPC (Avanti Polar Lipids, Alabaster, AL, USA), POPC with 33% mol cholesterol (Sigma) and DPPC (Avanti Polar Lipids), were obtained by extrusion of multi-lamellar vesicles (MLV) as described elsewhere [9,19]. Lipid vesicles suspensions with 500 μM of total lipid were incubated overnight with di-8-ANEPPS 10 μM, to ensure maximum incorporation of the probe. Sifuvirtide (a kind gift of FusoGen, Tianjin, PR China) was incubated at different concentrations with labeled erythrocytes (0.02% hematocrit), PBMC (100 cells/μL) or lipid vesicles (200 μM of total lipid) during 1 h for cells or 90 min for vesicles, with gentle agitation before measurements. These incubations times were checked to be adequate for an equilibrium to be reached. All the fluorescence spectroscopy measurements were made in a Varian Cary Eclipse (Mulgrave, Australia) fluorescence spectrophotometer. Membrane-bound di-8-ANEPPS excitation spectra and ratios were taken with emission at 670 nm in order to avoid membrane fluidity effects [9,20]. Excitation and emission slits for all measurements were 5 nm and 10 nm, respectively.

All the experiments were done in HEPES isotonic buffer (HEPES 10 mM, NaCl 150 mM) at pH 7.4 and at room temperature (25 °C).

3. Results

In order to qualitatively evaluate sifuvirtide–membrane interaction, these two types of cell populations were incubated with three concentrations of sifuvirtide and the differential spectra were obtained (Fig. 1). The shape of these graphs indicates that there is a decrease in the dipole potential due to the presence of the peptide. Moreover, the amplitude, which is proportional to the spectral shift of the probe, is dependent on the peptide concentration.

To further investigate this dependence, we defined the ratio R of fluorescence intensities (I) at the two excitation wavelengths of maximum signal variation $I_{455\ nm}/I_{525\ nm}$ (both measurements with emission at 670 nm) of cell membrane-bound di-8-ANEPPS, which is proportional to the dipole potential (Fig. 2A). The effect of the peptide concentration is identical for the two cell types.

The decrease in the dipole potential is almost linear with concentration, at variance with the hyperbolic-like variation previously observed for enfuvirtide and T-1249 (Fig. 3) [9]. This denotes that the overall affinity is much lower compared to those two other fusion inhibitors. High concentrations were needed in order to decrease the dipole potential in a comparable way to T-1249 and enfuvirtide. Nevertheless, a clear membranotropic behavior is observed.

We also assessed the dipole potential variation for membrane model systems of defined composition (Fig. 2B). For that we used large unilamelar vesicles (LUVs) labeled with the same probe, di-8-ANEPPS. To model a standard mammalian membrane we used POPC to form zwitterionic and fluid phase bilayers on the liquid disordered state (l_d). Lipid raft-like domains, on the liquid ordered state (l_o) were mimicked by POPC:cholesterol (2:1) LUV. Also, we used pure DPPC, a totally saturated, gel phase-forming phospholipid, to which sifuvirtide has preference [10]. The results agreed with the previous study using tryptophan intrinsic fluorescence, in which the extension of the interaction varied following the trend POPC < POPC:cholesterol < DPPC.

4. Discussion

The overall membranotropism of sifuvirtide is lower regarding blood cell membranes or even lipid vesicles (depending on the composition) in relation to enfuvirtide and T-1249. The primary explanation for this relates to the portion of the sequence of gp41 CHR that the peptide is based on. Sifuvirtide, like C34, lacks the lipid-binding domain present in enfuvirtide and T-1249, which reduces its membrane affinity. In fact, C34 (and also sifuvirtide) has a very low binding to POPC lipid vesicles, as measured by microcalorimetry [3]. However, regarding the blood cells, we measured an overall affinity that is the sum of the contributions of a complex mixture of components present on their membranes.

Apparently, there is no clear distinction between the interaction of sifuvirtide with erythrocytes and PBMC (Fig. 2A). Different levels of membrane interaction could be expected, considering the distinct lipid compositions of these two cell types that differ mainly in cholesterol composition. However, just for the sake of comparison with the model lipids used in this work, erythrocytes have nearly doubled cholesterol content, while having half of the DPPC content when compared to PBMC [21]; therefore, both factors may eventually level up.

Sifuvirtide prefers more rigid phosphatidylcholines-rich lipid domains and this specific targeting can potentially direct the peptide to the saturated PC-enriched viral envelope membranes and, probably, also to the raft-like regions of host cells, which are richer in membrane receptors, including CD4, constituting a preferential site for HIV binding. Moreover, the fusion peptide directs the virus to these receptor-harboring platforms [12,13].

The atypical shape of the dipole potential variation as a function of the fusion-inhibitor concentration, both for cell membranes and biomembrane model systems, should be the result of the combined effects of the different lipids present on them, and hence, different preferences that are difficult to dissect in the cell membrane context. However, by comparing the maximum extent of binding for the lipid vesicles and the cell membranes, one can conclude that the heterogeneity of the latter is an adjuvant to the binding of this peptide, as it performs much better than simple POPC and POPC:cholesterol lipid mixtures. Yet, atomic force microscopy results show that this is not related to the effect of membrane domain interfaces [11]. Negative inflexions on the R vs. concentration curves close to a sifuvirtide concentration of 60 μM are especially evident on the studies with LUVs, but can also be noticed on the measurements with erythrocytes. This effect can be explained by the previously reported oligomerization of sifuvirtide in solution, occurring above 60 μM [10]. However, the formation of sifuvirtide larger aggregates, detectable by dynamic light scattering, only occurs at concentrations above 600 μM [10].

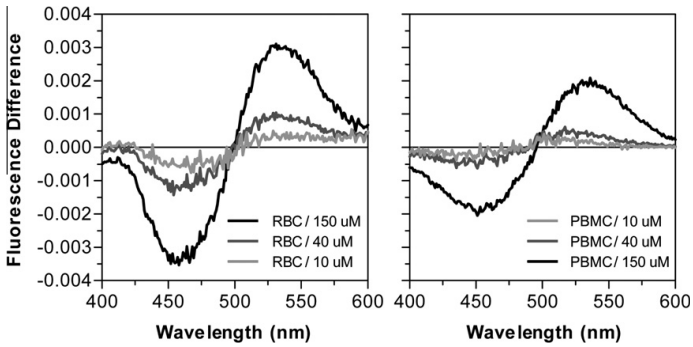

Fig. 1. Probe response to the presence of sifuvirtide in labeled blood cells membranes. Difference spectra of suspended cells with membrane-bound di-8-ANEPPS incubated with different concentrations of sifuvirtide, for erythrocytes (red blood cells, RBC; left) and PBMC (right) to assess the extent of excitation spectra shift. These were obtained by subtracting the normalized excitation spectra (to the integrated areas) of labeled cells in the presence of peptide from the spectrum in its absence. The shape and amplitude variation denotes a sifuvirtide concentration-dependent decrease in the dipole potential.

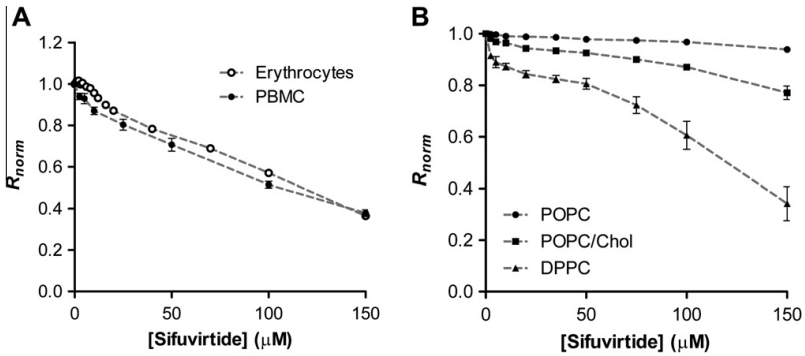

Fig. 2. Interaction of sifuvirtide with cell membranes and biomembrane model systems. (A) Variation of the di-8-ANEPPS excitation ratio R_{norm} with sifuvirtide concentration for erythrocytes and PBMC. $N = 6$ for erythrocytes and PBMC (blood samples from different donors). (B) Dipole potential variation for labeled LUV with defined lipid composition of POPC, POPC:cholesterol 2:1 and DPPC at 200 μM total lipid ($N = 2$). Ratio values were normalized for the initial value in the absence of sifuvirtide. Plotted values represent mean ± SEM.

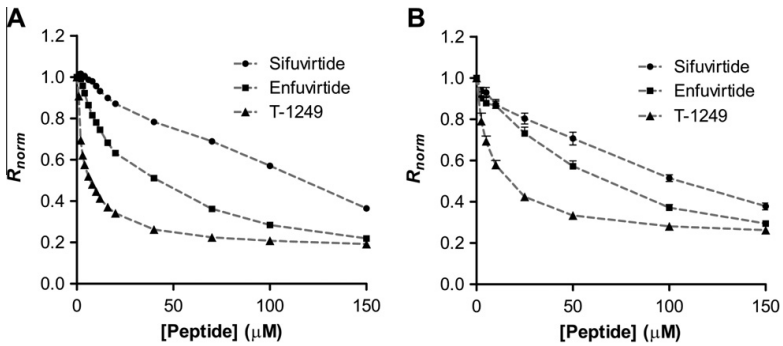

Fig. 3. Comparison with enfuvirtide and T-1249. The binding profile of sifuvirtide is shown here compared with previously obtained results for enfuvirtide and T-1249 [9], for erythrocytes (A) and PBMC (B), under the same experimental conditions. Ratio values were normalized for the initial value in the absence of peptide. Plotted values represent mean ± SEM.

The results presented in this report using erythrocytes and PMBC show that the membrane-association of sifuvirtide is potentially relevant in the biological context. The results obtained with vesicles show a weak and interfacial adsorption, which is consistent with the results now presented for cells. Sifuvirtide interacts with membranes, but not as extensively as enfuvirtide or T-1249. This can be related to the so-called "membrane catalysis" hypothesis, where one of the effect of membranes is to increase the local

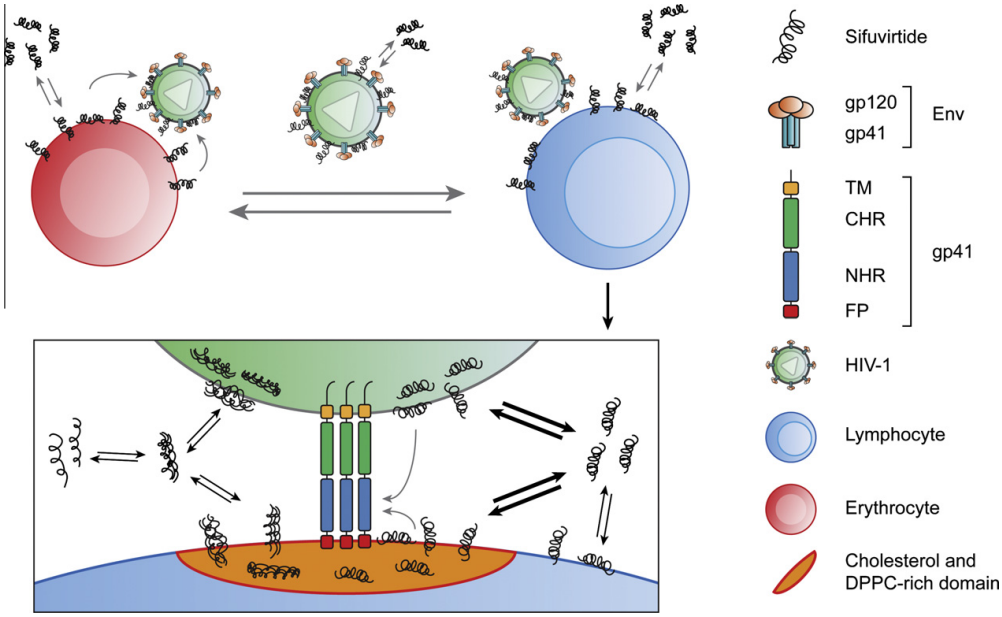

Fig. 4. Dynamics of sifuvirtide membranotropism. Sifuvirtide interacts to a certain extent with the membrane of circulating erythrocytes, PBMC and, presumably, HIV. Exchange of peptide would be facilitated by the contact of the virus with the erythrocyte surface. Sifuvirtide partitions preferentially to more rigid domains, enriched in DPPC and cholesterol, where the receptors are presumably located, facilitating the access to gp41 in its pre-fusion conformation, during the reduced timewindow in which it is accessible. Above a sifuvirtide concentration threshold of 60 μM, the oligomerization of the peptide enhances partition. Env, envelope; TM, transmembrane domain; NHR, N-terminal heptad repeat; CHR, C-terminal heptad repeat; FP, fusion peptide.

concentration of ligands in the vicinity of their targets [22]. A possible model for the relevance of the interaction of sifuvirtide with blood cells, based on information available on the literature, complemented by the present findings, is presented in Fig. 4. The virus was previously demonstrated to associate to the erythrocyte surface, allowing trans-infection to permissive cells [23–26], highlighting an importance in the context of drug distribution and delivery of sifuvirtide to the viral envelope, where it can also adsorb (the viral envelope is a DPPC- and cholesterol-rich bilayer). When the virus infects the preferential target cells, $CD4^+$ lymphocytes, the accumulation of sifuvirtide in the cell surface domains is a factor that could enhance the inhibition of HIV gp41-mediated fusion and entry.

Role of the funding source

This work was funded by Fundação para a Ciência e Tecnologia (FCT) of the Portuguese Ministry of Science, Technology and Higher Education (MCTES), including project PTDC/QUI-BIQ/104787/2008 and Ph.D. Grant SFRH/BD/42205/2007 for P.M.M. The funding source did not have a direct involvement in this study.

Acknowledgments

The authors thank Henri G. Franquelim (Instituto de Medicina Molecular, Lisbon, Portugal) for valuable discussions and to Fuso-Gen Pharmaceuticals Inc. (Tianjin, PR China) for the kind gift of sifuvirtide.

References

[1] E. De Clercq, The design of drugs for HIV and HCV, Nat. Rev. Drug Discov. 6 (2007) 1001–1018.
[2] T. Matthews, M. Salgo, M. Greenberg, J. Chung, R. DeMasi, D. Bolognesi, Enfuvirtide: the first therapy to inhibit the entry of HIV-1 into host CD4 lymphocytes, Nat. Rev. Drug Discov. 3 (2004) 215–225.
[3] Y.X. He, Y.H. Xiao, H.F. Song, Q. Liang, D. Ju, X. Chen, H. Lu, W.G. Jing, S.B. Jiang, L.Q. Zhang, Design and evaluation of sifuvirtide, a novel HIV-1 fusion inhibitor, J. Biol. Chem. 283 (2008) 11126–11134.
[4] R.R. Wang, L.M. Yang, Y.H. Wang, W. Pang, S.C. Tam, P. Tien, Y.T. Zheng, Sifuvirtide, a potent HIV fusion inhibitor peptide, Biochem. Biophys. Res. Commun. 382 (2009) 540–544.
[5] J.J. Eron, R.M. Gulick, J.A. Bartlett, T. Merigan, R. Arduino, J.M. Kilby, B. Yangco, A. Diers, C. Drobnes, R. DeMasi, M. Greenberg, T. Melby, C. Raskino, P. Rusnak, Y. Zhang, R. Spence, G.D. Miralles, Short-term safety and antiretroviral activity of T-1249, a second-generation fusion inhibitor of HIV, J. Infect. Dis. 189 (2004) 1075–1083.
[6] M.L. Greenberg, D. Davison, J. Jin, S. Mosier, T. Melby, P. Sista, R. Demasi, D. Miralles, N. Cammack, T.J. Matthews, In vitro antiviral activity of T-1249 a second generation fusion inhibitor, Antivir. Ther. 7 (Suppl.1) (2002) S10.
[7] A.S. Veiga, N.C. Santos, L.M.S. Loura, A. Fedorov, M.A.R.B. Castanho, HIV fusion inhibitor peptide T-1249 is able to insert or adsorb to lipidic bilayers. Putative correlation with improved efficiency, J. Am. Chem. Soc. 126 (2004) 14758–14763.
[8] S. Veiga, S. Henriques, N.C. Santos, M. Castanho, Putative role of membranes in the HIV fusion inhibitor enfuvirtide mode of action at the molecular level, Biochem. J. 377 (2004) 107–110.
[9] P.M. Matos, M.A.R.B. Castanho, N.C. Santos, HIV-1 fusion inhibitor peptides enfuvirtide and T-1249 interact with erythrocyte and lymphocyte membranes, PLoS One 5 (2010) e9830.
[10] H.G. Franquelim, L.M.S. Loura, N.C. Santos, M.A.R.B. Castanho, Sifuvirtide screens rigid membrane surfaces. Establishment of a correlation between efficacy and membrane domain selectivity among HIV fusion inhibitor peptides, J. Am. Chem. Soc. 130 (2008) 6215–6223.
[11] H.G. Franquelim, A.S. Veiga, G. Weissmuller, N.C. Santos, M.A. Castanho, Unravelling the molecular basis of the selectivity of the HIV-1 fusion inhibitor sifuvirtide towards phosphatidylcholine-rich rigid membranes, Biochim. Biophys. Acta 1798 (2010) 1234–1243.
[12] D. Gerber, M. Pritsker, S. Gunther-Ausborn, B. Johnson, R. Blumenthal, Y. Shai, Inhibition of HIV-1 envelope glycoprotein-mediated cell fusion by a D-amino acid-containing fusion peptide: possible recognition of the fusion complex, J. Biol. Chem. 279 (2004) 48224–48230.
[13] F.J. Quintana, D. Gerber, S.C. Kent, I.R. Cohen, Y. Shai, HIV-1 fusion peptide targets the TCR and inhibits antigen-specific T cell activation, J. Clin. Invest. 115 (2005) 2149–2158.

[14] B. Brugger, B. Glass, P. Haberkant, I. Leibrecht, F.T. Wieland, H.G. Krasslich, The HIV lipidome: a raft with an unusual composition, Proc. Natl. Acad. Sci. USA 103 (2006) 2641–2646.
[15] T. Asawakarn, J. Cladera, P. O'Shea, Effects of the membrane dipole potential on the interaction of saquinavir with phospholipid membranes and plasma membrane receptors of Caco-2 cells, J. Biol. Chem. 276 (2001) 38457–38463.
[16] J. Cladera, P. O'Shea, Intramembrane molecular dipoles affect the membrane insertion and folding of a model amphiphilic peptide, Biophys. J. 74 (1998) 2434–2442.
[17] E. Gross, R.S. Bedlack, L.M. Loew, Dual-wavelength ratiometric fluorescence measurement of the membrane dipole potential, Biophys. J. 67 (1994) 208–216.
[18] P.M. Matos, S. Goncalves, N.C. Santos, Interaction of peptides with biomembranes assessed by potential-sensitive fluorescent probes, J. Pept. Sci. 14 (2008) 407–415.
[19] L.D. Mayer, M.J. Hope, P.R. Cullis, Vesicles of variable sizes produced by a rapid extrusion procedure, Biochim. Biophys. Acta 858 (1986) 161–168.
[20] R.J. Clarke, D.J. Kane, Optical detection of membrane dipole potential: avoidance of fluidity and dye-induced effects, Biochim. Biophys. Acta 1323 (1997) 223–239.
[21] K. Leidl, G. Liebisch, D. Richter, G. Schmitz, Mass spectrometric analysis of lipid species of human circulating blood cells, Biochim. Biophys. Acta 1781 (2008) 655–664.
[22] M.A. Castanho, M.X. Fernandes, Lipid membrane-induced optimization for ligand–receptor docking: recent tools and insights for the "membrane catalysis" model, Eur. Biophys. J. 35 (2006) 92–103.
[23] C. Hess, T. Klimkait, L. Schlapbach, V. Del Zenero, S. Sadallah, E. Horakova, G. Balestra, V. Werder, C. Schaefer, M. Battegay, J.A. Schifferli, Association of a pool of HIV-1 with erythrocytes in vivo: a cohort study, Lancet 359 (2002) 2230–2234.
[24] Z. Banki, D. Wilflingseder, C.G. Ammann, M. Pruenster, B. Mullauer, K. Hollander, M. Meyer, G.M. Sprinzl, J. van Lunzen, H.J. Stellbrink, M.P. Dierich, H. Stoiber, Factor I-mediated processing of complement fragments on HIV immune complexes targets HIV to CR2-expressing B cells and facilitates B cell-mediated transmission of opsonized HIV to T cells, J. Immunol. 177 (2006) 3469–3476.
[25] W. He, S. Neil, H. Kulkarni, E. Wright, B.K. Agan, V.C. Marconi, M.J. Dolan, R.A. Weiss, S.K. Ahuja, Duffy antigen receptor for chemokines mediates trans-infection of HIV-1 from red blood cells to target cells and affects HIV-AIDS susceptibility, Cell Host Microbe 4 (2008) 52–62.
[26] Z. Beck, B.K. Brown, L. Wieczorek, K.K. Peachman, G.R. Matyas, V.R. Polonis, M. Rao, C.R. Alving, Human erythrocytes selectively bind and enrich infectious HIV-1 virions, PLoS One 4 (2009) e8297.

Article C

Declaration of authorship

I, Pedro Miguel Baptista de Matos, declare that I equally shared the tasks of experimental design, experimental work, data analysis and writing of initial manuscript draft with Dr. Axel Hollmann, under the supervisions of Prof. Nuno C. Santos and the help of Prof. Miguel Castanho. I was involved mainly in partition coefficient determination, acrylamide quenching and cell membrane interaction experiments. Marcelo T. Augusto carried out additional fluorescence spectroscopy experiments requested by the referees during editorial revision.

I, Nuno C. Santos, as supervisor of Pedro Matos and as corresponding author of the article mentioned above, hereby acknowledge and confirm that the information above is correct.

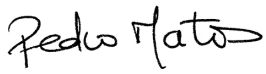

Pedro M. Matos

Nuno C. Santos

OPEN ACCESS Freely available online

PLOS ONE

Conjugation of Cholesterol to HIV-1 Fusion Inhibitor C34 Increases Peptide-Membrane Interactions Potentiating Its Action

Axel Hollmann[•], **Pedro M. Matos**[•], **Marcelo T. Augusto, Miguel A. R. B. Castanho, Nuno C. Santos***

Instituto de Medicina Molecular, Faculdade de Medicina, Universidade de Lisboa, Lisbon, Portugal

Abstract

Recently, the covalent binding of a cholesterol moiety to a classical HIV-1 fusion inhibitor peptide, C34, was shown to potentiate its antiviral activity. Our purpose was to evaluate the interaction of cholesterol-conjugated and native C34 with membrane model systems and human blood cells to understand the effects of this derivatization. Lipid vesicles and monolayers with defined compositions were used as model membranes. C34-cholesterol partitions more to fluid phase membranes that mimic biological membranes. Importantly, there is a preference of the conjugate for liquid ordered membranes, rich in cholesterol and/or sphingomyelin, as observed both from partition and surface pressure studies. In human erythrocytes and peripheral blood mononuclear cells (PBMC), C34-cholesterol significantly decreases the membrane dipole potential. In PBMC, the conjugate was 14- and 115-fold more membranotropic than T-1249 and enfuvirtide, respectively. C34 or cholesterol alone did not show significant membrane activity. The enhanced interaction of C34-cholesterol with biological membranes correlates with its higher antiviral potency. Higher partitions for lipid-raft like compositions direct the drug to the receptor-rich domains where membrane fusion is likely to occur. This intermediary membrane binding step may facilitate the drug delivery to gp41 in its pre-fusion state.

Citation: Hollmann A, Matos PM, Augusto MT, Castanho MARB, Santos NC (2013) Conjugation of Cholesterol to HIV-1 Fusion Inhibitor C34 Increases Peptide-Membrane Interactions Potentiating Its Action. PLoS ONE 8(4): e60302. doi:10.1371/journal.pone.0060302

Editor: Stefan Pöhlmann, German Primate Center, Germany

Received December 13, 2012; **Accepted** February 25, 2013; **Published** April 2, 2013

Funding: This work was funded by Fundação para a Ciência e Tecnologia, Portugal (fellowships SFRH/BPD/72037/2010 and SFRH/BD/42205/2007 to A.H. and P.M.M., respectively, and projects PTDC/QUI-BIQ/104787/2008, PTDC/QUI-BIQ/112929/2009 and VIH/SAU/0047/2011). The funders had no role in study design, data collection and analysis, decision to publish, or preparation of the manuscript.

Competing Interests: The authors have declared that no competing interests exist.

* E-mail: nsantos@fm.ul.pt

• These authors contributed equally to this work.

Introduction

The development of new drugs against the human immunodeficiency virus type 1 (HIV-1) has been the focus of intense research since its discovery [1]. The virus fusion with the cell membrane and the consequent entry into the host cell is a critical moment of its life cycle. Efficiently blocking this process prevents all the subsequent intracellular steps. Most importantly, the integration of the viral genome, which can stay silent for years, does not occur. Despite this promising approach, only two HIV entry inhibitors are available in the market: maraviroc, an inhibitor of envelope binding to the CCR5 co-receptor [2], and enfuvirtide, a fusion inhibitor peptide targeting gp41 in its pre fusion conformation [3]. Enfuvirtide, due to its peptide nature, has to be administered subcutaneously and is more sensitive to degradation while in circulation. It is important to overcome these limitations as peptide drugs can also have the advantage to be potentially less toxic.

Several HIV-1 fusion inhibitor peptides have been developed and studied *in vitro* [4–6]. The rationale for the development of these peptides is based on the structural rearrangements of gp41 after the binding of gp120 to CD4 and a co-receptor (CCR5 or CXCR4). The two heptad repeats fold into each other creating a hairpin structure (also named 6-helix bundle, due to the formation of a homotrimer of heterodimers) that brings the two membranes together and promotes the formation of the fusion pore used for the entry of the viral content into the target cell [7]. Most of these peptides were derived from the C-terminal heptad repeat (CHR) region of gp41, and hence bind to the opposite domain in order to prevent bundle formation. The rational design of higher efficacy peptides compared to the native sequence from gp41 CHR include rearrangements and substitutions in order to improve intrinsic characteristics such as solubility, helical stability, oligomerization, lipophilicity and resistance to proteolysis [4].

In our previous works, we emphasized the importance of the lipophilicity and membrane interaction properties of the fusion inhibitor peptides enfuvirtide, T-1249 and sifuvirtide [8–10]. The fact that these peptides can partition to the membranes and to the microdomains, where receptors are preferentially located, facilitates the interaction with gp41 in its exposed conformation. This intermediate is temporally and spatially constrained; thus, a pre-concentration effect in the membrane can be a strategy to overcome this poorly accessible target.

Previously, the peptide C34, a classical fusion inhibitor used also as a template for the structural characterization of gp41 [7], was conjugated with a cholesterol moiety in order to obtain higher efficacy and lifetime *in vivo* [11]. C34-cholesterol (with cholesterol covalently bound to the C-terminus of the peptide; also known as L'644) was shown to be 50-fold more potent than C34 alone in terms of IC_{50} (HXB2 strain). Moreover, in a mouse model, the

conjugated peptide was still detected 24 h after injection and with higher concentration, when compared with the unconjugated peptide, which was undetectable after 6 h [11]. In another recent work, a comparative pre-clinical evaluation of four fusion inhibitors (C34, T1249, enfuvirtide and C34-cholesterol) as potential microbicides showed that C34-cholesterol exhibits the highest anti HIV-1 activity as well as an extended window of activity. Moreover, C34-cholesterol is able to inhibit both wild type and reverse transcriptase inhibitors-resistant isolates [12].

The conjugation approach to improve fusion inhibitor peptides, such as by attaching acyl chains of various sizes [13–15] or human serum albumin [16,17], has been tried before; however, none has reached beyond pre-clinical tests. C34-cholesterol is a promising candidate [12].

In this article, we aimed at characterizing the interaction of C34 and C34-cholesterol with biomembranes to elucidate the peptide-membrane interaction and possible relations with the efficiency of these drugs. Our approach first covered a detailed study of the peptide partition towards biomembrane model systems, namely large unilamellar vesicles (LUV), by following the intrinsic fluorescence changes of the peptide tryptophan residues, located at the N-terminal region, when it adsorb or penetrate in the lipid environment. This methodology allows testing a diversity of lipid compositions, in order to dissect the role of the different lipid types. Insertion of the fusion inhibitors in lipid monolayers was also evaluated on a Langmuir-Blodgett trough. Finally, we studied the interaction with membranes of human blood cells, in an *ex vivo* setting. In this case, we used a lipophilic fluorescent probe (di-8-ANEPPS) that is sensitive to the membrane dipole potential and can report interactions of molecules that disturb the membrane order.

Experimental Section

Reagents

C34 (WMEWDREINNYTSLIHSLIEESQNQQEKNEQELL) was obtained from the NIH AIDS Research and Reference Reagent Program (Division of AIDS, NIAID, NIH). C34-cholesterol (L'644) was a kind gift from the International Partnership for Microbicides (licensed by Merck) and its sequence is C34-GSGC-Cholesterol. 5NS (5-doxyl-stearic acid) and 16NS (16-doxyl-stearic acid) were from Aldrich (Milwaukee, WI, USA). L-Tryptophan, acrylamide, HEPES and NaCl were from Merck (Darmstadt, Germany). POPC (1-palmitoyl-2-oleoyl-*sn*-glycero-3-phosphocholine), DPPC (1,2-dipalmitoyl-*sn*-glycero-3-phosphocholine), POPG (1-palmitoyl-2-oleoyl-*sn*-glycero-3-[phospho-*rac*-(1-glycerol)]), DHSM (N-dodecanoyl-sphinganine-1-phosphocholine), SM (egg sphingomyelin), POPE (1-palmitoyl-2-oleoyl-*sn*-glycero-3-phosphoethanolamine) and POPS (1-palmitoyl-2-oleoyl-*sn*-glycero-3-phospho-L-serine) were purchased from Avanti Polar Lipids (Alabaster, AL, USA), while cholesterol (Chol) were from Sigma (St. Louis, MO, USA).

Fluorescence Spectroscopy Measurements

C34 and C34-cholesterol peptides contain tryptophan residues, which make fluorescence techniques suitable tools to probe these molecules. The working buffer used throughout the studies was HEPES 10 mM pH 7.4 in NaCl 150 mM. C34 (150 μM) and Trp (500 μM) stock solutions were prepared in buffer. C34-cholesterol (500 μM) stock solutions were prepared in DMSO. Large unilamellar vesicles (LUV) were prepared by extrusion methods, as described elsewhere [18,19].

Membrane partition and fluorescence quenching studies using acrylamide were carried out in a Varian Cary Eclipse fluorescence spectrophotometer (Mulgrave, Australia) and time-resolved fluorescence spectroscopy studies in a LifeSpec II Fluorescence Lifetime spectrometer (Edinburgh Instruments).

The fluorescence spectral characterization of C34, C34-cholesterol and Trp was performed with an excitation wavelength of 280 nm, except for 5NS, 16NS and acrylamide quenching experiments, where the excitation was performed at 290 nm to minimize the relative quencher/fluorophore light-absorption ratios. For the quenching experiments, fluorescence emission was collected at a fixed wavelength of 350 nm and for the partition studies integrated spectra from 310 to 450 nm were used. Typical spectral bandwidths were 5 nm for excitation and 10 nm for emission. Excitation and emission spectra were corrected for wavelength-dependent instrumental factors [20]. During the quenching and partition experiments, emission was also corrected for successive dilutions, scatter [21] and simultaneous light absorptions of quencher and fluorophore. All the fluorescence measurements in this study were performed at room temperature (approximately 25°C).

Partition Coefficient Determination

Membrane partition studies were performed by successive additions to a 5 μM C34 or C34-cholesterol solution of small amounts of LUV suspensions with different lipid compositions, including: POPC, POPC:Chol (2:1 and 1:1), DPPC, POPC:-Chol:SM (1:1:1 and 2:2:1), POPC:SM (2:1), POPC:POPG (5:1), POPC:DHSM (1:0.06), and HIV membrane-like mixture with and without DHSM (POPC 5.3%, DPPC 3.5%, cholesterol 45.3%, SM 18.2%, POPE 19.3% and POPS 8.4% [22]), with a 10 min incubation time between each addition. The partition coefficients (K_p) were calculated using the equation [23]:

$$\frac{I}{I_W} = \frac{1 + K_p \gamma_L \frac{I_L}{I_W} [L]}{1 + K_p \gamma_L [L]} \quad (1)$$

where I_W and I_L are the fluorescence intensities in aqueous solution and in lipid, respectively, γ_L is the molar volume of the lipid [24,25], and [L] its concentration.

Surface Pressure

Changes on the surface pressure of lipid monolayers induced by C34, C34-cholesterol, enfuvirtide and T-1249 were measured in a Langmuir-Blodgett trough NIMA ST900 (Coventry, UK), at constant temperature (25±0.5°C). The surface of a HEPES buffer solution contained in a Teflon trough of fixed area was exhaustively cleaned by surface aspiration. Then, a solution of lipids in chloroform was spread on this surface, reaching a surface pressure of 20.5±1 mN/m. Peptide solutions were injected in the subphase and the changes on the surface pressure were followed during the necessary time to reach a constant value. The surface pressure of an air−water interface upon injecting the largest concentration of each peptide used throughout the studies was always below 15 mN/m (data not shown). For this reason, the lowest initial surface pressure of the lipid monolayers before the addition of the peptides to the subphase was above that value. In this condition, the changes in surface pressure observed upon the injection of the peptide can be attributed to an effect of the peptide on the monolayer interfacial tension.

The dissociation constant (K_d) was calculated from the adsorption Langmuir isotherm:

$$\Delta\Pi = \frac{\Delta\Pi_{max}[peptide]}{K_d + [peptide]} \quad (2)$$

where $\Delta\Pi$ are the changes of surface pressure, $\Delta\Pi_{max}$ is the maximum change of pressure achieved and [*peptide*] is the peptide concentration.

Acrylamide Quenching

The fluorescence quenching of 5 μM C34 or C34-cholesterol by acrylamide (0−60 mM) [8] was studied in buffer and in the presence of POPC or DPPC 3 mM LUV, by successive additions of small volumes of the quencher stock solution. For every addition, a minimal 10 min incubation time was allowed before measurement. Quenching data were analyzed by using the Stern−Volmer equation [23]:

$$\frac{I_0}{I} = 1 + K_{SV}\cdot[Q] \quad (3)$$

where I and I_0 are the fluorescence intensity of the sample in the presence and absence of quencher, respectively, K_{SV} is the Stern−Volmer constant and [Q] the concentration of quencher.

5NS and 16NS Quenching

Fluorescence quenching assays with the lipophilic probes 5NS and 16NS were performed by time-resolved fluorescence spectroscopy. These assays were carried out at the same peptide and lipid concentrations used for the acrylamide quenching, by successive additions of small amounts of these quenchers (in ethanol) to samples of peptide in POPC and POPC:Chol (2:1), keeping the ethanol concentration below 2% (v/v) [26]. The effective lipophilic quencher concentration in the membrane was calculated from the partition coefficient of both quenchers to the lipid bilayers [27]. For every addition, a minimal 10 min incubation time was allowed before measurement. Quenching data were analyzed by using the Stern−Volmer equation (eq. 1), or the Lehrer equation [27,28] when a negative deviation to the Stern–Volmer relationship is observed:

$$\frac{I_0}{I} = \frac{1 + K_{SV}[Q]}{(1 + K_{SV}[Q])(1 - f_b) + f_b} \quad (4)$$

where f_b is the fraction of light arising from the fluorophores accessible to the quencher.

In the case of dynamic quenching, the relationship $I_0/I = \tau_0/\tau$ is valid; thus, time-resolved quenching data can be analyzed by using the same equations (eq. 3 and 4).

Membrane Dipole Potential Assessed by di-8-ANEPPS

Human blood samples were obtained from healthy volunteers, with their previous written informed consent, at the Instituto Português do Sangue (Lisbon, Portugal). This study was approved by the ethics committee of the Faculdade de Medicina da Universidade de Lisboa. Isolation of erythrocytes and PBMC and labeling of these cells with di-8-ANEPPS (Invitrogen, Carlsbad, CA, USA) were performed as described before [9,29]. For erythrocytes isolation, blood samples were centrifuged at 1200 × *g* during 10 min, plasma and buffy-coat were removed, and remaining erythrocytes were washed twice in working buffer. They were incubated at 1% hematocrit in buffer supplemented with 0.05% (m/v) Pluronic F-127 (Sigma) and di-8-ANEPPS 10 μM. PBMC were isolated by density gradient using Ficoll-Paque Plus (GE Healthcare, Little Chalfont, UK) and counted in a Neubauer improved hemocytometer. They were incubated at 3000 cells/μL in Pluronic-supplemented buffer with 3.3 μM di-8-ANEPPS. Cells were incubated with the fluorescent probe during 1 h, with gentle agitation, and unbound probe was washed with Pluronic-free buffer on two centrifugation cycles. C34, C34-cholesterol (in DMSO stock solution) or cholesterol (in DMSO:ethanol 1:1 stock solution) were incubated with erythrocytes at 0.02% hematocrit and with PBMC at 100 cells/μL during 1 h, with gentle agitation, before the fluorescence measurements. For lipid vesicles labeling, suspensions with 500 mM of total lipid were incubated overnight with di-8-ANEPPS 10 μM, to ensure maximum incorporation of the probe. The maximum concentration of DMSO or DMSO:ethanol in the suspensions was 2.4% (v/v) at 6 μM of peptide or cholesterol. Excitation spectra and the ratio of intensities at the excitation wavelengths of 455 and 525 nm ($R = I_{455}/I_{525}$) were obtained with emission set at 670 nm to avoid membrane fluidity-related artifacts [30,31]. Excitation and emission slits for these measurements were set to 5 and 10 nm, respectively. The variation of R with the peptide concentration was analyzed by a single binding site model [32]:

$$\frac{R}{R_0} = 1 + \frac{R_{min}/R_0[peptide]}{K_d + [peptide]} \quad (5)$$

with the R values normalized for R_0, the value in the absence of peptide. R_{min} defines the asymptotic minimum value of R and K_d is the dissociation constant.

Data Analysis

Fitting of the equations mentioned in this article to the experimental data was done by non-linear regression using Graphpad Prism 5. Error bars on data presentation represent the standard error of mean (SEM).

Results

Membrane Partition

UV-visible absorption and fluorescence spectra in buffer of C34 are comparable to those of Trp in aqueous solution (Fig. 1); however, C34-cholesterol presents a blue shift, indicating that there is a change in the Trp surrounding environment in this conjugate.

As shown in Fig. 2, there is an increase in the fluorescence intensity of C34-cholesterol in the presence of LUV. The partition coefficient between the lipid and aqueous phases, K_p, was determined by fitting eq. 1 to the fluorescence intensity data, in order to quantify the extent of interaction of the peptides to the LUV (Table 1). For POPC, a lipid with packing density and fluidity properties similar to biological membranes, a K_p value of 1.57×10^3 was obtained, showing a significant interaction. When gel phase DPPC membranes were tested, a decreased K_p was found, probably due to the higher bilayer rigidity. In cholesterol-rich membranes (POPC:Chol, POPC:Chol:SM 2:2:1 and HIV-like mixture) a significant increase in the partition was observed, when compared with pure POPC, also with a decrease on I_L. Mixtures with cholesterol and SM mimic membrane microdomains usually named lipid rafts [33]. The same variation on I_L occurred for the addition of SM or DHSM (an unusual sphingolipid which does not contain a 4,5-*trans* double bond in its sphinganine backbone, significantly enriched in HIV-1 membranes [22]). The HIV-like mixture had the highest partition,

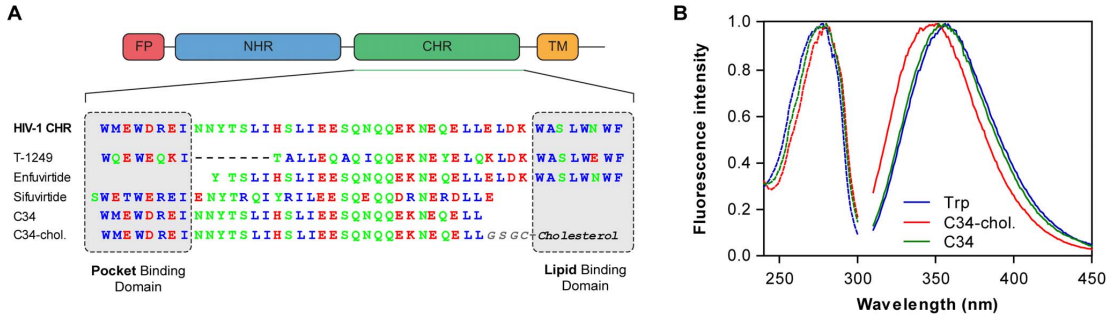

Figure 1. Characteristics of C34 and C34-cholesterol. (**A**) Schematic representation of HIV-1 gp41 main domains, depicting the relative position of the fusion peptide (FP), N-terminal heptad repeat domain (NHR), C-terminal heptad repeat domain (CHR) and transmembrane region (TM). The sequence of C34 was aligned with enfuvirtide, T-1249 and sifuvirtide, showing the pocket binding domain (PBD) and the lipid binding domain (LBD). Hydrophobic residues are represented in blue, non-charged polar residues in green, and charged polar residues in red. (**B**) Normalized fluorescence excitation (dashed line) and emission (solid line) spectra of 5 μM C34, C34-cholesterol or Trp in aqueous solution.
doi:10.1371/journal.pone.0060302.g001

hinting to an importance of the viral membrane in capturing the drug besides the cell membrane.

In the case of C34, except for DPPC, no significant changes in the fluorescence intensity were observed in the presence of membranes (Fig. 2A), indicating an absence of significant peptide-membrane interactions.

Surface Pressure Perturbation of Monolayers

Despite the negligible partition and quenching results, adsorption of C34 to the membrane surface cannot be discarded, as it may leave the Trp residues exposed to the bulk aqueous environment, with unchanged quantum yield (*i.e.*, not contributing for K_p calculation) [10]. In order to discard that situation, surface pressure measurements on POPC monolayer were carried out, using a low initial surface pressure (20.5 mN/m). Usually, the adsorption and penetration of molecules is favored at low surface density (loosely packed lipid monolayers), whereas high surface pressure (compact lipid packing) hinders the adsorption and penetration in the lipid monolayers [34]. As shown in Fig. 3A, C34 is not able to induce any significant change in the surface pressure, in contrast to C34-cholesterol.

We also measured the changes in surface pressures induced by enfuvirtide and T-1249, yielding similar results to C34-cholesterol (Fig. 3A). In contrast, with POPC:Chol (2:1) or POPC:Chol:SM (1:1:1) monolayers, C34-cholesterol was able to induce larger changes than the other inhibitors (Figure 3B,C). K_d and $\Delta\Pi_{max}$ values were determined by fitting eq. 2, in order to quantify the interaction of each peptide with the Langmuir monolayers (Table 2).

Direct comparison between the three peptides is difficult since they have different membrane binding domains. Therefore, they are not expected to modify the same way the surface tension of the membrane. However, comparing the same peptide for different lipids, we observe that C34-cholesterol presents an increased affinity to cholesterol rich membranes: an approximate ten-fold increase for POPC:Chol (2:1) and around six-fold for POPC:Chol:SM (1:1:1), when compared to pure POPC. This is in good agreement with data obtained from partition studies. In the case of enfuvirtide, no significant changes in the affinity were observed among each membrane composition tested, with just a slight decrease in the affinity for POPC:Chol, in a good agreement with previously published data [35]. Finally, T-1249 presented lower affinity for POPC:Chol, when compared with the other two compositions.

When the interaction kinetics were tested, a faster variation was observed for C34-cholesterol (Figure 3D). Control experiments were carried out using DMSO without C34-cholesterol and no significant changes were observed.

Table 1. Partition coefficients.

Lipid Mixture	K_p	I_L/I_w
POPC	1574±261	1.88±0.05
DPPC	331±44	2.98±0.16
POPC:Chol 2:1	3454±718	1.25±0.01
POPC:Chol:SM 2:2:1	4050±885	1.24±0.01
POPC:Chol 1:1	4612±436	1.32±0.01
POPC:DHSM (6%)	755±232	1.72±0.09
HIV-like mixture	8084±1190	1.14±0.004
HIV-like mixture with DHSM	1758±688	1.15±0.002

Parameters obtained from the fitting of the fluorescence data of the partition assays of C34-cholesterol 5 μM using eq. 1. All measures were made at least in triplicate. Values are presented as mean ± standard error of mean (SEM).
doi:10.1371/journal.pone.0060302.t001

Localization in the Lipid Bilayer

In order to test the accessibility of the fluorophores to the aqueous environment, the fluorescence quenching of the Trp residues of the peptide by acrylamide was studied. Linear Stern-Volmer plots were obtained in the absence of lipid (Fig. 4) and the quenching for C34-cholesterol is less efficient than C34, indicating that the fluorophore in the conjugate is less exposed to the surrounding aqueous medium. The cholesterol moiety may create hydrophobic pockets due to the formation of micro-aggregates, leading to this difference in the quenching in aqueous solution. Stern−Volmer plots and K_{sv} constants in the presence of 3 mM of lipid and 5 μM of C34 or C34-cholesterol were obtained in order to complement the partition assays (Fig. 4). For C34-cholesterol, both assays with lipids yielded K_{sv} values lower than the obtained in their absence (7.23±0.15 mM^{-1} in solution, 5.58±0.14 mM^{-1} with DPPC and 5.16±0.11 mM^{-1} with POPC). In contrast, for C34 only, DPPC was able to reduce the K_{sv} value from

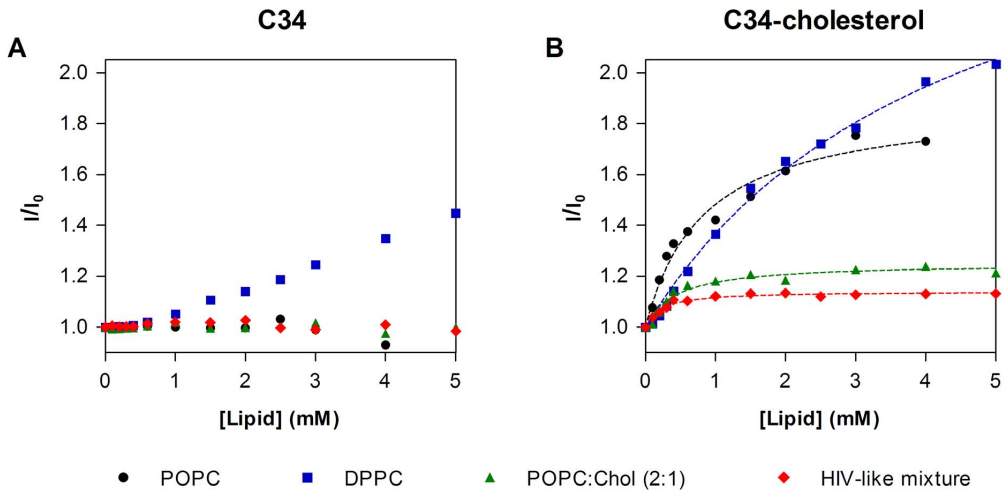

Figure 2. Partition of the peptides to lipid vesicles. Evaluation of Trp fluorescence variations of 5 μM C34 (**A**) or C34-cholesterol (**B**) upon titration with large unilamellar vesicles (LUV), performed by successive additions of POPC, POPC:Chol 2:1, DPPC or HIV-like mixture LUV suspension. Dashed lines are fittings of eq. 1 to the experimental data.
doi:10.1371/journal.pone.0060302.g002

$13.6\pm0.01\ mM^{-1}$ in solution to $11.5\pm0.39\ mM^{-1}$ in DPPC vesicles. These reductions on the Stern−Volmer constant indicate that the interaction with the membrane occurs with the fluorophores partially exposed to the aqueous environment.

Fluorescence quenching measurements were also used to evaluate the depth of insertion of Trp residues of the peptides inserted in POPC or POPC:Chol (2:1) vesicles. Stearic acid molecules derivatized with doxyl (quencher) groups either at carbon 5 (5NS) or 16 (16NS) were used. 5NS is a better quencher for molecules inserted in the membrane in a shallow position, close to the lipid-water interface, while 16NS is better for molecules buried deeply in the membrane [36]. Fig. 5A and B shows the Stern-Volmer plot obtained for C34-cholesterol on POPC or POPC:Chol (2:1), respectively, using the effective concentration of 5NS and 16NS in the bilayer matrix. For POPC, the K_{sv} with 5NS was higher ($4.43\pm0.41\ mM^{-1}$, calculated with the Lehrer equation) than for 16NS ($1.38\pm0.052\ mM^{-1}$, calculated with the linear Stern-Volmer equation). In the case of POPC:Chol (2:1), K_{sv} for 5NS was also higher ($9.23\pm0.67\ mM^{-1}$, with the Lehrer equation) than 16NS ($6.94\pm0.44\ mM^{-1}$, with the Lehrer equation). Fluorescence lifetime quenching data enabled the application of the SIMEXDA method [36] to obtain the depth of insertion of the Trp residues of C34-cholesterol (Fig. 5C). A similar mean shallow location, close to the membrane interface, was observed for both lipid membranes. However, in the presence of cholesterol, the depth distribution is narrower, and the location more superficial (more exposed to the aqueous media), in a good agreement with acrylamide quenching data. The location distribution of C34-cholesterol does not differ much from the determined previously for enfuvirtide or T-1249 [10,35]. As expected, no changes in the fluorescence intensity were detected in the presence of 5NS or 16NS for C34 (data not shown).

Interaction with Blood Cell Membranes

After the characterization using membrane-model systems, we studied this peptide-membrane interaction in biological settings. We used isolated human erythrocytes and PBMC, labeled with the fluorescent probe di-8-ANEPPS, which is sensitive to the membrane dipole potential [30]. If the peptides interact by inserting or adsorbing on the membrane, it is expected that they change the membrane order to some extent, inducing variations in its dipole potential. These changes can be reported by di-8-ANEPPS excitation spectrum shifts [30,37], becoming easier to assess in differential spectra (Fig. 6A–C). The fluorescence red shift indicates a decrease in the membrane dipole potential in a peptide concentration-dependent manner. In order to quantify this interaction, we measured the ratio R of the intensities at the excitation wavelengths 455 and 525 nm (with emission at 670 nm) for a range of peptide concentrations. R is a quantitative descriptor of spectral shifts and, hence, of the relative variation of dipole potential. The membrane dipole potential significantly decreased in the presence of C34-cholesterol (Fig. 6 D–F), in sharp contrast to the unconjugated C34 peptide that had almost no effect. This shows that, in agreement with the model membrane studies, C34 does not have tendency to interact with cell membranes, while C34-cholesterol does. Affinity constants derived from the dipole potential variation curves indicate a much higher affinity when compared with the previously studied HIV fusion inhibitor peptides enfuvirtide and T-1249 (Table 3).

For the sake of comparison with the data obtained for blood cell membranes, and in order to validate the comparison with previous data, we also labeled lipid vesicles with di-8-ANEPPS (Fig. 6A, D). Lipid vesicles were composed of POPC, POPC:Chol 2:1 and POPC:Chol 1:1. In a good agreement with the partition and pressure data, we found that the increase of the cholesterol percentage on the membrane also increased the interaction of C34-cholesterol. Additions of DMSO, cholesterol or C34 were also tested as control and no changes on the dipole potential were observed (data not shown).

Discussion

In previous works, we showed that the interaction of HIV fusion inhibitor peptides with membranes (using lipid membrane models

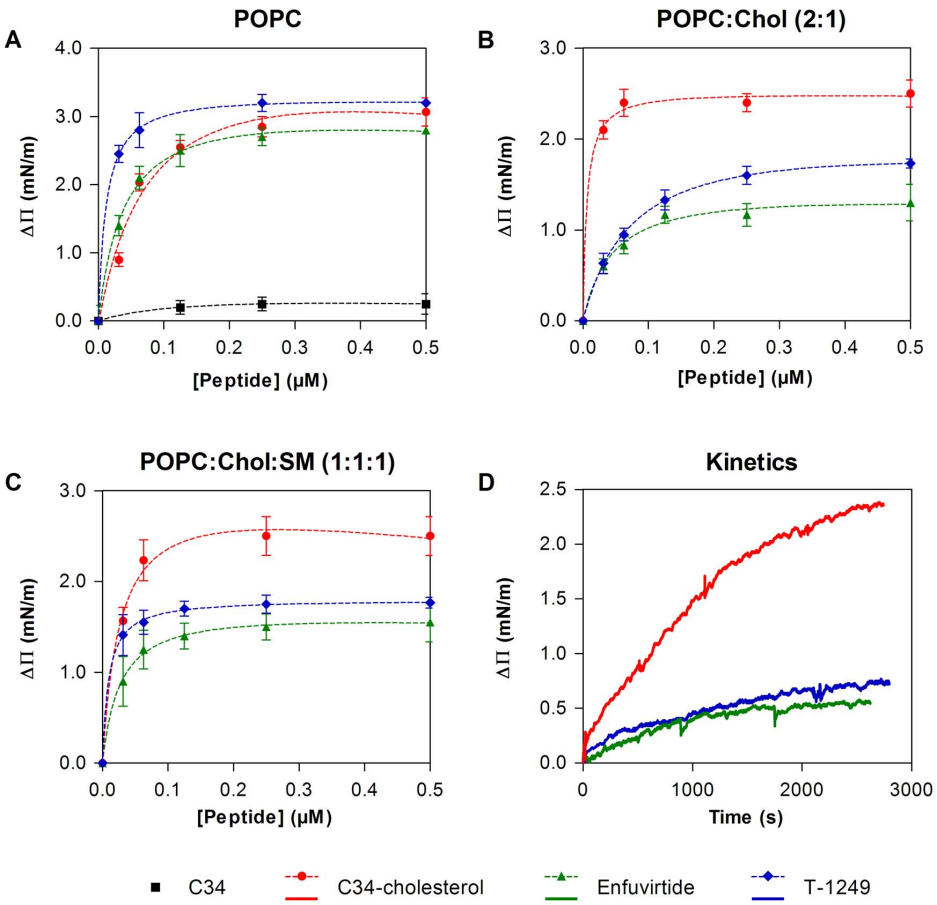

Figure 3. Interaction of the fusion inhibitor peptides with lipid monolayers. (**A–C**) Changes in surface pressure as a function of HIV-1 fusion inhibitor addition to pure POPC (**A**), POPC:Chol 2:1 (**B**) or POPC:Chol:SM 1:1:1 (**C**) monolayers. Dashed lines are fittings of eq. 2 to the experimental data. (**D**) Changes in surface pressure as a function of time after addition of HIV fusion inhibitors to achieve a final concentration of 31 nM on a POPC:Chol 2:1 monolayer. All assays were carried out at 25°C, using an initial pressure of 21.5±0.5 mN/m. Each point is the average of at least triplicates of independent samples. Error bars represent the standard error of mean (SEM).
doi:10.1371/journal.pone.0060302.g003

and blood cells) is a key aspect of their mechanism of action. The membranotropic properties of a peptide can increase its local concentration at the membrane and boost the efficiency of the drug [8–10,29,35,38]. In this context, we studied the membrane interactions of the C34 peptide, in comparison with its cholesterol conjugated version, C34-cholesterol, in order to understand the

Table 2. Dissociation constants, K_d, and $\Delta\Pi_{max}$ determined from surface pressure changes.

	C34-cholesterol		Enfuvirtide		T1249	
	K_d (nM)	$\Delta\Pi_{max}$ (mN/m)	K_d (nM)	$\Delta\Pi_{max}$ (mN/m)	K_d (nM)	$\Delta\Pi_{max}$ (mN/m)
POPC	59±15	3.5±0.3	31±3.7	3.1±0.1	12±0.6	3.3±0.02
POPC:Chol (2:1)	5.3±1.4	2.5±0.05	41±6.8	1.4±0.06	65±3.5	1.9±0.03
POPC:Chol:SM (1:1:1)	9.2±1.3	2.6±0.02	27±4.6	1.6±0.03	13±1.1	1.8±0.02

Parameters obtained from the fitting of the surface pressure data from Fig. 3 using eq. 2. All measures were made at least in triplicate. Values are presented as mean ± standard error of mean (SEM).
doi:10.1371/journal.pone.0060302.t002

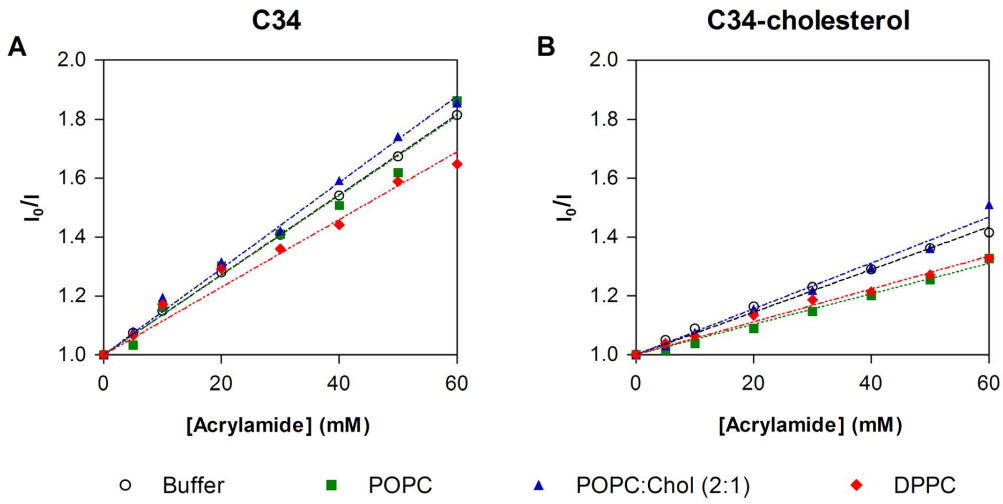

Figure 4. Accessibility of the peptide to the aqueous medium. Fluorescence quenching by acrylamide of C34 (**A**) and C34-cholesterol (**B**) in the presence (filled symbols) and absence (empty circles) of lipid vesicles (5 μM peptide and 3 mM total lipid). Lipid compositions tested were pure POPC, POPC:Chol 2:1 and pure DPPC. Dashed lines are fittings of the Stern-Volmer equation (eq. 3) to the experimental data.
doi:10.1371/journal.pone.0060302.g004

molecular basis of the dramatically increased antiviral efficiency of the conjugate [11].

This study demonstrates the membrane-binding ability of C34-cholesterol. Overall the results obtained from partition, surface pressure, quenching and dipole potential show that the addition of the cholesterol moiety to the C-terminus of C34 renders the peptide membranotropic. The partition coefficients for POPC obtained for this conjugated peptide are of the same order as the previously determined for enfuvirtide and T-1249 (Table 1). In contrast, C34 shows no partition for membranes of this lipid. Enfuvirtide and C34 share a common CHR sequence as a structural domain; however, C34 lacks a putative lipid-binding domain (LBD) that is Trp rich, which may explain its low membrane partition (Fig. 1A) [39]. This is also the case of the LBD-lacking fusion inhibitor peptide sifuvirtide, which also presents residual binding to POPC vesicles and the same preference for DPPC membranes (on the gel phase) [8,29]. When the interactions with cholesterol-rich membranes were studied, in contrast with the result previously obtained for enfuvirtide [35], membrane partition of C34-cholesterol still takes place and with a relatively high K_p (Table 1). A similar behavior was found for lipid raft-mimicking membranes (POPC:Chol:SM).

In order to interpret results on POPC:Chol binary mixtures, their phase diagram at 25°C needs to be considered [33]. In the case of pure POPC, the membrane is in the liquid disordered phase (L_d). For POPC:Chol 2:1 there is a phase coexistence between liquid ordered (L_o) and liquid disordered (L_d) phases, while for POPC:Chol 1:1 only L_o phase occurs (but close to the

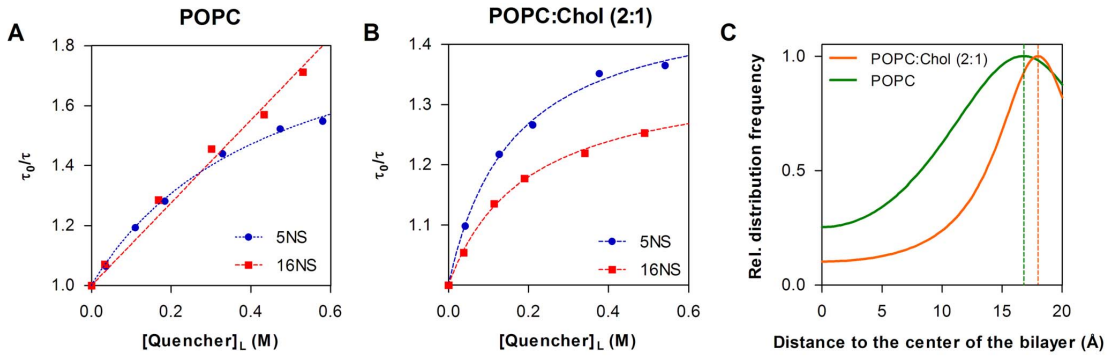

Figure 5. Localization of C34-cholesterol in the bilayer. (**A–B**) Stern-Volmer plots for the quenching of C34-cholesterol fluorescence by 5NS or 16NS in POPC (A) and POPC:Chol 2:1 (B) LUV, using time-resolved fluorescence measurements. Each point is the average of three independent measures. The dashed lines are fittings of the Lehrer equation (eq. 4) to the experimental data, except for 16NS in POPC (eq. 3). (**C**) Depth of insertion of C34-cholesterol Trp residues in the membrane using SIMEXDA method [36], yielding an average location 16.8 Å away from the center of the bilayer for POPC and 18.0 Å for POPC:Chol 2:1. Distributions' half-width at half-height were 8.9 Å for POPC and 6.5 Å for POPC:Chol.
doi:10.1371/journal.pone.0060302.g005

Table 3. Antiviral activity and cell membrane interaction parameters compared of HIV-1 fusion inhibitors.

		C34-cholesterol	T-1249	Enfuvirtide (T-20)
IC_{90} (nM)*	JRFL	0.36	8.3	20
	NL4-3	0.09	2.6	6.1
K_d (μM)	Erythrocytes	0.58±0.049	4.16±0.13†	35.4±1.33†
	PBMC	0.54±0.052	7.71±0.61†	62.2±10.2†

*[11];
†[9].
doi:10.1371/journal.pone.0060302.t003

boundary between L_o/L_d coexistence). Our partition data indicate that C34-cholesterol preferentially partitions to the L_o phase, displaying a K_p three-fold higher than for the L_d phase (pure POPC), and an intermediate behavior when both L_d and L_o phases coexist. Additionally, using di-8-ANEPPS labeled LUV (Fig. 6A, D), we showed that the interaction of the conjugated peptide increases with the amount of cholesterol present in the POPC:Chol binary mixture, suggesting again a preference for cholesterol-rich membranes.

Surface pressure measurements (Fig. 3) showed a higher membrane affinity of C34-cholesterol towards cholesterol and SM-rich membranes, when compared to pure POPC. Taking into account that C34 was unable to induce any change in any of the tested monolayers (data not show) these experiments also showed that the cholesterol moiety boosts the adsorption of C34 specifically on cholesterol-rich membranes. In comparison, enfuvirtide showed much less distinction between the three mixtures tested. Furthermore, regarding the kinetics of the interactions of the three HIV fusion inhibitors in POPC:Chol monolayers (Fig. 3D), we found that C34-cholesterol also exhibit a faster binding kinetic, which could only be assigned to the "membrane anchoring" cholesterol moiety.

This preference of the drug for cholesterol and "lipid raft-like" mixtures is very relevant regarding inhibiting HIV entry. The most important receptors for HIV entry, CD4 and CCR5, were shown to be associated with lipid raft microdomains and DRM (detergent resistant membranes) and this association is important for the binding of the virus to cells [40]. Several studies also demonstrated that depleting cholesterol from the host cells greatly

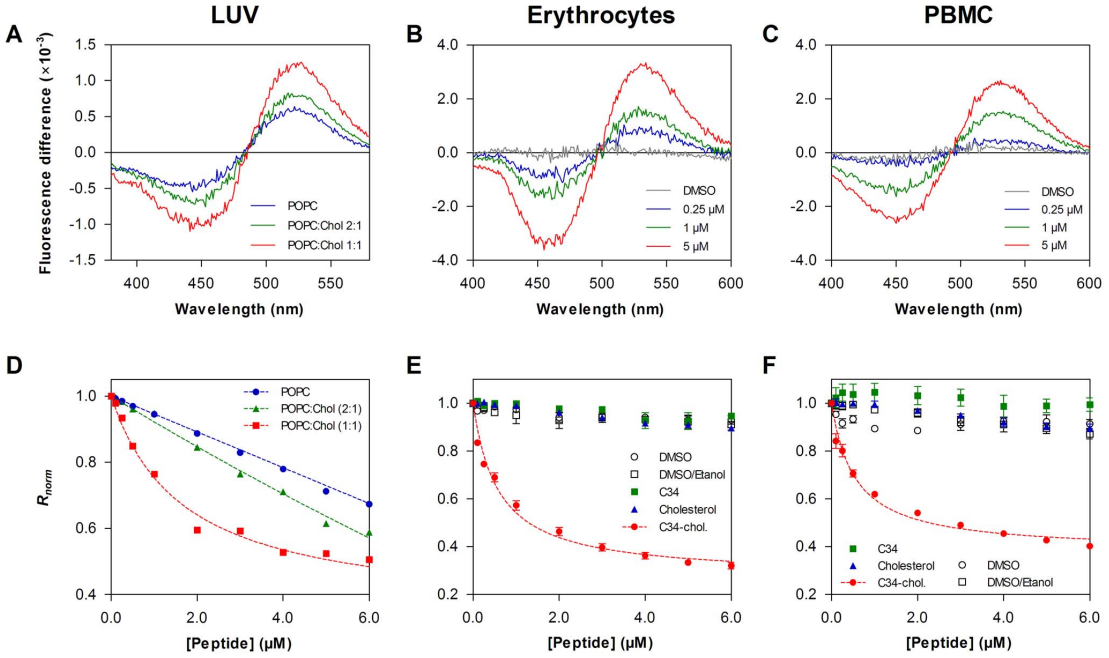

Figure 6. Peptide interactions with di-8-ANEPPS labeled LUV and cell membranes. (A–C) Differential spectra of di-8-ANEPPS bound to LUV (**A**) erythrocytes (**B**) and PBMC (**C**) membranes in the presence of C34-cholesterol and in its absence. Spectra were obtained by subtracting the excitation spectrum (normalized to the integrated areas) of labeled cells in the presence of peptide from the spectrum in the absence of the respective peptide. The shift to the red (decrease in dipole potential) is peptide concentration-dependent. For LUV, spectra traces represent C34-cholesterol 4 μM, in the presence of different lipid compositions: POPC, POPC:Chol 2:1 and POPC:Chol 1:1. For cells, spectra traces represent different C34-cholesterol concentrations: 0 μM, 0.25 μM, 1 μM and 5 μM. (**D**) Binding profiles of C34-cholesterol to LUV of POPC, POPC:Chol 2:1 and POPC:Chol 1:1, by plotting the di-8-ANEPPS excitation ratio, R (I_{455}/I_{525}, normalized to the initial value), as a function of the peptide concentration. DMSO, cholesterol and C34 (unconjugated) were also tested, as controls, and no significant changes on the dipole potential were observed (data not shown). (**E–F**) Binding profiles of C34-cholesterol, C34 and cholesterol to erythrocytes (**E**) and PBMC (**F**) cell membranes. Controls for DMSO (empty circles) and DMSO:ethanol (empty square) were also performed. Dashed curves represent the fitting to the single binding site equation (eq. 5). Affinity parameters for the cells are indicated in Table 3. Error bars represent SEM, with n = 5 for C34-cholesterol curves in cells and n = 3 for the control curves and LUV.
doi:10.1371/journal.pone.0060302.g006

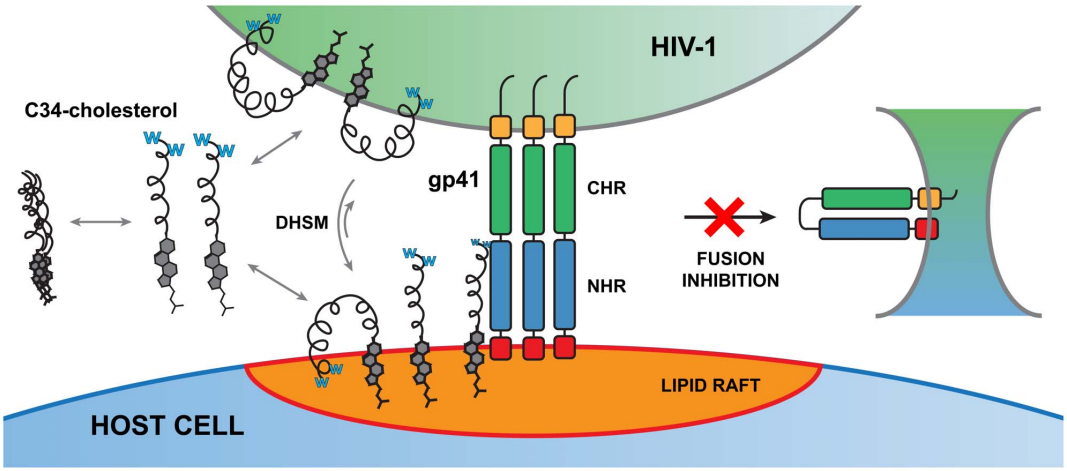

Figure 7. Putative mode of action of HIV-1 fusion inhibitor C34-cholesterol. In aqueous solution, the conjugate may form micro-aggregates when membranes are not present, due to its cholesterol moiety. The drug was demonstrated to partition to cell membranes and virus-like membranes. A preference towards cholesterol and SM-rich compositions was identified. These lipids are characteristic of the membrane microdomains designated as lipid rafts, which usually contain the receptors involved in HIV entry. C34-cholesterol anchors to the membrane *via* its cholesterol moiety and also, with a putative weaker binding, *via* its Trp (W)-rich N-terminal domain. In the context of HIV-1 gp41 engagement with the target cell, a confined space exits between the two membranes. Enrichment in DHSM in the viral membrane decreases the peptide partition, possibly shifting membrane partition equilibrium to the host cell membrane. The drug concentrated in the lipid raft environment may reach its target (gp41) more efficiently than through simple diffusion in aqueous solution. Moreover the anchoring promoted by the cholesterol at the C-terminus brings the peptide into contact in the correct orientation to compete with NHR binding site. This way, gp41 mediated fusion may be inhibited, blocking viral content entry into the cell.
doi:10.1371/journal.pone.0060302.g007

inhibits HIV infection [40–42]. Moreover, the substitution of the virion-associated cholesterol by the raft-inhibiting sterol analogues 4-cholestenone and coprostanol was shown to reduce infectivity, in contrast to other raft promoting sterols [43]. Overall, lipid rafts are considered to be essential for the virus entry process [44]. The preferential partition of C34-cholesterol to those domains would make the drug more available at the site where membrane fusion occurs.

Recently, the lipid composition of HIV-1 membrane, constituting its lipidome, has been precisely determined [22]. That allowed us to study lipid vesicles with compositions mimicking the virus envelope. The high C34-cholesterol partition observed for the HIV membrane-like mixture of lipids indicates that the viral membrane itself can also extensively capture and carry the conjugate drug on its surface, enhancing its availability at the required site of action. However, this interaction seems to be sensitive to the presence of DHSM, a lipid found to be unusually enriched at the viral membrane, when compared to the host cell membrane [22]. When present, DHSM decreases C34-cholesterol partition (Table 1). It is tempting to speculate that, in a context of virus and host cell engagement; this may be a factor that shifts the equilibrium of partition towards the cell membranes, where it anchors in the right direction to interact with the transiently exposed gp41 NHR domain.

Regarding the location of C34-cholesterol at the membrane level, our data show that the Trp residues of the peptide insert in the external leaflet of the bilayer, at a shallow position. Previously, the Trp-rich regions of enfuvirtide and T-1249 were also shown to insert superficially in lipid bilayers [10,35]. As the peptide is conjugated with cholesterol in a defined position, the peptide should adopt a consistent orientation, with the C-terminus anchored to the membrane by the cholesterol moiety (Fig. 1A). This is the proper orientation to align in an anti-parallel fashion with the NHR domain of gp41 when it extends towards the target membrane. The N-terminus, where the Trp residues are located, may interact freely with the nearby lipids, but cannot insert deep in the membrane.

In order to have a better understanding of what may happen in the bloodstream, we also studied the interaction of the peptides with human erythrocytes and mononuclear leukocytes. These peptide drugs must be injected, as oral administration is not feasible. HIV-1 is known to associate to the surface of erythrocytes in circulation [45–47], while PBMC are among the virus main targets. C34-cholesterol decreases the membrane dipole potential of the two cell types, indicating that an interaction is occurring (Fig. 6). In agreement with the partition data, C34 alone also does not interact with cell membranes. The same concentration of cholesterol alone is not sufficient to induce a detectable membrane potential change [48], indicating that the potential change is induced essentially by the peptide component of the conjugate. However this change only occurs in the conjugate, emphasizing the role of cholesterol in inducing the membrane partition of the peptide to cell membranes.

Quantitatively, C34-cholesterol was found to have approximately 115 or 14 times more affinity towards PBMC membranes than enfuvirtide or T-1249, respectively. Furthermore, the cell membrane affinities of the different fusion inhibitor peptides (C34-cholesterol>T-1249> enfuvirtide) correlate with the antiviral potency against HIV-1 (Table 3). Regarding the comparison with the K_p values determined with lipid vesicles, this is not straightforward, as the results obtained for the different compositions tested indicate that the process is lipid composition-dependent. Moreover, the partition is based on tryptophan fluorescence, which regards only the peptide part of the conjugate.

However, if we focus on cholesterol-containing mixtures, C34-cholesterol has the highest partition, contrasting with enfuvirtide, with negligible interaction [35]. T-1249 should fall in between, considering its partition to cholesterol-poor domains and ability to adsorb on cholesterol-rich domains [10].

These findings, relating membrane binding to improved antiviral potency of the peptides, indicate that this is a major factor to take into account when rationally designing HIV fusion inhibitor peptides. We demonstrated that C34-cholesterol has membranotropic behavior towards lipid vesicles and strongly interacts with circulating blood cells membranes. HIV fusion inhibitors have a restricted temporal and spatial window of opportunity to bind to their molecular target: the NHR region of gp41 in its extended conformation, when the virus and target cell are closely engaged. This makes aqueous diffusion of the peptide to its target less efficient. It has also been demonstrated that the forces governing protein–protein interactions in a membrane environment are different from those in solution [49]. The ability that these peptides have to bind to cell membranes facilitates the delivery of the peptides to this confined environment, as some peptide is already locally present (Figure 7). In this context, C34-cholesterol should be able to concentrate at the cell surface and also on the viral membrane. In agreement with this, previous results with cells after 48 h of treatment with C34-cholesterol showed the persistence of antiviral activity of residual peptide not cleared by washing steps [11], supporting the idea that cell membranes could work as C34-cholesterol reservoir. Importantly, the concentration effect would be higher on the lipid rafts, where the HIV receptors are present and fusion is more likely to occur [40,44]. This persistent antiviral activity may be ideal for this drug to be applied as a topical microbicide, for example as vaginal gel, to prevent infection [12]. C34-cholesterol was generally the most active inhibitor when tested in the context of human mucosal tissue explants (colorectal, penile and cervical), when compared to C34, enfuvirtide and T-1249 [12]. The first microbicides formulations against HIV were based on unspecific polyanions to present viral attachment to the cell surface; however, they largely failed in clinical trials [50]. Only recently a trial using a tenofovir gel (a reverse transcriptase inhibitor) showed 39% reduction on HIV-1 infection [51]. Using an entry inhibitor such as C34-cholesterol could prevent the viral entry in the first encountered immunological cells of the mucosa, blocking the virus at the earliest stage of infection.

Ultimately, the membrane may act as a "catalyst" to the binding reaction between gp41 and the peptide inhibitors, as it has been postulated in other receptor-ligand scenarios in membrane environments [38]. Thus, in this case, the marked increase in antiviral efficiency of C34-cholesterol in relation to C34 (and other fusion inhibitors) correlates with its higher affinity towards model and blood cells membranes.

Acknowledgments

We thank Teresa Freitas (IMM, FMUL) for the technical support on PBMC isolation.

Author Contributions

Conceived and designed the experiments: AH PMM MARBC NCS. Performed the experiments: AH PMM MTA. Analyzed the data: AH PMM NCS. Wrote the paper: AH PMM MARBC NCS.

References

1. De Clercq E (2009) Anti-HIV drugs: 25 compounds approved within 25 years after the discovery of HIV. Int J Antimicrob Agents 33: 307–320.
2. Lieberman-Blum SS, Fung HB, Bandres JC (2008) Maraviroc: a CCR5-receptor antagonist for the treatment of HIV-1 infection. Clin Ther 30: 1228–1250.
3. Matthews T, Salgo M, Greenberg M, Chung J, DeMasi R, et al. (2004) Enfuvirtide: the first therapy to inhibit the entry of HIV-1 into host CD4 lymphocytes. Nat Rev Drug Discov 3: 215–225.
4. Franquelim HG, Matos PM, Veiga AS (2011) HIV vs. HIV: Turning HIV-Derived Peptides into Drugs. In: Castanho MA, Santos NC, editors. Peptide Drug Discovery and Development. Weinheim, Germany: Wiley-VCH Verlag. 209–229.
5. Naider F, Anglister J (2009) Peptides in the treatment of AIDS. Curr Opin Struct Biol 19: 473–482.
6. He Y (2013) Synthesized Peptide Inhibitors of HIV-1 gp41-dependent Membrane Fusion. Curr Pharm Des 19: 1800–1809.
7. Chan DC, Fass D, Berger JM, Kim PS (1997) Core structure of gp41 from the HIV envelope glycoprotein. Cell 89: 263–273.
8. Franquelim HG, Loura LM, Santos NC, Castanho MARB (2008) Sifuvirtide screens rigid membrane surfaces. establishment of a correlation between efficacy and membrane domain selectivity among HIV fusion inhibitor peptides. J Am Chem Soc 130: 6215–6223.
9. Matos PM, Castanho MARB, Santos NC (2010) HIV-1 fusion inhibitor peptides enfuvirtide and T-1249 interact with erythrocyte and lymphocyte membranes. PLoS ONE 5: e9830.
10. Veiga AS, Santos NC, Loura LM, Fedorov A, Castanho MARB (2004) HIV fusion inhibitor peptide T-1249 is able to insert or adsorb to lipidic bilayers. Putative correlation with improved efficiency. J Am Chem Soc 126: 14758–14763.
11. Ingallinella P, Bianchi E, Ladwa NA, Wang YJ, Hrin R, et al. (2009) Addition of a cholesterol group to an HIV-1 peptide fusion inhibitor dramatically increases its antiviral potency. Proc Natl Acad Sci U S A 106: 5801–5806.
12. Harman S, Herrera C, Armanasco N, Nuttall J, Shattock RJ (2012) Preclinical Evaluation of the HIV-1 Fusion Inhibitor L'644 as a Potential Candidate Microbicide. Antimicrob Agents Chemother 56: 2347–2356.
13. Peisajovich SG, Gallo SA, Blumenthal R, Shai Y (2003) C-terminal octylation rescues an inactive T20 mutant: implications for the mechanism of HIV/SIMIAN immunodeficiency virus-induced membrane fusion. J Biol Chem 278: 21012–21017.
14. Wexler-Cohen Y, Shai Y (2007) Demonstrating the C-terminal boundary of the HIV 1 fusion conformation in a dynamic ongoing fusion process and implication for fusion inhibition. FASEB J 21: 3677–3684.
15. Zhang HY, Schneider SE, Bray BL, Friedrich PE, Tvermoes NA, et al. (2008) Process development of TRI-999, a fatty-acid-modified HIV fusion inhibitory peptide. Org Process Res Dev 12: 101–110.
16. Stoddart CA, Nault G, Galkina SA, Thibaudeau K, Bakis P, et al. (2008) Albumin-conjugated C34 peptide HIV-1 fusion inhibitor: equipotent to C34 and T-20 in vitro with sustained activity in SCID-hu Thy/Liv mice. J Biol Chem 283: 34045–34052.
17. Xie D, Yao C, Wang L, Min W, Xu J, et al. (2010) An albumin-conjugated peptide exhibits potent anti-HIV activity and long in vivo half-life. Antimicrob Agents Chemother 54: 191–196.
18. Mayer LD, Hope MJ, Cullis PR (1986) Vesicles of variable sizes produced by a rapid extrusion procedure. Biochim Biophys Acta 858: 161–168.
19. Szoka F, Olson F, Heath T, Vail W, Mayhew E, et al. (1980) Preparation of unilamellar liposomes of intermediate size (0.1–0.2 mumol) by a combination of reverse phase evaporation and extrusion through polycarbonate membranes. Biochim Biophys Acta 601: 559–571.
20. Kubista M, Sjoback R, Eriksson S, Albinsson B (1994) Experimental correction for the inner-filter effect in fluorescence spectra. Analyst 119: 417–419.
21. Ladokhin AS, Jayasinghe S, White SH (2000) How to measure and analyze tryptophan fluorescence in membranes properly, and why bother? Anal Biochem 285: 235–245.
22. Brugger B, Glass B, Haberkant P, Leibrecht I, Wieland FT, et al. (2006) The HIV lipidome: a raft with an unusual composition. Proc Natl Acad Sci U S A 103: 2641–2646.
23. Santos NC, Prieto M, Castanho MARB (2003) Quantifying molecular partition into model systems of biomembranes: an emphasis on optical spectroscopic methods. Biochim Biophys Acta 1612: 123–135.
24. Chiu SW, Subramaniam S, Jakobsson E (1999) Simulation study of a gramicidin/lipid bilayer system in excess water and lipid. II. Rates and mechanisms of water transport. Biophys J 76: 1939–1950.
25. Greenwood AI, Tristram-Nagle S, Nagle JF (2006) Partial molecular volumes of lipids and cholesterol. Chem Phys Lipids 143: 1–10.
26. Yamazaki M, Miyazu M, Asano T, Yuba A, Kume N (1994) Direct evidence of induction of interdigitated gel structure in large unilamellar vesicles of dipalmitoylphosphatidylcholine by ethanol: studies by excimer method and high-resolution electron cryomicroscopy. Biophys J 66: 729–733.
27. Santos NC, Prieto M, Castanho MARB (1998) Interaction of the major epitope region of HIV protein gp41 with membrane model systems. A fluorescence spectroscopy study. Biochemistry 37: 8674–8682.
28. Nagle JF, Wiener MC (1988) Structure of fully hydrated bilayer dispersions. Biochim Biophys Acta 942: 1–10.

29. Matos PM, Freitas T, Castanho MARB, Santos NC (2010) The role of blood cell membrane lipids on the mode of action of HIV-1 fusion inhibitor sifuvirtide. Biochem Biophys Res Commun 403: 270–274.
30. Gross E, Bedlack RS, Jr., Loew LM (1994) Dual-wavelength ratiometric fluorescence measurement of the membrane dipole potential. Biophys J 67: 208–216.
31. Clarke RJ, Kane DJ (1997) Optical detection of membrane dipole potential: avoidance of fluidity and dye-induced effects. Biochim Biophys Acta 1323: 223–239.
32. Cladera J, O'Shea P (1998) Intramembrane molecular dipoles affect the membrane insertion and folding of a model amphiphilic peptide. Biophys J 74: 2434–2442.
33. de Almeida RF, Fedorov A, Prieto M (2003) Sphingomyelin/phosphatidylcholine/cholesterol phase diagram: boundaries and composition of lipid rafts. Biophys J 85: 2406–2416.
34. Marsh D (1996) Lateral pressure in membranes. Biochim Biophys Acta 1286: 183–223.
35. Veiga S, Henriques S, Santos NC, Castanho MARB (2004) Putative role of membranes in the HIV fusion inhibitor enfuvirtide mode of action at the molecular level. Biochem J 377: 107–110.
36. Fernandes MX, Garcia de la Torre J, Castanho MARB (2002) Joint determination by Brownian dynamics and fluorescence quenching of the in-depth location profile of biomolecules in membranes. Anal Biochem 307: 1–12.
37. Matos PM, Franquelim HG, Castanho MA, Santos NC (2010) Quantitative assessment of peptide-lipid interactions. Ubiquitous fluorescence methodologies. Biochim Biophys Acta 1798: 1999–2012.
38. Castanho MARB, Fernandes MX (2006) Lipid membrane-induced optimization for ligand-receptor docking: recent tools and insights for the "membrane catalysis" model. Eur Biophys J 35: 92–103.
39. Liu S, Jing W, Cheung B, Lu H, Sun J, et al. (2007) HIV gp41 C-terminal heptad repeat contains multifunctional domains. Relation to mechanisms of action of anti-HIV peptides. J Biol Chem 282: 9612–9620.
40. Popik W, Alce TM, Au WC (2002) Human immunodeficiency virus type 1 uses lipid raft-colocalized CD4 and chemokine receptors for productive entry into CD4(+) T cells. J Virol 76: 4709–4722.
41. Liao Z, Cimakasky LM, Hampton R, Nguyen DH, Hildreth JE (2001) Lipid rafts and HIV pathogenesis: host membrane cholesterol is required for infection by HIV type 1. AIDS Res Hum Retroviruses 17: 1009–1019.
42. Manes S, del Real G, Lacalle RA, Lucas P, Gomez-Mouton C, et al. (2000) Membrane raft microdomains mediate lateral assemblies required for HIV-1 infection. EMBO reports 1: 190–196.
43. Campbell S, Gaus K, Bittman R, Jessup W, Crowe S, et al. (2004) The raft-promoting property of virion-associated cholesterol, but not the presence of virion-associated Brij 98 rafts, is a determinant of human immunodeficiency virus type 1 infectivity. J Virol 78: 10556–10565.
44. Campbell SM, Crowe SM, Mak J (2001) Lipid rafts and HIV-1: from viral entry to assembly of progeny virions. J Clin Virol 22: 217–227.
45. Beck Z, Brown BK, Wieczorek L, Peachman KK, Matyas GR, et al. (2009) Human erythrocytes selectively bind and enrich infectious HIV-1 virions. PLoS ONE 4: e8297.
46. He W, Neil S, Kulkarni H, Wright E, Agan BK, et al. (2008) Duffy antigen receptor for chemokines mediates trans-infection of HIV-1 from red blood cells to target cells and affects HIV-AIDS susceptibility. Cell Host Microbe 4: 52–62.
47. Hess C, Klimkait T, Schlapbach L, Del Zenero V, Sadallah S, et al. (2002) Association of a pool of HIV-1 with erythrocytes in vivo: a cohort study. Lancet 359: 2230–2234.
48. Haldar S, Kanaparthi RK, Samanta A, Chattopadhyay A (2012) Differential effect of cholesterol and its biosynthetic precursors on membrane dipole potential. Biophys J 102: 1561–1569.
49. Gerber D, Sal-Man N, Shai Y (2004) Structural adaptation of the glycophorin A transmembrane homodimer to D-amino acid modifications. J Mol Biol 339: 243–250.
50. Vanpouille C, Arakelyan A, Margolis L (2012) Microbicides: still a long road to success. Trends Microbiol 20: 369–375.
51. Abdool Karim Q, Abdool Karim SS, Frohlich JA, Grobler AC, Baxter C, et al. (2010) Effectiveness and safety of tenofovir gel, an antiretroviral microbicide, for the prevention of HIV infection in women. Science 329: 1168–1174.

Interaction of glycosaminoglycans with HIV-1 envelope glycoprotein gp120

Overview

This section presents the experiments to determine the major GAG structural requirements that enable the binding to HIV-1 envelope gp120. We use surface plasmon resonance, an optical based label-free technique to determine biological interactions at the molecular level. Different types of GAG, with different sequence, size and sulfation patterns, were chosen to probe this interaction. Protection strategies for the immobilization of the proteins were also tried.

These studies were done at IMIM, in Barcelona, Spain, with the assistance of Prof. Ricardo Gutiérrez-Gallego. They are presented as an unpublished manuscript currently submitted to a peer-reviewed journal.

Article D

Matos PM, Andreu A, Santos NC*, Gutiérrez-Gallego R*. Structural requirements of glycosaminoglycans for the interaction with HIV-1 envelope glycoprotein gp120. (2013) *Submitted for publication in a peer-reviewed journal.* (*Co-corresponding authors).

Article D

Declaration of authorship

I, Pedro Miguel Baptista de Matos, declare that the experimental design, all the experimental work, data analysis and writing of initial manuscript drafts were carried out by me under the supervision and assistance of Prof. Ricardo Gutiérrez-Gallego, supervision of Prof. Nuno C. Santos and the help on the initial planning of Prof. David Andreu.

I, Nuno C. Santos, as supervisor of Pedro Matos and one of the corresponding authors of the manuscript mentioned above, hereby acknowledge and confirm that the information above is correct.

I, Ricardo Gutiérrez-Gallego, as one of the corresponding authors of the manuscript mentioned above, hereby acknowledge and confirm that the information above is correct.

Pedro M. Matos Nuno C. Santos Ricardo Gutiérrez-Gallego

Structural requirements of glycosaminoglycans for the interaction with HIV-1 envelope glycoprotein gp120

Pedro M. Matos[1], David Andreu[2], Nuno C. Santos[1,*], Ricardo Gutiérrez-Gallego[2,3,*]

[1]Instituto de Medicina Molecular, Faculdade de Medicina, Universidade de Lisboa, 1649-028 Lisbon, Portugal. [2]Department of Experimental and Health Sciences, Pompeu Fabra University, Barcelona Biomedical Research Park, 08003 Barcelona, Spain. [3]Bio-analysis group, Neuroscience Research Program, IMIM-Parc Salut Mar, Barcelona Biomedical Research Park, 08003 Barcelona, Spain.

Heparan sulfate proteoglycans are known to assist HIV-1 entry into host cells, mediated by the viral envelope glycoprotein gp120. We aimed to determine the general structural features of glycosaminoglycans that enable their binding to gp120 by surface plasmon resonance. Binding was found to be dependent on sequence type, size and sulfation patterns. HIV-1 gp120 prefers heparin and heparan sulfate (with at least 16 monomers in extension) over chondroitin and dermatan. Sulfate groups were essential to promote this interaction. These results advance the understanding of the molecular level requirements for the mechanism of virus attachment and cell entry.

Introduction

Human immunodeficiency virus type 1 (HIV-1) envelope glycoproteins (gp120 and gp41) are the prime mediators of the virus capability to bind and enter into host $CD4^+$ cells. These viral glycoproteins are required for engagement with the target cell receptors CD4 and co-receptors CCR5 or CXCR4 and, as an enveloped virus, to drive the fusion between the viral and cell membranes [1, 2]. However, additional mediators at the cell surface help the virus to approach and attach to the target cells, before CD4 interaction [3]. These attachment mediators include adhesion molecules, lectins, heparan sulfate proteoglycans (HSPG), and the glycolipid GalCer (galactosylceramide). HSPG are proteins (either membrane-bound or secreted) with attached glycosaminoglycan (GAG) chains [4]. These GAG are linear polysaccharides consisting of repeating disaccharide units of hexosamine and uronic acid, which are often sulfated and/or acetylated. Syndecans are a transmembrane form of HSPG that have an extended ectodomain, with the heparan sulfate (HS) chains mainly attached in a distal position from the membrane [4]. HS is the major GAG of cell surface proteoglycans. Chondroitin and dermatan sulfate are mainly associated to the proteoglycans from the extracellular matrix and important constituents of blood vessels, heart valves, bone, cartilage, tendons and skin [5].

In vitro studies of glycosaminoglycan-protein interactions usually rely on the soluble heparin as GAG model. Heparin is a highly sulfated form of heparan that is produced by mast cells to act as adjuvant in anti-coagulation [5]. Heparin and HS have been shown to bind HIV-1 gp120 [6, 7] and the essential residues for

*Corresponding authors:
Nuno C. Santos, Instituto de Medicina Molecular, Faculdade de Medicina, Universidade de Lisboa, 1649-028 Lisboa, Portugal. Tel.: +351 217999480; fax: +351 217999477; e-mail: nsantos@fm.ul.pt.
Ricardo Gutiérrez-Gallego, Bio-analysis group, Neuroscience Research Program, IMIM-Parc Salut Mar, Barcelona Biomedical Research Park, 08003 Barcelona, Spain. Tel.: +34 933160482 fax: +34 933160467, e-mail: ricardo.gutierrez@upf.edu.

Keywords: HIV-1; gp120; viral attachment; heparan sulfate proteoglycans; glycosaminoglycans; surface plasmon resonance

this interaction were identified, included in the V2 and V3 loops, in the C-terminal domain and in the CD4-induced co-receptor binding site [8-10]. Cells treated with heparitinase [11] or knocked out for GAG production [12] have much lower levels of viral attachment and infection than their *wt* counterparts. Syndecans have also been implicated in attachment and trans-infection to T lymphocytes [13]. Moreover, syndecans present in macrophages are crucial for HIV-1 attachment, as they compensate for the lower CD4 levels of these cells, when compared to $CD4^+$ T cells [14]. Syndecan-3 was also identified as a specific attachment site during HIV-1 infection of dendritic cells [15]. Overall, the ubiquitously present proteoglycans, especially in the epithelial, endothelial cells and dendritic cells, can efficiently capture HIV virions, protect them and facilitate trans-infections to T lymphocytes, enhancing viral spreading and pathogenesis [16].

In this work, we explored the interaction of HIV-1 gp120 with distinct glycosaminoglycans, differing in their type/composition, sulfation pattern and size. We screened these molecules for gp120 binding via surface plasmon resonance (SPR), a technique that allows label-free characterization of molecular interactions, in order to understand the general structural requirements for the glycosaminoglycan-HIV-1 envelope binding that may contribute to the design of more efficient HIV-binding blockers.

Materials and Methods

High grade heparin from porcine mucosa, heparin oligosaccharides (dp4, dp8, dp12, dp16, dp20 and dp30, with dp stating the monomer number), selectively desulfated heparins (2-*O*-desulfated, 6-*O*-desulfated, *N*-desulfated and *N*-desulfated re-*N*-acetylated), heparan and dermatan sulfate from porcine mucosa and K5 polysaccharide were all from Iduron (Manchester, UK). Chondroitin sulfate from shark cartilage and bovine serum albumin (BSA) were from Sigma (St. Louis, MO, USA). Refer to Table 1 for molecular weights.

Recombinant HIV-1 BaL gp120 envelope glycoprotein (produced in HEK-293), in monomeric form, was obtained from the NIH AIDS Research and Reference Reagent Program (Division of AIDS, NIAID, NIH; Germantown, MD, USA).

Biacore CM5 sensorchips, amine coupling kit (containing 1-ethyl-3-(3-dimethylaminopropyl)carbodiimide hydrochloride (EDC), N-hydroxysuccinimide (NHS) and 1 M ethanolamine-HCl pH 8.5) and HBS-EP running buffer (10 mM HEPES pH 7.4, 150 mM NaCl, 3 mM EDTA, 0.005% v/v surfactant P20) were from Biacore GE Healthcare Life Sciences (Uppsala, Sweden). All the experiments were performed using a Biacore 3000 SPR instrument (GE Healthcare).

BSA or recombinant HIV-1 gp120 were immobilized in CM5 sensorchips via amine coupling. The chip surface was activated with freshly prepared 1:1 mixture of EDC and NHS (50 µL), followed by injection of 50 µg/mL of protein in acetate buffer pH 4.8 (60 µL) and blocking of the remaining active surface with 1 M ethanolamine-HCl pH 8.5 (60 µL). The flow was kept at 5 µL/min during the immobilization procedures.

To assess the influence of gp120 positive charges distribution, we employed two other immobilization methods that required pre-incubation of the proteins with *p*-nitrocatechol sulfate (pNCS, Sigma) or suramin (Tocris Bioscience, Bristol, UK), at room temperature. The pre-incubation of gp120 with pNCs was done at 50 µg/ml protein concentration, with a protein:pNCS 1:10 molar ratio, for 25 min, and the immobilization with acetate buffer pH 4.0. For suramin, the concentration of protein was doubled to 100 µg/mL and the molar ratio for incubation was 1:5 (protein:suramin), for 1 h, with following immobilization done at pH 4.0. Binding experiments were performed in the running buffer HBS-EP.

Results

Measuring the binding of proteins to glycosaminoglycans in SPR systems usually relies on the immobilization of biotinylated GAG (usually heparin) at the sensor surface via streptavidin linking and flowing the protein as analyte. This is because the heterogeneity of molecular masses and optical properties of GAG

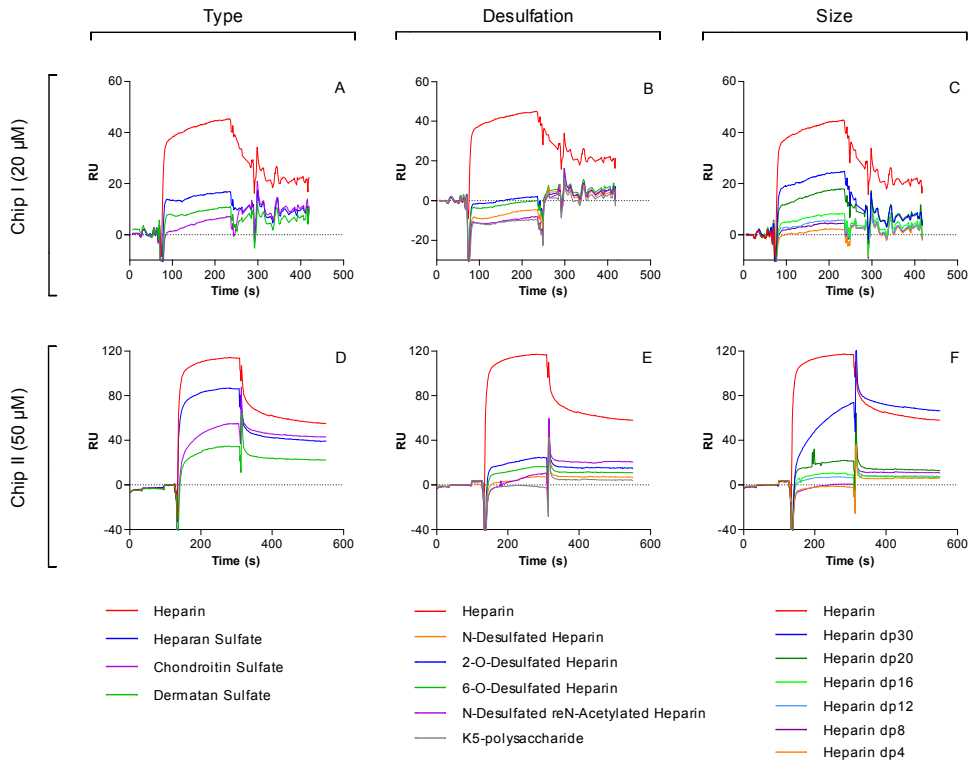

Figure 1 – Sensorgrams of glycosaminoglycans binding to immobilized HIV-1 gp120 BaL. All the soluble GAG were divided in three categories and tested against two independent chips with different proteins lots (chip I and II). Immobilized BSA was used as a control surface and all the traces were subtracted for this control. (A-C) For chip I, GAG were used at 20 µM and flown at 10 µL/min; immobilization levels were 19,835 RU for BSA and 16,103 RU for gp120. (D-F) For chip II, GAG were used at 50 µM and flown at 40 µL/min; immobilization levels were 15,094 RU for BSA and 16,482 RU for gp120. Plots are representative of duplicates.

in solution may not render the most adequate changes in order to be detected by the SPR sensor. However, since our objective was to test a diverse panel of different GAG under equivalent conditions, it was more appropriate to use them as analytes against the HIV-1 envelope glycoprotein. This strategy poses the analytical disadvantage of lower quality sensorgrams (in comparison to the reverse situation), which are required for detailed kinetic studies using SPR. Hence, in this work, we focused on the qualitative comparison of the binding degrees between each of the tested GAG.

In order to establish the requirements for GAG binding to HIV-1 gp120, we selected a panel of soluble GAG regarding their type (monomer sequence), desulfation pattern and oligomer size. We initially selected four GAG, namely heparin, heparan, chondroitin and dermatan sulfate, which differ in their disaccharide unit sequence, as well as in their distinct functions and locations in the human body. To assess the importance of the sulfate groups in the backbone of the GAG, we used heparins selectively desulfated in the position 2-*O* or 6-*O*, and an *N*-desulfated re-*N*-acetylated GAG. For a totally nonsulfated control, we used the K5 polysaccharide from *Escherichia coli*, a nonsulfated analogue of HS. Furthermore, we also tested different sizes of heparin olygosaccharides, ranging from dp4 to dp30.

Immobilization of HIV-1 gp120 BaL via amine coupling on carboxymethylated dextran surfaces was readily achieved, with immobilization levels around 1.6×10^4 RU.

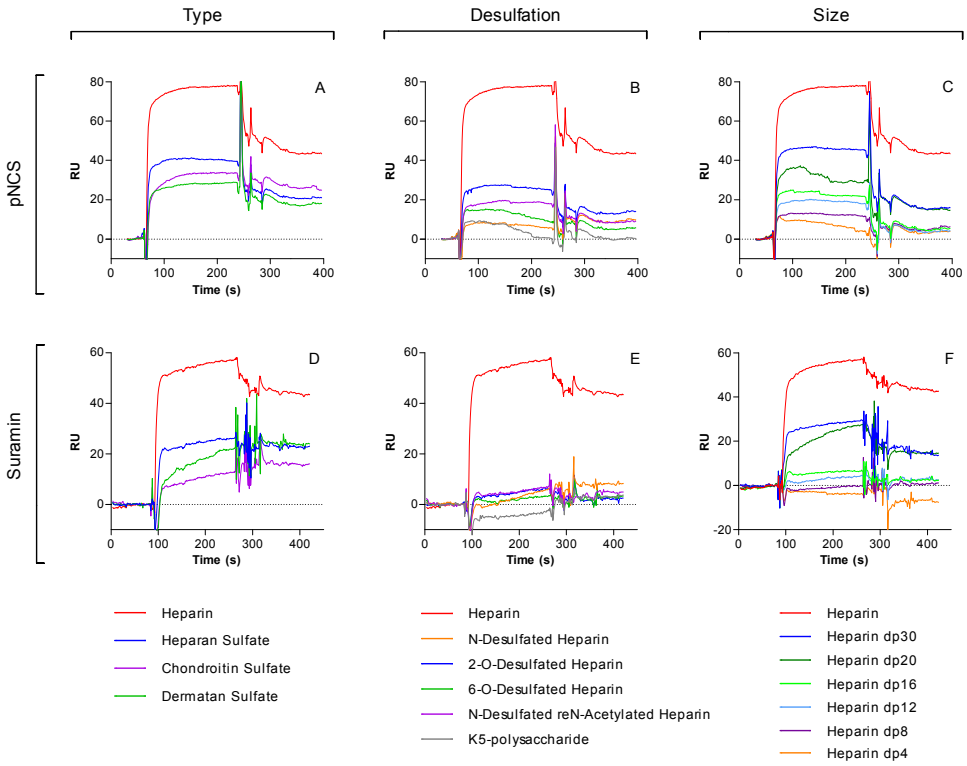

Figure 2 – Sensorgrams of glycosaminoglycans binding to HIV-1 gp120 BaL, pre-protected with sulfated compounds upon immobilization. The protein was incubated with *p*-nitrochatechol sulfate (A-C) or suramin (D-F), as described in the text, before being injected for immobilization. GAG were used at 20 μM and flown at 20 μL/min. Traces are subtracted for the control surface (BSA for suramin chip and activated/deactivated surface for pNCS chip). Immobilization levels for pNCS chip was 11,400 RU for gp120 and for suramin chip was 11,305 RU for gp120 and 9,970 RU for BSA. Plots are representative of duplicates.

Heparin, which is known to bind gp120 [6], was consistently the best binder to gp120 among the soluble GAG tested. Regarding the different types of GAG (Fig. 1A,D), HS followed heparin in affinity, while dermatan and chondroitin had lower binding. Comparing heparin with its selectively desulfated counterparts and the nonsulfated K5 (Fig. 1B,E), it can be observed that all the desulfated forms have considerably lower (almost residual) binding to gp120. However, the distinction between them is not clear. The binding of heparin is also size-dependent (Fig. 1C,F), with higher molecular masses having higher binding degree in the association phase. The binding was weak below dp16, indicating that 16 monomers is the minimum needed for a significant binding.

The direct immobilization of gp120 on the CM5 chip is directed by the electrostatic attraction to the negatively charged carboxymethylated surface (at pH > 3), before the covalent reaction occurs. To understand if any positively charged patches on the surface of gp120 were hidden following the immobilization procedure, we undertook a protection strategy by incubating with sulfated compounds prior to the immobilization. For this, we used the monosulfated small molecular *p*-nitrocatechol sulfate and the intermediate size hexasulfated suramin. The immobilization levels obtained when the gp120 was pre-incubated with the sulfated compounds was around 1.1×10^4 RU. A significant reduction is observed, when compared with the levels of the unprotected ones (1.6×10^4 RU), indicating that these compounds decrease the exposure of the glycoprotein

Table 1 – Molecular weights of the glycosaminoglycans and their interaction with gp120.

GAG Family	GAG Designation	Mean M_w [a]	Binding to gp120
Sequence distinct GAG	Heparin	15000	+++
	Heparan sulfate	22000	++
	Dermatan sulfate	41400	+
	Chondroitin sulfate	30000	+
Heparin oligomers	Heparin dp4	1340	-
	Heparin dp8	2680	-
	Heparin dp12	4020	+
	Heparin dp16	5360	+
	Heparin dp20	6700	++
	Heparin dp30	>9000	++
Desulfated GAG	2-*O*-desulfated heparin	15000	-
	6-*O*-desulfated heparin	15000	-
	N-desulfated heparin	15000	-
	N-desulfated re-*N*-acetylated heparin	15000	-
	K5 polysaccharide	30000	-

[a]Some values are estimates provided by the supplier.

positive patches, hence the attraction to the surface and thus the immobilization efficiency. However, the GAG interactions in the protected immobilized gp120 did not show significant differences (Fig. 2). Heparin was again the GAG type that bound with higher affinity, followed by heparan (based only on the association rate). Dermatan and chondroitin affinities seem also to depend on the type of protection applied. Desulfated heparins (Fig. 2B,E) bind at much lower degree than heparin itself, as previously observed in Fig. 1. In the case of suramin-treated gp120 (Fig. 2E), the binding of desulfated GAG is residual. However, for pNCS-treated gp120 (Fig. 2B), the levels of binding, although low, are significant, with 2-*O*-desulfated heparin having the highest affinity among them and K5 the lowest. Size dependent binding is retained also after protection, with the binding threshold maintained at dp16 (Fig. 2C, F).

Discussion

In this study we sought to qualitatively rank different glycosaminoglycans for their binding to HIV-1 gp120, under identical circumstances, using surface plasmon resonance. Despite the analytical challenge of monitoring directly the binding of compounds with low direct impact on the dielectric constants of the solutes, by running different GAG on immobilized gp120, we observe that the binding was dependent on GAG type (sequence), desulfation pattern and size. Heparin was the best binder for gp120. It is also the most sulfated GAG among the tested panel and the best characterized GAG binding partner to gp120 [6, 7]. Regarding the types of GAG, HS followed heparin in affinity, with dermatan and chondroitin possessing lower binding. Distinction between dermatan and chondroitin depended also on the protection of gp120 upon immobilization, but chondroitin usually showed higher RU levels in the dissociation phase. We can rank the binding as heparin > heparan > chondroitin ≈ dermatan (refer to the summary of the binding results in Table 1). This is consistent with the studies showing the ability of syndecans to capture HIV, since HS is the main GAG in those proteoglycans [13]. Chondroitin and dermatan sulfates are less relevant in the context of HIV infection as their locations and functions tend to be more at the level of the extracellular matrix [5].

Desulfated heparins presented residual binding, with little distinction achieved among them. The totally unsulfated K5 had the lowest absolute binding level. This confirms the crucial role of the GAG sulfate groups for their proper function and binding abilities, especially towards our protein of study, gp120. Desulfated heparins, especially *O*-desulfated, were previously shown not to have an inhibitory effect on HIV replication *in vitro*, similarly to what happened to heparin after desulfation [17].

The binding of heparin was also clearly dependent on the size of the oligomers, which can be interpreted both in terms of number and spatial distribution of the sulfate groups. The binding of dp12 and smaller oligomers was poorly detected, indicating that dp16 is the minimum size required for efficient binding. This size-dependency seems an actual biological differentiation, rather than experimental limitation, as the read-out for the species above dp16 are clear and proportional to size, whereas below this threshold value the read-outs are in the noise level. In the protected gp120 immobilization, despite a weak binding below dp16, the instrument can still differentiate among the different GAG. The length of HS chains in syndecans and other HSPG is subject to great variability [18, 19]. As such, a direct comparison between the minimum binding size determined by us and the lengths of the actual HSPG is difficult. However, the virions should bind more efficiently to those displaying longer and more sulfated chains. When gp120 interacts with CD4, the co-receptor binding site is exposed, which is also a known heparin binding domain [8]. For that case, the minimum size for binding was determined to be dp10 [8].

The binding we measure here is refer directly to gp120 in its monomeric form. At the viral envelope, gp120 forms trimers. Hence, increased sizes of GAG chain may present avidity effects towards the envelope, that is, the chain may span more than one gp120 monomer. As such, binding to the viral envelope in an *in vivo* setting should be more stable. The avidity effect may also be a concern when measuring binding of long GAG chains (in the case of dp30 and unfractionated heparin) to the immobilized gp120 monomer, as one chain may bind more than one protein.

New strategies targeting this HIV-proteoglycan interaction are starting to appear: a syndecan-Fc hybrid molecule showed potent antiviral activity and prevented trans-infection [20] and a synthetic CD4-mimetic peptide linked to an HS or an HS peptidomimetic chain also inhibited HIV-1 attachment and entry [21, 22]. These new inhibitors diversify the range of possible microbicides, increasing the probability of finding drug candidates with higher clinical potential.

Acknowledgements

This work was funded by Fundação para a Ciência e a Tecnologia – Ministério da Educação e Ciência (FCT-MEC, Portugal; projects PTDC/QUI-BIQ/104787/2008 and VIH/SAU/0047/2011, as well as P.M.M. PhD fellowship SFRH/BD/42205/2007) and the Spanish Ministry of Science and Innovation (project BIO2009-08983 to R.G.G.).

References

1. Klasse PJ (2012) The molecular basis of HIV entry. Cell Microbiol 14:1183-1192
2. Melikyan GB (2011) Membrane fusion mediated by human immunodeficiency virus envelope glycoprotein. Curr Top Membr 68:81-106
3. Ugolini S, Mondor I, Sattentau QJ (1999) HIV-1 attachment: another look. Trends Microbiol 7:144-149
4. Bernfield M, Gotte M, Park PW, Reizes O, Fitzgerald ML, Lincecum J, Zako M (1999) Functions of cell surface heparan sulfate proteoglycans. Annu Rev Biochem 68:729-777
5. Esko JD, Kimata K, Lindahl U (2009) Proteoglycans and Sulfated Glycosaminoglycans. In: Varki A, Cummings RD, Esko JD, Freeze HH, Stanley P, Bertozzi CR, Hart GW, Etzler ME (eds) Essentials of Glycobiology. Cold Spring Harbor Laboratory Press, Cold Spring Harbor (NY)
6. Mbemba E, Czyrski JA, Gattegno L (1992) The interaction of a glycosaminoglycan, heparin, with HIV-1 major envelope glycoprotein. Biochim Biophys Acta 1180:123-129
7. Roderiquez G, Oravecz T, Yanagishita M, Bou-Habib DC, Mostowski H, Norcross MA (1995)

Mediation of human immunodeficiency virus type 1 binding by interaction of cell surface heparan sulfate proteoglycans with the V3 region of envelope gp120-gp41. J Virol 69:2233-2239

8. Vives RR, Imberty A, Sattentau QJ, Lortat-Jacob H (2005) Heparan sulfate targets the HIV-1 envelope glycoprotein gp120 coreceptor binding site. J Biol Chem 280:21353-21357
9. Crublet E, Andrieu JP, Vives RR, Lortat-Jacob H (2008) The HIV-1 envelope glycoprotein gp120 features four heparan sulfate binding domains, including the co-receptor binding site. J Biol Chem 283:15193-15200
10. de Parseval A, Bobardt MD, Chatterji A, Chatterji U, Elder JH, David G, Zolla-Pazner S, Farzan M, Lee TH, Gallay PA (2005) A highly conserved arginine in gp120 governs HIV-1 binding to both syndecans and CCR5 via sulfated motifs. J Biol Chem 280:39493-39504
11. Mondor I, Ugolini S, Sattentau QJ (1998) Human immunodeficiency virus type 1 attachment to HeLa CD4 cells is CD4 independent and gp120 dependent and requires cell surface heparans. J Virol 72:3623-3634
12. Zhang YJ, Hatziioannou T, Zang T, Braaten D, Luban J, Goff SP, Bieniasz PD (2002) Envelope-dependent, cyclophilin-independent effects of glycosaminoglycans on human immunodeficiency virus type 1 attachment and infection. J Virol 76:6332-6343
13. Bobardt MD, Saphire AC, Hung HC, Yu X, Van der Schueren B, Zhang Z, David G, Gallay PA (2003) Syndecan captures, protects, and transmits HIV to T lymphocytes. Immunity 18:27-39
14. Saphire AC, Bobardt MD, Zhang Z, David G, Gallay PA (2001) Syndecans serve as attachment receptors for human immunodeficiency virus type 1 on macrophages. J Virol 75:9187-9200
15. de Witte L, Bobardt M, Chatterji U, Degeest G, David G, Geijtenbeek TB, Gallay P (2007) Syndecan-3 is a dendritic cell-specific attachment receptor for HIV-1. Proc Natl Acad Sci U S A 104:19464-19469
16. Gallay P (2004) Syndecans and HIV-1 pathogenesis. Microbes Infect 6:617-622
17. Rider CC, Coombe DR, Harrop HA, Hounsell EF, Bauer C, Feeney J, Mulloy B, Mahmood N, Hay A, Parish CR (1994) Anti-HIV-1 activity of chemically modified heparins: correlation between binding to the V3 loop of gp120 and inhibition of cellular HIV-1 infection in vitro. Biochemistry 33:6974-6980
18. Bishop JR, Schuksz M, Esko JD (2007) Heparan sulphate proteoglycans fine-tune mammalian physiology. Nature 446:1030-1037
19. Kato M, Wang H, Bernfield M, Gallagher JT, Turnbull JE (1994) Cell surface syndecan-1 on distinct cell types differs in fine structure and ligand binding of its heparan sulfate chains. J Biol Chem 269:18881-18890
20. Bobardt MD, Chatterji U, Schaffer L, de Witte L, Gallay PA (2010) Syndecan-Fc hybrid molecule as a potent in vitro microbicidal anti-HIV-1 agent. Antimicrob Agents Chemother 54:2753-2766
21. Baleux F, Loureiro-Morais L, Hersant Y, Clayette P, Arenzana-Seisdedos F, Bonnaffe D, Lortat-Jacob H (2009) A synthetic CD4-heparan sulfate glycoconjugate inhibits CCR5 and CXCR4 HIV-1 attachment and entry. Nat Chem Biol 5:743-748
22. Connell BJ, Baleux F, Coic YM, Clayette P, Bonnaffe D, Lortat-Jacob H (2012) A synthetic heparan sulfate-mimetic peptide conjugated to a mini CD4 displays very high anti- HIV-1 activity independently of coreceptor usage. Chem Biol 19:131-139

IV

Imaging single virus fusion with supported lipid bilayers

Overview

In this section we evolve our studies from peptides and proteins to actual viruses. We set up an experimental strategy to observe individual viruses fusing with supported lipid bilayers of defined lipid composition. VSV G protein was pseudotyped to a retrovirus core and double labeled in the membrane and in the nucleocapsid for fluorescence microscopy. Full fusion was observed by the dispersion of the membrane dye and disappearance of the fluorescent capsid signal, which allowed fusion kinetics to be evaluated. Anionic lipids were essential to promote these VSV G mediated viral fusion.

This work was done at Emory Childen's Center of Emory University, in Atlanta, USA, with the supervision of Prof. Gregory Melikyan.

Article E

Matos PM, Marin M, Ahn B, Lam W, Santos NC, Melikyan GB. Anionic lipids are required for Vesicular Stomatitis Virus G protein-mediated single particle fusion with supported lipid bilayers. *J. Biol. Chem.* **288**:12416-12425 (2013).

Article E

Declaration of authorship

I, Pedro Miguel Baptista de Matos, declare that the experimental design, the main experimental work involving microscopy, data analysis and writing of initial manuscript was carried out by me under the supervision and assistance of Prof. Gregory Melikyan, and supervision of Prof. Nuno C. Santos. Prof. Mariana Marin produced the fluorescent viruses, while Dr. Byungwook Ahn and Prof. Wilbur Lam produced the PDMS microfluidic chamber.

I, Nuno C. Santos, as supervisor of Pedro Matos and one of the authors of the manuscript mentioned above, hereby acknowledge and confirm that the information above is correct.

I, Gregory Melikyan, as corresponding author of the article mentioned above, hereby acknowledge and confirm that the information above is correct.

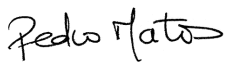

Pedro M. Matos

Nuno C. Santos

Gregory Melikyan

THE JOURNAL OF BIOLOGICAL CHEMISTRY VOL. 288, NO. 18, pp. 12416–12425, May 3, 2013

Anionic Lipids Are Required for Vesicular Stomatitis Virus G Protein-mediated Single Particle Fusion with Supported Lipid Bilayers*[S]

Received for publication, February 15, 2013, and in revised form, March 12, 2013 Published, JBC Papers in Press, March 14, 2013, DOI 10.1074/jbc.M113.462028

Pedro M. Matos[‡§], **Mariana Marin**[‡], **Byungwook Ahn**[‡], **Wilbur Lam**[‡], **Nuno C. Santos**[§], **and Gregory B. Melikyan**[‡¶1]

From the [‡]*Emory Children's Center, Department of Pediatrics, Emory University School of Medicine, Atlanta, Georgia 30322, the* [§]*Instituto de Medicina Molecular, Faculdade de Medicina, Universidade de Lisboa, Av. Prof. Egas Moniz, 1649-028 Lisbon, Portugal, and the* [¶]*Children's Healthcare of Atlanta, Atlanta, Georgia 30322*

Background: Regulation of virus entry by host lipids is poorly understood.
Results: Imaging of low pH-mediated fusion between single vesicular stomatitis pseudoviruses and lipid bilayers revealed a striking reliance on anionic lipids.
Conclusion: The dependence of fusion on late endosome-resident anionic lipids suggests a new means for regulating the virus entry sites.
Significance: Reliance on specific lipids for fusion may shed light on future antiviral strategies.

Viral glycoproteins mediate fusion between viral and cellular membranes upon binding to cognate receptors and/or experiencing low pH. Although activation of viral glycoproteins is thought to be necessary and sufficient for fusion, accumulating evidence suggests that additional cellular factors, including lipids, can modulate the fusion process. Understanding the role of lipids in virus entry via endocytosis is impeded by poor accessibility and the highly diverse nature of endosomes. Here we imaged fusion of single retroviral particles pseudotyped with the vesicular stomatitis virus (VSV) G protein with dextran-supported lipid bilayers. Incorporation of diffusible fluorescent labels into the viral membrane and the viral interior enabled detection of the lipid mixing (hemifusion) and content transfer (full fusion) steps of VSV G-mediated fusion at low pH. Although single virus fusion with supported bilayers made of zwitterionic lipids could not be detected, inclusion of anionic lipids, phosphatidylserine, and bis(monoacylglycero)phosphate (BMP), greatly enhanced the efficiency of hemifusion and permitted full fusion. Importantly, lipid mixing always preceded the opening of a fusion pore, demonstrating that VSV G-mediated fusion proceeds through a long-lived hemifusion intermediate. Kinetic analysis of lipid and content transfer showed that the lags between lipid and content mixing defining the lifetime of a hemifusion intermediate were significantly shorter for BMP-containing compared with PS-containing bilayers. The strong fusion-enhancing effect of BMP, a late endosome-resident lipid, is consistent with the model that VSV initiates fusion in early endosomes but releases its core into the cytosol after reaching late endosomal compartments.

Entry of enveloped viruses into a host cell is a complex, multistep process mediated by viral glycoproteins, which are activated upon encountering cellular receptor(s) and/or low pH (1, 2). Generally, the entry of enveloped viruses proceeds through attachment to a host cell, binding to cognate receptor(s), and either fusion of the viral membrane with the cell plasma membrane or virus internalization and low pH-dependent fusion with endosomes (3). Recent evidence suggests that viruses that do not rely on low pH can also enter through endocytic pathways (4–7). Viral envelope glycoproteins are thought to mediate energetically unfavorable membrane fusion events by releasing the energy stored in their native structure upon refolding into a thermodynamically favorable conformation (8–11). Despite the highly diverse structures of viral fusion glycoprotein, they are categorized into three classes on the basis of their structural and biochemical properties (2, 12).

VSV[2] G protein is a class III viral fusion protein that is well characterized both structurally and functionally (13–15). Interestingly, pH-induced conformational changes in VSV G are reversible, as the protein assumes the native conformation upon returning to neutral pH in the absence of a target membrane (16–18). This unusual feature of VSV G indicates that the difference between free energies of the initial "metastable" and final "stable" conformations is not large and that, therefore, little energy can be released by this protein to drive membrane fusion (19). These considerations warrant further studies of VSV G-mediated fusion to gain critical insights into the universal principles by which viral proteins promote membrane merger.

* This work was supported, in whole or in part, by National Institutes of Health Grant R01 AI053668 (to G. B. M.). This work was also supported by Fundação para a Ciência e Tecnologia, Ministério da Educação e Ciência (FCT-MEC, Portugal) Project Grant PTDC/QUI-BIQ/104787/2008 (to N. C. S.) and by Fellowship SFRH/BD/42205/2007 (to P. M. M.).
[S] This article contains supplemental Fig. 1 and Movies 1 and 2.
[1] To whom correspondence should be addressed: Department of Pediatrics Infectious Diseases, Emory University, 2015 Uppergate Dr., Atlanta, GA 30322. Tel.: 404-727-4652; Fax: 404-727-9223; E-mail: gmeliki@emory.edu.

[2] The abbreviations used are: VSV, vesicular stomatitis virus; PS, phosphatidylserine; BMP, bis(monooleoylglycero)phosphate; SLB, supported lipid bilayer(s); VSVpp, vesicular stomatitis virus G protein-pseudotyped particle(s); DiD, 1,1′-dioctadecyl-3,3,3′,3′-tetramethylindodicarbocyanine; POPS, 1-palmitoyl-2-oleoyl-*sn*-glycero-3-phospho-L-serine; POPC, 1-palmitoyl-2-oleoyl-*sn*-glycero-3-phosphocholine; CF-PE, 1,2-dioleoyl-*sn*-glycero-3-phosphoethanolamine-N-(carboxyfluorescein); Chol, cholesterol; PDMS, polydimethylsiloxane; mKO, CoralHue® monomeric Kusabira Orange fluorescent protein; FRAP, fluorescence recovery after photobleaching; ROI, region of interest; NC, nucleocapsid; MLV, murine leukemia virus.

Despite extensive efforts, the host cell receptor(s) for VSV entry has not been unambiguously identified. Phosphatidylserine (PS) has been shown to promote VSV fusion and entry into cells (20–23). However, this lipid is unlikely to be the primary VSV receptor because VSV binding and infection do not correlate with the level of PS in the plasma membrane, and blocking PS with annexin V does not inhibit VSV infection (24). Moreover, the fact that VSV can merge with lipid vesicles made of phosphatidylcholine at low pH (21, 25) indicates the lack of reliance on a proteinaceous receptor or a specific lipid. On the other hand, lipid composition is known to modulate the kinetics and efficiency of viral fusion (26) and could, therefore, play a role in the regulation of G protein-mediated fusion. Recent studies highlight the importance of an endosome-specific anionic lipid, bis(monoacylglycero)phosphate (BMP), also referred to as lysobisphosphatidic acid (27), in promoting fusion of unrelated viruses entering cells *via* endocytosis (28–31). For instance, dengue virus fusion with liposomes and with cell membranes has been shown to depend on anionic lipids, including BMP (30), which is one of the major lipid species in late endosomes and multivesicular bodies (27, 32). BMP is thought to facilitate cellular entry of different pathogens by regulating back-fusion between intralumenal vesicles and the limiting membrane of an endosome (33, 34). Interestingly, a BMP-dependent back-fusion process has also been implicated in the VSV nucleocapsid release into the cytosol following virus fusion with intralumenal vesicles (28, 29). However, this two-step VSV entry model is not universally accepted because this virus appears to quickly fuse with early endosomes prior to entry into multivesicular bodies (35, 36).

Single virus trafficking in host cells is an increasingly popular tool to study the viral entry process (37). However, real-time detection of fusion events that culminate in the viral content release is technically challenging and, therefore, less common (4, 38–40). The main advantage of these approaches is the ability to study events at a single virus level, which allows distinguishing specific subpopulations of particles or characteristics hidden in bulk assay data.

Although single virus imaging in live cells provides important insights into the entry process, the complexity of vesicular trafficking and the heterogeneity of endosomal compartments impede mechanistic studies of viral fusion. Dissecting the viral entry processes in a controlled environment can shed light on the mechanism of fusion and on the host factors required for completion of this reaction. A powerful approach to address these questions is to reconstitute viral fusion in model systems such as liposomes and supported lipid bilayers (SLB). Recent advances in imaging of membrane fusion using supported lipid bilayers or tethered single liposomes have brought new mechanistic insights into the membrane merger mediated by cellular fusion proteins (41–43) and viral glycoproteins (44–46). Rapid pH-dependent hemifusion/fusion of single influenza and Sindbis viruses with SLB was observed by monitoring redistribution of a lipophilic dye incorporated into the viral membrane (hemifusion) (46) or by visualizing the transfer of both viral membrane and content markers (full fusion) (44, 45).

Here, we report the direct visualization of VSV G-pseudotyped particle (VSVpp) fusion with dextran-supported lipid bilayers. We took advantage of the murine leukemia virus (MLV) pseudotyping system, which allows incorporation of a releasable fluorescent protein marker into the virus (5) and of a membrane dye into the viral envelope. This labeling strategy permitted the detection of both lipid mixing (hemifusion) and content release (full fusion) steps of the VSVpp fusion process. Imaging of single VSVpp revealed that both hemifusion and fusion with supported bilayers were markedly promoted by anionic lipids, POPS, or BMP. Although BMP-containing bilayers supported faster conversion of hemifusion to full fusion compared with POPS bilayers, similar probabilities of fusion and identical effective sizes of nascent fusion pores were consistent with the lack of requirement for a specific lipid for productive VSV entry. The strong fusion-stimulating effect of BMP indicates, however, that this endosome-resident lipid may modulate the outcome of low pH-induced VSV fusion with intracellular compartments.

EXPERIMENTAL PROCEDURES

Virus Production—Fluorescently labeled pseudoviruses were produced in HEK293T/17 cells using PolyFect transfection reagent (Qiagen, Valencia, CA). Cells grown on 10-cm dishes were transfected with 2 μg MLV-Gag-Pol, 1 μg MLV-Gag-mKO, 3 μg pMLV-LTR-LacZ, and 3 μg of pMDG-VSV-G. Twenty-four hours post-transfection, cells were labeled with 10 μM 1,1′-dioctadecyl-3,3,3′,3′-tetramethylindodicarbocyanine (DiD) for 4 h in a CO_2 incubator at 37 °C. Cells were washed, covered with 6 ml of fresh phenol red-free growth medium, and incubated for an additional 24 h. Virus-containing medium was collected 48 h post-transfection, passed through a 0.45 μM filter, aliquoted, and stored at −80 °C. The infectious titer was determined by a β-galactosidase assay in TZM-bl cells (47). Vectors expressing MLV-Gag-pol and MLV-LTR LacZ (48) were provided by Dr. Walther Mothes (Yale University). The pMDG-VSV-G expression vector was provided by Dr. John Young (Salk Institute). The construction of the MLV-Gag-mKo expression vector was described in Ref. 5.

Preparation of Small Unilamellar Vesicles—1-palmitoyl-2-oleoyl-*sn*-glycero-3-phosphocholine (POPC), 1-palmitoyl-2-oleoyl-*sn*-glycero-3-phospho-L-serine (POPS), BMP (S,R isomer) and 1,2-dioleoyl-*sn*-glycero-3-phosphoethanolamine-N-(carboxyfluorescein) (CF-PE) were purchased from Avanti Polar Lipids (Alabaster, AL). Cholesterol (Chol) was from Sigma. Lipids were mixed in chloroform and dried to a thin film in a round-bottom glass flask under an argon stream. Traces of solvent were removed by placing the flask in a vacuum chamber for at least 3 h. The lipid film was hydrated in PBS buffer (Cellgro, Mediatech, Inc., Manassas, VA) to make a final lipid concentration of 1 mM. The lipid suspension was subjected to several freeze/thaw cycles and sonicated with a probe sonicator (VWR, Radnor, PA) on ice to avoid sample heating. The obtained lipid suspension was cleared by centrifugation at 10,000 × *g* for 5 min.

Coverslip Cleaning and Functionalization with Dextran—Glass coverslips (no. 1.5, 22 × 22 mm, Corning, NY) were thoroughly cleaned using the following steps: 1) immersion into hot 2% Hellmanex (Hellma Analytics, Müllheim, Germany) for 30 min, 2) sonication in Hellmanex for 15 min while warm, 3)

rinsing extensively with Milli-Q water, 4) immersion into Piranha solution (3:1 concentrated sulfuric acid/hydrogen peroxide 30% without stabilizer) for 30 min, 5) rinsing extensively with Milli-Q water, 6) sonication in Milli-Q water for 10 min, and 7) rinsing extensively with Milli-Q water. The cleaned coverslips were dried in an oven for 1 h at ~100 °C.

Dextran functionalization was carried out as described previously (45). Briefly, cleaned coverslips were immersed in 0.2% (3-glycidyloxypropyl)trimethoxysilane (Sigma) in isopropanol for 5 min under gentle agitation. After rinsing with pure isopropanol, the coverslips were cured for 1 h at ~80 °C. A 30% (w/v) dextran (M_r 5 × 10^5, Sigma-Fluka) solution was prepared using Milli-Q water, and air bubbles were removed in a vacuum chamber. The coverslips were carefully covered with dextran solution (~1 ml) and incubated in a humidified chamber for ~24 h. Excess dextran was rinsed off by dipping repeatedly in water and leaving the coverslips in water for 2 days. The coverslips were dried in an oven for 1 h at 80 °C and stored in a vacuum desiccator.

Microfluidic Chamber Design and Fluorescence Microscopy—The microfluidic polydimethylsiloxane (PDMS) chamber was fabricated using both standard photolithography and soft lithography. To prepare the soft mold for the microfluidic channels, a negative photoresist (MicoChem, SU-8) was spin-coated and patterned on a 4-inch silicon wafer. The patterned wafers were silanized using hexamethyldisilazane so that the cured PDMS could be easily peeled off from the soft mold. PDMS mixed at a 10:1 ratio (w/w) of polymer to curing agent was then poured onto the silanized wafer and cured at 60 °C for about 24 h. The cured device was then peeled off from the wafer. The PDMS pieces were then rinsed thoroughly with deionized water and set to dry at 60 °C in an oven.

The 25 × 25-mm PDMS block had two 10-mm grooves that were 1 mm wide and 75 μm deep. Small holes were punched at each end of the grooves, and polytetrafluoroethylene tubing (microbore 0.03-inch (0.76-mm) diameter) was inserted into the holes (Fig. 1, *A* and *B*). The PDMS block was adhered to top of a dextran-functionalized coverslip, thus creating two flow channels between the PDMS block and the coverslip. Tight adhesion of the polymer to the glass surface was sufficient to seal the channels. This approach was similar to a method described previously for SLB formation in microfluidic cells (49).

All imaging experiments were carried out at room temperature using a confocal laser scanning microscope Zeiss LSM 780 and oil immersion Plan-Neofluar ×40/1.3 numerical aperture objective. The laser lines used to excite fluorophores were 488 (CF-PE), 561 (mKO), and 633 nm (DiD). The PDMS block with coverslip was affixed to a microscope stage and connected to a peristaltic pump (Fig. 1*A*). Solution flow during the imaging experiments was adjusted to ~48 μl/min.

Supported Lipid Bilayer Formation—SLB were formed by the vesicle fusion method (50). Small unilamellar vesicle suspensions with 0.1 mM of total lipids in PBS were injected into both microfluidic channels. After incubation for 30 min, the excess of liposomes was removed by flowing PBS for 5 min. The compositions used for the SLB were POPC:Chol:CF-PE, 84.5:15:0.5 mol %; POPC:Chol:POPS:CF-PE, 64.5:15:20:0.5 mol %; and POPC:Chol:BMP:CF-PE, 64.5:15:20:0.5 mol %. These mixtures are designated throughout the text as POPC, POPS, and BMP, respectively. Small amounts of the fluorescent lipid CF-PE were included for three reasons: to assess the uniformity of SLBs, to test whether lipids would diffuse freely in SLBs by performing FRAP experiments (see below), and to determine the exact time of the pH drop upon perfusion with acidic buffers (similar to Ref. 45).

FRAP Assay—SLB obtained by spontaneous rupture/fusion of small unilamellar vesicles over the hydrated dextran layer of the glass coverslip were usually uniform, as observed by the fluorescence of CF-PE incorporated in the lipids mixtures. Next, SLB were tested for fluidity using FRAP (51). Briefly, a circular region of interest (radius 8 μm) was photobleached using a brief pulse of the 488-nm line of an argon laser set at 100% power. The fluorescence recovery was monitored by low-intensity laser excitation for at least 5 min. The fluorescence of a distant circular region of interest (ROI) served as a reference signal.

Intensity profiles for the bleached and reference ROIs were analyzed using ImageJ software. The fluorescence recovery trace was double-normalized to take into account a possible inadvertent bleaching effect upon image acquisition

$$F_{norm} = \frac{F_{\text{Ref (pre)}}}{F_{\text{Ref}}(t)} \times \frac{F_{\text{FRAP}}(t)}{F_{\text{FRAP (pre)}}} \quad \text{(Eq. 1)}$$

where F_{Ref} is the mean fluorescence intensity of the reference ROI, F_{FRAP} is the intensity of the bleached ROI, t is the time after photobleaching, and *pre* stands for the mean intensity before photobleaching.

The normalized traces of the bleached ROI were fitted using a diffusion model for a circular spot (52)

$$F_{\text{FRAP(norm)}}(t) = a_0 + a_1 \cdot e^{-\frac{\tau}{2(t - t_{\text{bleach}})}} \cdot \left[I_0\left(\frac{\tau}{2(t - t_{\text{bleach}})}\right) + I_1\left(\frac{\tau}{2(t - t_{\text{bleach}})}\right)\right] \cdot \tau = \frac{w^2}{D} \quad \text{(Eq. 2)}$$

where t_{bleach} is the time of bleaching, τ is the characteristic diffusion time, w is the radius of the ROI, D is the diffusion coefficient, and $I_n(x)$ are modified Bessel functions. Nonlinear fit of the data was performed in GraphPad Prism version 5.

The results of the FRAP assay for each type of lipid mixture used are shown in Fig. 1*D*, and the corresponding diffusion coefficients are in the figure legend. Diffusion coefficients around 1 $\mu m^2/s$, corresponding to free lipid diffusion in bilayers, were deemed acceptable for virus fusion experiments. Systematic verification of the bilayer fluidity is important because a fraction of bilayers did not exhibit fluorescence recovery after photobleaching (see also Ref. 49).

Imaging of VSVpp Fusion—All experiments were performed at room temperature. For each imaging experiment, a sample of 5 μl of the virus stock solution was diluted in 100 μl of PBS and vortexed briefly. Approximately 90 μl of viral suspension was continuously flowing into a channel. Viruses adhered to the bilayer reasonably well, permitting subsequent washing with BPS for 1–2 min to remove unbound viruses. Next, image

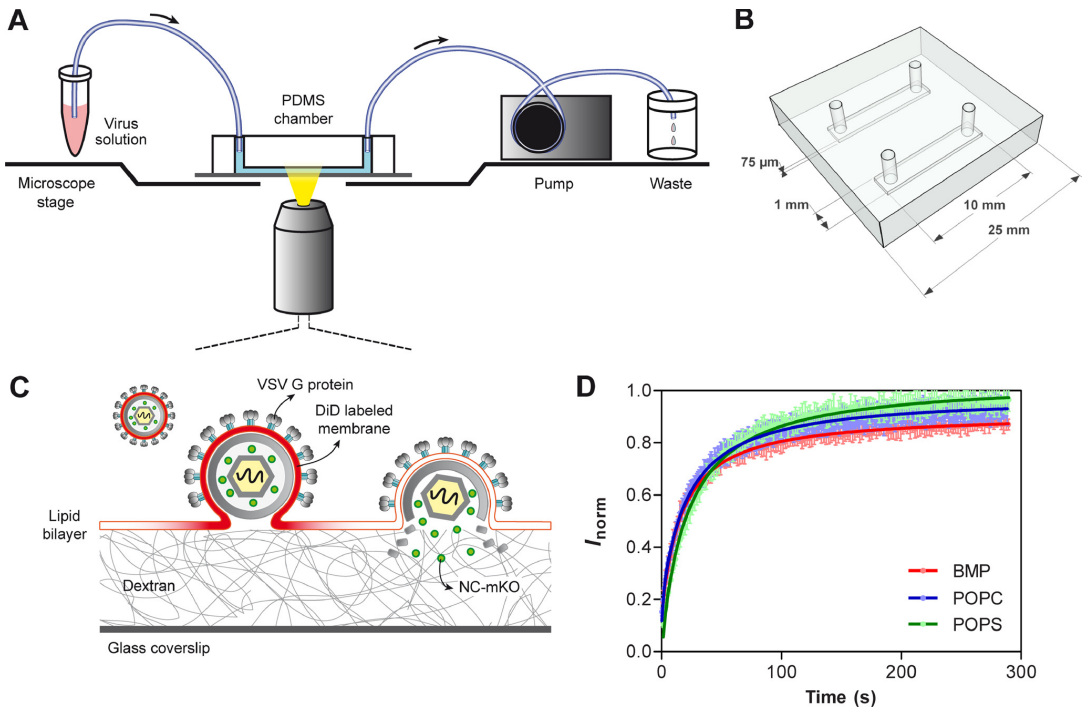

FIGURE 1. **Schematic representation of single virus fusion experiments.** *A*, schematic drawing of the microfluidic chamber mounted on a microscope stage. *B*, sketch of the microfluidic PDMS block (*top view*) that was attached to the glass coverslip to form two channels where the SLB were formed. *C*, single VSVpp fusion triggered by low pH detected by double fluorescent labeling with Gag-mKO (*green*) and DiD (*red*). VSV G-mediated lipid mixing is manifested in radial diffusion of DiD into the SLB. After pore formation, the fluorescent content marker is released into the dextran layer underneath the bilayer and disappears because of diffusion. *D*, FRAP assay to measure the fluidity of supported lipid bilayers. The recovery of CF-PE fluorescence after photobleaching of a defined circular region ($w = 8.02\ \mu m$) was followed over time. Plotted values are means with *error bars* from 95% confidence intervals ($n = 5$). Recovery data were fitted with equation 1. The resulting mean ± S.E. diffusion coefficients for CF-PE were 0.946 ± 0.022 $\mu m^2/s$ in POPC, 0.904 ± 0.026 $\mu m^2/s$ in POPS, and 1.16 ± 0.035 $\mu m^2/s$ in BMP bilayers.

acquisition was started, and perfusion with an MES (pH 5.5) buffer (144 mM NaCl, 2 mM $CaCl_2$, 30 mM MES) was initiated. This acidic buffer quenched the CF-PE fluorescence, marking the exact time of the pH change (similar to an approach introduced in Ref. 45). Images were acquired with 2-s intervals for 11 min. At the end of the acquisition, the flow channel was cleaned by flowing ~1 ml of 70% ethanol at a higher flow rate before removing the chamber from the microscope.

Image Analysis—Hemifusion and fusion events were initially identified by visual inspection of image sequences. Next, double-labeled (DiD and mKO) viral particles were detected, and their mean fluorescence intensities over time were measured using Speckle TrackerJ, a recent freely available ImageJ plug-in (53). The program identified fluorescent particles and tracked them until the fluorescence intensity/particle size decreased below a defined threshold. DiD-only labeled particles (likely dye aggregates) were excluded from the analysis. Virus hemifusion was defined as DiD redistribution into SLBs without the loss of mKO, whereas full fusion was defined as release of DiD followed by loss of the content marker. The mean fluorescence intensity profiles for each marker (CF-PE, DiD, and mKO) were obtained using small circular regions encompassing the particles. Analysis of these profiles yielded the following key events used for kinetic analysis. The pH drop was assessed by decay of the CF-PE signal; the onset of lipid mixing was defined as the onset of DiD dequenching or, when dequenching was weak, by the onset of fluorescence decay because of DiD dilution; the onset of content release was detected by mKO fluorescence decrease; and completion of content release was defined as the time point at which the mKO signal reached the background level. The non-parametric Mann-Whitney rank sum test was used to evaluate the differences among the kinetic parameters for bilayers of different composition.

RESULTS

Direct Visualization of Single VSVpp Hemifusion and Fusion Events—The microfluidic PDMS chamber allowed for an easy solution change and for a quick formation of supported lipid bilayers, as described under "Experimental Procedures" (Fig. 1, *A* and *B*). After testing the SLB fluidity by FRAP (Fig. 1*D*), double-labeled VSV pseudoviruses were drawn into the chamber and allowed to attach to the bilayer for 5 min. VSVpp readily adhered to bilayers and remained relatively immobile throughout the experiments despite the solution changes. The same volume of diluted viral stock was passed through a flow channel in each experiment, resulting in adhesion of 60–100 particles/

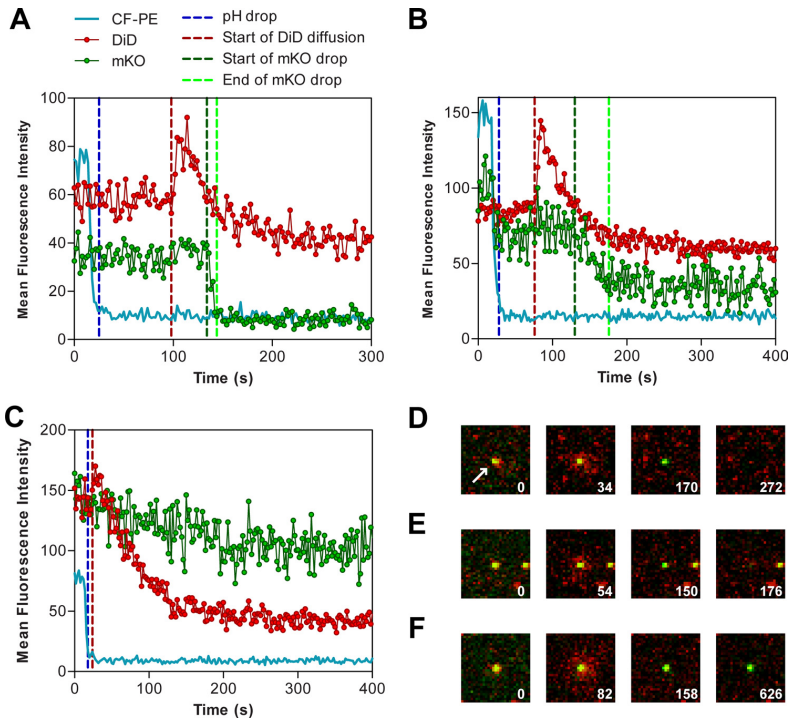

FIGURE 2. **Imaging single VSV pseudovirus fusion.** *A*, example of fluorescence intensity profiles for a single VSVpp-SLB fusion event (POPS). The drop of CF-PE signal (*blue*) marks the acidification of the image area to pH 5.5. Key events used for kinetic analysis are marked by *vertical lines* representing the time of acidification (*blue*), onset of lipid mixing (*red*), onset of content release (*green*), and end of content release (*light green*). *B*, intensity profiles for a single fusion event with BMP bilayers exhibiting a slow mKO release. The slight reduction in the mKO signal upon acidification reflects a spectral bleed-through from the CF-PE signal which was fully quenched by low pH. *C*, intensity profiles for a virus undergoing hemifusion (decay of the DiD signal without loss of the mKO signal). *D* and *E*, images of full VSVpp fusion events with POPS (*D*) and BMP (*E*) bilayers. The double-labeled pseudoviruses (*yellow*) released DiD (*red*) into the SLB by radial diffusion, followed by disappearance of green puncta because of release of NC-mKO. The first images in each panel are taken before acidification, the second and third images show the dequenching and spread of DiD while the mKO signal remains steady, and the last images were taken after completion of fusion (mKO release). *F*, example of a hemifusion event with BMP bilayer that did not culminate in full fusion. Here the mKO signal remained steady throughout the experiment. *White numbers* (*D–F*) indicate time after acidification in seconds. The image fields are 12×12 μm. The *white arrow* is pointed at the central particle of interest that will undergo fusion.

image field. VSVpp were colabeled with the membrane dye, DiD, and the viral content marker, the MLV-Gag polyprotein tagged with mKO (monomeric Kusabira Orange, Ref. 54), as described in Ref. 5. The Gag-mKO marker is cleaved upon MLV maturation, producing the nucleocapsid-mKO (NC-mKO) fragment, which is not associated with the viral core and is, therefore, readily released upon viral fusion (4, 5, 55). For low pH-triggered fusion, mKO is a better marker than GFP because its resistance to quenching by low pH ($pK_a \leq 5$ (54)) minimizes the possibility that the loss of mKO signal is due to acidification of the viral interior. This strategy allowed the detection of DiD transfer into SLB as a marker for hemifusion as well as detection of the viral content release as a marker for full fusion (Fig. 1*C*).

VSVpp fusion with SLB was initiated by perfusion with an acidic (pH 5.5) buffer. The exact time of acidification was determined on the basis of quenching of CF-PE fluorescence, similarly to the approach described in Ref. 45. Shortly after acidification, radial diffusion of DiD into a bilayer, away from the viral particles, was observed for a fraction of the virions (Fig. 2). Typical fluorescence intensity profiles for fusion events are shown in Fig. 2, *A* and *B*, and Fig. 3. The DiD signal usually increased because of fluorescence dequenching and then decayed upon spreading into the supported bilayer. These lipid mixing events reflecting virus-SLB hemifusion were not observed at neutral pH. Following the lipid mixing events, a fraction of particles lost their content marker, NC-mKO. Because the mKO signal from neighboring particles that had no change in DiD fluorescence remained stable, the loss of the mKO signal following the hemifusion step signified the viral content release through a fusion pore (Fig. 2, *D–E*, and supplemental movie 1). The existence of a hydrated dextran layer supporting the membrane provided sufficient space to accommodate the viral content marker and to permit its diffusion away from a particle. The four sequential events (acidification of the flow channel, onset of lipid mixing, as well as the onset and time of completion of content release) are marked by vertical lines in Fig. 2, *A* and *B*. These four parameters were used to compare the kinetics of VSVpp fusion with SLB of a different lipid composition (see examples in Fig. 3).

Anionic Lipids Are Essential for VSV G-mediated Hemifusion and Fusion—The total number of double-labeled VSVpp attached to POPS and BMP membranes was comparable, but a

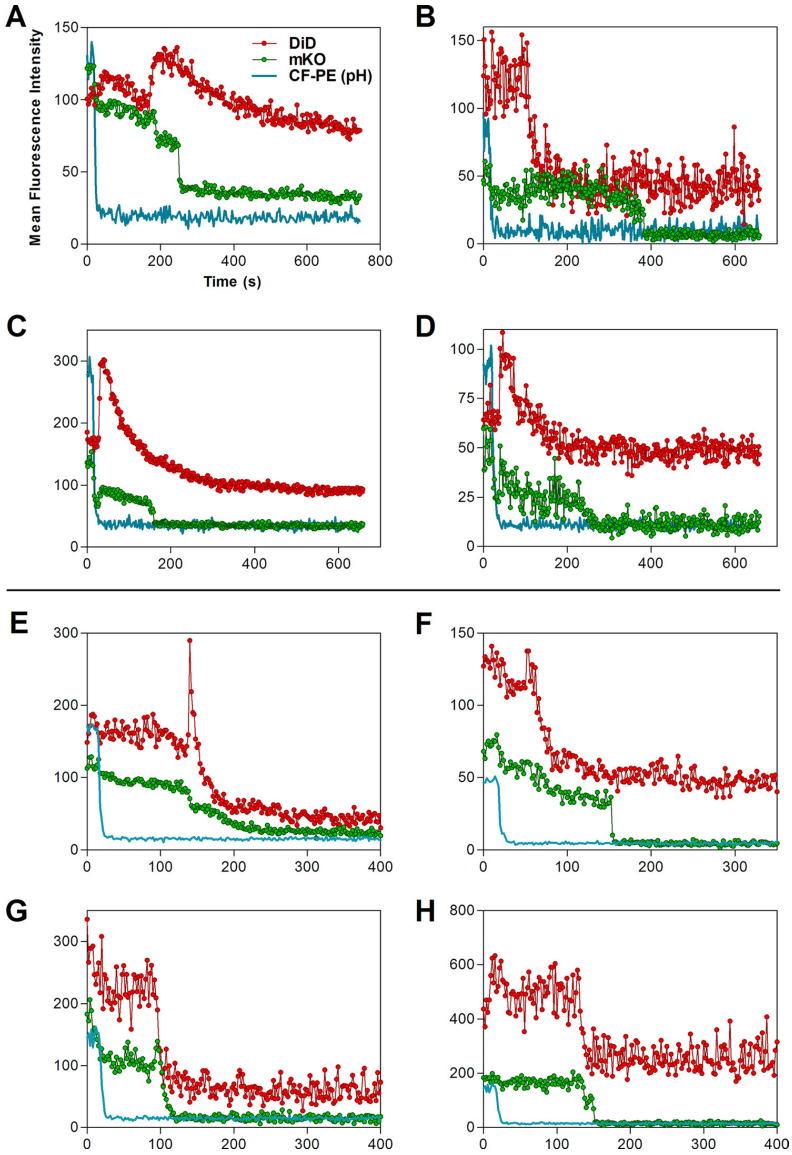

FIGURE 3. **Mean fluorescence intensity profiles of representative single virus fusion events with POPS (*A–D*) and BMP (*E–H*) bilayers.** MFIs of arbitrary circular regions encompassing individual particles are plotted. *Red traces* show the DiD signal, *green traces* show the mKO, and *blue traces* show the CF-PE signal (the pH indicator). Note that quenching of the CF-PE fluorescence upon acidification was often associated with a concomitant reduction in the mKO signal because of a spectral bleed-through. These initial changes in the mKO signal were ignored.

larger number of pseudoviruses adhered to POPC-based membranes lacking anionic lipids (see legend for Fig. 4*A*). However, despite the larger number of adhered particles, POPC bilayers did not support complete VSVpp fusion, and only 2.5% of double-labeled particles exhibited lipid mixing (hemifusion) with these bilayers (Fig. 4*A*). In sharp contrast, 31.1% and 41.5% of VSV pseudoviruses released DiD into POPS and BMP bilayers, respectively (Fig. 4*A*). BMP more potently facilitated lipid mixing than an equal amount of POPS. Under our experimental conditions, double-labeled particles released their lipid markers much more frequently than their contents. Complete fusion was detected for 6.6% of particles following their hemifusion with POPS bilayers and for 5.1% particles adhered to BMP bilayers. In other words, a significant fraction of viruses underwent hemifusion but did not form a fusion pore large enough to allow NC-mKO escape into the dextran layer underneath SLB (Figs. 1*C* and 2, *C* and *F*, and supplemental movie 2). Hemifusion always preceded full fusion. The fluorescence signal from

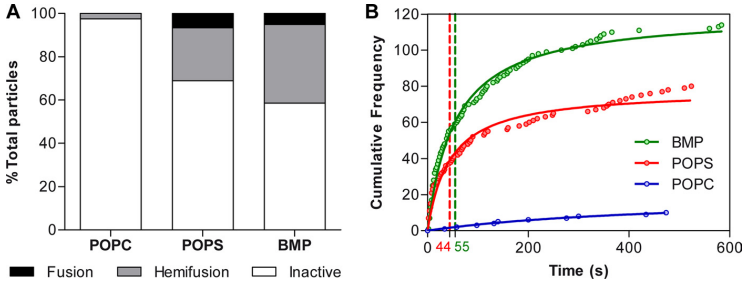

FIGURE 4. **Analyses of the extent and kinetics of VSV pseudovirus fusion.** *A*, the relative frequencies of fusion outcomes (no fusion, hemifusion, and full fusion) are shown for fusion of double-labeled VSVpp with SLBs of different lipid compositions. Hemifusion is defined as dequenching/loss of the DiD signal without the content release, whereas fusion is defined as the loss of both membrane and content markers (DiD and mKO, respectively). The total number of membrane-bound particles immediately after the pH drop was 398 for POPC, 257 for POPS, and 275 for BMP bilayers using four independent image fields for each lipid composition. *B*, distribution of the time elapsed between the pH drop (CF-PE fluorescence quenching) and the onset of lipid mixing for double-labeled particles that underwent hemifusion or fusion. The difference in the lag times before the lipid mixing for POPS and BMP was not significant ($p > 0.93$), but the differences between the hemifusion kinetics for these bilayers and POPC-based membranes were significant ($p < 0.006$ for POPS and $p < 0.023$ for BMP). The hemifusion half-time (t_{50}) was determined by fitting the data with equation $N = (A \cdot t)/(t_{50} + t)$, where A is the total number of events and t is the time. The *green* and *red dashed vertical lines* with corresponding numbers at the *x axis* correspond to the t_{50} values for BMP and POPS bilayers, respectively.

double-labeled particles that did not exhibit lipid or content mixing was stable over the course of the experiment, demonstrating that inadvertent photobleaching of fluorophores was negligible (supplemental Fig. 1). In conclusion, 20 mol % of POPS or BMP greatly enhanced the efficiency of VSVpp hemifusion and, importantly, enabled complete fusion compared with the basal lipid mixture lacking anionic lipids (Fig. 4*A*).

BMP Shortens the Lag Time between Lipid Mixing and Fusion Pore Formation—As indicated above, lipid mixing events were rare for POPC bilayers lacking anionic lipids. This is in contrast with POPS or BMP bilayers supporting a much greater number of lipid mixing events. To further assess the role of anionic lipids in VSVpp fusion, we analyzed the distribution of delay times from the pH drop to the onset of lipid mixing (Fig. 4*B*). After acidification, VSVpp hemifusion with POPS and BMP bilayers occurred with the half-times of 44 s and 55 s, respectively (Fig. 4*B*). The difference in lag times to the onset of lipid mixing with BMP and POPS bilayers was not statistically significant ($p > 0.93$). These results suggest that although anionic lipids promote VSVpp hemifusion, this process does not require a specific lipid. It thus appears that the enhanced VSVpp fusion with bilayers containing anionic lipids is due to an electrostatic effect.

The kinetics of VSVpp fusion were analyzed in more detail using the following parameters illustrated in Figs. 2 and 5: 1) time to the onset of lipid mixing/hemifusion, 2) time to the onset of content release, 3) lag time between lipid mixing and content release for a given particle, and 4) the time from the onset to completion of the NC-mKO release as a measure of the relative size of a fusion pore. All full fusion events were preceded by lipid mixing (Figs. 2 and 3), demonstrating that VSVpp fusion proceeded through a relatively long-lived hemifusion intermediate. This analysis revealed that the distribution of the times from acidification to content release was slightly faster for BMP bilayers than for POPS bilayers, but the difference was not statically significant (Fig. 5, *A* and *B*). Importantly, the lag time between lipid mixing and content release was significantly shorter for BMP when compared with POPS bilayers (Fig. 5, *A* and *B*). These results indicate that BMP can accelerate the conversion of a hemifusion intermediate into a functional fusion pore. Although POPS supports the efficient formation of fusion pores, this process is slower than with BMP bilayers.

We next asked whether the effective sizes of VSV G-mediated fusion pores are lipid-dependent. By analyzing the mKO release profiles for individual events on the basis of the fluorescence signal decay (Fig. 3), we found that the time required for complete release of NC-mKO varied. In many cases the mKO signal dropped virtually instantaneously (*e.g.* Figs. 2*A* and 3, *A*, *C*, and *F*), but there were also particles exhibiting a slow decrease of the signal (*e.g.* Figs. 2*B* and 3, *D* and *E*). Thus, VSV G formed fusion pores of different initial sizes. To assess whether lipids can alter the time between the onset and the end of the mKO signal decrease, we compared the VSVpp fusion with POPS and BMP bilayers and found that the distributions of this parameter were identical (Fig. 5*C*). These findings argue against a specific effect of anionic lipids on the apparent size of a fusion pore.

Another prominent feature of the VSV G-mediated fusion was the stepwise release of the mKO marker (Fig. 3, *A* and *H*). The two-step release of the viral content likely reflected the pore flickering. The transient halting of content release is likely due to pore closure or shrinkage, whereas resumption of release reflects subsequent pore dilation (56, 57). Thus, fusion pores formed by VSV G in supported bilayers exhibited dynamic features similar to those formed by other viral proteins (38, 56, 58, 59).

DISCUSSION

In this study, we successfully reconstituted VSV G-mediated membrane fusion in a minimal model system that enabled time-resolved imaging of single lipid mixing and content release events. The ability to mediated fusion with lipid bilayers at low pH implies that VSV G does not strictly require a proteinaceous receptor to induce fusion. On the other hand, VSVpp fusion was markedly augmented by anionic lipids, POPS, or BMP. Only bilayers containing POPS or BMP supported complete VSVpp fusion, whereas a POPC-based mixture supported only limited lipid mixing activity. Our results

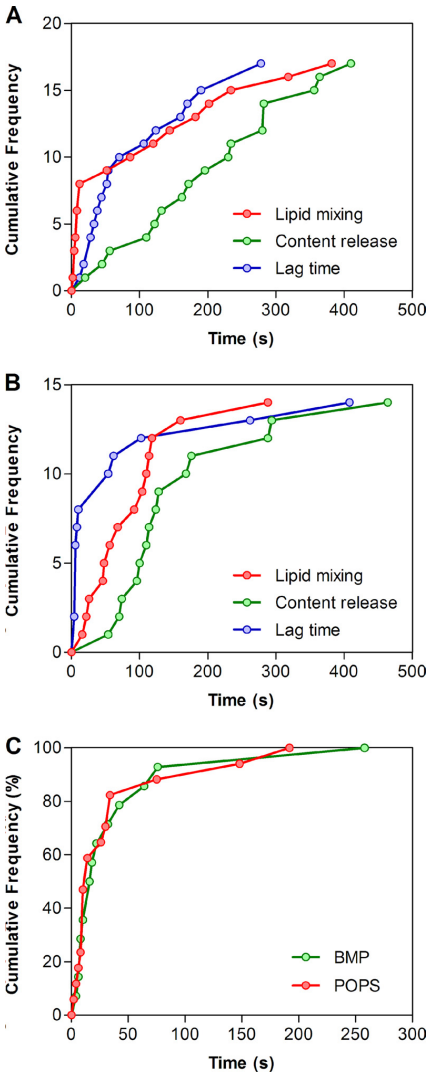

FIGURE 5. **Kinetics of distinct steps of single VSV pseudovirus fusion.** *A* and *B*, distributions of the delay times from acidification to the onset of lipid mixing (hemifusion, *red circles*) to the onset of content release (*green circles*) as well as the lag times between hemifusion and fusion for a given particle (*blue circles*) for bilayers containing POPS (*A*) and BMP (*B*). Only the lag time between lipid and content transfer was significantly different between POPS and BMP ($p < 0.045$). *C*, distributions of the duration of mKO release (*i.e.* time from the onset of mKO signal decrease to reaching the background fluorescence level) that reflect the relative diameter of fusion pores. The total number of full fusion events was 17 for the POPS mixture (*red circles*) and 14 for the BMP mixture (*green circles*). No fusion events were observed for the POPC-based mixture lacking the anionic lipids.

are in full agreement with the previous report that BMP somewhat selectively facilitates VSV G-mediated lipid mixing with liposomes (31). However, in that study, the beneficial effect of BMP was observed in the background of 50% POPS, thus complicating the evaluation of relative roles of these lipids in VSVpp fusion. We found that, although BMP supported more efficient lipid mixing and faster conversion from hemifusion to full fusion than POPS, these differences were modest. In addition, the average time required to complete the release of viral content, which is inversely proportional to the size of a fusion pore (60), was identical for BMP and POPS bilayers. These findings argue against POPS as the specific receptor for VSV and highlight the potential direct role of BMP in entry of this virus.

The BMP content in late endosomes was reported to be as high as 15% of total phospholipids, with the POPC:BMP molar ratio ~3:1 (32) being close to the lipid composition of the SLB used in our study. By contrast, late endosomal membranes contain only 5% of PS (32), which appears to be even lower that the PS content of the plasma membrane (61, 62). Furthermore, because VSV infection is not inhibited by the PS-binding protein annexin V (22), it is unlikely that the incoming VSV encounters PS at the cell surface or during intracellular trafficking. On the other hand, recent evidence suggests a role for BMP in VSV entry from late endosomes (28). The observation that lipid mixing between VSV and endosomes is not attenuated by BMP depletion with specific antibodies (28) suggests that, similarly to dengue virus (30), VSV may undergo hemifusion with early endosomes. It is conceivable that complete fusion can be delayed until VSV enters into late compartments enriched in BMP (28). However, given the evidence that VSV enters from early endosomes (36, 63), further studies are required to test this model.

The relatively low probability of full fusion between VSVpp and SLBs containing BMP or POPS may be due to incorporation of fewer G proteins compared with *bona fide* VSV (64, 65). In addition, fusion with liposomes appears to occur at the base of a bullet-shaped VSV particle (65), suggesting that the architecture of the virus and perhaps the interactions between G and M proteins regulate the fusion activity. Another explanation for the poor fusion efficiency is that low pH and anionic lipids may not be the only factors required for VSV fusion. Future studies of single VSV fusion with lipid bilayers should distinguish between these possibilities.

Regardless of the lipid composition of SLBs tested in this study, hemifusion always preceded or full fusion. For some particles, the lag time from lipid mixing to the onset of content release reached several minutes. These results agree with previous data on influenza (45), HIV-1 (55) and avian sarcoma and leucosis virus (66) fusion and show that hemifusion is a true and long-lived intermediate stage of VSV G-mediated fusion. Note, however, that for 10% of single influenza virus fusion events with SLB, viral content transfer preceded lipid mixing (45). No explanation for this rather unusual phenotype has been offered by the authors. In addition, our experiments detected transient closing/shrinkage of fusion pores formed by VSV G, a phenomenon known as pore flickering (38, 56, 58, 59).

In conclusion, the SLB model offers a number of important advantages for mechanistic studies of viral fusion at the single particle level. Also, pseudotyping the MLV core with VSV G or other viral glycoproteins provides a universal platform for future mechanistic studies of single virus fusion. The virus labeling and imaging strategies introduced in this study enable detailed studies of the role of lipids at distinct intermediate steps of VSVpp fusion: hemifusion and formation of a small

fusion pore. Future studies should help delineate the effects of other anionic and neutral lipids, as well as lipid domains, in regulation of membrane fusion mediated by VSV G and other viral glycoproteins. It would also be interesting to assess the pH dependence of VSVpp-SLB hemifusion and fusion. Of particular relevance are the efficiency and kinetics of viral fusion at a higher pH, around 6.0, typical of early endosomes (67, 68). Because the pH threshold of VSV fusion is only somewhat higher than 6.0 (65, 69, 70), fusion experiments carried out at this suboptimal pH can accentuate the stimulating effect of various lipids and cofactors compared with the optimal pH of 5.5 employed in this study.

Acknowledgments—We thank Dr. Erdem Karatekin (Yale University) for expert advice on techniques for supported bilayer formation and Matthew Smith (Lehigh University) for helpful hints in using the Speckle TrackerJ. We also thank José Rino (Instituto de Medicina Molecular) and Tanay Desai (Emory University) for critical reading of the manuscript.

REFERENCES

1. Cohen, F. S., and Melikyan, G. B. (2004) The energetics of membrane fusion from binding, through hemifusion, pore formation, and pore enlargement. *J. Membr. Biol.* **199,** 1–14
2. Harrison, S. C. (2008) Viral membrane fusion. *Nat. Struct. Mol. Biol.* **15,** 690–698
3. Marsh, M., and Helenius, A. (2006) Virus entry. Open sesame. *Cell* **124,** 729–740
4. Miyauchi, K., Kim, Y., Latinovic, O., Morozov, V., and Melikyan, G. B. (2009) HIV enters cells via endocytosis and dynamin-dependent fusion with endosomes. *Cell* **137,** 433–444
5. de la Vega, M., Marin, M., Kondo, N., Miyauchi, K., Kim, Y., Epand, R. F., Epand, R. M., and Melikyan, G. B. (2011) Inhibition of HIV-1 endocytosis allows lipid mixing at the plasma membrane, but not complete fusion. *Retrovirology* **8,** 99
6. Akhtar, J., and Shukla, D. (2009) Viral entry mechanisms. Cellular and viral mediators of herpes simplex virus entry. *FEBS J.* **276,** 7228–7236
7. Kolokoltsov, A. A., Deniger, D., Fleming, E. H., Roberts, N. J., Jr., Karpilow, J. M., and Davey, R. A. (2007) Small interfering RNA profiling reveals key role of clathrin-mediated endocytosis and early endosome formation for infection by respiratory syncytial virus. *J. Virol.* **81,** 7786–7800
8. Carr, C. M., and Kim, P. S. (1993) A spring-loaded mechanism for the conformational change of influenza hemagglutinin. *Cell* **73,** 823–832
9. Earp, L. J., Delos, S. E., Park, H. E., and White, J. M. (2005) The many mechanisms of viral membrane fusion proteins. *Curr. Top. Microbiol. Immunol.* **285,** 25–66
10. Kielian, M., and Rey, F. A. (2006) Virus membrane-fusion proteins. More than one way to make a hairpin. *Nat. Rev. Microbiol.* **4,** 67–76
11. Melikyan, G. B. (2008) Common principles and intermediates of viral protein-mediated fusion. The HIV-1 paradigm. *Retrovirology* **5,** 111
12. White, J. M., Delos, S. E., Brecher, M., and Schornberg, K. (2008) Structures and mechanisms of viral membrane fusion proteins. Multiple variations on a common theme. *Crit. Rev. Biochem. Mol. Biol.* **43,** 189–219
13. Albertini, A. A., Baquero, E., Ferlin, A., and Gaudin, Y. (2012) Molecular and cellular aspects of rhabdovirus entry. *Viruses* **4,** 117–139
14. Backovic, M., and Jardetzky, T. S. (2009) Class III viral membrane fusion proteins. *Curr. Opin. Struct. Biol.* **19,** 189–196
15. Roche, S., Albertini, A. A., Lepault, J., Bressanelli, S., and Gaudin, Y. (2008) Structures of vesicular stomatitis virus glycoprotein. Membrane fusion revisited. *Cell. Mol. Life Sci.* **65,** 1716–1728
16. Blumenthal, R., Bali-Puri, A., Walter, A., Covell, D., and Eidelman, O. (1987) pH-dependent fusion of vesicular stomatitis virus with Vero cells. Measurement by dequenching of octadecyl rhodamine fluorescence. *J. Biol. Chem.* **262,** 13614–13619
17. Puri, A., Winick, J., Lowy, R. J., Covell, D., Eidelman, O., Walter, A., and Blumenthal, R. (1988) Activation of vesicular stomatitis virus fusion with cells by pretreatment at low pH. *J. Biol. Chem.* **263,** 4749–4753
18. Gaudin, Y., Tuffereau, C., Segretain, D., Knossow, M., and Flamand, A. (1991) Reversible conformational changes and fusion activity of rabies virus glycoprotein. *J. Virol.* **65,** 4853–4859
19. Gaudin, Y. (2000) Reversibility in fusion protein conformational changes. The intriguing case of rhabdovirus-induced membrane fusion. *Subcell. Biochem.* **34,** 379–408
20. Carneiro, F. A., Bianconi, M. L., Weissmüller, G., Stauffer, F., and Da Poian, A. T. (2002) Membrane recognition by vesicular stomatitis virus involves enthalpy-driven protein-lipid interactions. *J. Virol.* **76,** 3756–3764
21. Eidelman, O., Schlegel, R., Tralka, T. S., and Blumenthal, R. (1984) pH-dependent fusion induced by vesicular stomatitis virus glycoprotein reconstituted into phospholipid vesicles. *J. Biol. Chem.* **259,** 4622–4628
22. Schlegel, R., Tralka, T. S., Willingham, M. C., and Pastan, I. (1983) Inhibition of VSV binding and infectivity by phosphatidylserine. Is phosphatidylserine a VSV-binding site? *Cell* **32,** 639–646
23. Schlegel, R., and Wade, M. (1983) Neutralized vesicular stomatitis virus binds to host cells by a different "receptor." *Biochem. Biophys. Res. Commun.* **114,** 774–778
24. Coil, D. A., and Miller, A. D. (2004) Phosphatidylserine is not the cell surface receptor for vesicular stomatitis virus. *J. Virol.* **78,** 10920–10926
25. Puri, A., Grimaldi, S., and Blumenthal, R. (1992) Role of viral envelope sialic acid in membrane fusion mediated by the vesicular stomatitis virus envelope glycoprotein. *Biochemistry* **31,** 10108–10113
26. Waheed, A. A., and Freed, E. O. (2010) The role of lipids in retrovirus replication. *Viruses* **2,** 1146–1180
27. Kobayashi, T., Stang, E., Fang, K. S., de Moerloose, P., Parton, R. G., and Gruenberg, J. (1998) A lipid associated with the antiphospholipid syndrome regulates endosome structure and function. *Nature* **392,** 193–197
28. Le Blanc, I., Luyet, P. P., Pons, V., Ferguson, C., Emans, N., Petiot, A., Mayran, N., Demaurex, N., Fauré, J., Sadoul, R., Parton, R. G., and Gruenberg, J. (2005) Endosome-to-cytosol transport of viral nucleocapsids. *Nat. Cell Biol.* **7,** 653–664
29. Luyet, P. P., Falguières, T., Pons, V., Pattnaik, A. K., and Gruenberg, J. (2008) The ESCRT-I subunit TSG101 controls endosome-to-cytosol release of viral RNA. *Traffic* **9,** 2279–2290
30. Zaitseva, E., Yang, S. T., Melikov, K., Pourmal, S., and Chernomordik, L. V. (2010) Dengue virus ensures its fusion in late endosomes using compartment-specific lipids. *PLoS Pathog.* **6,** e1001131
31. Roth, S. L., and Whittaker, G. R. (2011) Promotion of vesicular stomatitis virus fusion by the endosome-specific phospholipid bis(monoacylglycero)-phosphate (BMP). *FEBS Lett.* **585,** 865–869
32. Kobayashi, T., Beuchat, M. H., Chevallier, J., Makino, A., Mayran, N., Escola, J. M., Lebrand, C., Cosson, P., Kobayashi, T., and Gruenberg, J. (2002) Separation and characterization of late endosomal membrane domains. *J. Biol. Chem.* **277,** 32157–32164
33. Abrami, L., Lindsay, M., Parton, R. G., Leppla, S. H., and van der Goot, F. G. (2004) Membrane insertion of anthrax protective antigen and cytoplasmic delivery of lethal factor occur at different stages of the endocytic pathway. *J. Cell Biol.* **166,** 645–651
34. van der Goot, F. G., and Gruenberg, J. (2006) Intra-endosomal membrane traffic. *Trends Cell Biol.* **16,** 514–521
35. Sieczkarski, S. B., and Whittaker, G. R. (2003) Differential requirements of Rab5 and Rab7 for endocytosis of influenza and other enveloped viruses. *Traffic* **4,** 333–343
36. Johannsdottir, H. K., Mancini, R., Kartenbeck, J., Amato, L., and Helenius, A. (2009) Host cell factors and functions involved in vesicular stomatitis virus entry. *J. Virol.* **83,** 440–453
37. Brandenburg, B., and Zhuang, X. (2007) Virus trafficking. Learning from single-virus tracking. *Nat. Rev. Microbiol.* **5,** 197–208
38. Melikyan, G. B., Barnard, R. J., Abrahamyan, L. G., Mothes, W., and Young, J. A. (2005) Imaging individual retroviral fusion events. From hemifusion to pore formation and growth. *Proc. Natl. Acad. Sci. U.S.A.* **102,** 8728–8733
39. Koch, P., Lampe, M., Godinez, W. J., Müller, B., Rohr, K., Kräusslich, H. G.,

and Lehmann, M. J. (2009) Visualizing fusion of pseudotyped HIV-1 particles in real time by live cell microscopy. *Retrovirology* **6,** 84
40. Padilla-Parra, S., Matos, P. M., Kondo, N., Marin, M., Santos, N. C., and Melikyan, G. B. (2012) Quantitative imaging of endosome acidification and single retrovirus fusion with distinct pools of early endosomes. *Proc. Natl. Acad. Sci. U.S.A.* **109,** 17627–17632
41. Karatekin, E., Di Giovanni, J., Iborra, C., Coleman, J., O'Shaughnessy, B., Seagar, M., and Rothman, J. E. (2010) A fast, single-vesicle fusion assay mimics physiological SNARE requirements. *Proc. Natl. Acad. Sci. U.S.A.* **107,** 3517–3521
42. Fix, M., Melia, T. J., Jaiswal, J. K., Rappoport, J. Z., You, D., Söllner, T. H., Rothman, J. E., and Simon, S. M. (2004) Imaging single membrane fusion events mediated by SNARE proteins. *Proc. Natl. Acad. Sci. U.S.A.* **101,** 7311–7316
43. Bowen, M. E., Weninger, K., Brunger, A. T., and Chu, S. (2004) Single molecule observation of liposome-bilayer fusion thermally induced by soluble *N*-ethyl maleimide sensitive-factor attachment protein receptors (SNAREs). *Biophys. J.* **87,** 3569–3584
44. Costello, D. A., Lee, D. W., Drewes, J., Vasquez, K. A., Kisler, K., Wiesner, U., Pollack, L., Whittaker, G. R., and Daniel, S. (2012) Influenza virus-membrane fusion triggered by proton uncaging for single particle studies of fusion kinetics. *Anal. Chem.* **84,** 8480–8489
45. Floyd, D. L., Ragains, J. R., Skehel, J. J., Harrison, S. C., and van Oijen, A. M. (2008) Single-particle kinetics of influenza virus membrane fusion. *Proc. Natl. Acad. Sci. U.S.A.* **105,** 15382–15387
46. Wessels, L., Elting, M. W., Scimeca, D., and Weninger, K. (2007) Rapid membrane fusion of individual virus particles with supported lipid bilayers. *Biophys. J.* **93,** 526–538
47. Kimpton, J., and Emerman, M. (1992) Detection of replication-competent and pseudotyped human immunodeficiency virus with a sensitive cell line on the basis of activation of an integrated β-galactosidase gene. *J. Virol.* **66,** 2232–2239
48. Sherer, N. M., Lehmann, M. J., Jimenez-Soto, L. F., Ingmundson, A., Horner, S. M., Cicchetti, G., Allen, P. G., Pypaert, M., Cunningham, J. M., and Mothes, W. (2003) Visualization of retroviral replication in living cells reveals budding into multivesicular bodies. *Traffic* **4,** 785–801
49. Karatekin, E., and Rothman, J. E. (2012) Fusion of single proteoliposomes with planar, cushioned bilayers in microfluidic flow cells. *Nat. Protoc.* **7,** 903–920
50. Brian, A. A., and McConnell, H. M. (1984) Allogeneic stimulation of cytotoxic T cells by supported planar membranes. *Proc. Natl. Acad. Sci. U.S.A.* **81,** 6159–6163
51. Kenworthy, A. K. (2007) Fluorescence recovery after photobleaching studies of lipid rafts. *Methods Mol. Biol.* **398,** 179–192
52. Soumpasis, D. M. (1983) Theoretical analysis of fluorescence photobleaching recovery experiments. *Biophys. J.* **41,** 95–97
53. Smith, M. B., Karatekin, E., Gohlke, A., Mizuno, H., Watanabe, N., and Vavylonis, D. (2011) Interactive, computer-assisted tracking of speckle trajectories in fluorescence microscopy. Application to actin polymerization and membrane fusion. *Biophys. J.* **101,** 1794–1804
54. Karasawa, S., Araki, T., Nagai, T., Mizuno, H., and Miyawaki, A. (2004) Cyan-emitting and orange-emitting fluorescent proteins as a donor/acceptor pair for fluorescence resonance energy transfer. *Biochem. J.* **381,** 307–312
55. Markosyan, R. M., Cohen, F. S., and Melikyan, G. B. (2005) Time-resolved imaging of HIV-1 Env-mediated lipid and content mixing between a single virion and cell membrane. *Mol. Biol. Cell* **16,** 5502–5513
56. Melikyan, G. B., Niles, W. D., Peeples, M. E., and Cohen, F. S. (1993) Influenza hemagglutinin-mediated fusion pores connecting cells to planar membranes. Flickering to final expansion. *J. Gen. Physiol.* **102,** 1131–1149
57. Spruce, A. E., Iwata, A., and Almers, W. (1991) The first milliseconds of the pore formed by a fusogenic viral envelope protein during membrane fusion. *Proc. Natl. Acad. Sci. U.S.A.* **88,** 3623–3627
58. Spruce, A. E., Iwata, A., White, J. M., and Almers, W. (1989) Patch clamp studies of single cell-fusion events mediated by a viral fusion protein. *Nature* **342,** 555–558
59. Markosyan, R. M., Cohen, F. S., and Melikyan, G. B. (2000) The lipid-anchored ectodomain of influenza virus hemagglutinin (GPI-HA) is capable of inducing nonenlarging fusion pores. *Mol. Biol. Cell* **11,** 1143–1152
60. Padilla-Parra, S., Marin, M., Kondo, N., and Melikyan, G. B. (2012) Synchronized retrovirus fusion in cells expressing alternative receptor isoforms releases the viral core into distinct sub-cellular compartments. *PLoS Pathog.* **8,** e1002694
61. Leventis, P. A., and Grinstein, S. (2010) The distribution and function of phosphatidylserine in cellular membranes. *Annu. Rev. Biophys.* **39,** 407–427
62. Leidl, K., Liebisch, G., Richter, D., and Schmitz, G. (2008) Mass spectrometric analysis of lipid species of human circulating blood cells. *Biochim. Biophys. Acta* **1781,** 655–664
63. Mire, C. E., White, J. M., and Whitt, M. A. (2010) A spatio-temporal analysis of matrix protein and nucleocapsid trafficking during vesicular stomatitis virus uncoating. *PLoS Pathog.* **6,** e1000994
64. Ge, P., Tsao, J., Schein, S., Green, T. J., Luo, M., and Zhou, Z. H. (2010) Cryo-EM model of the bullet-shaped vesicular stomatitis virus. *Science* **327,** 689–693
65. Libersou, S., Albertini, A. A., Ouldali, M., Maury, V., Maheu, C., Raux, H., de Haas, F., Roche, S., Gaudin, Y., and Lepault, J. (2010) Distinct structural rearrangements of the VSV glycoprotein drive membrane fusion. *J. Cell Biol.* **191,** 199–210
66. Jha, N. K., Latinovic, O., Martin, E., Novitskiy, G., Marin, M., Miyauchi, K., Naughton, J., Young, J. A., and Melikyan, G. B. (2011) Imaging single retrovirus entry through alternative receptor isoforms and intermediates of virus-endosome fusion. *PLoS Pathog.* **7,** e1001260
67. Sieczkarski, S. B., and Whittaker, G. R. (2002) Dissecting virus entry via endocytosis. *J. Gen. Virol.* **83,** 1535–1545
68. Mercer, J., Schelhaas, M., and Helenius, A. (2010) Virus entry by endocytosis. *Annu. Rev. Biochem.* **79,** 803–833
69. Fredericksen, B. L., and Whitt, M. A. (1996) Mutations at two conserved acidic amino acids in the glycoprotein of vesicular stomatitis virus affect pH-dependent conformational changes and reduce the pH threshold for membrane fusion. *Virology* **217,** 49–57
70. Shokralla, S., He, Y., Wanas, E., and Ghosh, H. P. (1998) Mutations in a carboxy-terminal region of vesicular stomatitis virus glycoprotein G that affect membrane fusion activity. *Virology* **242,** 39–50

Supplementary Figure and Movie Legends

Supplementary Figure 1. Mean fluorescence intensity (MFI) profiles of VSV G pseudoparticles that failed to undergo hemifusion or fusion at low pH. The relatively stable signals from single particles indicate that photobleaching occurred at a significantly lower (in some cases undetectable) rate than loss of fluorescence due to DiD or mKO release. Two representative traces are shown for each lipid composition: POPC (A-B), POPS (C-D) and BMP (E-F). Note that quenching of the CF-PE fluorescence upon acidification was often associated with concomitant reduction in the mKO signal due to a spectral bleed through.

Supplementary Movie 1. Complete fusion of a VSV G pseudovirus with BMP-containing bilayers. A pseudovirus co-labeled with DiD (red) and NC-mKO (green) is marked by a white arrow (see the corresponding Figure 2C showing a sub-area from this movie). The size of the area shown here is 30×30 μm. DiD signal is in red and NC-mKO signal in green (the CF-PE fluorescence is not shown for clarity). The frame rate is 10 fps.

Supplementary Movie 2. Hemifusion of a VSV G pseudovirus with BMP-containing bilayer. Images of a pseudovirus co-labeled with DiD (red) and NC-mKO (green) correspond to Figure 2D, but show a somewhat larger area (24×24 μm). The CF-PE signal is not shown for clarity. The frame rate is 10 fps.

SUPPLEMENTARY FIGURE 1

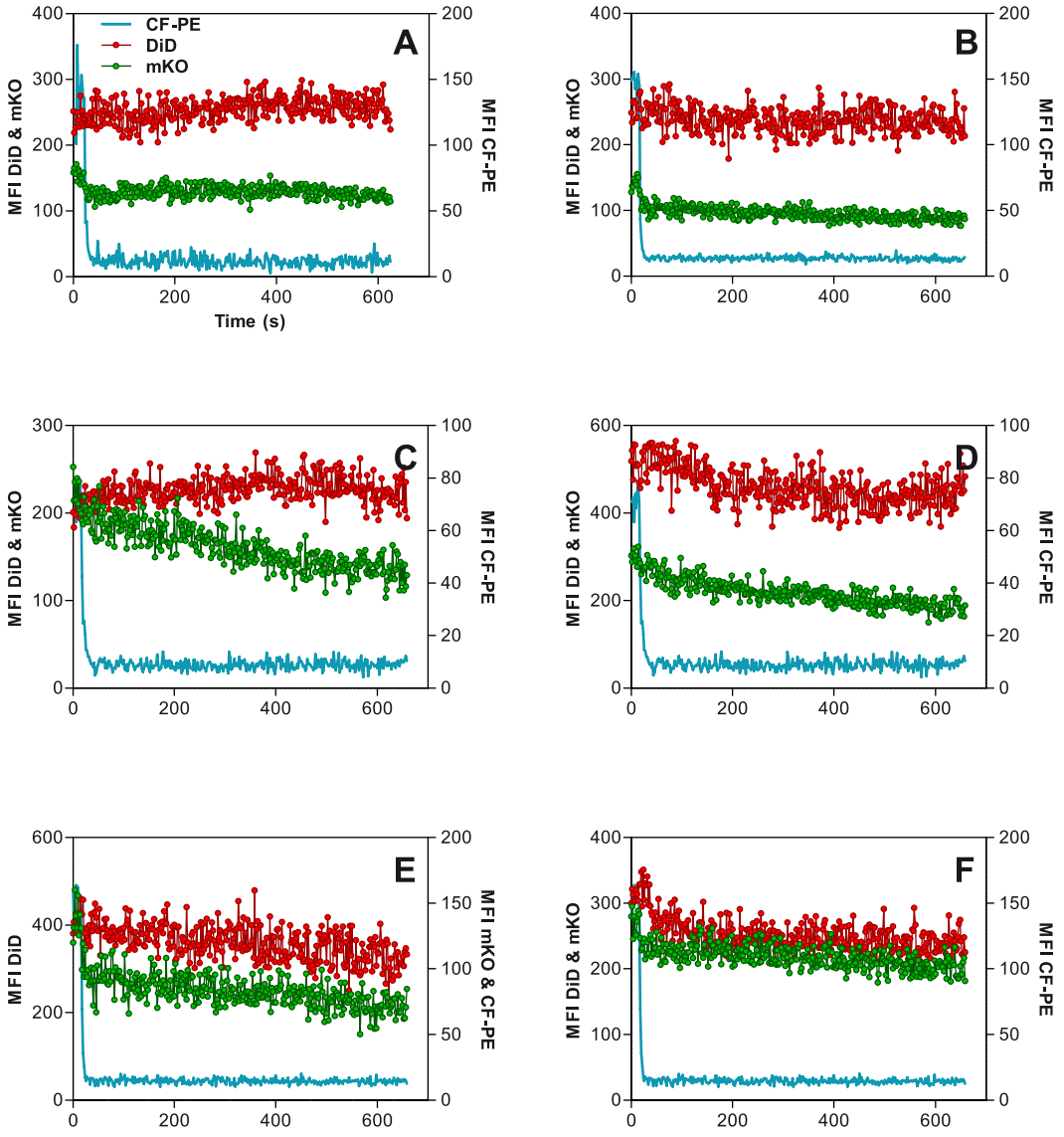

V

Imaging of endosome acidification and single retrovirus trafficking and fusion

Overview

Visualizing the capture and intracellular voyage of a virus is a challenging task that has become possible with the improvements in microscopes, fluorescent dyes and fluorescent proteins technologies. In this chapter, we present a study that follows the ASLV internalization though the endosomes until it fuses, observed by the fluorescent capsid release. We engineered the virus to have a fluorescent protein pair mTFP1-eYFP in its envelope, which allowed quantitative imaging of the pH variations along the viral path. The results shed new light on the entry pathway of the virus and on endosome dynamics.

This work was done at Emory Childen's Center of Emory University, in Atlanta, USA, with the supervision of Prof. Gregory Melikyan.

Article F

Padilla-Parra S, Matos PM, Kondo N, Marin M, Santos NC, Melikyan GB. Quantitative imaging of endosome acidification and single retrovirus fusion with distinct pools of early endosomes. *Proc. Natl. Acad. Sci. U.S.A.* **109**:17627-17632 (2012).

Article F

Declaration of authorship

I, Pedro Miguel Baptista de Matos, declare that I performed part of the experimental work of pH calibration curve and imaging of virus fusion with cells and assisted in some analysis of the data. Dr. Sergi Padilla-Parra planned the experimental design, did the majority of experimental work and analysis, Dr. Naoyuki Kondo and Prof. Mariana Marin produced the viruses and helped in the experiments. Prof. Gregory Melikyan supervised the work for the planning of experimental design, data analysis and manuscript writing. Prof. Nuno Santos helped with the experimental design and manuscript writing. All authors were involved in the manuscript writing.

I, Nuno C. Santos, as supervisor of Pedro Matos and one of the authors of the manuscript mentioned above, hereby acknowledge and confirm that the information above is correct.

I, Gregory Melikyan, as corresponding author of the article mentioned above, hereby acknowledge and confirm that the information above is correct.

Pedro M. Matos | Nuno C. Santos | Gregory Melikyan

Quantitative imaging of endosome acidification and single retrovirus fusion with distinct pools of early endosomes

Sergi Padilla-Parra[a,1], Pedro M. Matos[b], Naoyuki Kondo[a], Mariana Marin[a], Nuno C. Santos[b], and Gregory B. Melikyan[a,c,2]

[a]Department of Pediatrics, Division of Infectious Diseases, Emory Children's Center, Atlanta, GA 30322; [b]Unidade de Biomembranas, Instituto de Medicina Molecular, Faculdade de Medicina da Universidade de Lisboa, 1649-028 Lisbon, Portugal; and [c]Children's Healthcare of Atlanta, Atlanta, GA 30322

Edited by Peter Palese, Mount Sinai School of Medicine, New York, NY, and approved September 19, 2012 (received for review July 10, 2012)

Diverse enveloped viruses enter host cells through endocytosis and fuse with endosomal membranes upon encountering acidic pH. Currently, the pH dynamics in virus-carrying endosomes and the relationship between acidification and viral fusion are poorly characterized. Here, we examined the entry of avian retrovirus that requires two sequential stimuli—binding to a cognate receptor and low pH—to undergo fusion. A genetically encoded sensor incorporated into the viral membrane was used to measure the pH in virus-carrying endosomes. Acid-induced virus fusion was visualized as the release of a fluorescent viral content marker into the cytosol. The pH values in early acidic endosomes transporting the virus ranged from 5.6 to 6.5 but were relatively stable over time for a given vesicle. Analysis of viral motility and luminal pH showed that cells expressing the transmembrane isoform of the receptor (TVA950) preferentially sorted the virus into slowly trafficking, less acidic endosomes. In contrast, viruses internalized by cells expressing the GPI-anchored isoform (TVA800) were uniformly distributed between stationary and mobile compartments. We found that the lag times between acidification and fusion were significantly shorter and fusion pores were larger in dynamic endosomes than in more stationary compartments. Despite the same average pH within mobile compartments of cells expressing alternative receptor isoforms, TVA950 supported faster fusion than TVA800 receptor. Collectively, our results suggest that fusion steps downstream of the low-pH trigger are modulated by properties of intracellular compartments harboring the virus.

confocal imaging | nano-pH-meter | single virus tracking | FRET

Many enveloped viruses use endocytosis and vesicular trafficking to enter host cells, where acidification of an endosomal lumen serves as a trigger for viral fusion (1, 2). Viral fusion proteins are fine-tuned to respond to different pH values. Those that are activated at less acidic pH (~6.0) are thought to mediate fusion with early endosomes, whereas those with a lower pH threshold (~5.0) appear to direct the virus entry from late endosomes (1, 3). However, recent evidence implies that factors other than low pH, such as specific endosome-resident lipids, can determine the intracellular compartments from which the viral capsid is released into the cytosol (2, 4, 5). Progress in understanding the complex regulation of virus–endosome fusion has been hindered by poor accessibility of intracellular compartments and lack of direct techniques for monitoring this process in situ.

Single-virus imaging is a powerful tool for gaining critical insights into virus entry (reviewed in ref. 6), but detection of virus–endosome fusion (here defined as the release of viral content into the cytoplasm) is technically challenging (7, 8). To understand the relationship between the pH trigger and virus–endosome fusion, it is essential to visualize these events in real time. A ratiometric method developed by the Zhuang group (9, 10) permits monitoring endosomal pH around single influenza viruses colabeled with pH-sensitive and pH-insensitive fluorescent markers. However, simultaneous measurements of the pH drop and the resulting virus fusion have not been reported so far.

We previously developed tools to visualize virus uptake (11) and to detect single retrovirus–endosome fusion (7, 8, 12) for differently labeled viruses in separate experiments. Here, we incorporated a FRET-based pH sensor into the membrane of the avian sarcoma and leukosis virus (ASLV) and loaded virions with a fluorescent content marker. This technique permitted simultaneous measurements of the pH in virus-carrying endosomes and the kinetics of postacidification steps of fusion. Analyses of acidification and movement patterns of virus-carrying endosomes indicated that ASLV entered two distinct pools of endosomes: slow moving and generally less acidic or dynamic and more acidic compartments. The rate of virus fusion depended on the pH and endosome motility and on the ASLV receptor isoform. For the same pH value, the kinetics of fusion and sizes of nascent fusion pores differed in cells expressing alternative isoforms of the ASLV receptor, which appear to target the virus entry through distinct endocytic routes (13, 14). These findings suggest that late steps of ASLV entry are modulated by properties of intracellular membranes.

Results

Genetically Engineered Sensor for Single Virus-Based pH Measurements. We previously visualized virus entry into acidic endosomes by incorporating a membrane-anchored ecliptic pHluorin (15) into the viral membrane (7, 11). The nearly complete quenching of the ecliptic pHluorin signal at pH below 6.2 marked the ASLV entry into mildly acidic compartments but did not allow quantitative measurements of endosomal pH. To enable simultaneous measurements of endosomal pH and ASLV fusion, we used a modified version of the FRET-based pH sensor, pHlameleon (16). The CFP (donor) module of pHlameleon was replaced with the monomeric teal fluorescent protein, mTFP1 (Fig. 1*A*) (17). The higher photostability and brightness of mTFP1 compared with CFP make this protein more suitable for single-virus imaging. The mTFP1-eYFP tandem was appended to the N terminus of the transmembrane domain of human ICAM-1 (Fig. 1*A*), which is known to incorporate selectively into retroviral particles (e.g., ref. 18). As we have demonstrated previously (7, 11), coexpression of ICAM-1–anchored fluorescent proteins with viral structural proteins results in efficient labeling of the viral membrane. Labeled viruses

Author contributions: S.P.-P., N.C.S., and G.B.M. designed research; S.P.-P, P.M.M., and N.K. performed research; N.K. and M.M. contributed new reagents/analytic tools; S.P.-P. and G.B.M. analyzed data; and S.P.-P., P.M.M., N.K., M.M., N.C.S., and G.B.M. wrote the paper.

The authors declare no conflict of interest.

This article is a PNAS Direct Submission.

[1]Present address: Institut de Génétique et Développement de Rennes, Unité Mixte de Recherche 6290 Centre National de la Recherche Scientifique - Université Rennes 1, 35043 Rennes Cedex, France.

[2]To whom correspondence should be addressed. E-mail: gmeliki@emory.edu.

This article contains supporting information online at www.pnas.org/lookup/suppl/doi:10.1073/pnas.1211714109/-/DCSupplemental.

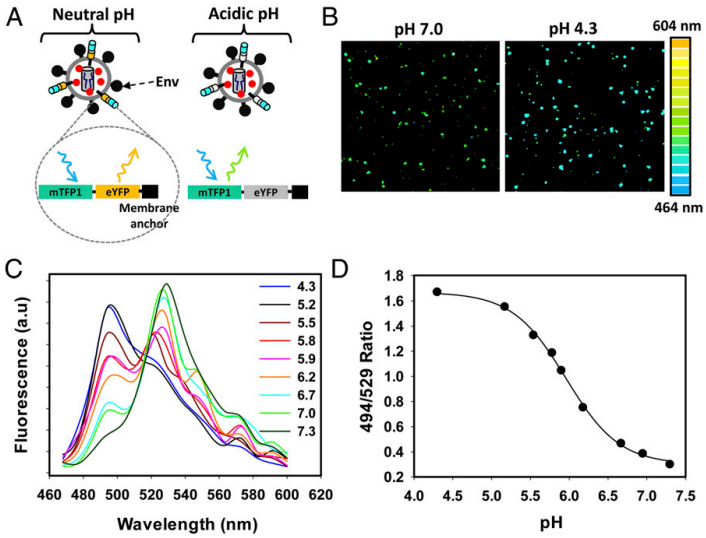

Fig. 1. Construction of pH-sensing ASLV particles and pH measurements. (*A*) Drawings of triple-labeled ASLV viruses bearing a pH-sensor in their membranes at different pH. The sensor consisted of a CFP (mTFP1) attached to an eYFP by a short linker (shown respectively as colored cylinders or boxes on the enlarged diagram), which was in turn fused to the N terminus of the ICAM-1 transmembrane domain. The virus interior was labeled with the MLV Gag-mKate2 (red dots). (*Left*) At basic pH, mTFP1 is poorly fluorescent because of FRET, which is manifested in intense sensitized eYFP emission. (*Right*) In an acidic environment, eYFP fluorescence is quenched (gray cylinders or boxes), and FRET is disrupted, leading to an increase in the mTFP1 signal. (*B*) The pH-dependent spectral shift in the tandem protein emission. ASLV pseudoviruses colabeled with mTFP1-eYFP-ICAM and Gag-mKate2 were allowed to adhere to poly-L-lysine–coated coverslips and were imaged at room temperature in citrate/phosphate buffers adjusted to different pH values. Representative micrographs taken at neutral pH (*Left*) and acidic pH (*Right*) are shown along with the coloring chart. The mKate2 fluorescence is not included for visual clarity. (*C*) The mTFP1-eYFP-ICAM emission spectra as a function of pH. (*D*) The calibration curve obtained by plotting the average ratio of the mTFP1 and eYFP signals from all viruses in the image field at different pH.

were immobilized on poly-L-lysine–coated coverslips and imaged using a Zeiss LSM780 confocal microscope in spectral mode (Fig. 1*B*). At basic pH, mTFP1 fluorescence is weak because of efficient FRET between donor and acceptor eYFP (Fig. S1 and ref. 19). Low pH markedly reduces sensitized emission of eYFP (pK_a 7.1) (20) by shifting its absorption peak (21) (Fig. 1 *B* and *C*) and thereby increases the signal from relatively pH-insensitive mTFP1 (pK_a 4.3) (17).

To determine the relationship between the pH and emission spectrum of the mTFP1-eYFP sensor, viruses were imaged in solutions of different acidity (Fig. 1 *B* and *C*). To ensure that the measured signal was from viruses, particles were colabeled with the content marker, murine leukemia virus (MLV) Gag-mKate2 (red emission). Only puncta positive for all three labels, mTFP1, eYFP, and mKate2, were analyzed, yielding the calibration curve that related the mTFP1/eYFP emission ratio to the external pH (Fig. 1*D*). The observed spectral shift in the tandem protein fluorescence enabled sensitive pH measurements in individual ASLV-carrying endosomes within a physiologically relevant range. Normally, FRET measurements using sensitized emission require corrections for direct excitation of the acceptor by the 458-nm laser line and spectral bleed-through (donor photons detected in the acceptor channel). However, for intramolecular FRET between the tandem mTFP1-eYFP proteins, the donor/acceptor stoichiometry and their emission ratio are fixed, thus providing a reliable direct measure of pH based on the emission ratio (17).

Imaging the pH Drop in a Single-Virus–Carrying Endosome and Viral Content Release into the Cytosol. Subtype A ASLV envelope glycoprotein (EnvA) becomes competent to mediate low-pH–dependent membrane fusion only after binding to the avian tumor virus receptor A (TVA receptor) (22, 23). Both isoforms of this receptor, the transmembrane (TVA950) and GPI-anchored (TVA800) proteins (24), support ASLV fusion but appear to direct the virus entry through different endocytic routes (13, 14). To determine the timing and the strength of the pH trigger that activates the receptor-primed ASLV entering through different routes, we imaged fusion of triple-labeled pseudoviruses into cells expressing either TVA800 or TVA950. Viruses were prebound to cells under cold conditions, and their entry was initiated by raising the temperature. ASLV internalization and delivery into acidic endosomes resulted in diminution of the eYFP signal and concomitant increase of the mTFP1 fluorescence (Fig. 2). These changes could be seen readily as a white-to-purple shift in the virus color (Fig. 2, a–b transitions). For most virions, endosomal pH dropped fairly quickly (<20 s) and usually stabilized around pH 6.0 (Fig. 2 *B* and *C* and Fig. S2).

Low-pH–dependent ASLV fusion was detected based on the loss of the viral content marker, nucleocapsid-mKate2, a product of the MLV Gag-mKate2 cleavage occurring upon virus maturation (Fig. 2) (25). We found that ~20% of triple-labeled particles fused with acidic endosomes, as evidenced by the quick loss of the mKate2 signal following the pH drop (Fig. 2, b–c transitions). In contrast to eYFP, the more acid-resistant mTFP1 signal persisted under acidic conditions and thus continued to mark the viral membrane after fusion took place. Similar acidification and fusion patterns were observed in cells expressing TVA950 and TVA800 (Fig. 2 *B* and *C*). Fusion was not detected in control experiments performed in the presence of a fully inhibitory dose (0.1 mg/mL) of the ASLV EnvA-derived R99 peptide (26). Thus we were able to measure the pH dynamics in virus-carrying endosomes and detect ASLV fusion in the same experiment.

Endosome Acidity and pH-Dependence of ASLV Fusion Are Not Affected by TVA Isoforms. Analysis of the changes in fluorescence of the virus-borne pH-sensor showed that acidity of individual endosomes was fairly stable over time (Fig. S2). We did not detect further acidification of lumen for as long as we could reliably measure the pH (usually up to 20 min, at which point most viruses entered the autofluorescent perinuclear area). Steady luminal pH aided more precise determination of this parameter for each vesicle by averaging the mTFP1/eYFP ratio signal (Fig. 2 *B* and *C*). The time-averaged values of pH in virus-carrying endosomes were broadly distributed (Fig. 3*A*, circles), and its mean value before fusion was independent of the receptor isoform: 5.98 ± 0.16 (n = 39) for TVA800 and 5.99 ± 0.14 (n = 57) for TVA950 cells (Fig. 3*A*, diamonds). The fraction of fusion events as a function of pH was distributed normally, with most events occurring between pH 5.8 and 6.1 (Fig. 3*B*, black and open bars).

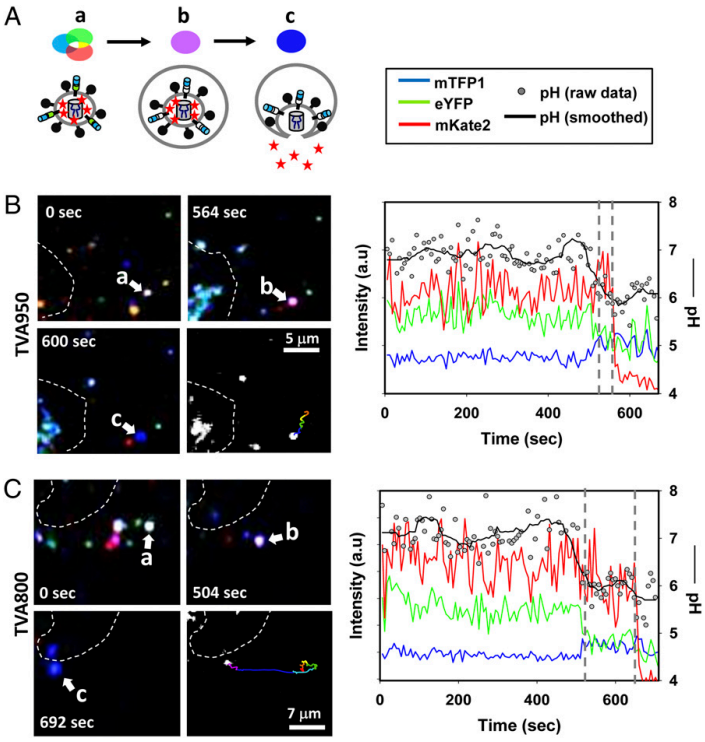

Fig. 2. Measuring the pH drop in ASLV-carrying endosomes and virus–endosome fusion. (*A*) Diagram of ASLV colabeled with mTFP1-eYFP-ICAM and Gag-mKate2 (*a*) and of the color changes associated with virus entry into acidic endosomes (*b*) and fusion (*c*). (*B* and *C*) Triple-labeled ASLV pseudoviruses (appearing as white puncta) were prebound to CV-1 cells expressing either TVA950 (*B*) or TVA800 (*C*) in the cold, and fusion was initiated by shifting to 37 °C. The mTFP1 fluorescence is shown in blue, the sensitized eYFP emission in green, and the mKate2 signal in red. Image panels represent consecutive snapshots of viruses before internalization (marked "a"), immediately after entry into acidic endosomes (purple puncta, "b"), and after fusion, which results in the release of mKate2 (blue puncta, "c"). White dashed lines in images *B* and *C* outline the cell nucleus. The lower left panels in *B* and *C* show the particle's trajectory pseudocolored according to the time from the onset of the experiment (see corresponding Movies S1 and S2). The graphs show the fluorescence intensities of viral markers as a function of time obtained by single-particle tracking using the mTFP1 channel. Endosomal pH (gray dots) and smoothed pH data (black lines) are shown also. Vertical gray dashed lines illustrate the lag time between acidification and fusion.

The reduced number of fusion events at more acidic pH (Fig. 3*B*) apparently was caused by the lower abundance of virus carriers with luminal pH below 5.8. This notion was verified by measuring the pH distribution around triple-labeled particles that entered acidic compartments but failed to fuse (Fig. 3*B*): Only a minor fraction of fusion-incompetent viruses were exposed to pH <5.8. On the other hand, the low occurrence of fusion events relative to the virus delivery into less acidic compartments (pH >6.2) likely reflects suboptimal activation of receptor-primed EnvA. This result is in agreement with the pH threshold of ~6.2 obtained from ensemble measurements of ASLV fusion (27) and from ASLV EnvA-mediated cell–cell fusion (28).

The mean pH in endosomes carrying nonfusogenic viruses was 6.10 ± 0.19 (n = 46) and 6.10 ± 0.22 (n = 43) in TVA800 and TVA950 cells, respectively. These values were significantly higher (P < 0.022) than the average pH in endosomes transporting fusion-competent viruses. Assuming that all endocytosed virions are fusion competent, one can estimate the pH-dependence of fusion by normalizing the number of viral content release events to the number of internalized particles (from Fig. 3*B*) across the pH range. ASLV fusion with TVA800 and TVA950 cells exhibited similar pH-dependence (Fig. 3*C*), indicating that both receptor isoforms efficiently primed EnvA for low-pH–induced fusion. The obtained pH-dependence of ASLV–endosome fusion appeared less steep than for EnvA-mediated cell–cell fusion, which reached the maximal level below pH 5.7 (28; see also ref. 27).

ASLV Enters and Fuses with Distinct Populations of Endosomes. Visual inspection of fusion events showed that a fraction of viruses entered acidic endosomes and released their content without undergoing considerable displacement from their initial position on the cell surface (Fig. 2*B*). In contrast, other particles moved quickly before being exposed to low pH and undergoing fusion. Because endosome acidification is coupled to their retrograde trafficking (29), we explored the relationship between endosome motility and luminal pH. Viruses/endosomes that moved faster than an arbitrary threshold (set at 0.5 μm/s) for at least two consecutive frames before or at the time of fusion were regarded as "fast" (Fig. 3*D* and Fig. S3). This relatively fast and directional movement is typical for trafficking along microtubules (10). Particles that did not reach the threshold velocity were designated "slow" In both cell lines, rapid movement correlated with acidification and usually occurred within 1 min from the pH drop (Fig. S3*C*). Interestingly, the average pH was significantly higher in slow endosomes than in fast compartments. Fast and slow endosomes in TVA800 cells exhibited average pH values of 6.04 ± 0.16 (n = 20) and 5.92 ± 0.15 (n = 19), respectively (P = 0.022) (Fig. 3*A*, squares). Likewise, slow endosomes in TVA950 cells were less acidic than fast endosomes: 6.02 ± 0.15 (n = 35) vs. 5.93 ± 0.13 (n = 14) (P = 0.048). The differences in average pH and different motion patterns of fast and slow endosomes suggest these endosomes are distinct, perhaps corresponding to quickly and slowly maturing pools of vesicles, respectively (9).

Velocity analysis for all triple-labeled particles, irrespective of whether they underwent fusion, revealed that the number of internalized ASLV was divided nearly evenly between fast and slow endosomes in both TVA800 and TVA950 cells. However, although the number of fusion events in TVA800 cells also was equally distributed between the two populations of endosomes, ASLV fused less frequently with fast endosomes in TVA950 cells (Fig. 3*E*). If fusing and nonfusing viruses are sorted similarly by TVA950 cells, the less frequent fusion with fast endosomes

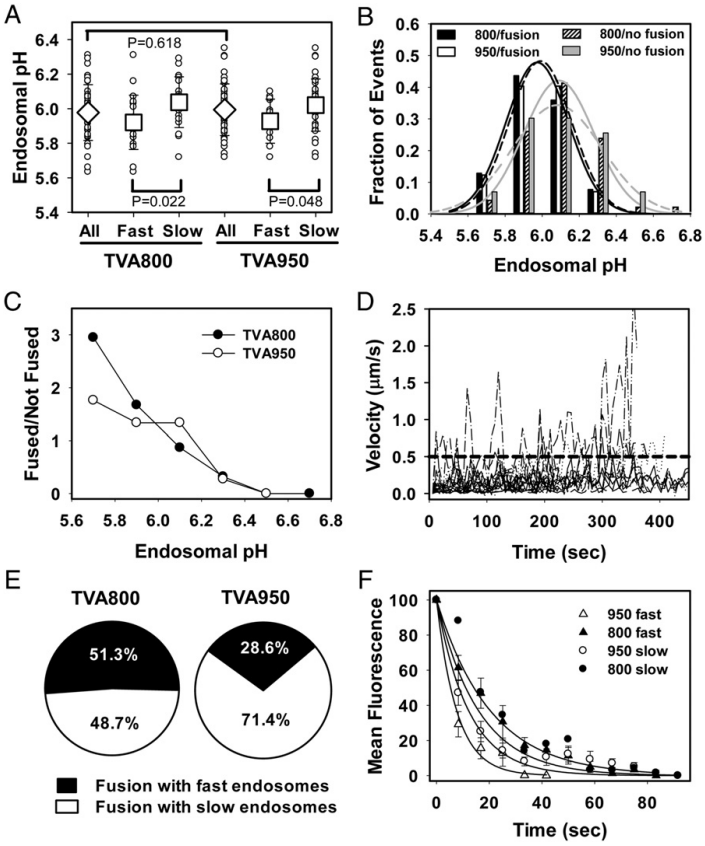

Fig. 3. Distribution of endosomal pH and pH-dependence of ASLV fusion. (*A*) Distributions of pH in virus-carrying endosomes in TVA800 and TVA950 cells from 10 independent experiments performed for each cell line. Mean pH values (diamonds) and scatterplots of individual pH values (circles) are shown. Also shown are the mean pH (squares) and scatterplots for mobile ("fast") and less mobile ("slow") subpopulations of endosomes. Error bars indicate SDs. (*B*) pH histograms for nonfusing (hatched and gray bars) and fusing particles (black and open bars). Solid and dashed lines are Gaussian fits to data for TVA800 and TVA950 cells, respectively; curve fits for fusion events are shown by black lines and for nonfusing particles by gray lines. (*C*) The pH-dependence of ASLV fusion with endosomes is shown as the ratio of fused vs. inactive particles for TVA800 (black circles) and TVA950 (open circles) cells. (*D*) Velocities as a function of time are shown for 20 representative fusion-competent virions in TVA950 cells before fusion. Velocities below 0.5 μm/s (marked by a thick dashed line) define slow endosomes. (*E*) Relative frequencies of ASLV fusion with fast (black segments) and slow (open segments) endosomes of TVA800 and TVA950 cells. (*F*) Decay times for the viral content (mKate2) signal upon ASLV fusion. Twenty individual fluorescence traces for fast (open triangles) and slow endosomes (open circles) in TVA950 cells and for fast (black triangles) and slow (black circles) endosomes in TVA800 cells were averaged and plotted as a function of time. Error bars indicate SEM. The corresponding single exponential fits are shown by solid lines. Pores were significantly larger in fast TVA950 endosomes than in fast TVA800 endosomes ($P = 0.001$) or in slow TVA950 endosomes ($P = 0.032$).

would indicate that these compartments are less permissive of fusion than slow endosomes.

To compare the fusion-permissiveness of fast and slow compartments, we assessed the effective sizes of fusion pores formed by ASLV EnvA. Larger initial fusion pores usually correlate with a more robust fusion process, consistent with the higher probability of ASLV fusion and faster release of the viral content (a measure of the pore diameter) in TVA950 as compared with TVA800 cells (7). We found that the decay of the mKate2 signal as a result of fusion with TVA950 cells was faster than for TVA800 cells (Fig. 3*F*). Thus, pores formed through the GPI-anchored receptor were smaller, because they restricted the efflux of mKate2 from virions. The fact that larger, more robust fusion pores were observed in mobile endosomes of TVA950 cells (Fig. 3*F*) argues against the possibility that these endosomes are less permissive to fusion than stationary compartments.

Quickly Moving Endosomes Support Faster ASLV Fusion than Less Mobile Compartments. Measurements of the lag times from shifting to 37 °C to individual acidification events showed that ASLV entered acidic compartments in TVA950 cells earlier than in TVA800 cells (Fig. S3*D*). This result was expected, based on our previous findings that TVA800 internalized ASLV more slowly than the transmembrane receptor (7, 14). In TVA800 cells, endosome acidification occurred with the same time course, irrespective of their motion pattern, whereas in TVA950 cells the lumen of fast endosomes became acidic at earlier times than in slow compartments ($P = 0.023$).

We next determined the true kinetics of acid-mediated ASLV fusion with different endosomes by measuring the interval between the pH drop below pH 6.3 (Fig. 3*C*) and the onset of mKate2 release, as illustrated in Fig. 2 *B* and *C* (vertical dashed lines). The lag times to fusion with fast endosomes in both TVA800 and TVA950 cells were considerably shorter than with their respective slow endosomes ($P = 0.012$ and 0.001, respectively) (Fig. 4*A*). In other words, the virus' ability to undergo quick fusion correlated with accelerated/directional movement of carrier endosomes. In addition, fusion with mobile endosomes was faster in TVA950 than in TVA800 cells ($P = 0.012$), whereas the fusion rates with slow endosomes in the two cell lines were not significantly different ($P = 0.151$). These shorter lags to ASLV fusion in fast endosomes in TVA950 cells are inconsistent with the possibility that these compartments are less permissive to fusion than slow endosomes.

Accelerated fusion with fast endosomes could be driven, at least in part, by their lower luminal pH compared with slow endosomes (Fig. 3*A*). However, the differences in the mean pH in dynamic and stationary endosomes in TVA950 cells were of only borderline significance (Fig. 3*A*). More importantly, the waiting times to fusion did not correlate strictly with luminal pH (Fig. 4*B*). For both TVA950 and TVA800 cells, lag times to fusion exhibited relatively weak dependences on endosomal pH with

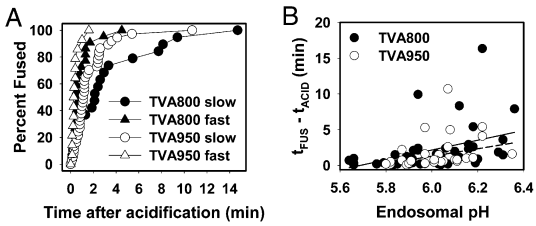

Fig. 4. Kinetics of low-pH–triggered ASLV fusion with fast and slow endosomes. (*A*) The time intervals between the pH drop below 6.3 and the onset of mKate2 release were determined for fusion events in TVA800 (filled symbols) and TVA950 (open symbols) cells and were plotted separately for fast and slow endosomes (triangles and circles, respectively). (*B*) Correlation between endosomal pH and the delay between acidification and fusion for TVA800 (filled circles) and TVA950 (open circles) cells. Solid and dashed lines are linear regressions for TVA800 and TVA950 data, respectively.

a greater scatter observed at pH above 5.95. This pattern suggests that, although low pH triggers fusion, other factors, such as heterogeneity of viruses and of endosomal membranes, can modulate postacidification steps of this process. It appears that endosomal compartments in TVA950 cells, but not in TVA800 cells, support the formation of a relatively long-lived (~1 min) hemifusion intermediate (7). The existence of such an intermediate is consistent with delays between acidification and content release (full fusion) observed in this work (Fig. 4). Together, our findings are in line with the idea that endosomes exhibiting distinct motion patterns vary in their propensity to support ASLV fusion.

Because dynamic endosomes support faster ASLV and faster release of the viral content in TVA950 than in TVA800 cells, it is unlikely that dynamic compartments disfavor ASLV fusion. We therefore reinterpreted the apparent probability of fusion obtained by comparing the frequencies of fusing and nonfusing particles across the pH range (Fig. 3*E*). It appears that, although nonfusing particles are distributed evenly between the two populations of endosomes, fusion-competent virions are sorted preferentially to slow endosomes in TVA950 cells. Although fewer virions enter fast endosomes, these compartments appear to support ASLV fusion optimally.

Discussion

In this study, retroviruses tagged with a genetically encoded pH-sensor and a fluorescent content marker enabled simultaneous measurements of the pH drop within virus-carrying vesicles and the resulting virus–endosome fusion. From several FRET-based sensors designed to measure endosomal pH (16, 30–32), we used a derivative of pHlameleon (16) incorporated into the viral membrane. Unlike other approaches, this strategy avoided chemical modifications of the virus, which could compromise its ability to undergo fusion. The ICAM-1–anchored pH sensors can be incorporated into retroviral particles pseudotyped with other viral fusion proteins (11) and thus may be used for studies of entry of other enveloped viruses.

The main limitation of single virus-based pH measurements is the relatively weak signal from the tandem fluorescent protein. Although this sensor allowed pH measurements around single viruses down to ~5.2 in vitro (Fig. 1*D*), the ability to determine the pH reliably in late endosomes was limited by cell autofluorescence. This problem can be alleviated by incorporating a larger number of pHlameleon-based sensors into the viral membrane and/or by implementing alternative labeling strategies (32). Further improvements in sensitivity and temporal resolution of pH measurements could shed light on biogenesis of acidic compartments. The initial pH drop to ~6.0 followed by a stationary phase (Fig. 2 and Fig. S2) appears surprising, considering that endosome maturation is thought to be coupled to gradual acidification. However, to our knowledge, pH measurements in a single maturing endosome have not been reported (perhaps with the exception of refs. 9 and 10). Ensemble measurements of endosomal pH are not likely to resolve the pH profile observed here for single endosomes.

Simultaneous measurements of endosomal pH and the release of viral content into the cytosol afford a unique opportunity to define the relationship between the strength of the fusion trigger and the rate and efficiency of this process. A weak correlation between endosomal pH and the lag before fusion (Fig. 4*B*) implies that additional factors, such as the property of endosomal membranes, can modulate the fusion reaction. Indeed, the ASLV fusion pores were larger (Fig. 3*F*) and the lag times to fusion were shorter (Fig. 4*A*) in dynamic endosomes than in slow endosomes of TVA950 cells. In contrast, nascent fusion pores formed in either fast or slow endosomes of TVA800 cells were not statistically different. A possible explanation is that, because the GPI-anchored receptor internalizes the virus through a raft-dependent pathway (14), particles trafficked to distinct compartments may remain associated with raft-like subdomains that are equally permissive to fusion.

Paradoxically, quick and robust ASLV fusion with fast endosomes in TVA950 cells (Figs. 3*F* and 4*A*) was observed relatively infrequently as compared with respective compartments in TVA800 cells (Fig. 3*E*). This difference could result from differential sorting of fusion-competent and -incompetent particles in TVA950 cells. If fusogenic particles incorporate more Env glycoproteins than fusion-incompetent ones, they could induce stronger signaling and be sorted into a different endosome population than inactive particles. The lack of selective sorting (and perhaps signaling) of ASLV in TVA800 cells is consistent with its slow uptake occurring at the rate of receptor-independent endocytosis in parental CV-1 cells (7).

The possibility of selective sorting of fusion-competent, but not inactive, ASLV into a subset of endosomes makes it difficult to evaluate the fusion efficiency simply by normalizing the number of fusion events to the total number of internalized particles. Thus it is possible that the real pH-dependence of ASLV–endosome fusion is steeper than shown in Fig. 3*C* and is similar to EnvA-mediated cell–cell fusion (28). The apparently selective ASLV entry into slow endosomes in TVA950 cells is in contrast to sorting of the influenza virus to mobile, quickly maturing endosomes (9). These differences likely reflect the markedly lower pH optimum for influenza fusion (pH 4.8–5.2) (33) compared with ASLV fusion (pH ~5.5) (27, 28). Entry into quickly maturing endosomes likely ensures faster delivery of influenza viruses into sufficiently acidic compartments.

Accumulating evidence supports the notion that TVA950 and TVA800 direct the ASLV entry through distinct routes (13, 14). It currently is not known whether ASLV fuses with early endosomes in both cell lines; such fusion would suggest quick convergence of different endocytic routes to early endosomes where fusion takes place shortly after acidification. Future studies with cells expressing specific markers of early and late endosomes, Rab5 and Rab7, should provide further insights into ASLV-trafficking pathways and reveal the identity of endosomes supporting the fusion reaction.

Methods

Cell Lines, Plasmids, and Virus Preparation. Cell lines and reagents used in this study, as well as pseudovirus production protocols, have been described before (7, 8, 12). For details, see *SI Methods*.

Calibration of a Nano-pH-Meter. MLV-based pseudoparticles carrying ASLV EnvA were colabeled with Gag-mKate2 (content marker) and mTFP1-eYFP-ICAM (membrane marker). Viruses were adhered to poly-L-lysine–coated

MICROBIOLOGY

eight-well coverslips (Nunc) and visualized using a Zeiss LSM780 confocal microscope (Carl Zeiss Microsystems). To relate changes in the mTFP1/YFP-sensitized emission to extraviral pH, viruses were exposed to a set of citrate/phosphate buffers between pH 4.3 and 7.3 and were imaged using a 63×/1.4 NA oil immersion objective. Fluorophores were excited with the 458-nm line of an argon laser, and emission spectra between 468 and 600 nm were acquired with a 32-channel GaAsP detector in the spectral mode. To minimize the effect of photobleaching, the calibration curve was obtained from nine separate experiments, each using a buffer of different acidity. The fluorescence ratios used for the calibration curve were obtained by summing the intensity of spectral images between 468–503 nm for the mTFP1 emission and 512–547 nm for the sensitized eYFP emission. This configuration was preserved when carrying out measurements in live cells using the same GaAsP detector. The fluorescence signal from all viruses in the image field (usually around 100 particles) was integrated and plotted as a function of wavelength. Background subtraction and a low-pass filter were applied on all spectral images using ImageJ (National Institutes of Health). The experimental points were fitted, as described in ref. 16, yielding the apparent pK_a 5.95.

Imaging Virus Entry into Acidic Compartments and Fusion. CV-1 cells expressing either TVA950 or TVA800 were grown to near confluency on glass-bottomed 35-mm Petri dishes (MatTek) in phenol red-free medium. Dishes were placed on ice, washed with cold HBSS, and centrifuged with $\sim 1.5 \times 10^4$ IU of pseudoviruses colabeled with mTFP1-eYFP-ICAM and Gag-mKate2 at 2,100 × *g* (4 °C) for 20 min. Unbound viruses were removed by washing, and cells were mounted onto a microscope stage maintained at 37 °C. Virus internalization and fusion were imaged using a Zeiss LSM 780 confocal microscope with a 63×/1.4 NA oil immersion objective. mTFP1 and mKate2 were excited with the 458- and 561-nm laser lines, respectively. Fluorescence emission was detected with the 32-channel spectral detector. The first 16 channels recorded the mTFP1 signal, and the remaining 16 channels acquired the sensitized eYFP emission signal. The mKate2 fluorescence was detected using a cooled photomultiplier tube. Images were acquired for 35–40 min approximately every 8 s.

Single-virus tracking was performed with Imaris (BitPlane) or Volocity (Perkin-Elmer). Changes in the average fluorescence ratio of mTFP1 fluorescence and of sensitized eYFP emission from internalized viruses were converted to pH units using the calibration curve. Virus-carrying endosomes were considered quickly moving ("fast") if (*i*) the particle's velocity exceeded 0.5 μm/s for at least three consecutive frames before virus fusion and (*ii*) increased velocity was associated with directional movement toward the nucleus. The endosomal pH distributions were compared using the two-tailed Student *t* test, and distributions of waiting times for fusion were compared using the Mann–Whitney rank sum test.

ACKNOWLEDGMENTS. This work has been supported by National Institutes of Health Grant AI053668 (to G.B.M.) and Fundação para a Ciência e a Tecnologia-Ministério da Educação e Ciência (FCT-MEC, Portugal) Grant PTDC/QUI-BIQ/104787/2008 (to N.C.S.). P.M.M. is the recipient of FCT-MEC Fellowship SFRH/BD/42205/2007.

1. Mercer J, Schelhaas M, Helenius A (2010) Virus entry by endocytosis. *Annu Rev Biochem* 79:803–833.
2. Gruenberg J (2009) Viruses and endosome membrane dynamics. *Curr Opin Cell Biol* 21 (4):582–588.
3. Sieczkarski SB, Whittaker GR (2002) Dissecting virus entry via endocytosis. *J Gen Virol* 83(Pt 7):1535–1545.
4. Pasqual G, Rojek JM, Masin M, Chatton JY, Kunz S (2011) Old world arenaviruses enter the host cell via the multivesicular body and depend on the endosomal sorting complex required for transport. *PLoS Pathog* 7(9):e1002232.
5. Zaitseva E, Yang S-T, Melikov K, Pourmal S, Chernomordik LV (2010) Dengue virus ensures its fusion in late endosomes using compartment-specific lipids. *PLoS Pathog* 6 (10)(e1001131. doi:10.1371/journal.ppat.1001131).
6. Brandenburg B, Zhuang X (2007) Virus trafficking - learning from single-virus tracking. *Nat Rev Microbiol* 5(3):197–208.
7. Jha NK, et al. (2011) Imaging single retrovirus entry through alternative receptor isoforms and intermediates of virus-endosome fusion. *PLoS Pathog* 7(1):e1001260.
8. Miyauchi K, Kim Y, Latinovic O, Morozov V, Melikyan GB (2009) HIV enters cells via endocytosis and dynamin-dependent fusion with endosomes. *Cell* 137(3):433–444.
9. Lakadamyali M, Rust MJ, Zhuang X (2006) Ligands for clathrin-mediated endocytosis are differentially sorted into distinct populations of early endosomes. *Cell* 124(5): 997–1009.
10. Lakadamyali M, Rust MJ, Babcock HP, Zhuang X (2003) Visualizing infection of individual influenza viruses. *Proc Natl Acad Sci USA* 100(16):9280–9285.
11. Miyauchi K, Marin M, Melikyan GB (2011) Visualization of retrovirus uptake and delivery into acidic endosomes. *Biochem J* 434(3):559–569.
12. Melikyan GB, Barnard RJ, Abrahamyan LG, Mothes W, Young JA (2005) Imaging individual retroviral fusion events: From hemifusion to pore formation and growth. *Proc Natl Acad Sci USA* 102(24):8728–8733.
13. Padilla-Parra S, Marin M, Kondo N, Melikyan GB (2012) Synchronized retrovirus fusion in cells expressing alternative receptor isoforms releases the viral core into distinct sub-cellular compartments. *PLoS Pathog* 8(5):e1002694.
14. Narayan S, Barnard RJ, Young JA (2003) Two retroviral entry pathways distinguished by lipid raft association of the viral receptor and differences in viral infectivity. *J Virol* 77(3):1977–1983.
15. Miesenböck G, De Angelis DA, Rothman JE (1998) Visualizing secretion and synaptic transmission with pH-sensitive green fluorescent proteins. *Nature* 394(6689):192–195.
16. Esposito A, Gralle M, Dani MA, Lange D, Wouters FS (2008) pHlameleons: A family of FRET-based protein sensors for quantitative pH imaging. *Biochemistry* 47(49): 13115–13126.
17. Ai HW, Henderson JN, Remington SJ, Campbell RE (2006) Directed evolution of a monomeric, bright and photostable version of Clavularia cyan fluorescent protein: Structural characterization and applications in fluorescence imaging. *Biochem J* 400 (3):531–540.
18. Capobianchi MR, et al. (1994) A simple and reliable method to detect cell membrane proteins on infectious human immunodeficiency virus type 1 particles. *J Infect Dis* 169 (4):886–889.
19. Padilla-Parra S, et al. (2009) Quantitative comparison of different fluorescent protein couples for fast FRET-FLIM acquisition. *Biophys J* 97(8):2368–2376.
20. Llopis J, McCaffery JM, Miyawaki A, Farquhar MG, Tsien RY (1998) Measurement of cytosolic, mitochondrial, and Golgi pH in single living cells with green fluorescent proteins. *Proc Natl Acad Sci USA* 95(12):6803–6808.
21. Elsliger MA, Wachter RM, Hanson GT, Kallio K, Remington SJ (1999) Structural and spectral response of green fluorescent protein variants to changes in pH. *Biochemistry* 38(17):5296–5301.
22. Mothes W, Boerger AL, Narayan S, Cunningham JM, Young JA (2000) Retroviral entry mediated by receptor priming and low pH triggering of an envelope glycoprotein. *Cell* 103(4):679–689.
23. Bates P, Young JA, Varmus HE (1993) A receptor for subgroup A Rous sarcoma virus is related to the low density lipoprotein receptor. *Cell* 74(6):1043–1051.
24. Elleder D, Melder DC, Trejbalova K, Svoboda J, Federspiel MJ (2004) Two different molecular defects in the Tva receptor gene explain the resistance of two tvar lines of chickens to infection by subgroup A avian sarcoma and leukosis viruses. *J Virol* 78(24): 13489–13500.
25. Markosyan RM, Cohen FS, Melikyan GB (2005) Time-resolved imaging of HIV-1 Env-mediated lipid and content mixing between a single virion and cell membrane. *Mol Biol Cell* 16(12):5502–5513.
26. Netter RC, et al. (2004) Heptad repeat 2-based peptides inhibit avian sarcoma and leukosis virus subgroup a infection and identify a fusion intermediate. *J Virol* 78(24): 13430–13439.
27. Delos SE, La B, Gilmartin A, White JM (2010) Studies of the "chain reversal regions" of the avian sarcoma/leukosis virus (ASLV) and ebolavirus fusion proteins: Analogous residues are important, and a His residue unique to EnvA affects the pH dependence of ASLV entry. *J Virol* 84(11):5687–5694.
28. Melikyan GB, Barnard RJ, Markosyan RM, Young JA, Cohen FS (2004) Low pH is required for avian sarcoma and leukosis virus Env-induced hemifusion and fusion pore formation but not for pore growth. *J Virol* 78(7):3753–3762.
29. Huotari J, Helenius A (2011) Endosome maturation. *EMBO J* 30(17):3481–3500.
30. Modi S, et al. (2009) A DNA nanomachine that maps spatial and temporal pH changes inside living cells. *Nat Nanotechnol* 4(5):325–330.
31. Grover A, et al. (2012) Genetically encoded pH sensor for tracking surface proteins through endocytosis. *Angew Chem Int Ed Engl* 51(20):4838–4842.
32. Dennis AM, Rhee WJ, Sotto D, Dublin SN, Bao G (2012) Quantum dot-fluorescent protein FRET probes for sensing intracellular pH. *ACS Nano* 6(4):2917–2924.
33. Doms RW, Helenius A, White J (1985) Membrane fusion activity of the influenza virus hemagglutinin. The low pH-induced conformational change. *J Biol Chem* 260(5): 2973–2981.

Supporting Information

Padilla-Parra et al. 10.1073/pnas.1211714109

SI Methods

Cell Lines and Plasmids. HEK293T/17 cells were obtained from the American Type Culture Collection. CV-1 cells stably expressing the avian tumor virus receptor A (TVA) receptor isoforms TVA800 or TVA950 have been described previously (1). CV-1–derived cells were grown in DMEM (Cellgro) supplemented with 10% (vol/vol) Cosmic Calf Serum (HyClone Laboratories) and 100 U penicillin-streptomycin (Gemini Bio-Products). HEK 293T/17 cells were cultured in high-glucose DMEM supplemented with 10% FBS (HyClone Laboratories), 100 U penicillin/streptomycin, and 0.5 mg/mL G418 sulfate (Cellgro). Vectors expressing murine leukemia virus (MLV) Gag-Pol, Gag-GFP, and MLV LTR lacZ were a gift from W. Mothes (Yale University, New Haven, CT). The avian sarcoma and leukosis virus (ASLV)-A envelope glycoprotein lacking cytoplasmic tail (EnvAΔCT) and MLV Gag-mKate2 plasmids have been described previously (2, 3).

Construction of mTFP1-ICAM and mTFP1-eYFP-ICAM was done as follows. The mTFP1 gene fragment was amplified using KOD Xtreme DNA polymerase (Novagen), mTFP1-eYFP plasmid (a gift from Maïté Coppey-Moisan, Université Paris Diderot, Paris) (4) as a template, and the forward and reverse primers 5′-T*AAGCTT*CTCGAG GTGAGCAAGGGCGAGGAGACCAC-3′ and 5′-T*GAATTC*TT CTTGTACAGCTCGTCCAT GCCGTC-3′, respectively. The amplified fragment was inserted into pCR4blunt-topo vector using a TOPO cloning kit (Invitrogen). After verifying the sequence, the mTFP1 gene was purified and ligated into EcpH-TM vector by replacing the EcpH gene with mTFP1 using HindIII and EcoRI restriction enzyme sites (corresponding to the italicized regions in primers). Cloning of the mTFP1-EYFP fragment into the EcpH-TM vector was done essentially as described above, except that the reverse primer 5′-T*GAATTC*TT CTTGTACAGCTCGTCCATGCCGAGAGTG-3′ was used for the amplification of the mTFP1-EYFP fragment by PCR.

Virus Production. ASLV EnvA-pseudotyped fluorescent viruses bearing mTFP1-ICAM or mTFP1-eYFP-ICAM on the surface and Gag-mKate2 as a content marker were produced as follows. ASLV EnvAΔCT (3 μg), MLV Gag-Pol (2 μg), pMLV-LTR-LacZ (3 μg), MLV Gag-mKate2 (1.2 μg), and mTFP1-ICAM or mTFP1-eYFP-ICAM (3 μg) expression plasmids were mixed with 300 μL of DMEM and 122 μL of Polyfect (Qiagen). The mixture was incubated for 10 min at room temperature, diluted to 1 mL with DMEM containing 10% FBS, and added onto HEK 293T cells grown to ∼60% confluency in a 100-mm dish. Twelve hours after transfection, the medium was replaced with 6 mL of fresh warm DMEM/10% FBS without phenol red. The plate was incubated further for 34 h at 37 °C. The culture supernatant was collected, passed through a 0.45-μm filter, aliquoted, and stored at −80 °C. The virus titer was determined by the β-gal assay using TVA800 cells, as described previously (5).

1. Jha NK, et al. (2011) Imaging single retrovirus entry through alternative receptor isoforms and intermediates of virus-endosome fusion. *PLoS Pathog* 7(1):e1001260.
2. Melikyan GB, Barnard RJ, Abrahamyan LG, Mothes W, Young JA (2005) Imaging individual retroviral fusion events: From hemifusion to pore formation and growth. *Proc Natl Acad Sci USA* 102(24):8728–8733.
3. Padilla-Parra S, Marin M, Kondo N, Melikyan GB (2012) Synchronized retrovirus fusion in cells expressing alternative receptor isoforms releases the viral core into distinct subcellular compartments. *PLoS Pathog* 8(5):e1002694.
4. Padilla-Parra S, et al. (2009) Quantitative comparison of different fluorescent protein couples for fast FRET-FLIM acquisition. *Biophys J* 97(8):2368–2376.
5. Miyauchi K, Kim Y, Latinovic O, Morozov V, Melikyan GB (2009) HIV enters cells via endocytosis and dynamin-dependent fusion with endosomes. *Cell* 137(3):433–444.

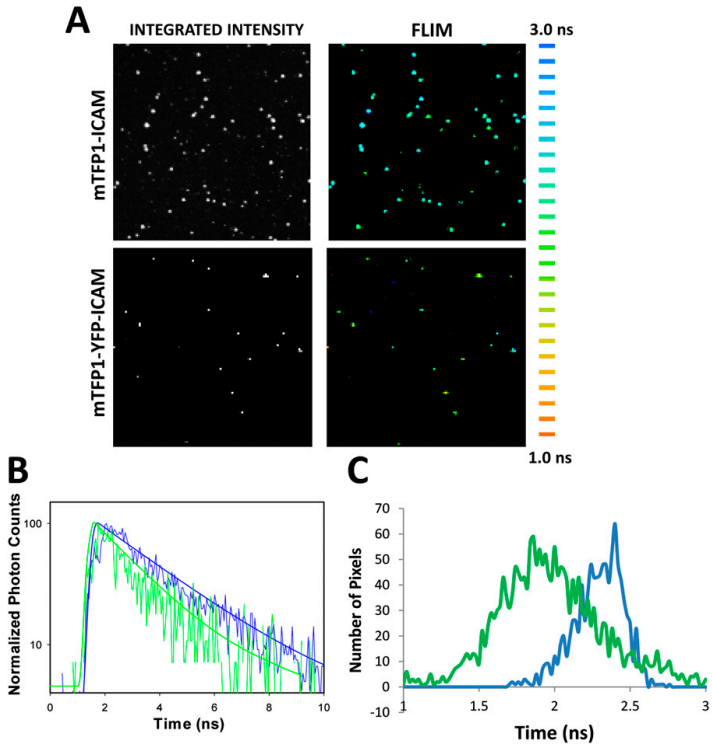

Fig. S1. Fluorescence lifetime imaging microscopy (FLIM) of FRET in the mTFP1-eYFP-ICAM sensor. FLIM measurements were performed using a Zeiss LSM780 confocal microscope equipped with an HPM-100–40 hybrid detector from Becker &. Time-correlated single-photon counting was performed using an SPC-830 (Becker & Hickl) acquisition card. A 63×/1.4 NA oil immersion objective was used for all measurements. Samples were excited with a Picosecond Laser Diode Head (Becker & Hickl) tuned at 440 nm with the repetition frequency of 80 MHz. (*A*) ASLV pseudoviruses colabeled with Gag-mKate2 and mTFP1-ICAM-1 (donor alone) or mTFP1-eYFP-ICAM-1 (tandem fluorescent protein) were allowed to adhere to poly-L-lysine–coated coverslips and were imaged at room temperature in Hanks' buffer. The average lifetime of mTFP1-ICAM-1 for the virus population was 2.4 ± 0.3 ns (*Upper*). The average lifetime of mTFP1 for pseudoviruses bearing mTFP1-eYFP-ICAM-1 was shortened to 1.9 ± 0.3 ns because of FRET between mTFP1 (donor) and eYFP (acceptor) (*Lower*). (*B*) Decay of the mTFP1 fluorescence of a single virus labeled with mTFP1-ICAM-1 (blue trace) and of a virus labeled with tandem protein (green trace) confirms FRET between donor and acceptor. (*C*) Analysis of the average lifetimes for multiple viruses in the image field. A clear blue shift of the mTFP1-eYFP-ICAM-1 lifetime at neutral pH shows efficient FRET.

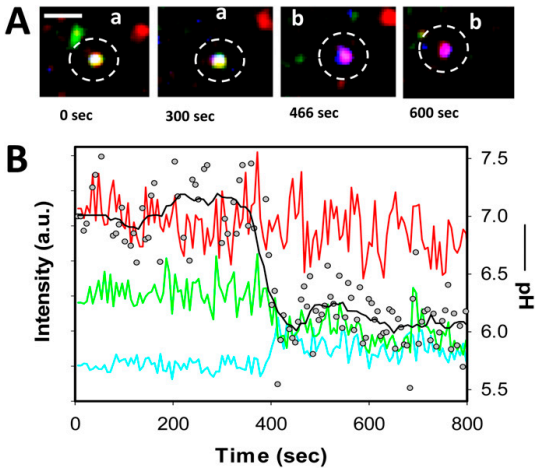

Fig. S2. ASLV entry into acidic endosomes without fusion. (*A*) Consecutive images of a representative pseudovirus (circled) colabeled with mTFP1-eYFP-ICAM (blue and green) and Gag-mKate2 (red) as it enters an acidic endosome (seen as transition from white to purple). (Scale bar, 5 μm.) (*B*) Mean fluorescence intensities of all three fluorophores are shown with respectively colored lines along with the calculated endosomal pH (gray circles and black line).

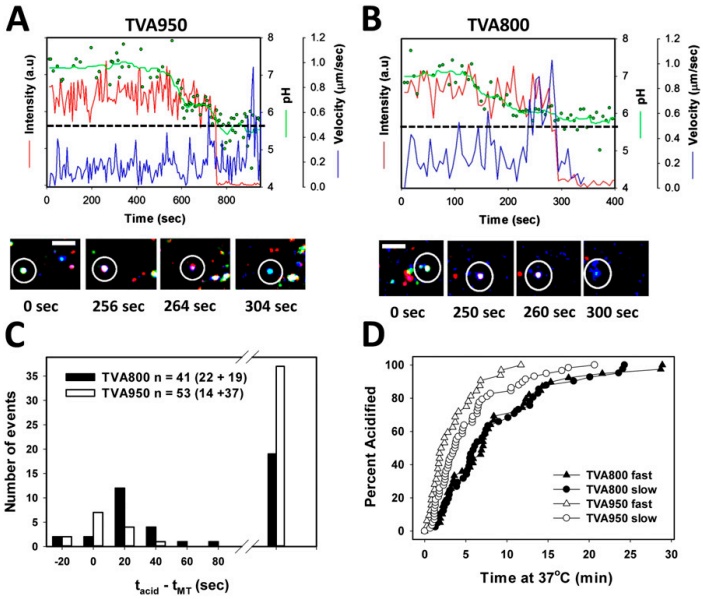

Fig. S3. Acidification and motility analyses for representative particles fusing with TVA950 and TVA800 cells. (*A* and *B*) The pH changes (green dots) and the mKate2 fluorescence profile for particles fusing with TVA950 (*A*) and TVA800 (*B*) cells. An additional axis on the right depicts particle velocity. Green solid lines are the running averages of raw pH data. Note the postfusion acceleration of an endosome in a TVA950 cell (*A*, blue line), which contrasts with the quick trafficking of in a TVA800 cell (*B*). Thick dashed lines show the arbitrary threshold that separates slow-moving particles (speed <0.5 μm/s) from fast particles. Fusion with a TVA800, but not with a TVA950 cell, is preceded by an increase in velocity above the threshold level for several consecutive image frames. Snapshots of sequential acidification and fusion steps are shown below the respective graphs. (Scale bar, 5 μm.) (*C*) Histograms of lag times between acidification and acceleration above 0.5 μm/s for TVA800 (black bars) and TVA950 (open bars) cells. The less mobile particles traveling in "slow" endosomes are grouped, and their number is shown on the right. (*D*) Kinetics of endosome acidification in TVA800 (black symbols) and TVA950 (open symbols) cells. The lag times from the temperature increase to the drop in pH were measured, ranked, and plotted as cumulative distributions for slow- (circles) and fast-moving (triangles) endosomes. Pooled data for fusing and nonfusing viruses are shown.

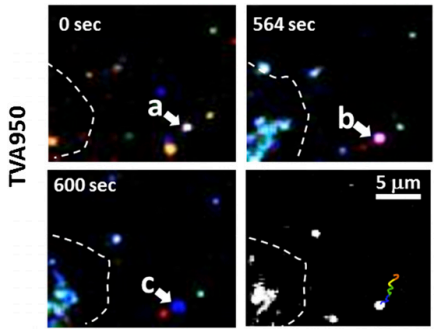

Movie S1. Visualization of ASLV entry into acidic endosomes and fusion with TVA950 cells. ASLV pseudoviruses colabeled with mTFP1-eYFP-ICAM (colored blue and green, respectively) and Gag-mKate2 (red) were prebound to CV-1 cells expressing TVA950 in the cold, and fusion was initiated by shifting to 37 °C. The circled virus enters into an acidic endosome, as seen by the color shift from white to purple caused by eYFP quenching, and then undergoes fusion (seen as purple-to-blue transition). The movie is played at 5 frames/s. See also corresponding Fig. 2*B*.

Movie S1

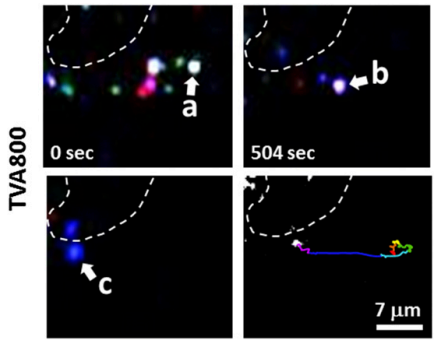

Movie S2. Visualization of ASLV entry into acidic endosomes and fusion with TVA800 cells. ASLV pseudoviruses colabeled with mTFP1-eYFP-ICAM (colored blue and green, respectively) and Gag-mKate2 (red) were prebound to CV-1 cells expressing TVA800 in the cold, and fusion was initiated by shifting to 37 °C. The circled virus enters into an acidic endosome, as seen by the color shift from white to purple caused by eYFP quenching, and then undergoes fusion (purple-to-blue transition). The movie is played at five frames/s. See also corresponding Fig. 2*C*.

Movie S2

VI

Final conclusions

This Thesis gathered different points of view regarding enveloped viruses attachment, fusion and entry steps of their lifecycles. Throughout this work, we diversified our objects of study from simple peptides, to glycoproteins, to whole viruses and cells. Moreover, we took advantage of membrane model systems from lipid vesicles to supported lipid bilayers. In terms of main techniques, we focused on optical based biophysical techniques, namely fluorescent spectroscopy, confocal microscopy and surface plasmon resonance. All of this came together and allowed us to achieved the following: **i)** establishment of the membranotropism towards lipid raft-like domains as a factor that influences the action of HIV-1 fusion inhibitor peptides; **ii)** elucidation that sequence type, size and sulfation pattern are determinants of HIV-1 gp120 interaction with glycosaminoglycans; **iii)** recognition of the importance of anionic lipids as an essential host factor that modulates the fusion of VSV; and **iv)** clarification on the entry pathways of ASLV via quantitative imaging of endosomal pH and fusion.

HIV-1 fusion inhibitor peptides constitute a relatively recent family of antiviral drugs, with enfuvirtide being the only one in the market. However, emergence of viral strains resistant to enfuvirtide [189-191] urged the development and trials of new drugs of this type. As described in the Introduction section, many experimental peptide fusion inhibitors were developed with different rational designs behind them. Some required sequence modifications to overcome resistance, to increase helical content, stability or solubility while others have conjugated the peptides with other proteins and lipophilic moieties [192,193] [Book Chapter A]. We were able to study different generations of HIV-1 fusion inhibitor peptides, from the only one approved, enfuvirtide, to T-1249, sifuvirtide, C34 and C34-cholesterol. The final target for these peptides is the extended conformation of gp41, when it is bridging the cellular and viral membranes before their fusion. This target is only exposed transiently and confined in a limited space between the membranes. As such, we proposed that fusion inhibitor peptides binding to the surrounding cell and viral membranes to constitute an intermediate step on their mechanism of action. The concentration of peptide in the cell and viral membranes would make the peptide more available to bind gp41 near the

possible sites of fusion, potentiating its antiviral activity. In our studies, we observed that the mentioned peptides had different affinities towards membranes and that it was dependent on the lipid compositions used, for the case of model membranes.

Enfuvirtide and T-1249 partition was first studied in model membranes. T-1249 was able to adsorb to cholesterol rich lipid vesicles, contrary to enfuvirtide [69,81]. In our work with model membranes, we observed that C34-cholesterol had notorious partition towards cholesterol-rich and cholesterol/SM mixtures mimicking lipid rafts. The development of the assays for evaluating the binding to cell membranes by the potential sensitive probe di-8-ANEPPS, allowed the translation of these evaluations from model membranes to cells. The results for cell membrane binding were elucidative enough to establish an increasing degree of membranotropism that correlated with their antiviral potency, for the following peptides: enfuvirtide < T-1249 < C34-cholesterol. The same sequence also applies for partitions to lipid raft mimicking model membranes (**Table 2**).

Table 2 – Summary of the relative antiviral potencies and membrane partition or binding for the studied HIV-1 fusion inhibitor peptides.

Peptides	Enfuvirtide	T-1249	C34-cholesterol	Sifuvirtide C34
Antiviral potency	+	++	+++	++
Partition to raft-mimicking model membranes	+	++	+++	Specific for rigid PC (DPPC) ++
Binding to cell membranes	+	++	+++	Low

The case of sifuvirtide proved to be particular. Despite being of a later generation and more potent than enfuvirtide [53,55], it was found that it had residual partition towards fluid phase POPC vesicles, but was highly specific towards rigid phosphatidylcholines, mainly DPPC [84,85]. In terms of cell membranotropism, we observed some degree of binding, but lower than enfuvirtide. Rigid domains are also a characteristic of lipid rafts, and hence one can assume that sifuvirtide screens very specifically for such domains, despite its

overall partition towards cholesterol and sphingomyelin-rich membranes being low [84,85]. As such, the intermediate step of lipid raft binding before gp41 binding should also be present at some extent for sifuvirtide. However, the higher potency of sifuvirtide compared to enfuvirtide should rely more on the sequence optimization that allows more stable binding to gp41 NHR [53].

Overall, targeting lipid raft binding for fusion inhibitor peptides is an important factor to take into account in the mode of action and potency of these drugs.

The search for better fusion inhibitor peptides is an ongoing effort and rational design has been of key importance to enhance the properties of these drugs at several levels. There are three major drawbacks in the clinical use of enfuvirtide, the only HIV fusion inhibitor currently approved: **i)** administration by injection, **ii)** appearance of resistance and **iii)** cost. The improvements in potency and stability of the peptides should allow less frequent injections, with lower doses, as already happens for sifuvirtide [53] and others [194,195]. Similarly, sequence modification in the peptide design taking into account known resistance patterns for enfuvirtide will delay viral resistance [196]. Moreover, the mutations that the virus has to develop in order to escape the later generation inhibitors can greatly reduce viral fitness and delay disease progression [197-200]. Regarding the financial burden of fusion inhibitors therapy, the development and large scale production of more peptide drugs should help bring the costs down. It is noteworthy that peptides are still cheaper to produce than antibodies.

The future of viral fusion inhibitors also lies on alternative therapy uses, mainly in combination therapy and in microbicide topical formulations [192]. Currently, the antiviral therapy is highly dependent on combinations of different types of drugs, constituting the HAART regimen (highly active antiretroviral therapy) [201]. As such, therapy regimens with future fusion inhibitor peptides should involve some kind of combination with other entry inhibitors and/or other intracellular acting antivirals. This has already been proven to be beneficial, mostly *in vitro* [202-206]. The success of fusion inhibitors may also be achieved through their use in topical formulations to prevent new infections (microbicides). As

mentioned before, studies *in vitro* and in animal models have shown promising results for gels containing T-1249 [50-52], sifuvirtide [58] or C34-cholesterol [60]. This is particularly interesting in the case of T-1249, which clinical trials for use as injected antiretroviral have been put on hold due to formulation problems [49]. Its new use as microbicide revives the potential of this drug to succeed clinically.

The potential for fusion inhibitor peptides also spans to other enveloped viruses that rely on the conserved mechanism of the viral fusion proteins hairpin folding. In fact, the derivation of peptides from the sequence of fusion proteins can constitute a robust framework to rapidly develop antivirals for emerging viral diseases. Examples of fusion inhibitors for influenza virus and paramyxoviruses, particularly the emerging Nipah and Hendra viruses [73,207], have already been given in the Introduction section. The case of development of entry inhibitors, either peptides or small molecules, for respiratory syncytial virus is interesting since in this particular case a inhalation route can be used to deliver the drug directly in the respiratory system [208,209]. Sequencing the fusion protein of new viruses can give the necessary information to synthesize potential peptide inhibitors against them.

The fusion inhibitors development is a great example of drug design that used the accumulated knowledge of fundamental molecular biology and biochemistry research on virus entry mechanisms. In that sense, we also pursued a study to evaluate the glycosaminoglycans characteristics that were essential for binding to HIV-1 envelope protein gp120. The importance of the GAGs in viral pathogenesis was clarified in the introduction section, as essential attachment helpers to the cell surface. Interaction with gp120 was dependent on sequence type, with preference for heparin and heparan sulfate, with minimum extension of 16 monomers and highly dependent on sulfate groups. We also applied the SPR methodology in an uncommon way. Usually glycosaminoglycans, mainly heparin, used as a model, are immobilized on the surface via biotin-streptavidin link, which limits the types of GAG one can use. We managed to (at least qualitatively) evaluate protein-GAG binding using several GAG types. Protection strategies such as the attempt to shield charges in the proteins to be immobilized using counteracting charged small

molecules are also uncommon. These findings help to understand the requirements for viral attachment via glycosaminoglycans, a step previous to virus fusion and entry. The relevance of this interaction is demonstrated by the recently developed drugs that make use of the binding sites in gp120 for heparan sulfate and block them, the previously mentioned syndecan-Fc hybrid and a CD4-mimetic peptide linked to heparan sulfate [105,106].

Besides receptors that allow the virus to enter and fuse with the host cell, we explored the role of host lipids in the promotion of fusion mediated by VSV G protein. Visualization of single pseudovirus fusion was achieved on supported lipid bilayers with defined lipid compositions. Hemifusion and content release were temporally distinguished and proved that a long-lived hemifusion intermediate can exist for VSV G. We focused on comparing the fusion efficiencies and kinetics in the presence of anionic lipids (POPS and BMP) and the zwitterionic POPC. Anionic lipids were required for full fusion processes and greatly enhance hemifusion efficiency compared to POPC. BMP, an endosome resident lipid, also presented a shorter lag time between hemifusion and content release. As such, VSV can start to hemifuse in early endosomes but complete its fusion in late endosomes upon encounter of BMP-rich compartments. We reproduced fusion with minimal components: the virus, a planar membrane and low pH. However, the low full fusion efficiencies obtained should mean that other factors are as important as the lipids studied, including the elusive receptor either at the cell surface or in an intracellular compartment. Just after the publication of our VSV fusion studies on Article E, a paper came out identifying the receptor of low-density lipoprotein as the receptor for VSV [131]. That study shows strong evidence that VSV binding, internalization and infection depends on the LDLR. However, it is still not clear if the receptor has a direct role on the fusion process itself. The use of supported lipid bilayer containing such receptor should help to characterize its influence on viral fusion kinetics.

The methodology we used on this VSV study is very recent and allows to study in detail, at the single particle level, the effect of the lipids in the fusion. This method was only previously used to characterize the kinetics of influenza fusion

[182,185]. However, in these studies, they used the intraviral aqueous dye sulforhodamine B to observe content leakage. We actually observe labeled nucleocapsid proteins being released, which can implicate that we only detect pore sizes that are large enough for viral proteins to be released. The full potential of this technique is yet to be achieved. Reconstitution of recombinant cellular receptors in the supported lipid bilayer should enable the study of receptor-dependent viruses and how the binding differ from lipid-only bilayers. Ultimately, this technique can be applied to study all enveloped viruses entry mechanisms and enable a fine control of the different parameters that modulate viral entry: pH, cellular receptors and membrane lipids. Consequently, this would also allow detailed mechanistic insights into the effects of entry inhibitors.

Fluorescent based single-particle imaging was also used to follow the entry pathways of ASLV in cells. In this study, a novel methodological approach was developed as we incorporated a FRET pair of fluorescent proteins in the virus envelope to quantify the pH of the surrounding environment. The distinct pK_a values of mTFP1 and eYFP allowed ratiometric imaging to be calibrated in actual pH values. Acidification to around pH 6 triggered viral core release shortly after, as measured by the disappearance of Gag-mKate2 signal. The single particle tracking revealed sorting of the viruses to distinct populations of early endosomes and that the TVA950 receptor isoform supported faster fusion than TVA800.

The ability of following single viruses in their trajectory inside the cell provides valuable information regarding their lifecycle and mechanisms of invasion. This technique may be also of broad interest to other viruses, which entry pathways are yet to be clarified. However, these tracking techniques still require laborious manual work to ensure the validity of what is being observed. Development of more robust automated methods of acquisition and analysis would help these experiments to go mainstream. Moreover, as better and brighter fluorescent probes are developed, and super resolution microscopies becomes increasingly available, more detailed views of viral infection processes should be uncovered.

Future perspectives

The studies presented here pave the way for novel approaches to understand viral entry and its inhibition.

The attachment of a cholesterol moiety to C34 proved to be a successful strategy to improve antiviral potency. C34 is an analogue of sifuvirtide, as both lack a putative LBD that renders them less membranotropic. Despite the fact that sifuvirtide may have similar activity comparing to C34, depending on the strain [210], a possible sifuvirtide-cholesterol conjugation should also be beneficial. Structurally, sifuvirtide is more stable than C34, due to its rational design. Providing it with a lipid anchor may render a highly potent and specific new drug. The new anti-HIV peptides to be developed should also account for a recently established aspect of HIV-1 entry: it was proved that HIV can use an endocytic pathway to enter cells [36,37]. In this scenario, fusion inhibitors should be able to be internalized together with the virus to act inside the endosomes. Partitioning to membranes, especially for peptides possessing a lipid anchor, may help these drugs to be internalized as the membranes invaginates. Indeed, a recent study already pointed that this occurs in the case of influenza virus, upon testing a cholesterol-conjugated anti-influenza peptide [43]. In this regard, single virus fusion imaging in cells can be a valuable tool to assess such specific endosome level inhibition.

The membranotropism evaluation of drugs, either from peptides or small molecules, can be a valuable tool to assess drug delivery to the right target. If intracellular, the drug needs to be capable of interacting with the membrane and crossing it. If it is a cell surface protein, its concentration at the membrane level may also boost the action of the drug, as it is exemplified for the fusion inhibitors. Moreover, crossing cellular barriers such as epithelia, endothelia or the blood-brain barrier should also benefit from membrane crossing properties. These assays of membrane partition and membrane interaction, with model membranes and cells can be applied to early drug development stages, in order to assure they have such properties [211].

VSV has long been used as a model for viral entry and fusion studies. However, all the requirements necessary for its entry are yet to be understood. More studies are necessary in this regards, and the single virus fusion technique presented here can bring more information. More detailed fusion kinetics data with varying pH, with varying concentrations of BMP and other important lipids, such as cholesterol, SM and PE, can inform on limiting steps of viral fusion. Moreover, now that we know the LDL receptor mediates at least the internalization of the virus, the performing of these further studies evaluating also the effect of the presence or absence of the receptor should clarify the precise roles of LDLR and if other receptors may eventually be necessary. This would help to improve our knowledge on the behavior of class III fusion proteins, the latest type to be classified.

Single virus imaging with cells allowed a finer dissection of viral entry pathways for several viruses, but several questions still remain. The properties of the different populations of endosomes in which ASLV are sorted into poses a new question for the cell biology field. More comprehensive co-localization studies with different markers of early and late endosomes, and even other known intracellular compartments, should inform on viral trafficking sites. Herpes virus, in certain cases, apparently needs a double stimulus for fusion, binding to a receptor and low pH, as ASLV [11-14]. Engineering fluorescent herpes virus for single virus tracking may elucidate if it shares this rare mechanism of entry with ASLV, despite having different classes of fusion proteins

Increasing the fundamental knowledge of virus entry is a necessity in today's world of emerging viral diseases. Targeting the proteins responsible for the initial steps of viral invasion should be an effective method to control infections. I hope this Thesis has helped to advance the knowledge in this area and contribute to the scientific community as a whole.

References

1. Cosset FL, Lavillette D. Cell entry of enveloped viruses. *Adv. Genet.* **73**: 121-183 (2011).

2. Melikyan GB, Smith EC, Dutch RE. Mechanisms of Enveloped Virus Entry by Membrane Fusion. In: Edward HE, editor. *Comprehensive Biophysics*. Amsterdam: Elsevier Academic Press. pp. 290-311 (2012).

3. Harrison SC. Viral membrane fusion. *Nat. Struct. Mol. Biol.* **15**: 690-698 (2008).

4. Weissenhorn W, Hinz A, Gaudin Y. Virus membrane fusion. *FEBS Lett.* **581**: 2150-2155 (2007).

5. Chernomordik LV, Kozlov MM. Protein-lipid interplay in fusion and fission of biological membranes. *Annu. Rev. Biochem.* **72**: 175-207 (2003).

6. Chernomordik LV, Kozlov MM. Membrane hemifusion: crossing a chasm in two leaps. *Cell* **123**: 375-382 (2005).

7. White JM, Delos SE, Brecher M, Schornberg K. Structures and mechanisms of viral membrane fusion proteins: multiple variations on a common theme. *Crit. Rev. Biochem. Mol. Biol.* **43**: 189-219 (2008).

8. Baquero E, Albertini AA, Vachette P, Lepault J, Bressanelli S, Gaudin Y. Intermediate conformations during viral fusion glycoprotein structural transition. *Curr. Opin. Virol.* **3**: 143-150 (2013).

9. Plemper RK, Melikyan GB. Membrane Fusion. In: Lennarz WJ, Lane MD, editors. *Encyclopedia of Biological Chemistry*. Waltham: Elsevier Academic Press. pp. 36-43 (2013).

10. Backovic M, Jardetzky TS. Class III viral membrane fusion proteins. *Adv. Exp. Med. Biol.* **714**: 91-101 (2011).

11. Dollery SJ, Delboy MG, Nicola AV. Low pH-induced conformational change in herpes simplex virus glycoprotein B. *J. Virol.* **84**: 3759-3766 (2010).

12. Dollery SJ, Wright CC, Johnson DC, Nicola AV. Low-pH-dependent changes in the conformation and oligomeric state of the prefusion form of herpes simplex virus glycoprotein B are separable from fusion activity. *J. Virol.* **85**: 9964-9973 (2011).

13. Milne RS, Nicola AV, Whitbeck JC, Eisenberg RJ, Cohen GH. Glycoprotein D receptor-dependent, low-pH-independent endocytic entry of herpes simplex virus type 1. *J. Virol.* **79**: 6655-6663 (2005).

14. Nicola AV, Hou J, Major EO, Straus SE. Herpes simplex virus type 1 enters human epidermal keratinocytes, but not neurons, via a pH-dependent endocytic pathway. *J. Virol.* **79**: 7609-7616 (2005).

15. Wyatt R, Sodroski J. The HIV-1 envelope glycoproteins: fusogens, antigens, and immunogens. *Science* **280**: 1884-1888 (1998).

16. Weissenhorn W, Dessen A, Harrison SC, Skehel JJ, Wiley DC. Atomic structure of the ectodomain from HIV-1 gp41. *Nature* **387**: 426-430 (1997).

17. Hart TK, Kirsh R, Ellens H, Sweet RW, Lambert DM, Petteway SR, Jr., Leary J, Bugelski PJ. Binding of soluble CD4 proteins to human immunodeficiency virus type 1 and infected cells induces release of envelope glycoprotein gp120. *Proc. Natl. Acad. Sci. U. S. A.* **88**: 2189-2193 (1991).

18. Moore JP, McKeating JA, Weiss RA, Sattentau QJ. Dissociation of gp120 from HIV-1 virions induced by soluble CD4. *Science* **250**: 1139-1142 (1990).

19. Ugolini S, Mondor I, Sattentau QJ. HIV-1 attachment: another look. *Trends Microbiol.* **7**: 144-149 (1999).

20. Dalgleish AG, Beverley PC, Clapham PR, Crawford DH, Greaves MF, Weiss RA. The CD4 (T4) antigen is an essential component of the receptor for the AIDS retrovirus. *Nature* **312**: 763-767 (1984).

21. Klatzmann D, Champagne E, Chamaret S, Gruest J, Guetard D, Hercend T, Gluckman JC, Montagnier L. T-lymphocyte T4 molecule behaves as the receptor for human retrovirus LAV. *Nature* **312**: 767-768 (1984).

22. Maddon PJ, Dalgleish AG, McDougal JS, Clapham PR, Weiss RA, Axel R. The T4 gene encodes the AIDS virus receptor and is expressed in the immune system and the brain. *Cell* **47**: 333-348 (1986).

23. Alkhatib G, Combadiere C, Broder CC, Feng Y, Kennedy PE, Murphy PM, Berger EA. CC CKR5: a RANTES, MIP-1alpha, MIP-1beta receptor as a fusion cofactor for macrophage-tropic HIV-1. *Science* **272**: 1955-1958 (1996).

24. Dragic T, Litwin V, Allaway GP, Martin SR, Huang Y, Nagashima KA, Cayanan C, Maddon PJ, Koup RA, Moore JP, Paxton WA. HIV-1 entry into CD4+ cells is mediated by the chemokine receptor CC-CKR-5. *Nature* **381**: 667-673 (1996).

25. Lapham CK, Ouyang J, Chandrasekhar B, Nguyen NY, Dimitrov DS, Golding H. Evidence for cell-surface association between fusin and the CD4-gp120 complex in human cell lines. *Science* **274**: 602-605 (1996).

26. Sattentau QJ, Moore JP. Conformational changes induced in the human immunodeficiency virus envelope glycoprotein by soluble CD4 binding. *J. Exp. Med.* **174**: 407-415 (1991).

27. Trkola A, Dragic T, Arthos J, Binley JM, Olson WC, Allaway GP, Cheng-Mayer C, Robinson J, Maddon PJ, Moore JP. CD4-dependent, antibody-sensitive interactions between HIV-1 and its co-receptor CCR-5. *Nature* **384**: 184-187 (1996).

28. Wu L, Gerard NP, Wyatt R, Choe H, Parolin C, Ruffing N, Borsetti A, Cardoso AA, Desjardin E, Newman W, Gerard C, Sodroski J. CD4-induced interaction of primary HIV-1 gp120 glycoproteins with the chemokine receptor CCR-5. *Nature* **384**: 179-183 (1996).

29. Wild C, Oas T, McDanal C, Bolognesi D, Matthews T. A synthetic peptide inhibitor of human immunodeficiency virus replication: correlation between solution structure and viral inhibition. *Proc. Natl. Acad. Sci. U. S. A.* **89**: 10537-10541 (1992).

30. De Clercq E. The design of drugs for HIV and HCV. *Nat. Rev. Drug Discov.* **6**: 1001-1018 (2007).

31. Miyamoto F, Kodama EN. Novel HIV-1 fusion inhibition peptides: designing the next generation of drugs. *Antivir. Chem. Chemother.* **22**: 151-158 (2012).

32. Allen WJ, Rizzo RC. Computer-Aided Approaches for Targeting HIVgp41. *Biology* **1**: 311-338 (2012).

33. Maddon PJ, McDougal JS, Clapham PR, Dalgleish AG, Jamal S, Weiss RA, Axel R. HIV infection does not require endocytosis of its receptor, CD4. *Cell* **54**: 865-874 (1988).

34. McClure MO, Marsh M, Weiss RA. Human immunodeficiency virus infection of CD4-bearing cells occurs by a pH-independent mechanism. *EMBO J.* **7**: 513-518 (1988).

35. Stein BS, Gowda SD, Lifson JD, Penhallow RC, Bensch KG, Engleman EG. pH-independent HIV entry into CD4-positive T cells via virus envelope fusion to the plasma membrane. *Cell* **49**: 659-668 (1987).

36. Miyauchi K, Kim Y, Latinovic O, Morozov V, Melikyan GB. HIV enters cells via endocytosis and dynamin-dependent fusion with endosomes. *Cell* **137**: 433-444 (2009).

37. de la Vega M, Marin M, Kondo N, Miyauchi K, Kim Y, Epand RF, Epand RM, Melikyan GB. Inhibition of HIV-1 endocytosis allows lipid mixing at the plasma membrane, but not complete fusion. *Retrovirology* **8**: 99 (2011).

38. Owens RJ, Tanner CC, Mulligan MJ, Srinivas RV, Compans RW. Oligopeptide inhibitors of HIV-induced syncytium formation. *AIDS Res. Hum. Retroviruses* **6**: 1289-1296 (1990).

39. Jiang S, Lin K, Strick N, Neurath AR. HIV-1 inhibition by a peptide. *Nature* **365**: 113 (1993).

40. Wild CT, Shugars DC, Greenwell TK, McDanal CB, Matthews TJ. Peptides corresponding to a predictive alpha-helical domain of human immunodeficiency virus type 1 gp41 are potent inhibitors of virus infection. *Proc. Natl. Acad. Sci. U. S. A.* **91**: 9770-9774 (1994).

41. Wild C, Greenwell T, Matthews T. A synthetic peptide from HIV-1 gp41 is a potent inhibitor of virus-mediated cell-cell fusion. *AIDS Res. Hum. Retroviruses* **9**: 1051-1053 (1993).

42. Chan DC, Fass D, Berger JM, Kim PS. Core structure of gp41 from the HIV envelope glycoprotein. *Cell* **89**: 263-273 (1997).

43. Lee KK, Pessi A, Gui L, Santoprete A, Talekar A, Moscona A, Porotto M. Capturing a fusion intermediate of influenza hemagglutinin with a cholesterol-conjugated peptide, a new antiviral strategy for influenza virus. *J. Biol. Chem.* **286**: 42141-42149 (2011).

44. Kilby JM, Hopkins S, Venetta TM, DiMassimo B, Cloud GA, Lee JY, Alldredge L, Hunter E, Lambert D, Bolognesi D, Matthews T, Johnson MR, Nowak MA, Shaw GM, Saag MS. Potent suppression of HIV-1 replication in humans by T-20, a peptide inhibitor of gp41-mediated virus entry. *Nat. Med.* **4**: 1302-1307 (1998).

45. Lazzarin A, Clotet B, Cooper D, Reynes J, Arasteh K, Nelson M, Katlama C, Stellbrink HJ, Delfraissy JF, Lange J, Huson L, DeMasi R, Wat C, Delehanty J, Drobnes C, Salgo M, Group TS. Efficacy of enfuvirtide in patients infected with drug-resistant HIV-1 in Europe and Australia. *N. Engl. J. Med.* **348**: 2186-2195 (2003).

46. Lalezari JP, Henry K, O'Hearn M, Montaner JS, Piliero PJ, Trottier B, Walmsley S, Cohen C, Kuritzkes DR, Eron JJ, Jr., Chung J, DeMasi R, Donatacci L, Drobnes C, Delehanty J, Salgo M, Group TS. Enfuvirtide, an HIV-1 fusion inhibitor, for drug-resistant HIV infection in North and South America. *N. Engl. J. Med.* **348**: 2175-2185 (2003).

47. Matthews T, Salgo M, Greenberg M, Chung J, DeMasi R, Bolognesi D. Enfuvirtide: the first therapy to inhibit the entry of HIV-1 into host CD4 lymphocytes. *Nat. Rev. Drug Discov.* **3**: 215-225 (2004).

48. Eron JJ, Gulick RM, Bartlett JA, Merigan T, Arduino R, Kilby JM, Yangco B, Diers A, Drobnes C, DeMasi R, Greenberg M, Melby T, Raskino C, Rusnak P, Zhang Y,

Spence R, Miralles GD. Short-term safety and antiretroviral activity of T-1249, a second-generation fusion inhibitor of HIV. *J. Infect. Dis.* **189**: 1075-1083 (2004).

49. Martin-Carbonero L. Discontinuation of the clinical development of fusion inhibitor T-1249. *AIDS Rev.* **6**: 61 (2004).

50. Barouch DH, Klasse PJ, Dufour J, Veazey RS, Moore JP. Macaque studies of vaccine and microbicide combinations for preventing HIV-1 sexual transmission. *Proc. Natl. Acad. Sci. U. S. A.* **109**: 8694-8698 (2012).

51. Veazey RS, Klasse PJ, Schader SM, Hu Q, Ketas TJ, Lu M, Marx PA, Dufour J, Colonno RJ, Shattock RJ, Springer MS, Moore JP. Protection of macaques from vaginal SHIV challenge by vaginally delivered inhibitors of virus-cell fusion. *Nature* **438**: 99-102 (2005).

52. Veazey RS, Ketas TA, Klasse PJ, Davison DK, Singletary M, Green LC, Greenberg ML, Moore JP. Tropism-independent protection of macaques against vaginal transmission of three SHIVs by the HIV-1 fusion inhibitor T-1249. *Proc. Natl. Acad. Sci. U. S. A.* **105**: 10531-10536 (2008).

53. He Y, Xiao Y, Song H, Liang Q, Ju D, Chen X, Lu H, Jing W, Jiang S, Zhang L. Design and evaluation of sifuvirtide, a novel HIV-1 fusion inhibitor. *J. Biol. Chem.* **283**: 11126-11134 (2008).

54. Dai SJ, Dou GF, Qiang XH, Song HF, Tang ZM, Liu DS, Liu XW, Yang LM, Zheng YT, Liang Q. Pharmacokinetics of sifuvirtide, a novel anti-HIV-1 peptide, in monkeys and its inhibitory concentration in vitro. *Acta Pharmacol. Sin.* **26**: 1274-1280 (2005).

55. Wang RR, Yang LM, Wang YH, Pang W, Tam SC, Tien P, Zheng YT. Sifuvirtide, a potent HIV fusion inhibitor peptide. *Biochem. Biophys. Res. Commun.* **382**: 540-544 (2009).

56. FusoGen company webpage. http://fusogen.com/en/company/milestones. Accessed on 11/04/2013.

57. Yao X, Chong H, Zhang C, Waltersperger S, Wang M, Cui S, He Y. Broad antiviral activity and crystal structure of HIV-1 fusion inhibitor sifuvirtide. *J. Biol. Chem.* **287**: 6788-6796 (2012).

58. Li L, Ben Y, Yuan S, Jiang S, Xu J, Zhang X. Efficacy, stability, and biosafety of sifuvirtide gel as a microbicide candidate against HIV-1. *PLoS One* **7**: e37381 (2012).

59. Ingallinella P, Bianchi E, Ladwa NA, Wang YJ, Hrin R, Veneziano M, Bonelli F, Ketas TJ, Moore JP, Miller MD, Pessi A. Addition of a cholesterol group to an HIV-1 peptide fusion inhibitor dramatically increases its antiviral potency. *Proc. Natl. Acad. Sci. U. S. A.* **106**: 5801-5806 (2009).

60. Harman S, Herrera C, Armanasco N, Nuttall J, Shattock RJ. Preclinical Evaluation of the HIV-1 Fusion Inhibitor L'644 as a Potential Candidate Microbicide. *Antimicrob. Agents Chemother.* **56**: 2347-2356 (2012).

61. Peisajovich SG, Gallo SA, Blumenthal R, Shai Y. C-terminal octylation rescues an inactive T20 mutant: implications for the mechanism of HIV/SIMIAN immunodeficiency virus-induced membrane fusion. *J. Biol. Chem.* **278**: 21012-21017 (2003).

62. Wexler-Cohen Y, Shai Y. Demonstrating the C-terminal boundary of the HIV 1 fusion conformation in a dynamic ongoing fusion process and implication for fusion inhibition. *FASEB J.* **21**: 3677-3684 (2007).

63. Zhang HY, Schneider SE, Bray BL, Friedrich PE, Tvermoes NA, Mader CJ, Whight SR, Niemi TE, Silinski P, Picking T, Warren M, Wrings SA. Process development of TRI-999, a fatty-acid-modified HIV fusion inhibitory peptide. *Org. Process Res. Dev.* **12**: 101-110 (2008).

64. Campbell SM, Crowe SM, Mak J. Lipid rafts and HIV-1: from viral entry to assembly of progeny virions. *J. Clin. Virol.* **22**: 217-227 (2001).

65. Liao Z, Cimakasky LM, Hampton R, Nguyen DH, Hildreth JE. Lipid rafts and HIV pathogenesis: host membrane cholesterol is required for infection by HIV type 1. *AIDS Res. Hum. Retroviruses* **17**: 1009-1019 (2001).

66. Lingwood D, Simons K. Lipid rafts as a membrane-organizing principle. *Science* **327**: 46-50 (2010).

67. Popik W, Alce TM, Au WC. Human immunodeficiency virus type 1 uses lipid raft-colocalized CD4 and chemokine receptors for productive entry into CD4(+) T cells. *J. Virol.* **76**: 4709-4722 (2002).

68. Manes S, del Real G, Lacalle RA, Lucas P, Gomez-Mouton C, Sanchez-Palomino S, Delgado R, Alcami J, Mira E, Martinez AC. Membrane raft microdomains mediate lateral assemblies required for HIV-1 infection. *EMBO Rep.* **1**: 190-196 (2000).

69. Veiga AS, Santos NC, Loura LM, Fedorov A, Castanho MARB. HIV fusion inhibitor peptide T-1249 is able to insert or adsorb to lipidic bilayers. Putative correlation with improved efficiency. *J. Am. Chem. Soc.* **126**: 14758-14763 (2004).

70. Zhao L, Tong P, Chen YX, Hu ZW, Wang K, Zhang YN, Zhao DS, Cai LF, Liu KL, Zhao YF, Li YM. A multi-functional peptide as an HIV-1 entry inhibitor based on self-concentration, recognition, and covalent attachment. *Org. Biomol. Chem.* **10**: 6512-6520 (2012).

71. Vanpouille C, Arakelyan A, Margolis L. Microbicides: still a long road to success. *Trends Microbiol.* **20**: 369-375 (2012).

72. McEnery R. Oral tenofovir arm of VOICE trial discontinued early. *IAVI Rep.* **15**: 21 (2011).

73. Porotto M, Yokoyama CC, Palermo LM, Mungall B, Aljofan M, Cortese R, Pessi A, Moscona A. Viral entry inhibitors targeted to the membrane site of action. *J. Virol.* **84**: 6760-6768 (2010).

74. Porotto M, Rockx B, Yokoyama CC, Talekar A, Devito I, Palermo LM, Liu J, Cortese R, Lu M, Feldmann H, Pessi A, Moscona A. Inhibition of Nipah virus infection in vivo: targeting an early stage of paramyxovirus fusion activation during viral entry. *PLoS Pathog.* **6**: e1001168 (2010).

75. Pessi A, Langella A, Capito E, Ghezzi S, Vicenzi E, Poli G, Ketas T, Mathieu C, Cortese R, Horvat B, Moscona A, Porotto M. A general strategy to endow natural fusion-protein-derived peptides with potent antiviral activity. *PLoS One* **7**: e36833 (2012).

76. Ashkenazi A, Viard M, Unger L, Blumenthal R, Shai Y. Sphingopeptides: dihydrosphingosine-based fusion inhibitors against wild-type and enfuvirtide-resistant HIV-1. *FASEB J.*: (2012).

77. Cai L, Gochin M, Liu K. Biochemistry and biophysics of HIV-1 gp41 - membrane interactions and implications for HIV-1 envelope protein mediated viral-cell fusion and fusion inhibitor design. *Curr. Top. Med. Chem.* **11**: 2959-2984 (2011).

78. Martin I, Defrise-Quertain F, Mandieau V, Nielsen NM, Saermark T, Burny A, Brasseur R, Ruysschaert JM, Vandenbranden M. Fusogenic activity of SIV (simian immunodeficiency virus) peptides located in the GP32 NH2 terminal domain. *Biochem. Biophys. Res. Commun.* **175**: 872-879 (1991).

79. Slepushkin VA, Melikyan GB, Sidorova MS, Chumakov VM, Andreev SM, Manulyan RA, Karamov EV. Interaction of human immunodeficiency virus (HIV-1) fusion peptides with artificial lipid membranes. *Biochem. Biophys. Res. Commun.* **172**: 952-957 (1990).

80. Kliger Y, Gallo SA, Peisajovich SG, Munoz-Barroso I, Avkin S, Blumenthal R, Shai Y. Mode of action of an antiviral peptide from HIV-1. Inhibition at a post-lipid mixing stage. *J. Biol. Chem.* **276**: 1391-1397 (2001).

81. Veiga S, Henriques S, Santos NC, Castanho MARB. Putative role of membranes in the HIV fusion inhibitor enfuvirtide mode of action at the molecular level. *Biochem. J.* **377**: 107-110 (2004).

82. Liu S, Jing W, Cheung B, Lu H, Sun J, Yan X, Niu J, Farmar J, Wu S, Jiang S. HIV gp41 C-terminal heptad repeat contains multifunctional domains. Relation to mechanisms of action of anti-HIV peptides. *J. Biol. Chem.* **282**: 9612-9620 (2007).

83. Qi Z, Shi W, Xue N, Pan C, Jing W, Liu K, Jiang S. Rationally designed anti-HIV peptides containing multifunctional domains as molecule probes for studying the mechanisms of action of the first and second generation HIV fusion inhibitors. *J. Biol. Chem.* **283**: 30376-30384 (2008).

84. Franquelim HG, Loura LM, Santos NC, Castanho MARB. Sifuvirtide screens rigid membrane surfaces. establishment of a correlation between efficacy and membrane domain selectivity among HIV fusion inhibitor peptides. *J. Am. Chem. Soc.* **130**: 6215-6223 (2008).

85. Franquelim HG, Veiga AS, Weissmuller G, Santos NC, Castanho MARB. Unravelling the molecular basis of the selectivity of the HIV-1 fusion inhibitor sifuvirtide towards phosphatidylcholine-rich rigid membranes. *Biochim. Biophys. Acta* **1798**: 1234-1243 (2010).

86. Fortin JF, Cantin R, Lamontagne G, Tremblay M. Host-derived ICAM-1 glycoproteins incorporated on human immunodeficiency virus type 1 are biologically active and enhance viral infectivity. *J. Virol.* **71**: 3588-3596 (1997).

87. Pantaleo G, Butini L, Graziosi C, Poli G, Schnittman SM, Greenhouse JJ, Gallin JI, Fauci AS. Human immunodeficiency virus (HIV) infection in CD4+ T lymphocytes genetically deficient in LFA-1: LFA-1 is required for HIV-mediated cell fusion but not for viral transmission. *J. Exp. Med.* **173**: 511-514 (1991).

88. Geijtenbeek TB, Kwon DS, Torensma R, van Vliet SJ, van Duijnhoven GC, Middel J, Cornelissen IL, Nottet HS, KewalRamani VN, Littman DR, Figdor CG, van Kooyk Y. DC-SIGN, a dendritic cell-specific HIV-1-binding protein that enhances trans-infection of T cells. *Cell* **100**: 587-597 (2000).

89. Gallay P. Syndecans and HIV-1 pathogenesis. *Microbes Infect.* **6**: 617-622 (2004).

90. Gandhi NS, Mancera RL. The structure of glycosaminoglycans and their interactions with proteins. *Chem. Biol. Drug Des.* **72**: 455-482 (2008).

91. Bernfield M, Gotte M, Park PW, Reizes O, Fitzgerald ML, Lincecum J, Zako M. Functions of cell surface heparan sulfate proteoglycans. *Annu. Rev. Biochem.* **68**: 729-777 (1999).

92. Mbemba E, Czyrski JA, Gattegno L. The interaction of a glycosaminoglycan, heparin, with HIV-1 major envelope glycoprotein. *Biochim. Biophys. Acta* **1180**: 123-129 (1992).

93. Roderiquez G, Oravecz T, Yanagishita M, Bou-Habib DC, Mostowski H, Norcross MA. Mediation of human immunodeficiency virus type 1 binding by interaction of cell surface heparan sulfate proteoglycans with the V3 region of envelope gp120-gp41. *J. Virol.* **69**: 2233-2239 (1995).

94. Crublet E, Andrieu JP, Vives RR, Lortat-Jacob H. The HIV-1 envelope glycoprotein gp120 features four heparan sulfate binding domains, including the co-receptor binding site. *J. Biol. Chem.* **283**: 15193-15200 (2008).

95. Vives RR, Imberty A, Sattentau QJ, Lortat-Jacob H. Heparan sulfate targets the HIV-1 envelope glycoprotein gp120 coreceptor binding site. *J. Biol. Chem.* **280**: 21353-21357 (2005).

96. de Parseval A, Bobardt MD, Chatterji A, Chatterji U, Elder JH, David G, Zolla-Pazner S, Farzan M, Lee TH, Gallay PA. A highly conserved arginine in gp120 governs HIV-1 binding to both syndecans and CCR5 via sulfated motifs. *J. Biol. Chem.* **280**: 39493-39504 (2005).

97. Bulow HE, Hobert O. The molecular diversity of glycosaminoglycans shapes animal development. *Annu. Rev. Cell. Dev. Biol.* **22**: 375-407 (2006).

98. Hacker U, Nybakken K, Perrimon N. Heparan sulphate proteoglycans: the sweet side of development. *Nat. Rev. Mol. Cell Biol.* **6**: 530-541 (2005).

99. Mondor I, Ugolini S, Sattentau QJ. Human immunodeficiency virus type 1 attachment to HeLa CD4 cells is CD4 independent and gp120 dependent and requires cell surface heparans. *J. Virol.* **72**: 3623-3634 (1998).

100. Zhang YJ, Hatziioannou T, Zang T, Braaten D, Luban J, Goff SP, Bieniasz PD. Envelope-dependent, cyclophilin-independent effects of glycosaminoglycans on human immunodeficiency virus type 1 attachment and infection. *J. Virol.* **76**: 6332-6343 (2002).

101. Saphire AC, Bobardt MD, Zhang Z, David G, Gallay PA. Syndecans serve as attachment receptors for human immunodeficiency virus type 1 on macrophages. *J. Virol.* **75**: 9187-9200 (2001).

102. de Witte L, Bobardt M, Chatterji U, Degeest G, David G, Geijtenbeek TB, Gallay P. Syndecan-3 is a dendritic cell-specific attachment receptor for HIV-1. *Proc. Natl. Acad. Sci. U. S. A.* **104**: 19464-19469 (2007).

103. Argyris EG, Acheampong E, Nunnari G, Mukhtar M, Williams KJ, Pomerantz RJ. Human immunodeficiency virus type 1 enters primary human brain microvascular endothelial cells by a mechanism involving cell surface proteoglycans independent of lipid rafts. *J. Virol.* **77**: 12140-12151 (2003).

104. Bobardt MD, Salmon P, Wang L, Esko JD, Gabuzda D, Fiala M, Trono D, Van der Schueren B, David G, Gallay PA. Contribution of proteoglycans to human immunodeficiency virus type 1 brain invasion. *J. Virol.* **78**: 6567-6584 (2004).

105. Bobardt MD, Chatterji U, Schaffer L, de Witte L, Gallay PA. Syndecan-Fc hybrid molecule as a potent in vitro microbicidal anti-HIV-1 agent. *Antimicrob. Agents Chemother.* **54**: 2753-2766 (2010).

106. Baleux F, Loureiro-Morais L, Hersant Y, Clayette P, Arenzana-Seisdedos F, Bonnaffe D, Lortat-Jacob H. A synthetic CD4-heparan sulfate glycoconjugate inhibits CCR5 and CXCR4 HIV-1 attachment and entry. *Nat. Chem. Biol.* **5**: 743-748 (2009).

107. Connell BJ, Baleux F, Coic YM, Clayette P, Bonnaffe D, Lortat-Jacob H. A synthetic heparan sulfate-mimetic peptide conjugated to a mini CD4 displays very high anti-HIV-1 activity independently of coreceptor usage. *Chem. Biol.* **19**: 131-139 (2012).

108. Coffin JM, Hughes SH, Varmus H. *Retroviruses*. Plainview, New York: Cold Spring Harbor Laboratory Press (1997).

109. Young JA, Bates P, Varmus HE. Isolation of a chicken gene that confers susceptibility to infection by subgroup A avian leukosis and sarcoma viruses. *J. Virol.* **67**: 1811-1816 (1993).

110. Bates P, Young JA, Varmus HE. A receptor for subgroup A Rous sarcoma virus is related to the low density lipoprotein receptor. *Cell* **74**: 1043-1051 (1993).

111. Connolly L, Zingler K, Young JA. A soluble form of a receptor for subgroup A avian leukosis and sarcoma viruses (ALSV-A) blocks infection and binds directly to ALSV-A. *J. Virol.* **68**: 2760-2764 (1994).

112. Balliet JW, Berson J, D'Cruz CM, Huang J, Crane J, Gilbert JM, Bates P. Production and characterization of a soluble, active form of Tva, the subgroup A avian sarcoma and leukosis virus receptor. *J. Virol.* **73**: 3054-3061 (1999).

113. Damico R, Bates P. Soluble receptor-induced retroviral infection of receptor-deficient cells. *J. Virol.* **74**: 6469-6475 (2000).

114. Mothes W, Boerger AL, Narayan S, Cunningham JM, Young JA. Retroviral entry mediated by receptor priming and low pH triggering of an envelope glycoprotein. *Cell* **103**: 679-689 (2000).

115. Barnard RJ, Elleder D, Young JA. Avian sarcoma and leukosis virus-receptor interactions: from classical genetics to novel insights into virus-cell membrane fusion. *Virology* **344**: 25-29 (2006).

116. Matsuyama S, Delos SE, White JM. Sequential roles of receptor binding and low pH in forming prehairpin and hairpin conformations of a retroviral envelope glycoprotein. *J. Virol.* **78**: 8201-8209 (2004).

117. Earp LJ, Delos SE, Netter RC, Bates P, White JM. The avian retrovirus avian sarcoma/leukosis virus subtype A reaches the lipid mixing stage of fusion at neutral pH. *J. Virol.* **77**: 3058-3066 (2003).

118. Markosyan RM, Bates P, Cohen FS, Melikyan GB. A study of low pH-induced refolding of Env of avian sarcoma and leukosis virus into a six-helix bundle. *Biophys. J.* **87**: 3291-3298 (2004).

119. Narayan S, Barnard RJ, Young JA. Two retroviral entry pathways distinguished by lipid raft association of the viral receptor and differences in viral infectivity. *J. Virol.* **77**: 1977-1983 (2003).

120. Jha NK, Latinovic O, Martin E, Novitskiy G, Marin M, Miyauchi K, Naughton J, Young JA, Melikyan GB. Imaging single retrovirus entry through alternative receptor isoforms and intermediates of virus-endosome fusion. *PLoS Pathog.* **7**: e1001260 (2011).

121. Padilla-Parra S, Marin M, Kondo N, Melikyan GB. Synchronized retrovirus fusion in cells expressing alternative receptor isoforms releases the viral core into distinct sub-cellular compartments. *PLoS Pathog.* **8**: e1002694 (2012).

122. Cardone G, Brecher M, Fontana J, Winkler DC, Butan C, White JM, Steven AC. Visualization of the two-step fusion process of the retrovirus avian sarcoma/leukosis virus by cryo-electron tomography. *J. Virol.* **86**: 12129-12137 (2012).

123. Albertini AA, Baquero E, Ferlin A, Gaudin Y. Molecular and cellular aspects of rhabdovirus entry. *Viruses* **4**: 117-139 (2012).

124. Doms RW, Keller DS, Helenius A, Balch WE. Role for adenosine triphosphate in regulating the assembly and transport of vesicular stomatitis virus G protein trimers. *J. Cell Biol.* **105**: 1957-1969 (1987).

125. Schlegel R, Tralka TS, Willingham MC, Pastan I. Inhibition of VSV binding and infectivity by phosphatidylserine: is phosphatidylserine a VSV-binding site? *Cell* **32**: 639-646 (1983).

126. Carneiro FA, Bianconi ML, Weissmuller G, Stauffer F, Da Poian AT. Membrane recognition by vesicular stomatitis virus involves enthalpy-driven protein-lipid interactions. *J. Virol.* **76**: 3756-3764 (2002).

127. Schlegel R, Wade M. Neutralized vesicular stomatitis virus binds to host cells by a different "receptor". *Biochem. Biophys. Res. Commun.* **114**: 774-778 (1983).

128. Eidelman O, Schlegel R, Tralka TS, Blumenthal R. pH-dependent fusion induced by vesicular stomatitis virus glycoprotein reconstituted into phospholipid vesicles. *J. Biol. Chem.* **259**: 4622-4628 (1984).

129. Coil DA, Miller AD. Phosphatidylserine is not the cell surface receptor for vesicular stomatitis virus. *J. Virol.* **78**: 10920-10926 (2004).

130. Bloor S, Maelfait J, Krumbach R, Beyaert R, Randow F. Endoplasmic reticulum chaperone gp96 is essential for infection with vesicular stomatitis virus. *Proc. Natl. Acad. Sci. U. S. A.* **107**: 6970-6975 (2010).

131. Finkelshtein D, Werman A, Novick D, Barak S, Rubinstein M. LDL receptor and its family members serve as the cellular receptors for vesicular stomatitis virus. *Proc. Natl. Acad. Sci. U. S. A.* **110**: 7306-7311 (2013).

132. Gaudin Y, Tuffereau C, Segretain D, Knossow M, Flamand A. Reversible conformational changes and fusion activity of rabies virus glycoprotein. *J. Virol.* **65**: 4853-4859 (1991).

133. Gaudin Y. Reversibility in fusion protein conformational changes. The intriguing case of rhabdovirus-induced membrane fusion. *Subcell. Biochem.* **34**: 379-408 (2000).

134. Gaudin Y, Tuffereau C, Durrer P, Flamand A, Ruigrok RW. Biological function of the low-pH, fusion-inactive conformation of rabies virus glycoprotein (G): G is transported in a fusion-inactive state-like conformation. *J. Virol.* **69**: 5528-5534 (1995).

135. Johannsdottir HK, Mancini R, Kartenbeck J, Amato L, Helenius A. Host cell factors and functions involved in vesicular stomatitis virus entry. *J. Virol.* **83**: 440-453 (2009).

136. Superti F, Seganti L, Ruggeri FM, Tinari A, Donelli G, Orsi N. Entry pathway of vesicular stomatitis virus into different host cells. *J. Gen. Virol.* **68 (Pt 2)**: 387-399 (1987).

137. Sieczkarski SB, Whittaker GR. Differential requirements of Rab5 and Rab7 for endocytosis of influenza and other enveloped viruses. *Traffic* **4**: 333-343 (2003).

138. Le Blanc I, Luyet PP, Pons V, Ferguson C, Emans N, Petiot A, Mayran N, Demaurex N, Faure J, Sadoul R, Parton RG, Gruenberg J. Endosome-to-cytosol transport of viral nucleocapsids. *Nat. Cell Biol.* **7**: 653-664 (2005).

139. Kobayashi T, Stang E, Fang KS, de Moerloose P, Parton RG, Gruenberg J. A lipid associated with the antiphospholipid syndrome regulates endosome structure and function. *Nature* **392**: 193-197 (1998).

140. Luyet PP, Falguieres T, Pons V, Pattnaik AK, Gruenberg J. The ESCRT-I subunit TSG101 controls endosome-to-cytosol release of viral RNA. *Traffic* **9**: 2279-2290 (2008).

141. Roth SL, Whittaker GR. Promotion of vesicular stomatitis virus fusion by the endosome-specific phospholipid bis(monoacylglycero)phosphate (BMP). *FEBS Lett.* **585**: 865-869 (2011).

142. Zaitseva E, Yang ST, Melikov K, Pourmal S, Chernomordik LV. Dengue virus ensures its fusion in late endosomes using compartment-specific lipids. *PLoS Pathog.* **6**: e1001131 (2010).

143. Szabo A, Stolz L, Granzow R. Surface plasmon resonance and its use in biomolecular interaction analysis (BIA). *Curr. Opin. Struct. Biol.* **5**: 699-705 (1995).

144. Canziani G, Zhang W, Cines D, Rux A, Willis S, Cohen G, Eisenberg R, Chaiken I. Exploring biomolecular recognition using optical biosensors. *Methods* **19**: 253-269 (1999).

145. Wilson WD. Analyzing biomolecular interactions. *Science* **295**: 2103-2105 (2002).

146. Cooper MA. Optical biosensors in drug discovery. *Nat. Rev. Drug Discov.* **1**: 515-528 (2002).

147. Tanious FA, Nguyen B, Wilson WD. Biosensor-surface plasmon resonance methods for quantitative analysis of biomolecular interactions. *Methods Cell Biol.* **84**: 53-77 (2008).

148. Leonard P, Safsten P, Hearty S, McDonnell B, Finlay W, O'Kennedy R. High throughput ranking of recombinant avian scFv antibody fragments from crude lysates using the Biacore A100. *J. Immunol. Methods* **323**: 172-179 (2007).

149. Jung SO, Ro HS, Kho BH, Shin YB, Kim MG, Chung BH. Surface plasmon resonance imaging-based protein arrays for high-throughput screening of protein-protein interaction inhibitors. *Proteomics* **5**: 4427-4431 (2005).

150. Homola J. Present and future of surface plasmon resonance biosensors. *Anal. Bioanal. Chem.* **377**: 528-539 (2003).

151. Brandenburg B, Zhuang X. Virus trafficking - learning from single-virus tracking. *Nat. Rev. Microbiol.* **5**: 197-208 (2007).

152. Crowther D, Melnick JL. The incorporation of neutral red and acridine orange into developing poliovirus particles making them photosensitive. *Virology* **14**: 11-21 (1961).

153. Brandenburg B, Lee LY, Lakadamyali M, Rust MJ, Zhuang X, Hogle JM. Imaging poliovirus entry in live cells. *PLoS Biol.* **5**: e183 (2007).

154. Griffin BA, Adams SR, Tsien RY. Specific covalent labeling of recombinant protein molecules inside live cells. *Science* **281**: 269-272 (1998).

155. Das SC, Panda D, Nayak D, Pattnaik AK. Biarsenical labeling of vesicular stomatitis virus encoding tetracysteine-tagged m protein allows dynamic imaging of m protein and virus uncoating in infected cells. *J. Virol.* **83**: 2611-2622 (2009).

156. Pereira CF, Ellenberg PC, Jones KL, Fernandez TL, Smyth RP, Hawkes DJ, Hijnen M, Vivet-Boudou V, Marquet R, Johnson I, Mak J. Labeling of multiple HIV-1 proteins with the biarsenical-tetracysteine system. *PLoS One* **6**: e17016 (2011).

157. Chalfie M, Tu Y, Euskirchen G, Ward WW, Prasher DC. Green fluorescent protein as a marker for gene expression. *Science* **263**: 802-805 (1994).

158. Heim R, Cubitt AB, Tsien RY. Improved green fluorescence. *Nature* **373**: 663-664 (1995).

159. Chudakov DM, Lukyanov S, Lukyanov KA. Fluorescent proteins as a toolkit for in vivo imaging. *Trends Biotechnol.* **23**: 605-613 (2005).

160. Giepmans BN, Adams SR, Ellisman MH, Tsien RY. The fluorescent toolbox for assessing protein location and function. *Science* **312**: 217-224 (2006).

161. Stephens DJ, Allan VJ. Light microscopy techniques for live cell imaging. *Science* **300**: 82-86 (2003).

162. Swedlow JR, Platani M. Live cell imaging using wide-field microscopy and deconvolution. *Cell Struct. Funct.* **27**: 335-341 (2002).

163. Axelrod D. Total internal reflection fluorescence microscopy in cell biology. *Traffic* **2**: 764-774 (2001).

164. Abbe E. Beiträge zur Theorie des Mikroskops und der mikroskopischen Wahrnehmung. *Archiv f. mikrosk. Anatomie* **9**: 413-418 (1873).

165. Schermelleh L, Heintzmann R, Leonhardt H. A guide to super-resolution fluorescence microscopy. *J. Cell Biol.* **190**: 165-175 (2010).

166. Galbraith CG, Galbraith JA. Super-resolution microscopy at a glance. *J. Cell Sci.* **124**: 1607-1611 (2011).

167. Lefman J, Scott K, Stranick S. Live, video-rate super-resolution microscopy using structured illumination and rapid GPU-based parallel processing. *Microsc Microanal* **17**: 191-196 (2011).

168. Georgi A, Mottola-Hartshorn C, Warner A, Fields B, Chen LB. Detection of individual fluorescently labeled reovirions in living cells. *Proc. Natl. Acad. Sci. U. S. A.* **87**: 6579-6583 (1990).

169. Helenius A, Kartenbeck J, Simons K, Fries E. On the entry of Semliki forest virus into BHK-21 cells. *J. Cell Biol.* **84**: 404-420 (1980).

170. Elliott G, O'Hare P. Live-cell analysis of a green fluorescent protein-tagged herpes simplex virus infection. *J. Virol.* **73**: 4110-4119 (1999).

171. Desai P, Person S. Incorporation of the green fluorescent protein into the herpes simplex virus type 1 capsid. *J. Virol.* **72**: 7563-7568 (1998).

172. Suomalainen M, Nakano MY, Keller S, Boucke K, Stidwill RP, Greber UF. Microtubule-dependent plus- and minus end-directed motilities are competing processes for nuclear targeting of adenovirus. *J. Cell Biol.* **144**: 657-672 (1999).

173. Pelkmans L, Puntener D, Helenius A. Local actin polymerization and dynamin recruitment in SV40-induced internalization of caveolae. *Science* **296**: 535-539 (2002).

174. Pelkmans L, Kartenbeck J, Helenius A. Caveolar endocytosis of simian virus 40 reveals a new two-step vesicular-transport pathway to the ER. *Nat. Cell Biol.* **3**: 473-483 (2001).

175. McDonald D, Vodicka MA, Lucero G, Svitkina TM, Borisy GG, Emerman M, Hope TJ. Visualization of the intracellular behavior of HIV in living cells. *J. Cell Biol.* **159**: 441-452 (2002).

176. Seisenberger G, Ried MU, Endress T, Buning H, Hallek M, Brauchle C. Real-time single-molecule imaging of the infection pathway of an adeno-associated virus. *Science* **294**: 1929-1932 (2001).

177. Lakadamyali M, Rust MJ, Babcock HP, Zhuang X. Visualizing infection of individual influenza viruses. *Proc. Natl. Acad. Sci. U. S. A.* **100**: 9280-9285 (2003).

178. Melikyan GB, Barnard RJ, Abrahamyan LG, Mothes W, Young JA. Imaging individual retroviral fusion events: from hemifusion to pore formation and growth. *Proc. Natl. Acad. Sci. U. S. A.* **102**: 8728-8733 (2005).

179. Markosyan RM, Cohen FS, Melikyan GB. Time-resolved imaging of HIV-1 Env-mediated lipid and content mixing between a single virion and cell membrane. *Mol. Biol. Cell* **16**: 5502-5513 (2005).

180. Hubner W, McNerney GP, Chen P, Dale BM, Gordon RE, Chuang FY, Li XD, Asmuth DM, Huser T, Chen BK. Quantitative 3D video microscopy of HIV transfer across T cell virological synapses. *Science* **323**: 1743-1747 (2009).

181. Lelek M, Di Nunzio F, Henriques R, Charneau P, Arhel N, Zimmer C. Superresolution imaging of HIV in infected cells with FlAsH-PALM. *Proc. Natl. Acad. Sci. U. S. A.* **109**: 8564-8569 (2012).

182. Floyd DL, Ragains JR, Skehel JJ, Harrison SC, van Oijen AM. Single-particle kinetics of influenza virus membrane fusion. *Proc. Natl. Acad. Sci. U. S. A.* **105**: 15382-15387 (2008).

183. Wessels L, Elting MW, Scimeca D, Weninger K. Rapid membrane fusion of individual virus particles with supported lipid bilayers. *Biophys. J.* **93**: 526-538 (2007).

184. Castellana ET, Cremer PS. Solid supported lipid bilayers: From biophysical studies to sensor design. *Surf. Sci. Rep.* **61**: 429-444 (2006).

185. Costello DA, Lee DW, Drewes J, Vasquez KA, Kisler K, Wiesner U, Pollack L, Whittaker GR, Daniel S. Influenza virus-membrane fusion triggered by proton uncaging for single particle studies of fusion kinetics. *Anal. Chem.* **84**: 8480-8489 (2012).

186. Belogurov AA, Jr., Stepanov AV, Smirnov IV, Melamed D, Bacon A, Mamedov AE, Boitsov VM, Sashchenko LP, Ponomarenko NA, Sharanova SN, Boyko AN, Dubina MV, Friboulet A, Genkin DD, Gabibov AG. Liposome-encapsulated peptides protect against experimental allergic encephalitis. *FASEB J.* **27**: 222-231 (2013).

187. Konstantinov I, Belogurov A, Kovalevsky A, Korbut A, Kondratenko G. The use of liposomes in the treatment of multiple sclerosis. http://visualscience.ru/projects/liposomes-multiple-sclerosis/illustration/. Accessed on 08/04/2013.

188. Hamai C, Yang T, Kataoka S, Cremer PS, Musser SM. Effect of average phospholipid curvature on supported bilayer formation on glass by vesicle fusion. *Biophys. J.* **90**: 1241-1248 (2006).

189. Xu L, Pozniak A, Wildfire A, Stanfield-Oakley SA, Mosier SM, Ratcliffe D, Workman J, Joall A, Myers R, Smit E, Cane PA, Greenberg ML, Pillay D. Emergence and evolution of enfuvirtide resistance following long-term therapy involves heptad repeat 2 mutations within gp41. *Antimicrob. Agents Chemother.* **49**: 1113-1119 (2005).

190. Wei X, Decker JM, Liu H, Zhang Z, Arani RB, Kilby JM, Saag MS, Wu X, Shaw GM, Kappes JC. Emergence of resistant human immunodeficiency virus type 1 in patients receiving fusion inhibitor (T-20) monotherapy. *Antimicrob. Agents Chemother.* **46**: 1896-1905 (2002).

191. Greenberg ML, Cammack N. Resistance to enfuvirtide, the first HIV fusion inhibitor. *J. Antimicrob. Chemother.* **54**: 333-340 (2004).

192. Berkhout B, Eggink D, Sanders RW. Is there a future for antiviral fusion inhibitors? *Curr. Opin. Virol.* **2**: 50-59 (2012).

193. Naider F, Anglister J. Peptides in the treatment of AIDS. *Curr. Opin. Struct. Biol.* **19**: 473-482 (2009).

194. Kajiwara K, Watanabe K, Tokiwa R, Kurose T, Ohno H, Tsutsumi H, Hata Y, Izumi K, Kodama E, Matsuoka M, Oishi S, Fujii N. Bioorganic synthesis of a recombinant

HIV-1 fusion inhibitor, SC35EK, with an N-terminal pyroglutamate capping group. *Bioorg. Med. Chem.* **17**: 7964-7970 (2009).

195. Dwyer JJ, Wilson KL, Davison DK, Freel SA, Seedorff JE, Wring SA, Tvermoes NA, Matthews TJ, Greenberg ML, Delmedico MK. Design of helical, oligomeric HIV-1 fusion inhibitor peptides with potent activity against enfuvirtide-resistant virus. *Proc. Natl. Acad. Sci. U. S. A.* **104**: 12772-12777 (2007).

196. Eggink D, Langedijk JP, Bonvin AM, Deng Y, Lu M, Berkhout B, Sanders RW. Detailed mechanistic insights into HIV-1 sensitivity to three generations of fusion inhibitors. *J. Biol. Chem.* **284**: 26941-26950 (2009).

197. Eggink D, Bontjer I, Langedijk JP, Berkhout B, Sanders RW. Resistance of human immunodeficiency virus type 1 to a third-generation fusion inhibitor requires multiple mutations in gp41 and is accompanied by a dramatic loss of gp41 function. *J. Virol.* **85**: 10785-10797 (2011).

198. Lu J, Sista P, Giguel F, Greenberg M, Kuritzkes DR. Relative replicative fitness of human immunodeficiency virus type 1 mutants resistant to enfuvirtide (T-20). *J. Virol.* **78**: 4628-4637 (2004).

199. Melby T, Demasi R, Cammack N, Miralles GD, Greenberg ML. Evolution of genotypic and phenotypic resistance during chronic treatment with the fusion inhibitor T-1249. *AIDS Res. Hum. Retroviruses* **23**: 1366-1373 (2007).

200. Nijhuis M, Deeks S, Boucher C. Implications of antiretroviral resistance on viral fitness. *Curr. Opin. Infect. Dis.* **14**: 23-28 (2001).

201. Zolopa AR. The evolution of HIV treatment guidelines: current state-of-the-art of ART. *Antiviral Res.* **85**: 241-244 (2010).

202. Kopetzki E, Jekle A, Ji C, Rao E, Zhang J, Fischer S, Cammack N, Sankuratri S, Heilek G. Closing two doors of viral entry: intramolecular combination of a coreceptor- and fusion inhibitor of HIV-1. *Virol. J.* **5**: 56 (2008).

203. Nagashima KA, Thompson DA, Rosenfield SI, Maddon PJ, Dragic T, Olson WC. Human immunodeficiency virus type 1 entry inhibitors PRO 542 and T-20 are potently synergistic in blocking virus-cell and cell-cell fusion. *J. Infect. Dis.* **183**: 1121-1125 (2001).

204. Nakata H, Steinberg SM, Koh Y, Maeda K, Takaoka Y, Tamamura H, Fujii N, Mitsuya H. Potent synergistic anti-human immunodeficiency virus (HIV) effects using combinations of the CCR5 inhibitor aplaviroc with other anti-HIV drugs. *Antimicrob. Agents Chemother.* **52**: 2111-2119 (2008).

205. Pan C, Cai L, Lu H, Qi Z, Jiang S. Combinations of the first and next generations of human immunodeficiency virus (HIV) fusion inhibitors exhibit a highly potent

synergistic effect against enfuvirtide- sensitive and -resistant HIV type 1 strains. *J. Virol.* **83**: 7862-7872 (2009).

206. Tremblay CL, Kollmann C, Giguel F, Chou TC, Hirsch MS. Strong in vitro synergy between the fusion inhibitor T-20 and the CXCR4 blocker AMD-3100. *J. Acquir. Immune Defic. Syndr.* **25**: 99-102 (2000).

207. Aguilar HC, Lee B. Emerging paramyxoviruses: molecular mechanisms and antiviral strategies. *Expert Rev. Mol. Med.* **13**: e6 (2011).

208. Weiss WJ, Murphy T, Lynch ME, Frye J, Buklan A, Gray B, Lenoy E, Mitelman S, O'Connell J, Quartuccio S, Huntley C. Inhalation efficacy of RFI-641 in an African green monkey model of RSV infection. *J. Med. Primatol.* **32**: 82-88 (2003).

209. Sun Z, Pan Y, Jiang S, Lu L. Respiratory syncytial virus entry inhibitors targeting the F protein. *Viruses* **5**: 211-225 (2013).

210. Pang W, Wang RR, Gao YD, Yang LM, Sun Y, Huang JF, Tien P, Zheng YT. A novel enzyme-linked immunosorbent assay for screening HIV-1 fusion inhibitors targeting HIV-1 Gp41 core structure. *J. Biomol. Screen.* **16**: 221-229 (2011).

211. Ribeiro MM, Melo MN, Serrano ID, Santos NC, Castanho MARB. Drug-lipid interaction evaluation: why a 19th century solution? *Trends Pharmacol. Sci.* **31**: 449-454 (2010).

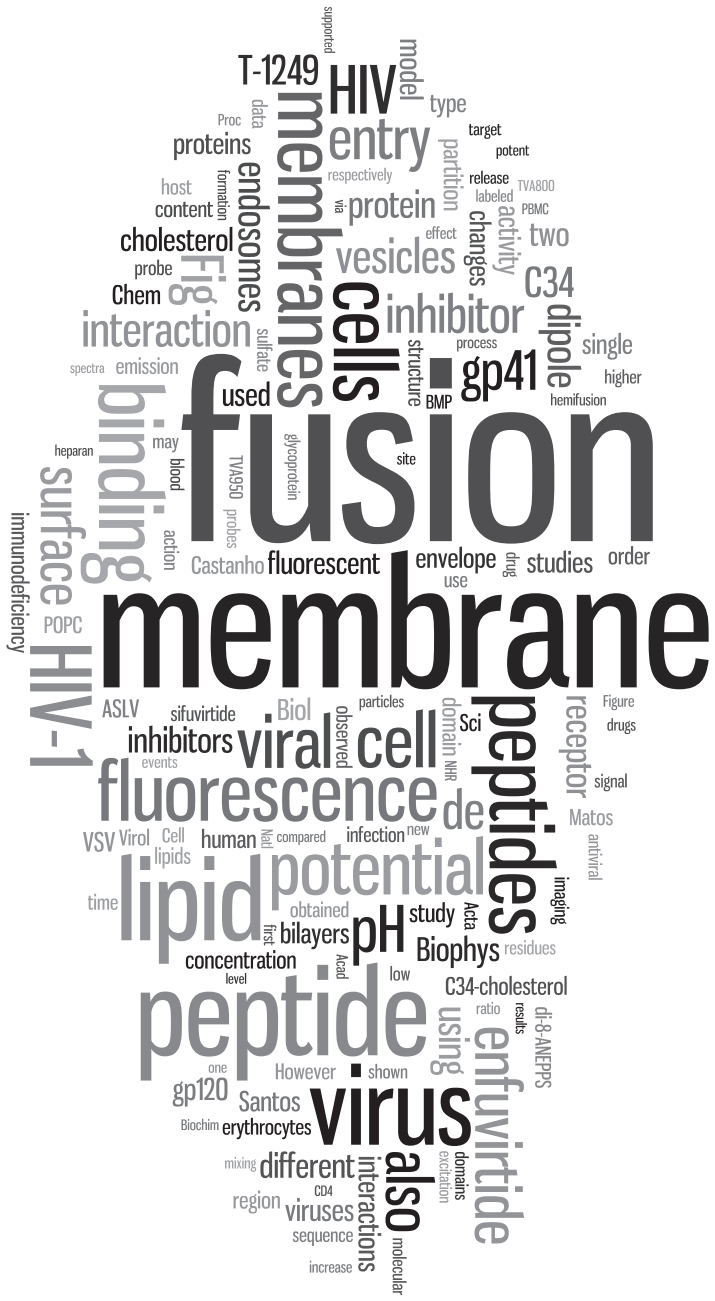

Shedding Light on Enveloped Viruses Entry and its Inhibition Using Optical Techniques

Pedro Matos

Doctoral Thesis

2013